CONSEQUENCES OF THE INTERACTION OF AMYLOID BETA WITH AMYLOID BINDING ALCOHOL DEHYDROGENASE AND THE RECEPTOR FOR ADVANCED GLYCATION END PRODUCTS

Yimin Ren

A Thesis Submitted for the Degree of PhD
at the
University of St. Andrews

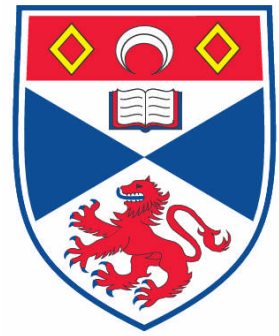

2008

Consequences of the interaction of Amyloid Beta with Amyloid Binding Alcohol Dehydrogenase and the Receptor for Advanced Glycation End products

By Yimin Ren, BM, MSc.

A thesis submitted to the University of St. Andrews in partial fulfillment of the requirement of the degree of Doctor of Philosophy

School of Biology and School of Medicine

CONTENTS

Declaration

I, Yimin Ren, hereby certify that this thesis, which is approximately 37,200 words in length, has been written by me, that it is the record of work carried out by me and that it has not been submitted in any previous application for a higher degree.

Date _____ _____

I was admitted as a candidate for the degree of Ph.D. in September, 2004; the higher study for which this is a record was carried out in the University of St Andrews between 2004 and 2008.

Date _____ _____

I hereby certify that the candidate has fulfilled the conditions of the Resolution and Regulations appropriate for the degree of Ph.D. in the University of St Andrews and that the candidate is qualified to submit this thesis in application for that degree.

Date _____ _____

Copyright declaration

In submitting this thesis to the University of St Andrews I understand that I am giving permission for it to be made available for use in accordance with the regulations of the University Library for the time being in force, subject to any copyright vested in the work not being affected thereby. I also understand that the title and abstract will be published, and that a copy of the work may be made and supplied to any bona fide library or research worker, that my thesis will be electronically accessible for personal or research use, and that the library has the right to migrate my thesis into new electronic forms as required to ensure continued access to the thesis. I have obtained any third-party copyright permissions that may be required in order to allow such access and migration.

Date _____ _____

Acknowledgement

I would like to express my deepest gratitude to my supervisor, Dr. Frank Gunn-Moore, for giving me the opportunity to work in his lab, for his kindness, encouragement and for the many valuable things he taught me over the past three years.

I would like to thank my second supervisor, Dr. Jim Aton, who is always delightful, approachable and ready to help.

I owe my sincere thanks to all the people in our group, Fleur Davey, Lisa Herron, Brian Powell and Dave Stevenson for their friendly help and company.

I want to thank all the people on E floor for making my PhD a nice and enjoyable experience.

My special thanks to Alex and Ian for their help with the order.

My deep thanks go to my best friends, Bo and Liang, for providing me a very tempting motivation to finish my thesis.

Finally, my most heartfelt thanks belong to my family: my parents, my brother and my sister for their understanding, endless support and patience.

This work was financially supported by the Alzheimer's Research Trust.

Abbreviations used in this thesis

A	adenine
Aβ	amyloid beta
ABAD	amyloid binding alcohol dehydrogenase (also known as 3β-HSD, ERAB, MHBD, HAD
AD	Alzheimer's disease
ADP	adenosine diphosphate
ATP	adenosine triphosphate
AGEs	advanced glycation end products
mAPP	mutant amyloid precursor protein
AICD	APP intracellular domain
Apaf1	apoptotic protease–activating factor-1
ANT	adenine nucleotide translocase
ATCC	American Tissue Culture Collection
Bis-Tris	bis(2-hydroxyethyl)iminotris(hydroxymethyl)methane
BFA	brefeldin A
bp	base pair
BSA	bovine serum albumin
C	cytosine
cDNA	complementary DNA
Cdk-5	cyclin-dependent kinase 5
CNS	central nervous system
C-terminus	carboxy terminus
CIN85	cbl-interacting protein of 85 kDa
COX	Complex IV, cytochrome c oxidase of the mitochondrial respiratory chain
CoQ	coenzyme Q
CypD	cyclophilin D
CsA	cyclosporin A
CTF	APP carboxyl-terminal derivative
SH3	cytoplasmic Src homology 3 domain
DMEM	Dulbecco's modified Eagle's medium
DMSO	dimethyl sulfoxide
DN	dominant negative
DNA	deoxyribonucleic acid
dNTP	deoxynucleoside triphosphate
DTT	dithiothreitol
E. coli	*Escherichia coli*
ECFP	enhanced cyan blue fluorescent protein
ECL	enhanced chemiluminescence

EDTA	ethylenediaminetetraacetic acid
EFABP	epidermal fatty acid binding protein
EGTA	ethyleneglycol-bis-(β-aminoethyl)-N,N'-tetraacetic acid
EIF-5A	ukaryotic translation initiation factor 5A
ER	endoplasmic reticulum
ETC	electron transport chain
EYFP	enhanced yellow fluorescent protein
FAD	flavin adenine dinucleotide
FCS	foetal calf serum
FRET	fluorescence resonance energy transfer
G	guanine
GFP	green fluorescent protein
GLK	germinal center kinase like kinase
GLO1	glyoxylase 1
GMFB	glia maturation factor-β
GSK3β	Glycogen synthase kinase 3β
HEK	human embryonic kidney cell line
HIV-1	human immunodeficiency virus-1
HNE	4-hydroxynonenal
HRP	horseradish peroxidase
HS	horse serum
IAP	inhibitor of apoptosis
IEF	isoelectric focusing
IPG	immobilized pH gradient
IPTG	isopropyl-β-D-thiogalactopyranoside
JNK	c-Jun N-terminal kinase
kb	kilobase pairs
LB	luria broth
LDH	lactate dehydrogenase
LPAAT	lysophosphatidic acid acyltransferase-β
MAP	mitogen-activated protein
MCP-1	monocyte chemotactic protein-1
M-CSF	macrophage-colony stimulating factor
MEM	minimum essential medium Eagle
MES	2-(*N*-morpholino)ethanesulfonic acid
MG	methylglyoxal
MHBD	2-methyl-3-hydroxybutyryl-CoA dehydrogenase
MIP	macrophage inflammatory protein
MMP	mitochondrial membrane permeabilization
MPT	mitochondrial membrane permeability transition
MPTP	mitochondrial membrane permeability transition pore
MQ	milli-Q purified water
mRNA	messenger ribonucleic acid

NAD	nicotinamide adenine dinucleotide
NDUFV2	NADH dehydrogenase ubiquinone flavoprotein 2
NEAA	non-essential amino acids
NFκβ	nuclear transcription factor κβ
NGF	nerve growth factor
Nit2	nitrilase family, member 2
NO	nitric oxide
non-Tg	wild type transgenic mice
NP-40	nonidet P40
N-terminus	amino terminus
PCR	polymerase chain reaction
pen	penicillin
PfuTurbo	DNA polymerase derived from Pyrococcus furiosus
PMSA2	alpha-type HC3
PMSF	phenylmethylsulfonyl fluoride
PS	presenilin
PSMB4	proteasome subunit, beta type 4
PVDF	polyvinylidine fluoride
RAGE	receptor for advanced glycation end products
RIPA	radio-immunoprecipitation assay
ROIs	region of interests
ROS	reactive oxygen species
rpm	revolutions per minute
SAD	sporadic Alzheimer’s disease
SBT	spectral bleedthrough
SDS	sodium dodecyl sulfate
SDS-PAGE	sodium dodecyl sulfate polyacrylamide gel electrophoresis
SK-N-SH	human neuroblastoma cell line
SH-SY-5Y	human neuroblastoma cell line
SNEV	senescence evasion factor
SOC	super optimal catabolite repression broth
T	thymine
TBE	tris-borate-EDTA buffer
TBS	tris buffered saline
TBS-T	tris buffered saline with Tween 20
TEMED	tetramethylethylenediamine
Tg	transgenic
Tris	tris(hydroxymethyl) methylamine
Tris-HCl	tris(hydroxymethyl) aminomethane hydrochloride
Triton X-100	t-Octylphenoxypolyethoxyethanol
Tween 20	Polyoxyethylenesorbitan, monolaurate
UV	ultraviolet
VDAC	voltage-dependent anion channel

Abstract

Amyloid beta (Aβ) has been postulated to be the principle initiator of the pathogenesis of Alzheimer's disease (AD). Therefore, understanding the underlying mechanisms of Aβ induced neurotoxicity in the early stages of AD would be essential for finding potential therapeutic targets of AD.

Aβ-binding alcohol dehydrogenase (ABAD) has been shown to be a mitochondrial binding site for Aβ. Expression of ABAD has been found to be increased in brains of AD sufferers. Two dimensional electrophoresis studies have revealed that endophilin 1 was upregulated in Tg mAPP/ABAD mice brains as compared to Tg mAPP, Tg ABAD and non-Tg mice brains. Increased expression of endophilin 1 has also been found in brains of AD patients as compared to non-demented control brain tissues. Endophilin1 has been reported to regulate c-Jun N-terminal kinase (JNK) activation. In this study, expression of dominant negative forms of endophilin 1 (DN-endophilin 1) in mouse cortical neurons exhibited a significant reduction of Aβ induced JNK activation. Furthermore, using cell counting methods, it was shown that the transfection of DN-endophilin 1 increased neuron survival after Aβ treatment.

Aβ has also been proposed to disrupt the interaction of ABAD and Cyclophilin D (CypD), which would trigger mitochondrial permeable transition, thereby leading to neurotoxicity. For fluorescence resonance energy transfer (FRET) analysis of the interaction of ABAD and CypD, a mitochondria targeted, EYFP tagged ABAD

plasmid (pMito-ABAD-EYFP) and an ECFP tagged CypD (pCypD-ECFP) plasmid were developed. Positive FRET signals in SK-N-SH cells co-expressing pMito-ABAD-EYFP and pCypD-ECFP indicated that ABAD interacts with CypD in the mitochondria of mammalian cells.

RAGE (receptor for advanced glycation end products) has been reported to bind to Aβ and mediate the toxic effects of Aβ peptides on neurons and microglia. It has been shown previously that Tg mAPP/DN-RAGE mice display preserved cognitive function as compared to Tg mAPP mice. To investigate possible mechanisms involved in rescuing cognitive function by RAGE blockage, two dimensional electrophoresis was used to analyze differential protein expression between Tg mAPP and Tg mAPP/DN-RAGE mice cortex. Altered expression of four proteins, including NADH dehydrogenase flavoprotein 2 (NDUFV2), glyoxalase 1 (GLO1), proteasome subunit beta type 4 (PSMB4, or β7 subunit of proteasome) and nitrilase family, member 2 (Nit2) have been observed between Tg mAPP/DN-RAGE mice cortex and Tg mAPP mice cortex. NDUFV2 is a 24kDa subunit of complex 1 which is involved in ATP synthesis. GLO1 is a cytosolic enzyme that plays a role the glutathione-dependent detoxification of α-oxoaldehydes, such as methylglyoxal. PSMB4 is a subunit of the 26s proteosome which is in the degradation of ubiquitinylated proteins. The function of Nit2 is still unclear.

Table of Contents

List of Figures

List of Tables

Chapter 1: Introduction

Chapter 1: Introduction

1.1 An overview of Alzheimer's disease

Alzheimer's disease (AD) is the most prevalent cause for dementia in the aged population and affects almost half of all patients with dementia. Advancing age is the dominant risk factor for AD. The diagnosis of AD is still rare in people under 65, but becomes more prevalent with each decade of life. 10% of those over 65 and almost 50% of those over the age of 85 have AD (Jones *et al.* 1993). With the aging of the world population, AD has become a major health problem worldwide. It has been estimated that there are 26.6 million cases of AD in the world and the number of people with AD will double every 20 years to 106.8 million by 2050 (Brookmeyer *et al.* 2007).

AD is a fatal, progressive neurodegenerative disorder. Clinically, the usual first symptom of AD is memory loss which progresses from minor forgetfulness to a more pervasive loss of short-term memory, then of long-term memories. As the disorder progresses, aphasia, disorientation and disinhibition often occur. In the later stages, Alzheimer's disease may also include behavioural and personality changes. The average duration of the disease from onset of symptoms to death is approximately 7-10 years (Smith and Swash 1978).

Alzheimer's disease is imposing a severe burden upon the individuals affected, along with their families and care givers. AD also has a substantial negative economic impact on the society. Recent research shows that, in the UK, the cost to

provide long-term care to older people with dementia will increase to £16.7 billion by 2031 (Comas-Herrera *et al.* 2007).

1.1.1 Neuropathology of Alzheimer's disease

At present, clinical diagnosis of AD is based on progressive impairment of memory and decline in at least one other cognitive domain, and exclusion of other diseases that might also cause dementia, such as frontotemporal dementia, dementia with Lewy-bodies, stroke, brain tumor, normal pressure hydrocephalus or depression. While the clinical diagnostic accuracy for Alzheimer's disease can exceed 90% in mid or late stages, definitive diagnosis of AD is only possible through direct pathologic examination of brain tissue derived from either biopsy or autopsy due to the absence of biologic markers (Jobst *et al.* 1994).

The characteristic neuropathology of AD was first described by a German psychiatrist, Alois Alzheimer, in 1907. There are two hall mark pathological findings in the brains of AD sufferers (Alzheimer 1907; Mott and Hulette 2005; Souder 2005):

- Extracellular amyloid plaques (or fibrils) including diffuse and neuritic plaques, which are mainly composed of the amyloid beta peptide (Aβ) (Selkoe 2001). The neuritic plaques are intimately surrounded by dystrophic axons and dendrites, reactive astrocytes and activated microglia.
- Intracellular neurofibrillary tangles (NFTs) which are intraneuronal bundles of paired helical filaments. The main structural component of NFTs is an

abnormally phosphorylated form of tau protein. Tau is a widely expressed phosphoprotein from the microtubule associated family, the main function of which is to maintain microtubule stability. In Alzheimer's disease, hyperphosphorylated tau aggregates, reducing its ability to bind microtubules and leading to cytoskeletal degeneration and neuronal death (Lovestone and Reynolds 1997). NFTs are not specific to Alzheimer's disease, and are also found in a variety of other neurodegenerative disorders such as frontotemporal dementia, subacute sclerosing panencephalitis, Hallervorden-Spatz disease, Parkinson dementia complex and dementia pugilistica (Perl 2000).

Besides plaques and tangles, AD brains also exhibit a number of pathological abnormalities, including cerebrovascular deposition of amyloid, a profound loss of neurons and synapses, profuse reactive gliosis, microglial activation and inflammatory processes (Roher 1993; Aisen 2002).

1.1.2 APP processing

Although numerous proteins are associated with the amyloid plaques in AD, the principal protein component of the plaques is the approximately 4-kDa Aβ. Aβ is derived from the amyloid precursor protein (APP) via endoproteolytic cleavage. APP is a ubiquitously expressed type I integral membrane glycoprotein. It is abundantly expressed in the brain. The human APP gene is located on the long arm of chromosome 21, and spans approximately 240 kb and contains at least 18 exons (Kang *et al.* 1987). Alternative splicing generates APP mRNAs encoding several

isoforms that range from 365 to 770 amino acid residues. The major Aβ peptide encoding proteins are 695, 751, and 770 amino acids (referred to as APP695, APP751 and APP770). APP processing is a normal event in nearly all neuronal and nonneuronal cells. Full-length APP is sequentially processed by at least three proteinases termed α-, β- and γ-secretases (Wilquet and De 2004). This process can be divided in two different pathways, the nonamyloidogenic and the amyloidogenic pathway. The majority of APP is processed in the nonamyloidogenic pathway. In the nonamyloidogenic pathway, full-length APP is first cleaved by α-secretase within the Aβ peptide domain, leading to the release of APPsα, production of membrane-tethered α-carboxyl-terminal fragments (α-CTFs) and precluding the generation of intact Aβ. Membrane-anchored α-CTF is then cleaved by γ-secretase within the membrane, releasing the p3 peptide and APP intracellular domain (AICD). In the amyloidogenic pathway, APP is cleaved at the amino-terminus of Aβ by a β-secretase. This cleavage generates a large secreted derivative (APPsβ) and a membrane-bound β-CTFs. Cleavage of CTF by γ-secretase results in the production of Aβ peptides of varying length. The two species of most interest are a 40–amino acid Aβ peptide (Aβ40) and a 42–amino acid Aβ peptide (Aβ42) (Figure 1.1). The molecules responsible for these proteolytic activities of APP processing have been identified. Several lines of studies indicate that α-secretase is a member of the ADAM (adisintegrin and metalloprotease) family of proteases (Allinson *et al.* 2003). The identity of β-secretase has been shown to be the novel transmembrane aspartic protease, beta-site APP-cleaving enzyme 1 (BACE1; also called Asp2 and memapsin 2). BACE2, a protease homologous to

BACE1, was also identified (Stockley and O'Neill 2007). γ-secretase is a multiprotein complex consisting of presenilin (PS), nicastrin, aph-1 (anterior pharynx-defective-1), and pen-2 (PS-enhancer-2) and that all four proteins are necessary for full proteolytic activity (De Strooper 1993).

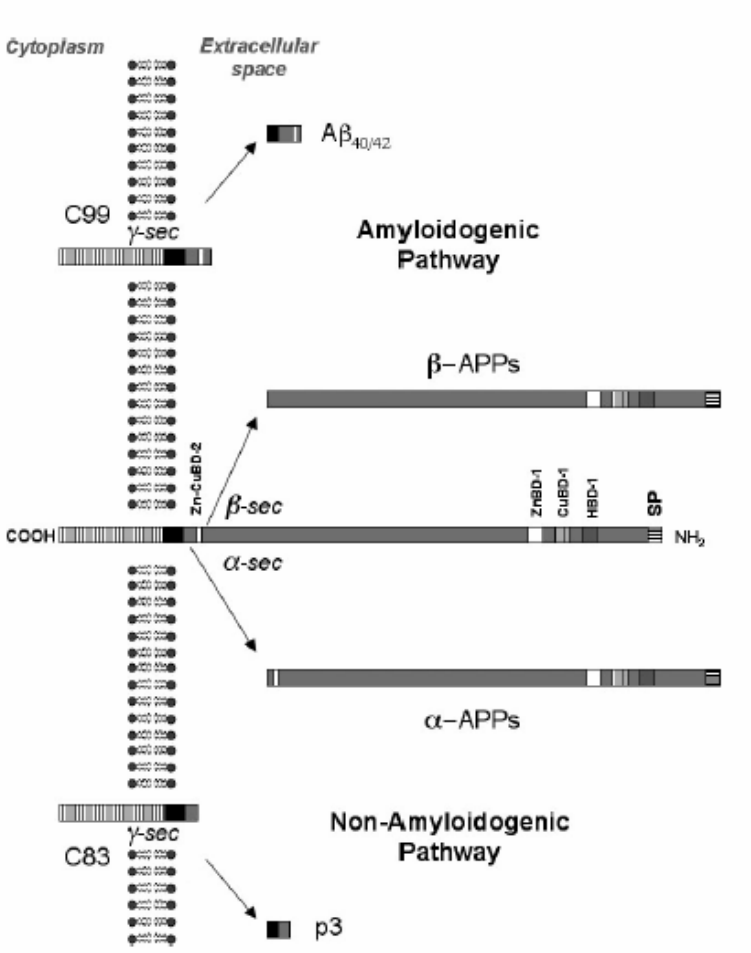

Figure 1.1 Proteolytic processing of amyloid precursor protein (APP). APP is first cleaved by α-secretase within the Aβ domain, leading to APPsα secretion and precluding Aβ generation. Membrane-anchored α-carboxy terminal fragment (α-CTF) is then cleaved by γ-secretase within the membrane, releasing the p3 peptide and APP intracellular domain (AICD). Alternatively, amyloidogenesis takes place when APP is first cleaved by β-secretase, producing APPsβ. Aβ and AICD are generated upon cleavage by γ-secretase of the β-CTF retained in the membrane.
From: Wilquet and De (2004) *Curr Opin Neurobiol.* 14, 582-588

1.1.3 Early-onset AD

Although the exact mechanisms of the pathophysiology of AD are still unknown, increasing evidence from histopathological, biochemical, genetic and animal model studies suggested that Aβ plays a key role in the pathogenesis of Alzheimer's disease.

There are two broad types of AD, the familial AD (FAD) and the sporadic AD (SAD). In FAD, the disease segregates in families, following an autosomal dominant inheritance pattern. FAD only affects a small subset of patients of younger age, usually before their fifties (Mullan *et al.* 1993). In SAD, no clear family history is indicated and the disease usually occurs over the age of 60s. Because of the variation in age at onset, AD is also categorized into early onset and late onset forms. People suffering AD before the age of 60 are generally placed in the early-onset category and account for about 1% of all AD cases.

1.1.3.1 Genetic mutations linked with early onset AD

Early onset AD is usually familial and follows an autosomal dominant inheritance pattern with a high penetrance. To date three different genes have been implicated in the pathology of the rare early onset familial Alzheimer's disease: mutations of the APP (mAPP) gene on chromosome 21(Goate *et al.* 1989; Levy *et al.* 1990), mutations in the presenilin 1 and 2 (PS1 and PS2) genes on chromosome 14 and 1, respectively (Rogaev et al. 1995; Levy-Lahad *et al.* 1995). Presenilin 1, presenilin 2 and amyloid precursor protein have a clear-cut autosomal dominant pattern with a

penetrance above 85%. Although the precise functions of presenilins are unclear, several studies indicated that PS1 and PS2 are catalytic components of γ-secretases (De Strooper *et al.* 1999; Haass and De 1999). In vitro studies demonstrated that the pathogenic mutations in the APP and presenilin genes are associated with abnormal processing of APP, which leads to increased production and elevated plasma levels of Aβ, especially Aβ42 or increased ratio of Aβ42: Aβ40 (Citron *et al.* 1992; Cai *et al.* 1993; Suzuki *et al.* 1994).

Transgenic (Tg) animals carrying mutations in amyloid precursor protein and presenilin genes displayed enhanced production and progressive aggregation of Aβ. These animal models also reproduced the major features of Alzheimer's disease: amyloid plaques and memory impairment. However, no significant tau pathology or extensive neuron loss, as found in AD brain, was detected in these transgenic animals (Games *et al.* 1995; Hsiao *et al.* 1996).

Although the mutations in APP, PS1 and PS2 genes account for only 1% of all AD cases, they have provided important insights for understanding some of the key underlying biological mechanisms of AD. These various genetic mutations, all lead to overproduction of Aβ42 in the brain before Alzheimer's disease symptoms arise, indicating that the accumulation of Aβ42 is the initiating factor in the pathogenesis of Alzheimer's disease.

Biochemical analysis of Aβ further supported this idea. In vitro, Aβ peptides aggregate via a complex multistep-nucleated polymerization involving formation of dimers and small oligomers followed by growth into protofibrils and fibrils. On

electron microscopy, amyloid fibrils are composed of multiple protofibrils wrapped around each other, forming a crossed β-pleated sheet (Caughey and Lansbury 2003). Moreover, Aβ42, which is up-regulated by most of the genetic mutations that have been linked to early onset AD, has a higher propensity to aggregate than the shorter species (Jarrett *et al.* 1993).

Additionally, Down syndrome patients, who have three copies of chromosome 21 which harbours the APP gene, began to develop amyloid plaques and tau tangles in their 30s and 40s (Kang *et al.* 1987).

1.1.3.2 Amyloid deposition precedes NFT formation

NFT is another characteristic neuropathologic lesion in AD brain. In patients with the presenilin 1 mutations or individuals with Down's syndrome, the presence of amyloid plaques preceded the appearance of neurofibrillary tangles (Lippa *et al.* 1998). Furthermore, transgenic mice overexpressing both mutant human tau and mutant human APP had the same number and structure of amyloid plaques but a significantly higher number of tau positive NFTs than transgenic mice overexpressing only mutant human tau (Lewis *et al.* 2001). These results indicated that the mutant amyloid precursor protein and the consequent Aβ production precede and promote the formation of NFTs.

In summary, these data collectively supported the hypothesis that increased production or deposition of Aβ is the initiating signaling event in AD.

1.1.4 Late onset AD

Late onset AD is the most common form of AD. Most late onset AD cases are sporadic, with no family history of the disease. In early onset AD, gene mutations lead to overproduction of Aβ, whereas, in late onset AD, the pathological mechanisms leading to increased Aβ generation are unclear. A twin study on incident cases indicated that almost 50% of the late onset AD risk is attributable to genetic factors (Raiha *et al.* 1996). It is probable that environmental factors have to interact with genetic susceptibility at multiple genes to cause development of the disease.

Several non-genetic risk factors for late-onset AD including female gender, poor early-childhood education, head injury, small cranial diameter and high cholesterol level were proposed (Tol *et al.* 1999). The evidence for these risk factors, however, was not convincing. The most well established risk factor for AD is increasing age. It was estimated that everyone would develop AD if we live to 140 years of age (Serretti *et al.* 2005).

The ApoE gene on chromosome 19q13 was identified as a strong risk factor for late onset AD. There was an increased prevalence of apolipoprotein E (ApoE) epsilon in late onset AD (Corder *et al.* 1998). The precise mechanism by which the ApoE4 allele is associated with late onset AD is unclear. It appears that, like the effects of APP mutations, PS1and PS2 mutations on APP processing, ApoE4 can promote the deposition of Aβ42 (Esler *et al.* 2002; Golabek *et al.* 1996).

Despite the robust association of the ApoE4 allele with late onset AD, the ApoE4

allele is not required for late onset AD. 50% of late onset AD patients did not posses the ApoE4 allele. This indicated that the ApoE4 allele functions as a susceptibility marker, which in conjunction with other genetic and/or environmental factors can increase the risk of late onset AD (Pirttila *et al.* 1996). This also pointed to the possibility that there remains additional, yet to be discovered susceptibility genes for late onset AD.

1.1.5 The toxic species of Aβ

The central role of Aβ in the pathogenesis of AD has been well established. Aβ is initially produced from APP intracellularly and then secreted (Hartmann *et al.* 1997). In vivo, Aβ peptides exist in various conformations including monomeric form, different oligomeric states and β sheet fibrils. Due to the dynamic nature of this peptide, the nature of the toxic species of Aβ remains unknown (Pedersen and Otzen 2008).

1.1.5.1 Soluble Aβ levels correlate with AD progression

The presence of amyloid plaques did not correlate well with clinical progression of AD. In contrast, synaptic loss was shown to correlate well with the degree of cognitive decline in AD patients (Lue *et al.* 1999). Moreover, soluble Aβ levels were found to correlate best with memory and cognitive deficits in AD patients. Even in very mildly impaired AD patients, soluble Aβ levels in the cortex showed a significant correlation with the degree of synaptic loss (Lue *et al.* 1999). Comparisons of transgenic lines having varying APP expression indicated that

decrease in presynaptic terminals is critically dependent on soluble Aβ oligomer levels, not on amyloid plaques (Selkoe 2002).

Consistent with these results, several studies demonstrated that diffusible soluble Aβ oligomers, but not monomers or insoluble amyloid fibrils, are toxic to cultured neurons and responsible for the neurotoxicity and synaptic dysfunction present in Alzheimer's disease (Walsh *et al.* 2002). For example, micro-injection of soluble Aβ oligomers into rats inhibited long-term potentiation in the hippocampus (Walsh *et al.* 2002). Moreover, synaptic toxicity was observed in young transgenic mice overexpressing mutant APP before plaque formation (Mucke *et al.* 2000).

These data collectively indicated that the soluble Aβ oligomers are involved in the early stages of the pathogenesis of AD. Three types of Aβ oligomers were identified in vitro: 1) very short oligomers ranging from dimer to hexamer size (Bitan *et al.* 2003); 2) Aβ-derived diffusible ligands (ADDLs), small oligomers ranging from 17 to 42 kDa (Lambert *et al.* 1998); 3) protofibrils, which can be seen on electron microscopy as short fibril intermediates (Yong *et al.* 2002). Detailed relationships between these different oligomers are not clear yet. The diversity and unstable nature of these Aβ intermediates, however, makes it difficult to identify the specific species of Aβ oligomers that is responsible for the neurotoxic effects in AD.

1.1.5.2 Intraneuronal Aβ accumulation causes the onset of synaptic dysfunction in AD

Another important question is: Do Aβ oligomers induce neurotoxicity via an

intracellular pathway or an extracellular pathway?

Aβ peptides are generated intracellularly at different subcellular sites. Aβ40 is generated solely in the trans-Golgi network (TGN), whereas Aβ42 is generated in the endoplasmic reticulum (ER) as well as Golgi compartments (Hartmann *et al.* 1997; Greenfield *et al.* 1999). Although much of the intracellularly generated Aβ is enroute to secretion, there is a significant pool of Aβ peptides which is not secreted. Stable oligomers of Aβ, were initially formed intracellularly in a variety of cell types, including primary human neurons (Walsh *et al.* 2000). In a 3XTg-AD mouse model, which developed an age-dependent accumulation of both plaques and tangles in disease-relevant brain region (Oddo *et al.* 2003), earliest cognitive impairment manifested at 4 months and correlated with the accumulation of intraneuronal Aβ in the hippocampus and amygdala, before any plaques or tangles appeared. Clearance of the intraneuronal Aβ by immunotherapy rescued the early cognitive deficits (Billings *et al.* 2005).

Taken together, these experiments suggested that deficits in synaptic plasticity, learning and memory in AD may be induced by the accumulation of both intracellular and extracellular Aβ oligomers.

1.1.6 Amyloid cascade hypothesis

When all the above data is taken together, this supports a modified version of the amyloid cascade hypothesis (Golde 2003) (Figure 1.2). Initially, it was proposed that an imbalance between the production and removal of Aβ leads to its

progressive accumulation, triggering a series of signaling cascades leading to synaptic dysfunction and neuronal loss, clinically manifested with memory loss and impaired cognitive functions (Selkoe 2000). This hypothesis remains valid, except that soluble Aβ oligomers and intraneuronal Aβ, instead of amyloid plaques, initiate the cascade leading to neuronal death and dysfunction.

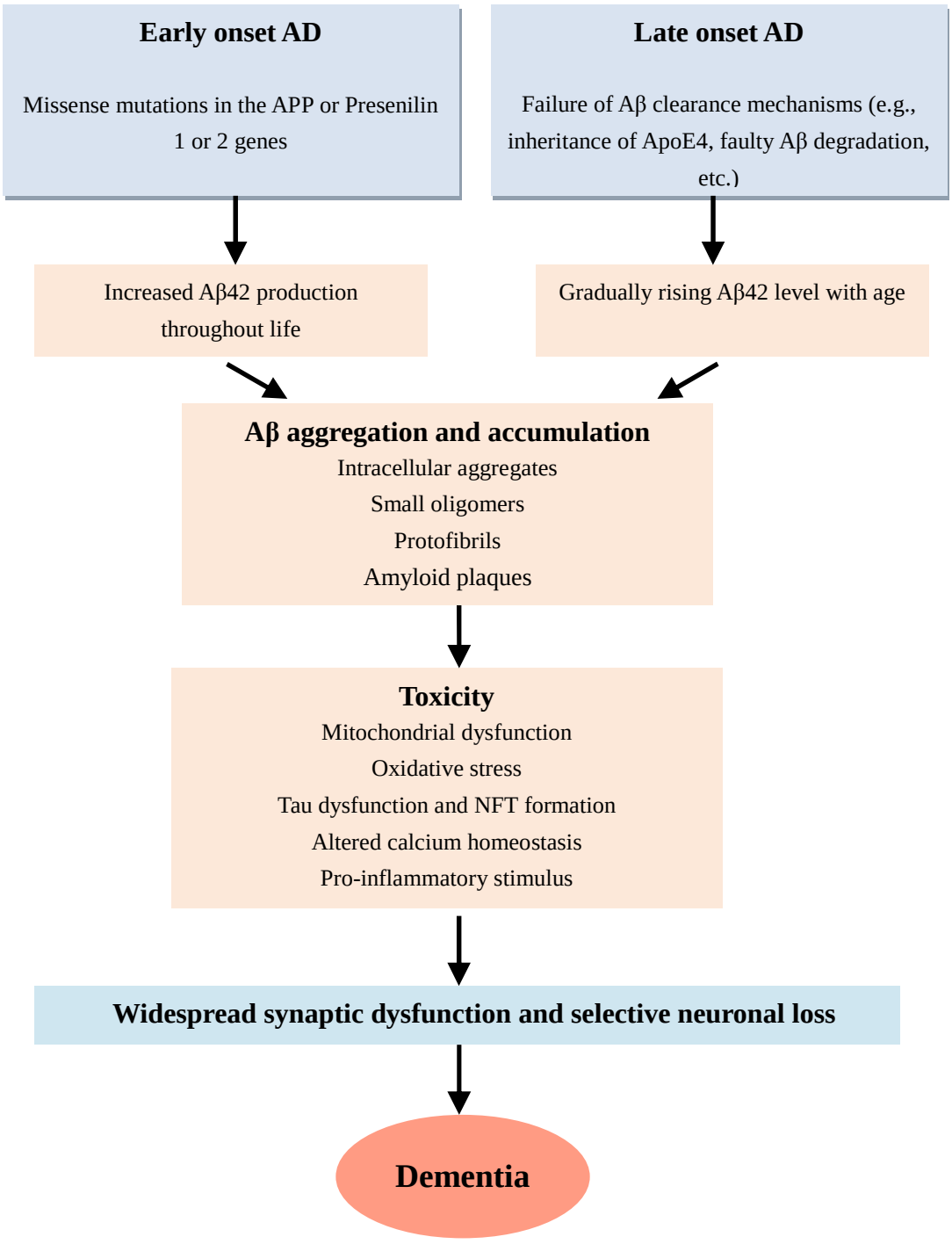

Figure 1.2 Schematic illustration of a modified version of the amyloid cascade hypothesis. This version takes into account the possibility that soluble Aβ oligomers and intraneuronal Aβ oligomers other than those found in amyloid deposits initiate the pathological cascade. This a schematic illustration of a hypothetical sequence of the pathogenetic steps of AD, based on currently available evidence.
Modified from: Golde (2003) *J Clin Invest*, 111, 11-18

1.2 Mitochondrial dysfunction and oxidative stress in AD

Although the etiology of AD is still unclear, mitochondrial dysfunction and oxidative stress have been proposed as underlying mechanisms of disease pathogenesis in AD. In contrast to amyloid plaques and NFTs, mitochondrial dysfunction and oxidative stress are two early events in the pathology of AD.

1.2.1 Mitochondria is the major site for ATP production and ROS generation

Mitochondria consist of two lipid membranes: the inner and the outer mitochondrial membrane (Sherratt 1991). The inner membrane houses the electron transport chain (ETC) and also covers the mitochondrial matrix, which contains the components of tricarboxylic acid cycle and β-oxidation. The outer membrane is basically porous, allowing low-molecular-weight substances to move between the cytosol and the intermembrane space (Sherratt 1991).

There are several important cellular functions of mitochondria: producing ATP, generating reactive oxygen species (ROS), regulating intracellular Ca^{2+}, and releasing proteins that activate the apoptotic pathway.

Mitochondria are the major source of energy for the brain (Ricci *et al.* 2003). Mitochondrial ATP is produced via oxidative phosphorylation (Leuner *et al.* 2007). Electrons from oxidative substrates are transferred to oxygen, through a series of oxidation and reduction reactions, to generate water. In the process, protons are pumped from the matrix across the mitochondrial inner membrane through the ETC which consists of five membrane-spanning enzyme complexes (Figure 1.3). NAD

(Nicotinamide adenine dinucleotide)H, is initially oxidized at complex I. The electrons from NADH are transferred to the first mobile electron acceptor, oxidized Coenzyme Q (CoQ). CoQ can also accept electrons from complex II donated by FAD (flavin adenine dinucleotide)H. CoQ donates electrons in the next step to cytochrome b of complex III. In complex III, electrons are transferred to cytochrome c1. Cytochrome c1 passes its electron to the second mobile electron acceptor, cytochrome c. This in turn reduces molecular oxygen to water in complex IV. The oxidation–reduction reactions are coupled to transfer of protons across the inner mitochondrial membrane. This proton efflux creates a proton electrochemical gradient, forming a mitochondrial membrane potential. The mitochondrial membrane potential is maintained at ∼150–180 mV negative to the cytosol and provides the force that drives an influx of protons and calcium into the mitochondria. This potential energy is in turn used to phosphorylate ADP to ATP via complex V (Parker *et al.* 1994).

An important aspect of ETC is the generation of ROS, which is a physiologically important by-product of respiration (Reddy and Beal 2005). During the transfer of electrons to molecular oxygen, an estimated 1–5% of electrons in the ETC divert their direction and participate in the formation of superoxide radicals ($O2^-$). The production of mitochondrial O_2- occurs at discrete points in the ETC at complexes I, II and III) (Pollodori *et al.* 2007) (Figure 1.3).

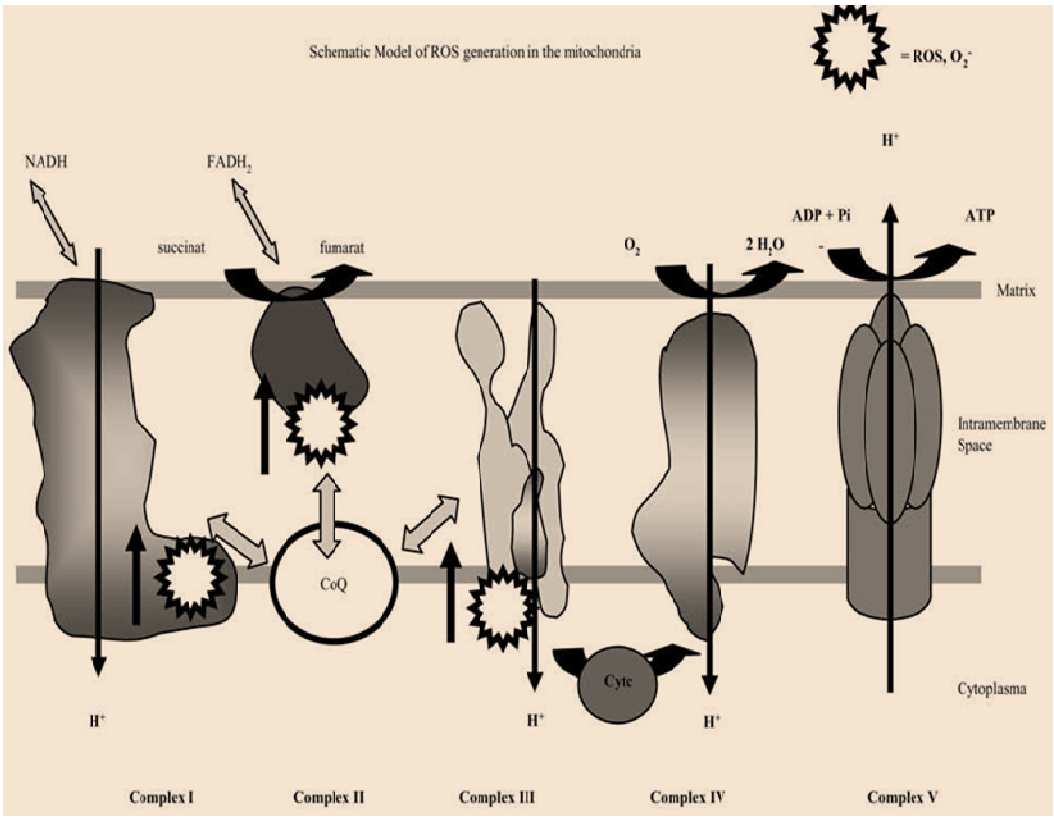

Figure 1.3 A schematic model of the energy transfer down the mitochondrial respiratory chain and ROS generation in mitochondria. The mitochondrial respiratory chain generates energy through the flow of electrons down the respiratory chain composed of five complexes. Complexes I, II, and III are involved in the generation of ROS.
From: Leuner *et al.* (2007) *Antioxid Redox Signa*. 9, 1659-1675

The mitochondrial electron transport system is the major intracellular source of oxygen radicals and H_2O_2. Paradoxically, mitochondria are one of the major targets of ROS. ROS can cause oxidative damage to lipids, proteins, and nucleic acids in the mitochondria (Ricci *et al.* 2003; Pollodori *et al.* 2007).

The brain is particularly vulnerable to ROS damage because of its high oxygen consumption rate, abundant lipid content, and relative paucity of antioxidant

enzymes compared with other organs (Vera 2005; Pollodori *et al.* 2007). One of the main etiologic hypotheses regarding AD is the involvement of free radical–induced oxidative damage in neuronal degeneration. Impairment of mitochondrial function leads to ATP reduction and increased free radical generation, which then results in neurodegeneration and neuron loss in AD (Zhu *et al.* 2004).

1.2.2 Mitochondria dysfunction and oxidative stress identified in postmortem tissue of AD patients

Direct evidence of the involvement of mitochondrial dysfunction in AD came from postmortem studies of AD brain. The alterations of mitochondrial efficiency and function were mostly related to alterations in concentration and efficiency of the constituents of the respiratory chain. In the brains of AD patients, there was a mild generalized reduction of the activity of the electron transport chain complexes (I-IV) (Parker, Jr. *et al.* 1994). In a positron emission tomography study (Kessler *et al.* 1991), a decline in cerebral metabolic rate in parietal and temporal lobes in AD subjects was observed indicating possible abnormalities in mitochondrial function. Metabolic defects were present in those at high risk for the disease before symptoms develop. More interestingly, a correlation was reported between decreased COX (complex IV) activity and deficits in cognitive abilities (Salmon *et al.* 2005).

Several lines of evidences indicated a role of oxidative stress in the pathogenesis of AD. An elevated level of 4-hydroxynonenal (HNE), a markers for lipid

peroxidation, was detected in the cortex and hippocampus of patients with AD compared to control subjects (McGrath *et al.* 2001). Moreover, increased levels of oxidized proteins and DNA were observed in brain tissues of AD patients as compared to age matched, non-demented controls (Lyras *et al.* 1997).

1.2.3 A causal relationship between Aβ and mitochondrial dysfunction/oxidative stress

Several in vitro studies demonstrated that Aβ can induce mitochondrial dysfunction and oxidative stress. Extracellular Aβ treatment led to a significant decrease in mitochondrial membrane potential and ATP levels in neuronal cell culture (Canevari *et al.* 2004). It was also observed that after exposure to Aβ, there was a significant decrease in mitochondrial respiratory chain enzymatic complexes I, II/III, and IV activities, with complex IV being the most affected (Canevari *et al.* 2004).

Intracellular Aβ accumulation was suggested as an early step in the neurotoxicity cascade of Aβ. APP containing the Swedish mutation (APPsw) resulted in an overall increase of Aβ including both Aβ40 and Aβ42. PC12 cells bearing the APPsw exhibited an increased Aβ secretion compared to control PC12 cells. PC12 cells bearing APPsw also displayed mitochondria impairment, including decreased mitochondrial membrane potential, reduced ATP level, and reduced cytochrome c oxidase activity (Marques *et al.* 2003). Using the fluorescence dye DAF-2DA, it was found that nitric oxide (NO) levels were significantly enhanced in PC12 APPsw cells compared to control cells. DAPT is a functional γ-secretase inhibitor

which reduces intracellular Aβ production. PC12 APPsw cells treated with DAPT, exhibited a normalization of NO and ATP levels as well as mitochondrial membrane potential (Keil *et al.* 2004).

Evidence from transgenic animal models of AD provided further support that Aβ accumulation is responsible for the impairment of mitochondria and oxidative stress observed in AD. For example, Tg2576 mice, an AD transgenic mouse model that overexpress mutant human APP, developed amyloid plaques and cognitive defects at 6-7 months of age. Increased H_2O_2 levels and decreased cytochrome c oxidase activity were found in 2-month-old Tg2576 mice (Manczak *et al.* 2006) when compared with their age-matched non-Tg littermates. More interestingly, a correlative analysis revealed that soluble Aβ40 and soluble Aβ42 directly correlated with H_2O_2 production whereas insoluble Aβ40 and insoluble Aβ42 did not (Manczak *et al.* 2006). This result is consistent with the modified amyloid hypothesis that suggests it is the soluble Aβ oligomers that trigger the pathologic mechanisms in AD. Findings from immunofluorescent analysis showed the presence of mitochondrial oxidative DNA damage in 2-month-old Tg2576 mice and increases in DNA damage corresponding to the stages of disease development in Tg2576 mice indicating that free radicals generated by overproduction of Aβ may be responsible for the mitochondrial oxidative DNA damage found in Tg2576 mice (Manczak *et al.* 2006).

These data together suggested that intraneuronal Aβ accumulation or extracellular Aβ oligomers lead to mitochondrial dysfunction and oxidative stress, which in turn,

results in synaptic dysfunction and ultimately neuron death in AD. However, the underlying signaling events linking Aβ and abnormalities in mitochondria are unclear. Both direct and indirect pathways have been proposed to mediate Aβ induced mitochondrial toxicity.

1.2.4 Mitochondrial Aβ

Emerging evidence suggested that Aβ progressively accumulates in mitochondria (Manczak *et al.* 2006). Tg mAPP mice were Tg mice with targeted overexpression of a mutant human form of amyloid precursor protein (a minigene encoding hAPP695, 751, and hAPP770 bearing V717/F, K670M, N671L) (Caspersen *et al.* 2005). Cortical neurons cultured from Tg mAPP mice demonstrated mitochondrial deposition of Aβ. Aβ was also detected in mitochondria in patients with Alzheimer's disease. Furthermore, Aβ was more abundant in the inner mitochondrial membrane and matrix fractions than in the outer mitochondrial membrane. The distribution of mitochondrial Aβ appears to parallel that of brain regions affected by AD-type pathology (Caspersen *et al.* 2005).

Consequently, there arises the question: How does Aβ gain access to mitochondria? Whether Aβ is produced in mitochondria or reaches the mitochondria from other subcellular locations is still unclear.

APP carries a dual leader sequence, permitting targeting to the endoplasmic reticulum (ER), or to mitochondria (Lin and Beal 2006) (Figure 1.4). In cultured cells overexpressing APP, using immunoelectron microscopy, immunoreactivity of

APP was detected in mitochondria. No mitochondrial localization was observed when the leader sequence was mutated (Lin and Beal 2006; Anandatheerthavarada *et al.* 2003; Anandatheerthavarada and Devi 2007). More importantly, studies of post-mortem brain samples from human Alzheimer's disease and control subjects found that full-length and C-terminally-truncated APP was associated with mitochondria in samples from the brains of individuals with Alzheimer disease, but not with mitochondria in samples from subjects without the disease. Furthermore, in brain samples of AD patients, levels of mitochondrial APP were higher in more affected brain areas and in subjects with more advanced disease (Devi *et al.* 2006). These data imply that localization of APP to mitochondria may possibly be an AD specific process.

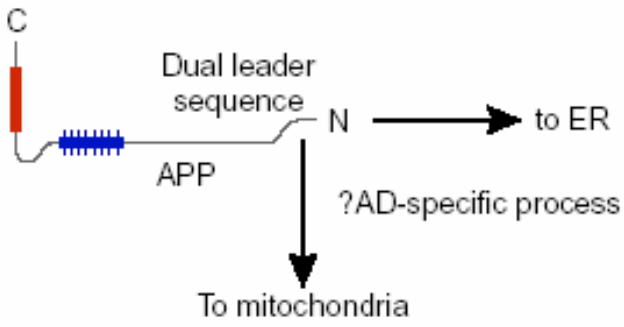

Figure 1.4 Mitochondria and Alzheimer disease. Amyloid precursor protein (APP) has a dual leader sequence, permitting targeting to the endoplasmic reticulum or to mitochondria. The targeting of APP to mitochondria may be an Alzheimer disease–specific process: mitochondrial localization of APP occurs only in disease subjects and only in affected brain areas and mitochondrial APP levels increase with disease severity.
From: Lin and Beal (2006) *Nat Med,* **12,** 1241-1243

Active γ-secretase complexes were detected in mitochondria (Hansson *et al.* 2004). However, β-APP is incompletely translocated through the mitochondrial outer membrane. It was suggested that a 22-kDa region (N-terminal) of β-APP is located inside the mitochondria and that the remaining 73-kDa portion, containing the Aβ sequence and γ-secretase cleavage site, is exposed on the cytoplasmic side (C-terminal). The Aβ sequence and γ-secretase cleavage site have to be in the transmembrane region for a correct processing by the γ-secretase (Lin and Beal 2006). These data indicated that Aβ may not be generated intramitochondrially.

It was reported that Aβ is generated intracellularly at ER or trans-Golgi network (TGN) site (Greenfield *et al.* 1999). Brefeldin A (BFA) is an inhibitor of protein transport from ER/intermediate compartment. Mitochondrial fractions from Tg mAPP cortical neurons displayed an immunoreactive Aβ band whereas mitochondria from non-Tg littermates under the same conditions did not. When cultured neurons from Tg mAPP mice were incubated with BFA for 16 hours, the intensity of the immunoreactive Aβ band increased. (Caspersen *et al.* 2005). These results suggested that transfer of Aβ from ER to mitochondria may occur in neurons.

These findings collectively indicated that Aβ peptides can enter the mitochondria and impair mitochondrial function, which in turn results in overproduction of reactive oxygen species, eventually leading to neuron loss in AD.

1.3 Identification of Aβ binding alcohol dehydrogenase, a mitochondrial receptor for Aβ

Using a yeast two-hybrid system, Yan *et al.* 1997 identified an intracellular receptor for Aβ, termed Aβ binding alcohol dehydrogenase (ABAD) (Yan *et al.* 1997). ABAD is also named as endoplasmic reticulum amyloid binding protein (ERAB), 3 hydroxyacyl CoA dehydrogenase type 2 (HADH 2), Short chain L 3 hydroxyacyl CoA dehydrogenase type 2 (SCHAD) and MHBD.

ABAD is a member of the short chain dehydrogenase family. It shares features with other members of this family, such as the requirement for a dinucleotide cofactor, NAD(H), and a Rossmanfold structural topology with an invariant sequence, Tyr-*X*-*XX*- Lys, corresponding to residues 168–172 in ABAD, all of which are required for enzymatic activity. Unique features of ABAD include its presence in endoplasmic reticulum and mitochondria, its capacity to bind Aβ and promote Aβ-induced cell stress, and its ability to use a broad array of substrates, including linear alcohols, 3-hydroxyacyl-CoA derivatives, D-β-hydroxybutyrate, and steroids. In neurons, ABAD is especially enriched in mitochondria where it appears to serve important functions in metabolic homeostasis (He *et al.* 1998).

Expression of ABAD was found to be increased in brains of AD patients compared to non-demented age matched controls (Yan and Stern 2005). It was proposed that the interaction of ABAD and Aβ results in mitochondrial dysfunction/oxidative stress, which account for neurodegeneration and neuron death in AD.

1.3.1 The physiological functions of ABAD

Although firstly identified as a mitochondrial receptor for Aβ, ABAD is an important enzyme that is required for regulation of development and maintenance of homeostasis.

1.3.1.1 Scully/ABAD deficiency in Drosophila

Studies of ABAD deficiency have provided considerable insight into the role of the enzyme during development and neuronal homeostasis. Inactivation of the *Drosophila* counterpart of ABAD, termed *scully*, resulted in a lethal phenotype with multiple developmental abnormalities. Certain salient features of the scully/ABAD deficient flies included mutant testes which were small and undeveloped. The testes displayed deficiency of 3-hydroxyacyl-coA dehydrogenase activity, indicating that ABAD is the principal enzyme with such activity in this tissue. Photoreceptor cell mitochondria appeared smaller, and showed fewer and swollen cristae compared with neighboring wild-type cells. This mitochondrial phenotype (pleomorphism) is a typical pathology in humans with inherited β-oxidation deficiencies. (Torroja *et al.*1998).

These data together strongly suggested a role of ABAD in fatty acid β-oxidation. However, considering that fatty acids are not a key energy substrate in the central nervous system, ABAD clearly has other properties in mammalian systems.

1.3.1.2 ABAD and the metabolism of β-Hydroxybutyrate

The broad enzymatic properties of ABAD as an oxidoreductase suggested that

ABAD might facilitate cellular utilization of ketone bodies such as D-β-hydroxybutyrate by promoting the generation of acetyl-CoA to feed into the tricarboxylic acid cycle. Ketone bodies can reach appreciable concentrations in normal humans/adult animals during starvation. Under these conditions, the oxidation of D-β-hydroxybutyrate becomes the dominant source for energy production in brain. This has led researchers to study a role for ABAD in the cellular response to nutritional/metabolic stress (Yan and Stern 2005).

A severe form of metabolic stress was induced by cerebral ischemia. Wild-type mice were subjected to transient middle cerebral artery occlusion and displayed increased levels of ABAD in neurons near the infarcted area, compared with the nonischemic hemisphere, using a polyclonal antibody to mouse ABAD. Immunohistochemical analysis demonstrated an ～5-fold increase of ABAD expression in cortical neurons consequent to stroke indicating the involvement of ABAD in the cellular response to metabolic stress (Yan *et al.* 2000).

In vitro studies showed that ABAD promotes utilization of ketone bodies, probably at the level of D-β-hydroxybutyrate. For example, overexpression of ABAD in COS cells, which have low endogenous levels of this enzyme, maintained cellular functions under conditions where D-β-hydroxybutyrate is the principal energetic substrate. Furthermore, there was an increased flux of acetyl-CoA through the tricarboxylic acid cycle in ABAD-transfected COS cells (Yan *et al.* 2000).

A murine stroke model in transgenic mice was employed to determine consequences of overexpressing ABAD in cortical neurons. ABAD transgenic mice

displayed a reduction in stroke volume and maintenance of neurologic function. Overexpression of ABAD in Tg mice was associated with increased flux of acetyl-CoA through the tricarboxylic acid cycle and increased ATP in cerebral cortex following infusion of D-β-hydroxybutyrate (Yan *et al.* 2000). These data indicated that increased expression of ABAD confers a protective response under metabolic stress, such as that imposed by ischemia.

Another important piece of evidence came from observations in patients with methyl-3-hydroxybutyryl-CoA dehydrogenase (MHBD) deficiency. MHBD, which was identified based on its participation in the catabolism of isoleucine and branched-chain fatty acids, was found to be identical to ABAD. Patients with defects in MHBD/ABAD activity showed severe neurologic symptoms, including psychomotor retardation and progressive infantile neurodegeneration (Chen and Yan 2007).

Taken together, these data indicated that ABAD might play several important roles in metabolic homeostasis related to energy metabolism and catabolism of isoleucine and branched-chain fatty acids.

1.3.2 Pathologic role of ABAD in an Aβ rich environment

Although ABAD seems to protect neurons under metabolic stress, it takes on a quite different role in cells subjected to an environment rich in Aβ (Yan *et al.* 1999).

1.3.2.1 In vitro studies of the Aβ-ABAD interaction

Following exposure to aggregated Aβ, cell stress was increased in neuroblastoma cells transfected to overexpress ABAD (Canevari *et al.* 2004; Lustbader *et al.* 2004). COS or SK-N-SH cells, which were simultaneously cotransfected with constructs encoding ABAD and mutant APP, displayed mitochondrial dysfunction, DNA fragmentation and cell death. Similar cotransfection studies with ABAD mutants devoid of enzymatic activity did not induce cell toxicity, although the level of expression of the transfected constructs was comparable (Yan and Stern 2005). These data suggested that ABAD might contribute to the Aβ induced mitochondrial dysfunction/oxidative stress.

1.3.2.2 In vivo studies of the Aβ-ABAD interaction

To further investigate the pathologic function of ABAD in an Aβ rich environment, double transgenic mice overexpressing both ABAD and mutant APP (Tg mAPP/ABAD) were developed (Lustbader *et al.* 2004). These double Tg mice exhibited exaggerated oxidative stress and elevated generation of ROS in comparison with brains from non-Tg littermates and Tg mAPP, Tg ABAD mice. Moreover, brains of Tg mAPP/ABAD mice displayed a strong reduction in brain COX activity by 4 months of age and brain ATP levels were significantly reduced at 9 months. A ßradial-arm water maze test was used to detect hippocampal-dependent learning and memory deficits in Tg mice. Young mice (4.5 to 5 months of age) of non-Tg, Tg mAPP, or Tg ABAD transgenic littermates all showed strong learning and memory capacity. In contrast, Tg mAPP/ABAD mice

failed to learn efficiently, indicating severe impairment in spatial learning and memory (Lustbader *et al.* 2004).

Studies of primary culture neurons from different genotypes found that, after 4 days in culture, neurons from Tg mAPP/ABAD displayed exaggerated mitochondrial dysfunction including decreased activity of COX, leakage of ROS, decreased membrane potential, and diminished ATP. After culturing for 6 days, there was an increase in caspase-3 like activity and DNA fragentation in Tg mAPP/ABAD mice. Using lactate dehydrogenase **(**LDH) assay, it was found that cell viability was strongly decreased in double transgenic mice. In the presence of antioxidants including vitamin E and N-acetylcysteine (NAC), increase of caspase-3-like activity, DNA fragmentation, and loss of cell viability in neurons from Tg mAPP/ABAD mice were strongly attenuated (Takuma *et al.* 2005).

1.3.2.3 Colocalization of Aβ and ABAD

Using immunoprecipitation and immunoblotting methods, Aβ-ABAD complexes were detected in AD brain. Very few Aβ-ABAD complexes were observed in age-matched non-demented brain. In Tg mAPP and Tg mAPP/ABAD mice brain, evident Aβ-ABAD complexes were detected whereas non-Tg mice brains displayed very low levels of Aβ-ABAD complexes. Confocal studies showed that Aβ and ABAD colocalize in mitochondria matrix in both Tg mAPP/ABAD mice brain and AD brain (Caspersen *et al.* 2005). These data together supported the hypothesis that ABAD and Aβ directly interact in mitochondria in AD, and that this interaction

promotes leakage of ROS, mitochondrial dysfunction and cell death.

1.3.2.4 Structural analysis of the Aβ-ABAD interaction

The interaction between ABAD and Aβ is highly specific and starts to occur at nanomolar concentrations. At micromolar concentrations, Aβ, likely in its oligomeric form, inhibited ABAD enzyme activity (Yan *et al.* 1999).

Crystal structural studies demonstrated that Aβ inhibits ABAD activity by preventing NAD binding to the enzyme (Lustbader *et al.* 2004) (Figure 1.5). Aβ-bound ABAD displayed substantial distortion of the NAD-binding pocket and the catalytic triad. The majority of the LD loop, the beginning of the following α helix, and the latter part of the LF loop of human ABAD were disordered. In the absence of Aβ, the LF loop was still disordered in the ABAD structure in complex with NAD, whereas the LD loop region was well ordered. This indicated that Aβ binding may have influenced the dynamics and conformation of the LD loop. Subsequent site-directed mutagenesis within and beyond the disordered LD loop region prevented interaction with Aβ using surface plasmon resonance (Yan *et al.* 1999; Lustbader *et al.* 2004). A synthesized peptide encompassing LD loop of human ABAD [termed ABAD decoy peptide (ABAD-DP)] inhibited binding of Aβ40 and Aβ42 to immobilized intact ABAD. These data further confirmed that the LD region alone is sufficient to mediate Aβ-ABAD interaction. To test the effects of ABAD-DP in cell culture, the cell-membrane transduction domain of the human immunodeficiency virus-1 (HIV-1) Tat protein was added to ABAD-DP to generate

Tat-ABAD-DP. Pretreatment of primary cortical neurons with Tat-ABAD-DP prevented ROS generation and cytochrome C release though the reversed peptide was without effects (Lustbader *et al.* 2004).

Based on these data, Yan and Stern 2005 proposed that endogenous levels of ABAD interacting with the amyloid peptide in an Aβ-rich environment are sufficient to trigger a series of events ultimately leading to neuronal dysfunction (Yan and Stern 2005). This hypothesis provides new insight into the initiative events in the pathogenesis of AD. However, the signaling cascade linking ABAD-Aβ interaction to mitochondrial dysfunction remains elusive.

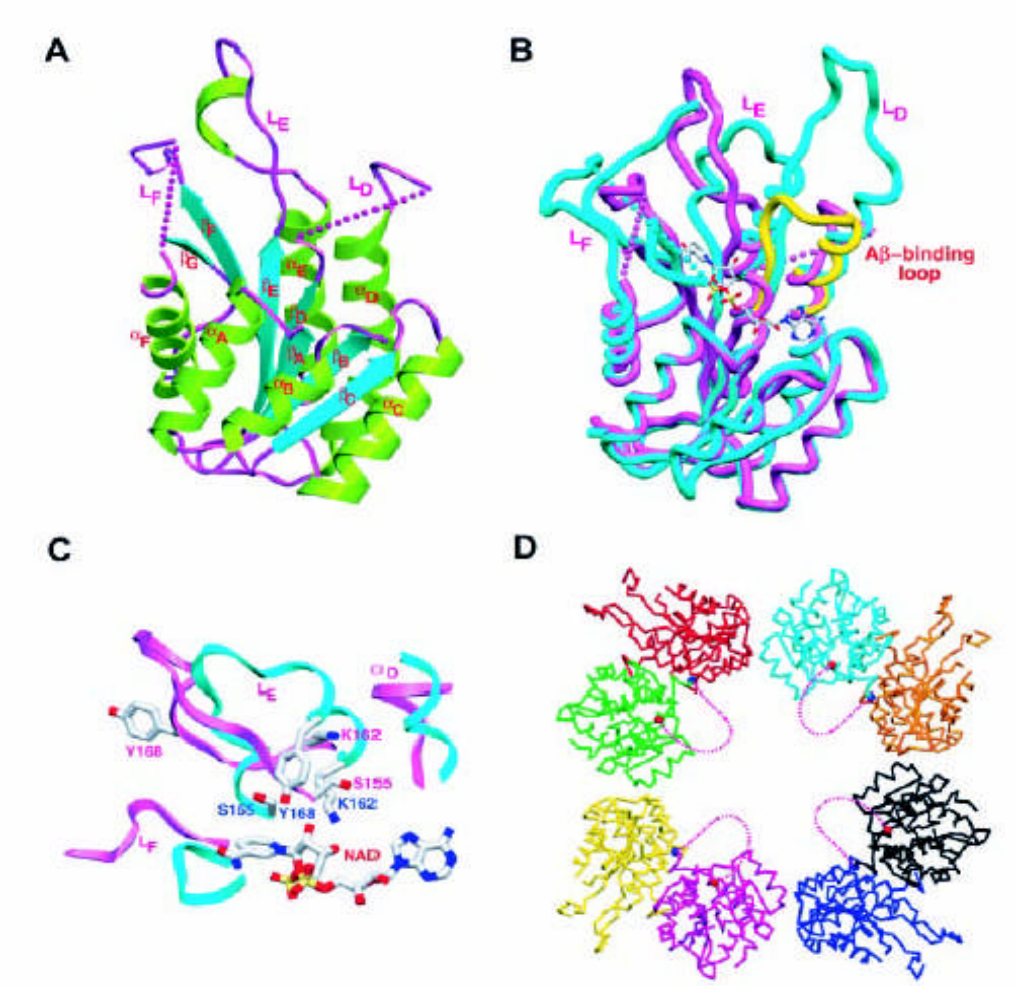

Figure 1.5 Crystal structure of Aβ bound human ABAD (β-Amyloid-binding alcohol dehydrogenase). (A) A ribbon diagram with labeled secondary structures and the LD, LE, and LF loops. Helices are shown in green, β strands are shown in blue, and loops are shown in pink. Disordered regions are shown by dotted lines. (B) Superposition of Aβ-bound human ABAD (pink) and rat ABAD in complex with NAD (blue). The LD loop of 3β-hydroxysteroid dehydrogenase (3β-HSD) (PDB code 1FJH) is shown in yellow. NAD is shown as a stick model with gray for carbon atoms, red for oxygen atoms, blue for nitrogen atoms, and yellow for phosphate atoms. The proposed Aβ-binding loop is indicated. (C) Superposition of the active sites of Aβ-bound human ABAD (pink) and rat ABAD (blue), showing distortion of the NAD binding site and the catalytic triad S155, K162, and Y168. Colors are the same as in (B). (D) A section of the crystal packing interactions, showing the large solvent channels. Each ABAD molecule is shown in a different color. The ordered ends of the LD loop, residues 94 and 114, are marked as red and blue balls, respectively, and the hypothetical loops are shown in pink as dotted lines.

From: Lustbader *et al.* (2004) *Science*, 304, 448-452

1.4 Identification of Endophilin 1 by two dimensional electrophoresis analysis

To investigate possible signaling events subsequent to ABAD-Aβ interaction, previous experiments done by Jim Aiton and Margaret Taylor in our laboratory, studied differential protein expression between different genotypes of mice brain using a proteomic approach. They identified differential expression of several proteins such as creatine kinase, peroxiredoxin II and ATP beta subunit, which have been associated with AD or oxidative stress, between Tg mAPP/ABAD, Tg mAPP, Tg ABAD, and non-Tg littermates. More interestingly, they found upregulation of endophilin 1 in Tg mAPP/ABAD and Tg mAPP mice compared to Tg ABAD and non-Tg animals. Immunoblotting studies with a monoclonal antibody to endophilin 1 further confirmed the result of the proteomic studies. More importantly, they also found that endophilin 1 is increased in brains of AD sufferers as compared to age-matched non-demented controls.

1.4.1 Endophilin 1 is a multifunctional protein

Endophilin 1 is a cytoplasmic Src homology 3 (SH3) domain-containing protein. It is abundantly expressed in the brain and is localized in synaptic terminals (Ringstad *et al.* 2001). Endophilin 1 contains an N-terminal domain with predicted α helical and coiled-coil conformation, the C-terminal SH3 domain and a short hinge region. Endophilin 1 exists as 80–90 kDa homodimer or heterodimer in rat brain cytosol and its dimerisation required the coiled-coil region (Reutens and Begley 2002).

Endophilin 1 plays a critical role in regulating synaptic vesicle formation in the clathrin-coated vesicle endocytic pathway. It participates in invagination, fission and vesicle release. The N-terminal portion of endophilin 1 was shown to have lysophosphatidic acid acyl transferase (LPAAT) activity. Conversion of the inverted cone-shaped lysophosphatidic acid into cone-shaped phosphatidic acid was hypothesized to induce positive-to-negative lipid membrane curvature required for vesicle formation (Schmidt *et al.* 1999). Through its SH3 domain, endophilin 1 was reported to interact with the endocytic proteins including synaptojanin 1, dynamin 1, and the amphiphysins and this interaction is critical for the clathrin-mediated endocytosis (Micheva *et al.* 1997; Gat *et al.* 2000) (Figure 1.6)

Through its interaction with non-endocytic proteins, endophilin 1 also functions in many non-endocytic pathways. For example, The SH3 domain of endophilin 1 bound to a proline-rich domain in the third intracellular loop of the G-protein-coupled β1-adrenergic receptor. Overexpression of endophilin 1 led to an increase of isoproterenol-induced receptor internalization and a decrease of receptor coupling to the G-protein. The SH3 domain of endophilin 1 also bound to the Cbl-interacting protein of 85 kDa (CIN85). This complex, when recruited by Cbl, can influence internalization, degradation and intracellular signaling of tyrosine kinase receptors for hepatocyte and epidermal growth factor (Reutens and Begley 2002).

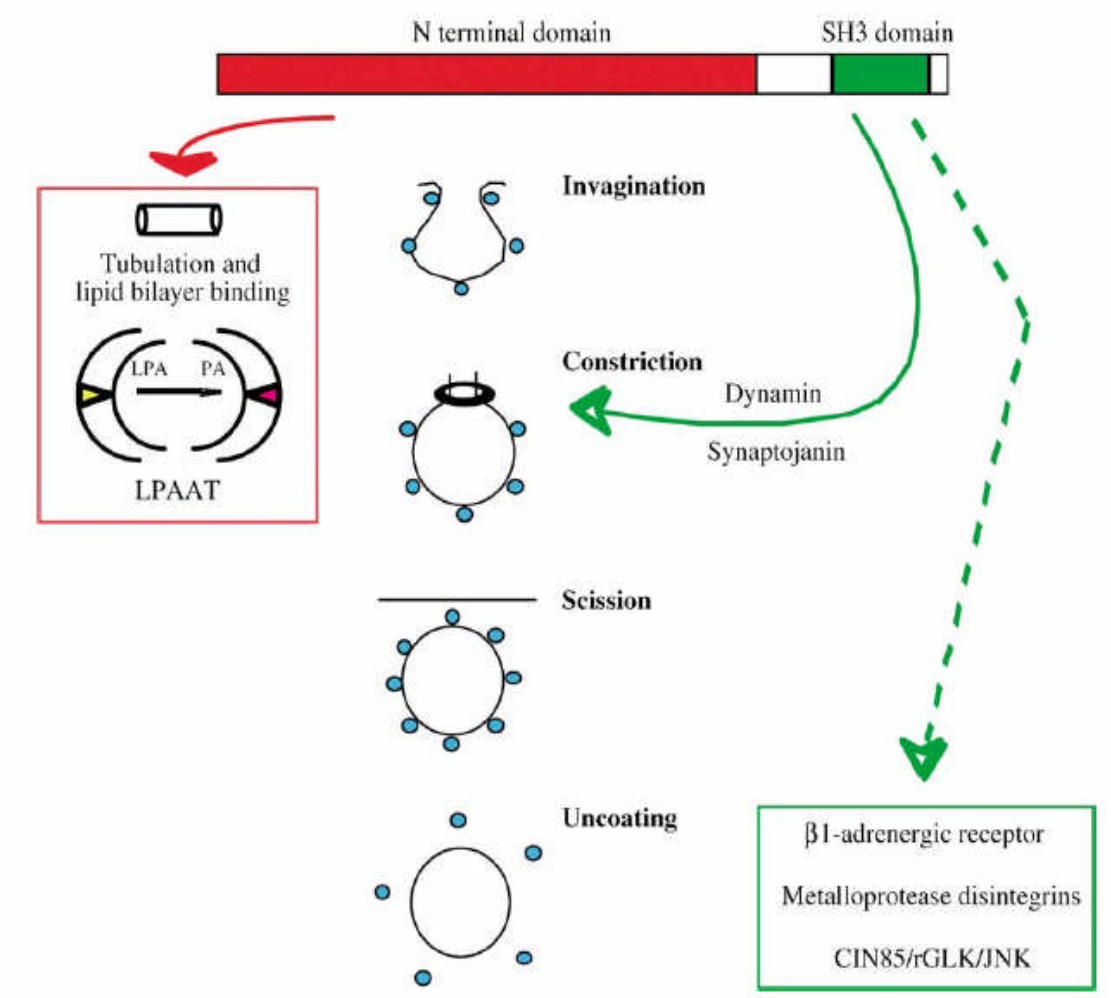

Figure 1.6 Multiple functions of endophilin 1. Endophilin 1 affects the clathrin-coated vesicle endocytic pathway, at steps from invagination through to vesicle uncoating. Shown inset are the properties of the N-terminal domain of endophilin 1 required for endocytosis: binding to lipid bilayers, tubulation and lysophosphatidic acid acyl transferase activity (LPAAT), which converts lysophosphatidic acid (LPA) to phosphatidic acid (PA). The SH3 domain interacts with other endocytic proteins such as dynamin and synaptojanin. Also, the SH3 domain of endophilin 1 modulates signaling pathways by interacting with non-endocytic proteins including Rat germinal centre kinase-like kinase (rGLK), metalloprotease disintegrins and G-protein-coupled β1-adrenergic receptor.
From: Reutens and Begley (2002) *Int J Biochem Cell Biol,* **34,** 1173-1177

1.4.2 Endophilin 1 regulates GLK induced JNK activation

McPherson‘s group (Department of Neurosurgery and Neurology, McGill University) screened a rat brain expression library with the SH3 domain of endophilin 1 and identified rat germinal center kinase like kinase (rGLK) as an endophilin 1 binding partner. Overlay assays of rat brain extracts revealed endophilin 1 as a major SH3 domain-binding partner for rGLK (Ramjaun *et al.* 2001).

GLK is a member of the second class of the Ste20 family of kinases. It is composed of an N-terminal kinase domain and a C-terminal regulatory domain with multiple SH3 domain consensus-binding sites. Overexpression of GLK specifically activated the JNK (c-Jun N-terminal kinase) pathway in HEK293 cells. Furthermore, expression of dominant-negative forms of MEKK1 and MKK4 inhibited GLK-induced JNK activation, suggesting that GLK may function upstream of MEKK1 and MKK4 (Diener *et al.* 1997).

To determine whether endophilin 1 regulates GLK-mediated JNK activation, specifically, Ramjaun *et al.* 2001 evaluated JNK activation using an anti-phospho-JNK antibody following transfection of HEK293 cells with GLK and different endophilin 1 constructs. Overexpression of FLAG tagged GLK and FLAG tagged JNK induced JNK activation. Overexpression of full-length, untagged endophilin 1 along with FLAG-GLK and FLAG-JNK caused a further increase in JNK activation versus coexpression of FLAG-GLK and FLAG-JNK in HEK293 cells. In contrast, overexpression of a GFP-tagged form of the SH3 domain of

endophilin 1(GFP-SH3) or of the untagged N terminus of endophilin 1 lacking the SH3 domain (delta SH3) along with FLAG-GLK and FLAG-JNK completely blocked GLK mediated JNK activation (Ramjaun *et al.* 2001). Together, these data suggested that endophilin 1 regulates GLK mediated JNK activation in HEK 293 cells.

1.4.3 JNKs in the Central Nervous System

1.4.3.1 JNK is a member of the mitogen-activated protein (MAP) kinase family

Eukaryotic cells respond to external stimuli via signal transduction pathways, many of which include protein kinases of the mitogen-activated protein (MAP) kinase family. These pathways are characterized by modules composed of three protein kinases: MAPKKKs phosphorylate and thereby activate MAPKKs, which in turn phosphorylate MAPKs. JNK cascade is one of the three major subfamilies of MAPKs. The others are extracellular signal-regulated kinase (ERK) and p38 (Zhu *et al.* 2002).

JNK protein kinases with molecular masses of 46 kDa and 55 kDa are coded for by 3 genes, JNK1, JNK2 and JNK3. JNK1 and JNK2 are ubiquitously expressed in all tissues whereas JNK3 is predominantly restricted to brain and is expressed in neurons (Brecht *et al.* 2005). JNK1 is present as the 46 kDa isoform, JNK2 is equally expressed as 46 kDa and 54 kDa isoforms, and JNK3 dominates as the 46 kDa isoform. Thus, the 46 kDa proteins comprise all three JNK proteins, whereas the 54 kDa proteins are mainly restricted to JNK2 (Brecht *et al.* 2005).

JNK is activated by dual phosphorylation of the Thr-Pro-Tyr motif located in the activation loop by a number of MAPKKs such as MKK (mitogen-activated kinase kinase) 4 and MKK7. At the MAPKKK level, the JNK activating kinases are more diverse, including MEKKs (MAPK kinase kinases), MLKs (mixed-lineage kinases), DLKs (dual leucine-zipper kinases), ASK (activator of S-phase kinase), and TAK (transforming growth factor β-activated kinase). JNKs and upstream kinases also interact with scaffold proteins, which have been reported as important regulatory elements of the JNK pathway including JIP, β-arrestin and JSAP1 (Bossello and Folorni 2007; Okazawa and Estus 2002). As described in the previous section, in HEK293 cells, GLK functions upstream of MKK4 and MEKK1 and specifically activates JNK. Further studies revealed that endophilin 1 regulates GLK mediated JNK activation (Ramjaun *el al.* 2001).

1.4.3.2 High basal activity of JNK in the central nervous system

Biochemical analysis revealed a high level of basal JNK activity in the CNS. The activity of JNK was 10- to 24-fold higher in the neocortex, hippocampus, brainstem, hypothalamus and amygdala than in peripheral organs (Xu *et al.* 1997). Western blot analysis with an antibody specific for JNKs revealed that protein levels of JNK in most regions of the CNS were similar to those in peripheral organs, indicating that the high levels of JNK activity in the CNS are not caused by increased JNK expression (Xu *et al.* 1997). JNK signaling cascade can be rapidly and strongly activated throughout the brain by noninvasive stimulation such as physical restraint

and exploration of a new environment suggesting the possibility that the JNK cascade plays an important physiological role in the CNS (Xu *et al.* 1997). JNK1 appears to be the major isoform responsible for the high level of basal JNK activity in the CNS as deletion of JNK1 markedly reduced the basal JNK activity of the whole brain lysates (Xu *et al.* 1997). The physiological functions of JNKs are still poorly understood.

1.4.3.3 JNK cascade leads to apoptosis via both mitochondrial and transcriptional pathways

On top of the high basal activity, JNK signaling can be activated by stress or cytokines, which often leads to apoptosis. An important role of JNK signaling in stress-induced apoptosis has been demonstrated in the CNS (Kumage *et al.* 1999; Brecht *et al.* 2005). Gene targeting studies showed that JNK3 is an essential component of the stress induced JNK signaling whereas JNK1 and JNK2 have a critical role in neural development (Kuan *et al.* 1999; Kuan *et al.* 2003). These results indicated the functional diversity of JNK isoforms and suggested that JNK3 may have a preferential role in stress-induced neuronal apoptosis.

The downstream events of JNK activation leading to apoptosis involve both mitochondrial and transcriptional mechanisms. For the mitochondrial mechanism, several studies demonstrated that JNK directly phosphorylates Bim, leading to activation of Bax/Bak-mediated cytochrome c-release and apoptosis (Dougherty *et al.* 2004). Besides Bim, JNK was shown to phosphorylate Bad to trigger the

mitochondrial cell death pathway. Moreover, evidences also indicated that JNK can induce the release of another pro-apoptosis factor Smac from the mitochondria (Aoki *et al.* 2002).

Upon activation, JNKs translocate into the nucleus to phosphorylate and activate nuclear transcription factors. Several substrates for JNK have been identified, such as c-Jun, ATF-2, Elk1, and p53 (Zhang and Zhang 2005). c-Jun is the major substrate of JNK. Once phosphorylated by JNK, the transcription activity of c-Jun was increased, leading to upregulation of many genes with AP-1 enhancer sequences (Ham *et al.* 2000). Transgenic mice carrying a mutated form of c-Jun that can no longer be phosphorylated by JNK displayed increased resistance to glutamate excitotoxicity (Kuan and Burke 2005). These data indicated that the induction of c-Jun/AP-1-mediated transcription is a major component of the apoptotic pathway downstream of JNK signaling.

1.4.4 JNK cascade and Alzheimer's disease

1.4.4.1 Increased JNK activation in the brains of AD patients

Increased activation of JNK has been associated with the pathogenesis of AD. With a monoclonal anti-activated JNK antibody, immunoblot analysis of cortical brain homogenates revealed an upregulation of activated JNK in AD compared to age-matched non-demented control cases (Zhu *et al.* 2001). Furthermore, an immunohistochemistry study found that JNK was activated in cerebral neurons of PS1-linked AD patients. Activated JNK was localized to both neuronal cell bodies

and neurites around amyloid deposits (Shoji *et al.* 2000).

Consistent with the in vivo findings, under oxidative stress condition, PC12 cells overexpressing mutant APP demonstrated significant increase of JNK activation as compared to cells transfected with control vector plasmid (Marques *et al.* 2003). Moreover, exposure of cortical neurons to Aβ peptides resulted in an increase in JNK activation. Activated JNK was found to activate the c-Jun transcription factor, which in turn stimulates the transcription of Fas ligand. The binding of Fas ligand to its receptor Fas induced a cascade of signaling events that eventually lead to cell death (Morishima *et al.* 2001).Additionally, intraneuronal Aβ has been reported to induce JNK activation in neuronal cell cultures (Shouji *et al.* 2000). These studies collectively suggested that elevated JNK signaling is associated with AD.

There are two ways through which JNK signaling might be involved in the pathogenesis of Alzheimer's disease. First, Aβ peptides activate JNK signaling in neurons which then lead to cell death. Secondly, JNK may directly phosphorylate tau leading to the formation of neurofibrillary tangles.

Normally the inactive JNK resides quiescently in the cytosol. After Aβ treatment, activated JNK translocate into the nucleus and activates transcription factors such as c-Jun and ATF-2 (Kihiko *et al.* 1999). Immunoreactivity of activated JNK was also localized to discrete regions within cytosol after exposure to Aβ and displayed a punctate distribution (Bosello and Forloni 2007). This may reflect mitochondrial targeting of JNK or association of JNK with cytosolic substrates such as tau.

1.4.4.2 Activation of JNK/C-Jun cascade leads to neuron death in AD

Massive neuron loss is a major characteristic in the brains of patients suffering from AD (Shimohama 2000). Therefore, elucidating the signaling events that underlie Aβ-mediated induction of cell death should provide insights into the mechanisms of the pathogenesis of AD.

As stated above, an enhanced activation of JNK was detected in neuronal cultures after exposure to Aβ. Application of synthetic inhibitors of JNK to these neuronal cultures protected against Aβ-mediated neuron death (Marques *et al.* 2003; Morishima *et al.* 2001). These observations indicated a causal role for JNK activation in Aβ-mediated neuron death in CNS.

Phospho-JNK can translocate into the nucleus and activate transcription factors. c-Jun, a component of transcription factor AP-1, is a major substrate for JNK in the nucleus. c-Jun immunoreactivity was increased in affected brain areas of patients with AD and colocalized with TUNEL labeling, an indicator of apoptosis (Marcus *et al.* 1998). Neurons from c-Jun null mice showed resistance to Aβ toxicity (Kihiko *et al.* 1999). Moreover, in primary neuronal cultures, Aβ induced JNK activation led to c-Jun activation which eventually results in neuron death via the Fas signaling cascade (Morishima *et al.* 2001). These observations indicated a positive correlation of the activation of the JNK/c-Jun pathway and neuron loss in AD.

1.4.4.3 Colocalization of activated JNK and Tau

In AD, NFTs correlate with neuronal loss and clinical symptoms of dementia. NFTs accumulate over the years in affected brain regions of AD and largely are comprised of abnormally hyperphosphorylated tau protein (Mckee *et al.* 1991). Many kinases have been implicated in tau hyperphosphorylation such as Glycogen synthase kinase-3 (GSK-3), cyclin dependent kinase-5 (cdk-5), extracellular signal-regulated kinases and JNK (Crespo-Biel *et al.* 2007). Unlike other tau phosphorylation kinases, JNK phosphorylate Thr^{205} and Ser^{422} of tau, which are more highly phosphorylated in Alzheimer tau than in normal adult tau (Sato *et al.* 2002; Okazawa and Estus 2002).

As noted above, the expression of activated JNK was upregulated in AD. In severe AD cases, phospho-JNK immunoreactivity was exclusively associated with cytoplasmic NFTs. However, in mild cases of AD, in addition to neurofibrillary pathology, immunoreactivity of phospho-JNK was also localized to neuronal nuclei (Zhu *et al.* 2001).

These findings together suggested that enhanced JNK activation in AD may be involved in the phosphorylation of tau, which could contribute to the progress of the disease.

1.4.4.4 The molecular mechanisms of Aβ induced JNK activation

The precise molecular mechanisms, by which Aβ induces JNK activation and neuronal apoptosis, especially at early stages, remain to be established. It was

proposed that reactive oxygen species might mediate Aβ induced neurotoxicity (Tamagno *et al.* 1996). Support of this hypothesis came from a study which showed that JNK was activated in Tg APP mice with extensive oxidative stress but not in Tg APP mice without oxidative stress (Hensley *et al.* 1996; Zhu *et al.* 2004). Furthermore, an in vitro study showed that Aβ peptides elicited both activation of JNK as well as apoptosis through simultaneous production of hydrogen peroxide and HNE (4-hydroxy-2-nonenal) (Tamagno *et al.* 1996).

Based on the finding that protein expression level of endophilin 1 was increased in brains of AD patients and AD transgenic mice models, a novel signaling mechanism that may mediate Aβ induced JNK activation in AD is proposed (See Chapter 3). In an Aβ rich enviroment, Aβ-ABAD interaction results in enhanced expression of endophilin 1, which then stimulates GLK mediated JNK activation (Figure 1.7).

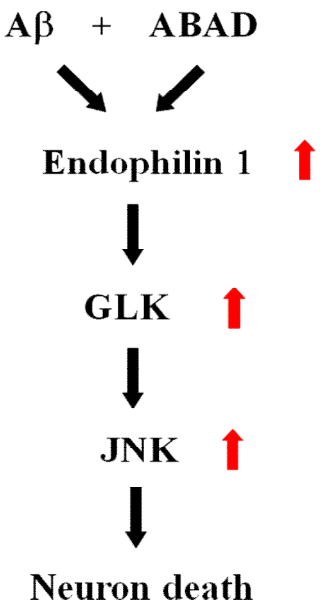

Figure 1.7 Hypothetic signaling cascade linking Aβ and ABAD interaction to neuron death.

1.5 ABAD-Cyclophilin D interaction

1.5.1 Mitochondrial membrane permeabilization

In addition to its role in Ca^{2+} homeostasis regulation, ATP and ROS production, mitochondria also plays a major role in apoptosis induction. Cell death stimuli induce mitochondrial membrane permeabilization (MMP), upon which, prodeath proteins sequestered in the inner mitochondrial membrane space are released into the cytosol (Mattson and Kroemer 2003). For example, cytochrome c is confined to the mitochondrial intermembrane space preventing it from interacting with apoptotic-protease-acting factor 1 (Apaf1), a cytosolic protein. Upon permeabilization, cytochrome C binds to Apaf-1, leading to activation of pro-caspase-9. Caspase-9 then proteolytically activates caspase-3, one of the principle proteases that participate in apoptosis pathway. Similarly, Smac/DIABLO and Omi/HtrA2, two intermembrane proteins, are normally physically separated from cytosolic inhibitors of apoptosis proteins (IAP), Smac/DIABLO and Omi/HtrA2 neutralize IAPs, and thus relieve the IAP-mediated inhibition of caspase-3 and -9 (Norenberg and Rao 2007). MMP is a major event in physiological as well as pathological cell death. Mitochondrial dysfunction and subsequent oxidative stress can lead to MMP and cell death (Norenberg and Rao 2007).

1.5.2 Mitochondria permeability transition

A number of mechanisms have been reported to trigger MMP, one of which has been proposed to occur by means of the phenomenon of mitochondria permeability transition (MPT) (Schinzel *et al.* 2005). MPT is described as an abrupt increase of inner membrane permeability to solutes with molecular masses of <1,500Da. These events are caused by the opening of a highly regulated MPT pore (MPTP), which leads to dissipitation of the mitochondrial membrane potential and an influx of solutes, causing expansion of the matrix. The latter event may lead to rupture of the outer mitochondrial membrane and cause cytochrome C release and subsequent caspase activation, resulting in cell death (Schinzel *et al.* 2005).

MPTP is a complex which is formed at contact sites between the inner and outer mitochondrial membranes (Crompton 1999) (Figure 1.8). It is comprised of the voltage-dependent anion channel (VDAC), the adenine nucleotide translocator (ANT), and cyclophilin D (CypD) which is the mitochondrial isoform of the peptidylprolyl cis-trans isomerase cyclophilin chaperone family. ANT is located in the inner mitochondrial membrane and VDAC in the outer mitochondrial membrane. CypD can be isolated from the matrix fraction, and generally assumed to reside in that compartment. Upon oxidative stress or other stimuli for MPT, CypD are recruited to the ANT, resulting in the formation of MPTP (Norenberg and Rao 2007).

ANT acts as a regulatory component of the MPTP (Halestrap and Brennerb 2003). CypD has been postulated to be an essential component of MPTP. An in vitro study

showed that CypD deficiency protected cells from H_2O_2 induced cell death. In a middle cerebral artery occlusion mice model, CypD deficiency was reported to confer significant protection against ischemic brain injury (Schinzel *et al.* 2005).

1.5.3 The interaction of ABAD and Cyclophilin D

As stated in section 1.3.1 and 1.3.2, overexpression of ABAD protected cells from metabolic stress. In contrast, overexpression of ABAD in an Aβ rich environment accentuated Aβ induced neuron toxicity.

Interestingly, Yan and Stern observed that ABAD binds CypD (unpublished observation, Yan and Stern, 2004). Therefore, they hypothesized that another contributor to the beneficial effects of ABAD on cellular functions might be related to its sequestration of CypD in the mitochondrial matrix. By maintaining the CypD in the matrix compartment, this chaperone molecule is unable to translocate to the inner mitochondrial membrane, where it could bind to the ANT and potentially lead to MPT and neuron death. However, in an Aβ rich environment, the Aβ-ABAD interaction might displace CypD, resulting in its translocation to the inner mitochondrial membrane, thereby leading to the induction of MPT (Yan and Stern 2005) (Figure 1.9).

Cyclosporine A (CsA) is an immunosuppressant drug, which interacts with CypD and inhibits the opening of the MPTP (Mattson and Kroemer 2003). In Tg mAPP/ABAD neuron cultures, CsA treatment virtually completely suppressed induction of caspase-3-like activity and DNA fragmentation. A significant

reduction of neuron death was also observed (Takuma 2005). These data indicated that the opening of the MPTP is likely to be involved in the cell death pathway of cultured neurons from Tg mAPP/ABAD mice.

To examine the hypothesis that the interaction of ABAD and CypD protect neurons from MPT and cell death, FRET (Fluorescence Resonance Energy Transfer) method was used to study if ABAD interacts with CypD in mitochondria.

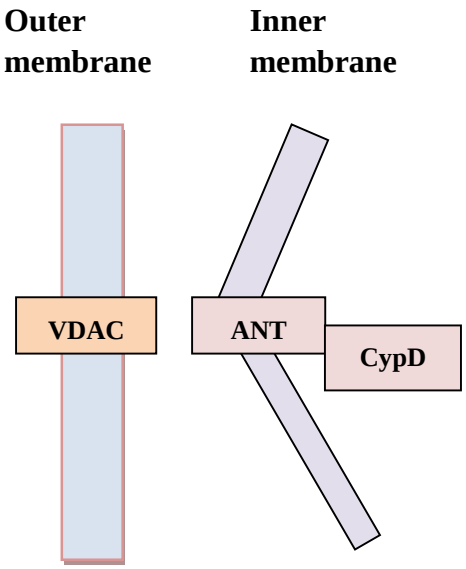

Figure 1.8 MPTP topology.
The basic unit of the MPTP is the VDAC-ANT-CypD complex located at contact sites between the mitochondrial inner and outer membranes.

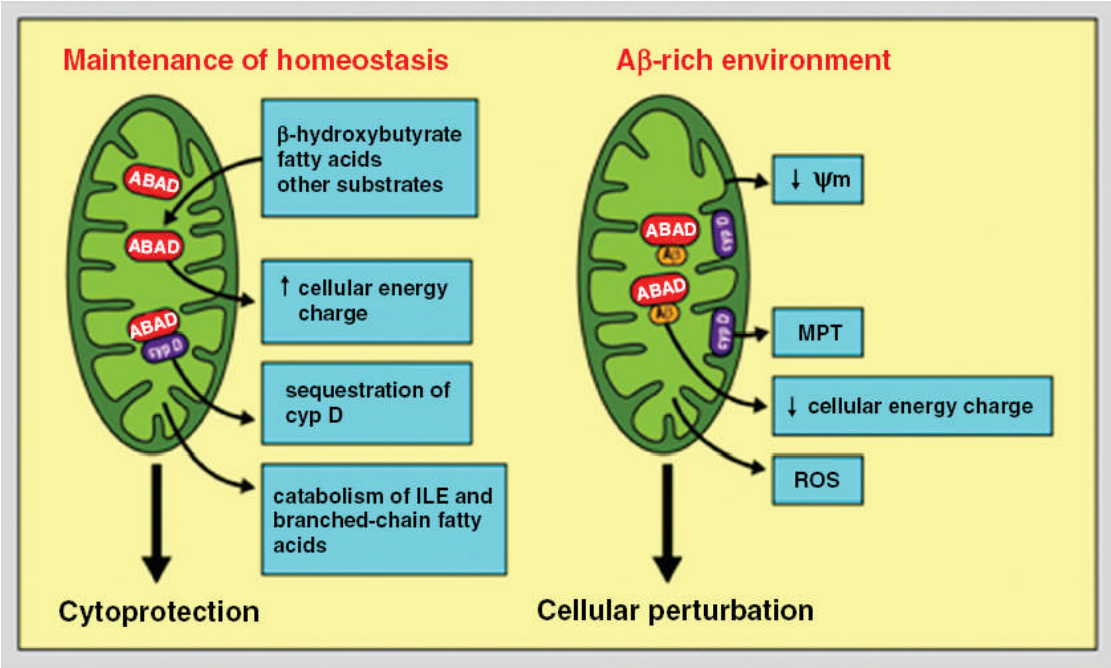

Figure 1.9 A schematic illustration of potential roles of ABAD in physiologic and pathophysiologic conditions. Under physiological conditions, ABAD-CypD interaction maintains CypD in the mitochondrial matrix, preventing it to translocate to the inner membrane of mitochondria. In an Aβ rich environment, ABAD-Aβ interaction displaces CypD, results in its translocation to the inner membrane of mitochondria, which leads to the opening of MPTP and cell death. Ψm, inner mitochondrial membrane potential; MPT, membrane permeability transition pore; ROS, reactive oxygen species.
From: Yan and Stern (2005) *Int J Exp Pathol,* **86,** 161-171

1.6 Receptor for advanced glycation end products

It is well established that Aβ accumulation plays a key role in neuronal dysfunction and neuropathologic changes of Alzheimer's disease. It has been proposed that, early in the disease process, low levels of Aβ are recruited to cellular receptors. Thus, the interaction between Aβ and cellular receptors could contribute importantly to amplifying Aβ induced neurotoxicity in AD (Yan *et al.* 2000).

Many cellular receptors have been identified to bind Aβ such as receptor for advanced glycation end products (RAGE), macrophage scavenger receptors, formyl peptide receptor-like-1, N-methyl-D-aspartate receptor, α7 nicotinic acetylcholine receptor, insulin receptor and integrin receptors (Lue *et al.* 2005; Verdier *et al.* 2004).

RAGE is the most ubiquitously expressed receptor that binds Aβ. It is expressed by neurons, microglia, astrocytes, cerebral endothelial cells, pericytes, and smooth muscle cells (Yan *et al.* 2000). My PhD focused on studying the involvement of RAGE in the pathogenesis of AD.

1.6.1 RAGE and its ligands

RAGE is a multi-ligand cell surface receptor in the immunoglobulin superfamily (Schmidt *et al.* 2000). It is an integral transmembrane protein composed of 404 amino acids. Full length RAGE contains three immunoglobulin-like domains; an N-terminal V-type (variable) region, followed by two C-type (constant regions). The V domain is responsible for ligand binding and contains two putative

N-glycosylation sites. Deglycosylation was shown to affect RAGE binding of certain ligands. The transmembrane domain of full-length RAGE is followed by a short cytoplasmic domain consisting of a sequence of highly-charged amino acids, which is essential for RAGE-mediated signal transduction. Three major types of splice isoforms of RAGE have been identified: full-length, C-truncated, and N-truncated (Ding and Keller 2005). C-truncated RAGE lacks the transmembrane and cytoplasmic domains and is a secreted protein (sRAGE), whereas N-truncated RAGE, which lacks the V-type domain and is incapable of binding ligands, is expressed in the plasma membrane.

RAGE was first indentified as a receptor for advanced glycation end products (AGEs) (Schmidt *et al.* 1996). AGEs are post-translational modifications of proteins that are formed when the amino group of proteins, especially N-terminal amino groups and side chains of lysine and arginine, react nonenzymatically with monosaccharides. This leads to protein-bound Amadori products by way of intermediate Schiff base products. The Amadori products, through oxidation and dehydration, ultimately lead to irreversible AGEs. The levels of AGEs were shown to be increased in aging and AD brain (Staniszewska *et al.* 2005; Takeuchi *et al.* 2004).

RAGE was identified as an extracellular binding site for Aβ. Binding of both soluble and fibrillar Aβ preparation to RAGE were observed (Yan *et al.* 1998). However, it is difficult to define the exact species of Aβ bound to RAGE since soluble oligomers are quite prone to fibrillogenesis.

RAGE also engages other physiologically and pathophysiologically relevant ligands. S100/Calgranulins are a family of low molecular weight, calcium binding proteins. Upon binding calcium, these proteins underwent conformational changes allowing for interaction with target proteins and induce diverse cellular responses. S100 proteins were associated with sites of inflammation and AD-affected regions (Lue *et al.* 2005). Amphoterin is a highly conserved, 30kDa polypeptide, which functions as an inflammatory mediator and act as a marker of necrotic cell damage. In AD brain, amphoterin levels were significantly increased and localized in amyloid plaques and activated microglia (Taguchi *et al.* 2000). RAGE functions as a signal transduction receptor for both S100 proteins and amphoterin.

1.6.2 Increased expression of RAGE in AD

RAGE expression in brain varies at different stages of life. It is highly expressed in the embryonic stage and can be colocalized to outgrowing neurites. During the adult period, levels of RAGE mRNA/protein fall off. However, RAGE expression levels are increased again during normal aging (Luth *et al.* 2005).

Several studies demonstrated that RAGE antigen levels are enhanced in AD-affected regions such as the hippocampus and superior frontal gyrus, compared to age-matched non-demented controls. In contrast, no differences in RAGE levels in brain regions that had limited amyloid plaques and NFTs were detected (Sasaki *et al.* 2001). Furthermore, immunohistochemistry studies of AD brain revealed that RAGE overexpressing cells are located in proximity to AD pathology sites. In the

hippocampal region of AD brain, there was an increase of RAGE immunoreactivity in neurons, microglia, and astrocytes. Double immunohistochemistry for RAGE and an activated microglia marker, MHC II showed that activated microglia clustered at amyloid plaques displayed the most intense RAGE immunoreactivity (Sasaki *et al.* 2001). Together, these data implicated that enhanced RAGE expression is associated with the pathologic changes in AD.

1.6.3 The effects of Aβ-RAGE interaction on neuronal cells

In vitro studies showed that Aβ treatment causes early activation of MAP kinase pathways and nuclear translocation of nucleofactor kappa B (NF-κB) in neuronal cultures that overexpress RAGE. At a later time point, activation of caspase 3 was observed, resulting in induction of apoptotic pathway (Yan *et al.* 1996). Moreover, exposure of neuroblastoma cells to aggregated Aβ40/42 resulted in increased expression of macrophage colony stimulating factor (M-CSF) in a dose-dependent manner. Increased production of M-CSF antigen was associated with enhanced expression of M-CSF transcripts and activation of NF-κB. Anti-RAGE IgG and antioxidant *N*-acetylcysteine can block M-CSF expression (Yan *et al.* 1998).

NF-κB is a transcription factor involved in the regulation of several cellular target genes. In the absence of stimulatory signals, NF-κB resides in the cytoplasm as a heterodimer by its physical interaction with an inhibitory phosphoprotein, IκB. Upon stimulation, NF-κB dissociates from IκB and then enters into the nucleus, where it induces expression of many genes involved in immune and inflammatory

responses (Widera *et al.* 2006). This factor is widely expressed in the central nervous system and is present in both neurons and glial cells, where it could be a positive regulator of genes whose products mediate a full array of inflammatory cytokines. Previous experiments showed that NF-κB activation is increased in AD brains compared with controls (Ferrer and Lopez 2008). Consistent with this observation in human AD, the level of activated NF-κB was found to be increased in brains of Tg2576 (described in section 1.2.3) compared with wild-type littermates, and this increase was associated with amyloid plaques (Townsend and Pratico 2005).

M-CSF is a neuronal survival and microglial growth and activation factor. M-CSF released by neurons stimulates its cognate receptor, c-fms on microglia. M-CSF mediates microglial activation through enhancing cell proliferation and migration, as well as cell survival (Lue *et al.* 2005). Increased expression of M-CSF was observed in neurons near amyloid plaques. Furthermore, M-CSF levels in the cerebrospinal fluid of patients with AD were elevated ～5 fold and its receptor, c-fms was also increased in AD brain (Lue *et al.* 2005).

These data suggested that in neuron cells, binding of Aβ to RAGE leads to oxidant-mediated activation of NF-κB, followed by increased levels of M-CSF transcripts and the protein.

1.6.4 The effects of Aβ-RAGE interaction on microglial cells

Exposing human microglia to pre-aggregated Aβ42 resulted in secretion of

inflammatory cytokines, chemokines including interleukin IL-6, tumor-necrosis-factor (TNF)-α and monocyte chemoattractant protein-1 (MCP-1), IL-8, macrophage inflammatory protein (MIP)-1α and M-CSF (Lue *et al.* 2001).

When human microglia cells were exposed to oligomeric/fibrillar Aβ42 in the presence of anti-RAGE, Aβ induced M-CSF production was significantly reduced (Yan *et al.* 1996). Moreover, in the presence of Aβ42 oligomers, blockade of RAGE in RAGE-bearing human microglia caused a marked decrease in MCP-1 and TNF-α secretion (Yan *et al.* 1998).

These data together indicated that RAGE mediates Aβ induced microglial activation, and this event may have influence over the course of inflammatory processes in AD.

There are two salient features of RAGE-dependent signaling. First, RAGE expression is upregulated in the presence of its ligands, thus ligand-receptor interaction is prolonged and causes sustained changes of cellular properties. Second, interaction of ligands with RAGE activates divergent signaling pathways, which, in many cases, results in the activation of NF-κB. The promoter of the RAGE gene contains three NF-κB binding sites (Yan *et al.* 2000). Therefore, as a result of RAGE-ligand interaction, activation of NF-κB positively regulates RAGE gene expression. These characteristics of RAGE may possibly underlie the contribution of the receptor to the pathogenesis of AD. During AD, accumulation of RAGE ligands leads to an ascending spiral of the receptor-induced inflammatory responses as a consequence of the positive feedback loops described above.

1.6.5 Neuropathological characterization of Tg mAPP/RAGE mice

Studies on transgenic animal models have provided important insights into the involvement of RAGE in cellular dysfunction associated with Aβ. Tg mAPP animals have been widely used as an animal model for AD. Most of these Tg models displayed only subtle changes in neuronal function and neuropathology, especially at early time points. It has been hypothesized that RAGE act as a cofactor magnifying Aβ-induced cell stress at early stages. Arancio *et al.* 2004 developed Tg mice with neuronal overexpression of wild-type (WT) RAGE and double Tg mice with targeted neuronal expression of transgenes for mAPP and RAGE (Arancio *et al.* 2004).

The nuclear binding activity of NF-κB was studied by gel shift analysis using nuclear extracts from cerebral cortex. At 3-4 months of age, Tg mAPP/RAGE mice displayed a strong gel shift band whereas non-Tg littermates, Tg mAPP and Tg RAGE displayed no corresponding changes.

In respect to the association of NF-κB activation with inflammation, microgliosis and astrocytosis in double Tgs and single Tgs were compared. Studies of Tg mAPP/RAGE at 3-4 and 7-8 months of age did not find a significant increase in microgliosis or astrocytosis compared with non-Tg littermates or single Tgs. However, at 14-18 months, double Tgs showed significantly more plaque-associated reactive microglia and astrocytes. It is possible that the latter represent an exaggerated secondary inflammatory response to amyloid plaques (Arancio *et al.* 2004).

The perturbation of neuronal function was studied using the radial arm water maze. At 3-4 months of age, non-Tg littermates showed strong learning and memory capability. Similar results were obtained with Tg RAGE, as well as Tg mAPP mice. However, Tg mAPP/RAGE mice displayed impairment of spatial learning and memory. At 5-6 months, the deficit in learning/memory in Tg mAPP/RAGE was worse than in younger double Tg animals. A deficit, though less severe, was also observed in age-matched Tg mAPP mice whereas Tg RAGE and non-Tg littermates still showed intact spatial memory. Decreased density of cholinergic fibres and synapses were identified as AD-like pathology. These pathological changes were found to be temporarily associated with altered spatial learning/memory in young Tg mAPP/RAGE mice. Taken together, these data suggested that neuronal dysfunction and neuropathologic changes are accelerated in Tg mAPP/RAGE mice (Arancio *et al.* 2004). .

1.6.6 Neuropathological characterization of Tg mAPP/DN-RAGE mice (Arancio *et al.* 2004).

To further verify a direct role of RAGE in signal transduction for Aβ induced cellular perturbation, double Tgs with neuron targeted overexpression of a dominant negative form of RAGE (DN-RAGE) and mAPP were employed. DN-RAGE is a truncated form of the receptor with intact extracellular and transmembrane domains, but a deleted cytosolic tail.

At 3-4 months of age, Tg mAPP/ DN-RAGE displayed a marked decrease of the

activation of NF-κB compared to Tg mAPP/RAGE mice. Consistently, at the same time point, Tg mAPP/ DN-RAGE also showed a preserved spatial learning/memory compared with Tg mAPP/RAGE. Furthermore, at 5-6 months of age, when Tg mAPP mice displayed a significant deficit in learning/memory, Tg mAPP/ DN-RAGE animal showed a better maintained cognitive function.

Neuropathologic changes, as evaluated by cholinergic-positive fibers in the subiculum, were virtually completely prevented in Tg mAPP/DN-RAGE mice, compared with Tg mAPP animals, at both 3-4 and 14-18 months of age.

Together, these data provided further support to the idea that RAGE functions as a signal transduction receptor mediating neuronal dysfunction in the Aβ-rich environment provided by the mutant APP transgene.

In summary, these data indicated that increased levels of RAGE in an Aβ-rich environment promote neuronal dysfunction, even prior to appearance of amyloid plaques. At later stages, the neuroinflammatory response seems to be accelerated in Tg mAPP/RAGE animals.

Chapter 2： Materials and Methods

Chapter 2： Materials and Methods

General chemicals and reagents were obtained from Sigma unless otherwise indicated. See Appendix 1 for a list of suppliers.

2.1 Molecular Biology Techniques

2.1.1 Polymerase Chain Reaction (PCR)

PCR was performed in a 50 μl reaction volume containing 10 μM of forward and reverse primers (Invitrogen), 200 μM dNTPs (Promega), 1.25 unit of PfuTurbo DNA polymerase (Strategene) and 1X PCR buffer (supplied with DNA polymerase) and 100-200 ng template DNA. Typical PCR conditions were: initial denaturation at 95°C for 10 minutes followed by 30 cycles of 95°C for 45 seconds, 52°C for 45 seconds and 72°C for 1 minute with a final extension of 10 minutes at 72°C.

2.1.2 Restriction enzyme digest

Restriction digestion was performed using restriction enzymes (New England Biolab) following the manufacture's instructions. In general, 2 μg plasmid DNA or PCR products were incubated with 5-10 units of appropriate restriction enzymes in the appropriate buffer as recommended by the supplier. These reactions were incubated routinely at 37 °C for 4 hours to insure complete digestion.

2.1.3 Agarose gel electrophoresis and gel purification

Linearized plasmid DNA, PCR products and DNA fragments produced by restriction digestion were separated based on molecular weight using agarose gel electrophoresis. Agarose was melted in tris-borate ethylenediamine-tetraacetic acid (TBE) buffer and ethidium bromide was added to a final concentration of 0.5 μg/ml and poured into and set in an AGTI submarine gel casting apparatus unit (VWR). 20% 6X agarose gel loading buffer (50% glycerol, 49.75% TBE, 0.25% bromophenol blue) were added to the samples. Samples with DNA fragments ≤1kb were loaded onto 1% (w/v) agarose gels and samples ≥1kb onto 2% (w/v) agarose gels. For sizing and quantification of DNA, Hyperladder 1 (New England Biolab) was loaded into the lanes beside the samples. Gel electrophoresis was carried out in TBE at 60-80V for 30-45 minutes. Analytical gels were visualized with a UV lamp and photographed by a digital camera (Mitsubishi 85mm lens, Thistle Scientific). To extract digested DNA fragments and PCR products for ligation reaction, DNA bands on preparation gels were visualized under a low intensity UV lamp (230V-50Hz, Ultratec, Ltd.) and then excised from the gel using a sterile scalpel blade. DNA purification was conducted using the Wizard SV Gel and PCR Cleanup Kit (Promega) according to the manufacture's instructions.

2.1.4 Ligation reaction

Ligation of plasmid vector and insert DNA was carried out in a final reaction volume of 20 μl. Both 1:1 and 1:3 insert/vector molar ratios were used for each

ligation. 100 ng insert was mixed with appropriate amount of vector and incubated at 65°C for 5 minutes. The reaction was left on ice to cool down, after which 0.5 µl T4 DNA ligase (Strategene) and 2 µl ligase buffer (supplied with T4 ligase) were added and the reaction mixture was incubated for 16-20 hours in a water bath at 16°C.

2.1.5 Preparation of Competent E. coli Strains (DH5α and BL21)

E. coli strains glycerol stocks (laboratory stocks) were inoculated into 5 ml LB (Lubria broth) and incubated overnight for 16-20 hours at 37°C by shaking at 210rpm. Next day, 1 ml overnight culture was diluted in 50 ml LB, grow with shaking until an OD at 600 nm of 0.3-0.4 was reached. The cells were centrifuged at 3500g for 10 minutes at 4°C. The supernatant was discarded and the cell pellet was resuspended in 20 ml sterile $CaCl_2$ (100 mM), left on ice for 30 minutes. Then the cells were centrifuged at 1000g for 5 minutes at 4°C. After incubation on ice for a further 30 minutes, the cells were used immediately for transformation or flash-frozen in liquid nitrogen and stored at -80°Cfor future use.

2.1.6 Transformation of Competent E. coli Strains (DH5α and BL21)

1-10 µl of plasmid DNA/ligation reaction was added to 200 µl competent bacteria and incubated on ice for 30 minutes. The bacteria were heat shocked for 45 seconds at 42°C and chilled on ice for 2 minutes. 1 ml LB or SOC medium (2% w/v tryptone, 0.5% bacto-yeast extract, 10 mM NaCl, 2.5 mM KCl, 10 mM MgCl2, 10 mM MgSO4, 20 mM glucose) was added to the transformed bacteria and the

cultures were incubated for 1 hour at 37°C with shaking at 210rpm. 100 µl of the culture medium were spread onto an agar plate containing the appropriate antibiotic. The remaining bacteria culture was centrifuged, and the pellet was resuspended in 100 µl culture medium and spread onto a second agar plate. Agar plates were placed inverted in a 37°C incubator for 16-20 hours, after which single colonies corresponding to transformants were isolated for screening/inoculation into LB.

2.1.7 Preparation of Glycerol Stocks of Transformed E. coli

Glycerol stocks were prepared from overnight bacterial cultures. 0.6 ml of bacterial culture was mixed with 0.4 ml of 50% sterile glycerol and frozen at -80°C for future use.

2.1.8 Preparation of plasmid DNA

Bacteria were cultured overnight at 37°C in LB supplemented with the appropriate antibiotic (ampicillin 50 µg/ml, kanamycin 35 µg/ml). Small-scale preparation of DNA for analysis, cloning and transfection was carried out using Qiagen's miniprep kit according to the manufacturer's instructions. Large-scale preparation of DNA for analysis, cloning and transfection was carried out with the Qiagen Endofree Maxi Kit or the Promega PureYield Midi Prep kit according to manufacturer's instructions.

2.2 Cell culture

All plastic-ware used was from Nunc (VMR) unless otherwise stated. All cells were cultured in T-75 flasks (80cm^3) at 37°C in a humidified atmosphere containing 5% CO_2.

2.2.1 General cell culture

SK-N-SH human neuroblastoma cells (ATCC) were routinely cultured in Dulbecco's modified Eagle medium (DMEM) supplemented with 10% (v/v) foetal calf serum (FCS) (Globepharm), 2 mM L-glutamine, 100 units/ml of penicillin (pen) and 0.1 mg/ml streptomycin (strep). Human Embryonic Kidney (HEK293) cells (Laboratory stocks) were routinely cultured in MEM supplemented with 10% FCS, 5% (v/v) non-essential amino acids (NEAA), 2 mM L-glutamine, 100 units/ml of pen and 0.1 mg/ml strep. SH-SY-5Y human neuroblastoma stable cell line overexpressing APP Swedish mutation (Dr Richard Killick, Institute of Psychiatry, King's College London) was maintained in the same medium for SK-N-SH cells with the addition of 500 μg/ml G-418 sulfate (Gibco).

2.2.2 Passage of cell lines

Cells were passaged at 70–80% confluency by washing with 2-3 ml trypsin/ethylenediaminetetraacetic acid (EDTA) (Gibco) at 37°C for 2-3 minutes. 10 ml of appropriate culture medium was added to the detached cells and they were then seeded into flasks or petri dishes/coverslips (VWR) at appropriate densities.

2.2.3 Primary cortical neuron culture

Brains of 14 day mouse embryos were taken and the cortices were removed under a dissecting microscope. The cortices were placed in a 15 ml tube containing PBS (Phosphate buffer saline; 0.01 M NaH_2PO_4, 0.14 M NaCl, pH 7.4) with 25 µl trypsin (1mg/ml), and incubated at 37°C for 5 minutes. After addition of 10 ml Trypsin stop [MEM, 10% FCS and 300 µl DNase (1000 unit/ml)], the tube was inverted several times and left to settle for 5 minutes. All but ~ 400 µl supernatant was removed. The cells were triturated 20-30 times with a glass pasteur pipette in order to dissociate the cells into a single-cell suspension. 5 ml of cortical neuron medium was added to the cell suspension and the number of cells was counted using a haemocytometer.

Cortical neurons were cultured in MEM supplemented with 5 mg/ml glucose, 24.5 mM KCl, 2 mM L-glutamine, 25 unit/ml pen, 25 µg/ml strep, 10% FCS and 10% horse serum (HS). Prior to amyloid beta (Aβ) treatment, cortical neurons were maintained in serum free medium containing MEM, 24.5 mM KCl, 2 mM L-glutamine, 25 unit/ml pen, 25 µg /ml strep and 1 mg/ml B27 (Gibco).

2.2.4 Preparation of aggregated Amyloid Beta

1 mM stock solution was made by dissolving 5 mg of Aβ25-35 (Bachem) in 5 ml of sterile milli-Q purified water (MQ), aliquot and stored at -40°C. Aggregated Aβ was prepared by mixing an equal amount of sterile PBS to the Aβ25-35 stock solution and incubating at 37°C for 3 to 5 days. Aggregated Aβ25-35 was then applied to

cortical neurons at a concentration of 50 μM. Neurons were serum-deprived for 72 hours prior to Aβ treatment.

2.2.5 Transfection of different cell lines

HEK, SK-N-SH and SH-SY-5Y cells were transfected using Genejammer Reagent (Strategene). Appropriate amount of Genejammer (three times the volume in μl of Genejammer reagent per 1.0 μg of DNA) was incubated in reduce serum Optimem ™ medium (Gibco) for 5 minutes. The appropriate amount of DNA was added to the transfection reaction and incubated for a further 10-15 minutes. The standard culture medium was removed from the culture dishes and replaced with fresh serum containing medium. The reaction mixture was applied dropwise to the culture dishes. Four hours later, an equal volume of serum containing medium was added to the cells. For transient transfections, after 48 hours incubation under standard growth conditions (i.e., 37°C and 5% CO_2 in a humidified incubator), cells were either harvested for electrophoresis or fixed for immunocytochemistry.

SK-N-SH cells were also transfected with the Amaxa Cell line nucleofector Solution V following the manufacture's instructions. A cell suspension containing $2X10^6$ to $3X10^6$ cells was centrifuged at 800g for 10 minutes and the cell pellet was resuspended in 100 μl nucleofector solution V and mixed with 2-6 μg of DNA plasmids. The reaction mixture was transferred into an Amaxa cuvette and the nucleofector program X-05 was selected. Transfected cells were then seeded onto 35 mm petri dishes containing glass coverslips.

Cortical neurons were transfected using Amaxa mouse neuon nucleofactor kit according to the manufacture's protocol. A cell suspension containing $5X10^6$ neurons was centrifuged at 800g for 5 minutes. The supernatant was discarded and the cell pellet was resuspended in 100 µl nucleofactor reagent. 2 µg of plasmid DNA was transfected into the cell suspension using program O-05. Transfected neurons were then seeded onto 35 mm petri dishes pre-coated with poly-D-lysine.

Poly-D-lysine petri dishes were prepared by covering the 35 mm petri dish surface with 2 ml of 50 µg/ml poly-D-lysine in sterile PBS overnight. The petri dishes were washed once with sterile MQ before use.

2.2.6 Liquid nitrogen cell stocks preparation and recovery

Liquid nitrogen stored cell stocks were prepared by trypsinizing confluent cultures and centrifuging the dissociated cells (1000g, 5 minutes, room temperature). Cell pellets were resuspended in medium containing 50% FCS, 40% normal growth medium for that cell line and 10% dimethyl sulfoxide (DMSO). 1 ml aliquots were pipetted into cryotubes, which were brought to -80°C slowly by placing in an acryo 1°C freezing container (Naglene) in a -80°C freezer overnight. The cryotubes were then placed in liquid nitrogen for long term storage. Cell stocks were recovered by thawing for 1 minute in a water bath at 37°C and placing in a T-75 flask together with 10 ml pre-warmed culture medium. Media was replaced 24 hours later to remove DMSO.

2.3 Fluorescence microscopic analysis

2.3.1 Immunocytochemistry

48 hours after transfection, cells were washed in pre-chilled PBS three times for five minutes. The cells were fixed in 4% paraformaldehyde (PFA) for 20 minutes at room temperature, followed by four washes in PBS. Coverslips were mounted onto glass slides in Mowiol 488(Calbiochem) with Dapi solution [10% (wt/vol) Moviol 488, 1 µg/ml DAPI] and sealed using clear nail varnish. The slides were kept at 4°C or -20°C prior to confocal microscopy. Fluorescence images were visualized and recorded using a Leica TCS SP2 Confocal Laser Scanning Microscope (Leica, Heidelberg, Germany), equipped with a DMIRBE inverted microscope (Leica) with 63X 1.32 NA and 40X 1.25 NA oil immersion HCX Plan Apo objectives.

2.3.2 Fluorescence resonant energy transfer (FRET) analysis

FRET is a phenomenon that occurs when two fluorophores tagged proteins are in sufficient proximity (<10 nm) and an appropriate relative orientation such that an excited fluorophore (donor) can transfer its energy to a second, longer-wavelength fluorophore (acceptor). Thus, excitation of the donor can produce light emission from the acceptor, with attendant loss of emission from the donor when the two proteins are in such proximity that they interact with each other. Therefore, FRET can be used as an assay to detect direct protein–protein interactions in cells. In this study, enhanced cyan fluorescent protein (ECFP) and enhanced yellow fluorescent protein (EYFP) were used as one pair of fluorophores for FRET study. Acceptor

photobleaching method was used to determine FRET in this study. Its principle is that energy transfer is reduced or eliminated when the acceptor is bleached, thereby yielding an increase in donor fluorescence.

SK-N-SH cells were transfected with plasmids encoding ECFP or EYFP tagged proteins. 48 hours after transfection, cells were fixed and mounted in Movial with Dapi solution. The slides were examined on a Leica Multiphoton confocal laser scanning microscope system (TCS MP; Leica), which contained 405, 458, 476, 488, 514, 543, and 633 nm laser lines. ECFP and EYFP were excited using 458 and 514 nm laser lines respectively. Detection parameters were optimized to eliminate crosstalk. ECFP emission was collected at 460-500 nm and EYFP emission was collected at 525-600 nm.

The FRET analysis was performed using the regulator function of the Leica Confocal Software Acceptor Photobleach module. Three to four fields with fluorescent cells on each slide and up to eight regions of interest (ROIs) within each cell were selected. Pre-bleach images of ECFP and EYFP were captured using 458 and 514 nm lasers at 20% of their full power. For EYFP acceptor photobleaching experiments, cells were photobleached in the ROIs to approximately 20% of its prebleach intensity by the 514 nm laser at its full power. Postbleach images were then captured. FRET efficiency (FRETeff) was calculated using the formula FRETeff = (Dpost – Dpre)/Dpost where Dpre and Dpost are the fluorescence intensities of ECFP before and after photobleaching, respectively.

2.4 Western Blotting

2.4.1 Sample preparation for SDS-PAGE

48 hours after transfection, culture media was removed from cell culture dishes and washed with pre-chilled PBS twice. To obtain cell extracts, 2X SDS sample buffer was added to the dishes and the cells were harvested using a cell scraper. 2X SDS sample buffer is composed of Tris-HCl (62.5 mM, pH6.8), 2% SDS, 10% Glycerol, 50 mM DTT, and 0.01% bromphenol blue. For each 35 mm petri dish, 100-200 µl 2X SDS sample buffer and for each 60 mm petri dish, 500 µl 2X SDS sample buffer were applied. Cell extracts were sonicated four times for five seconds and left on ice for 30 minutes. The cell lysates were then centrifuged at 13,000g for 15 minutes at 4°C. The supernatants were collected and stored at -20°C or -80°C until further use.

Mouse cortex was minced in 1 ml pre-chilled radioimmunoprecipitation (RIPA) buffer, sonicated for six times, each of ten seconds. RIPA buffer contained 10 mM Tris-HCl, pH8, 50 mM NaCl, 0.5% Na-deoxycholate, 0.2% SDS and 1% Nonidet P-40. This buffer also contained 1x Protease Inhibitor Cocktail (Roche) and 2 mM phenylmethylsulfonylfluoride (PMSF). The cortex extract was left on ice for 15 minutes and centrifuged at 13,000g for 15 minutes at 4°C. The supernatant was aliquot and frozen at -80°C until assayed.

To prepare cell lysates for detection of activated JNK, SH-SY-5Y cells or cortical neurons were harvested in kinase buffer containing 20 mM Tris (pH7.5), 150 mM

NaCl, 1 mM EDTA (pH 7.4), 1 mM EGTA, 10% Triton, 2.5 mM Sodium pyrophosphate, 1 mM Beta-Glycerolphosphate, 1 mM Sodium orthovanadate, 1 μg/ml Leupeptin, 1X Protease Inhibitor Cocktail and 2 mM PMSF. The cell extracts were sonicated for four times, each of five seconds, centrifuged at 13,000g for 15 minutes. The supernatants were then stored at -80°C.

2.4.2 Sodium orthovanadate activation

Sodium orthovanadate solution was prepared by adjusting a 200 mM stock solution to pH 10.0 using either NaOH or HCl as appropriate. The solution was boiled until colourless and left to cool to room temperature. Adjust pH of this solution back to 10.0 and repeat boiling, cooling and pH adjusting until the solution remained colourless and stabilized at pH 10.0.

2.4.3 Bradford assay

Protein concentration was determined using Bradford's reagent. Samples were diluted in MQ to a final volume of 500 μl, to which 500 μl of Bradford reagent was added. A series of 0, 2, 4, 8 μg/ml sample of bovine serum albumin (BSA) were used to make standard curve. Absorbencies were read at 595 nm using a Beckman DU 530 life science UV spectrometer. The protein concentrations of samples were calculated based on their absorbencies and dilution fold.

2.4.4 SDS-PAGE

Protein samples were prepared as described in section 2.4.1 and diluted in

Invitrogen NuPAGE LDS Sample buffer (4X) in the presence of reducing agent. The samples were boiled for five minutes and loaded onto Invitrogen NuPAGE Bis-Tris precast gradient (4-12%) polyacrylamide gels together with 5 µl of SeeBlue Plus2 protein standards (Invitrogen). The proteins were separated by electrophoresis in a Novex Xcell Mini-cell (Invitrogen) using Invitrogen NuPAGE morpholineethanesulfonic acid (MES) running buffer (50 mM MES, 50 mM Tris base, 3.5 mM SDS and 1 mM EDTA). Electrophoresis was conducted at a constant 200volts (V) for 40 minutes. After electrophoresis, protein gels were either visualized by Coomassie staining or blotted to membranes for immunoreactivity detection.

2.4.5 Coomassie staining of SDS-PAGE gels

Gels were stained with Coomassie stain solution [0.1% (w/v) Coomassie brilliant blue R-250, 45% (v/v) ethanol, 10% (v/v) glacial acetic acid)] for 40 minutes at room temperature. To remove excess Coomassie brilliant blue, the gels were destained for 3-4 hours or overnight in destaining solution [10% (v/v) glacial acetic acid, 40% (v/v) methanol] with 3-4 changes of destaining solution.

2.4.6 *Western blotting*

The SDS-PAGE resolved proteins were transferred onto nitrocellulose membranes or polyvinylidene difluoride (PVDF) membranes by electroblotting using the Novex X cell blot module (Invitrogen). Electroblotting was carried out at 30V for one hour in Invitrogen NuPAGE transfer buffer supplemented with appropriate

amounts of methanol and antioxidant according to the manufacturer's instructions. The efficiency of the transfer was evaluated by staining membranes with Ponceau S solution [0.1% Ponceau S (w/v), 5% acetic acid)] for three to five minutes at room temperature. Ponceau was washed off with PBS.

Detailed protocols for different antibodies are described in Appendix 2. In general, nonspecific binding sites on the membranes were blocked by incubating the blots in 5% non-fat dry milk in TBS/T (Tris buffer saline; 20 mM Tris-HCl, 137mM NaCl, and 0.1% Tween-20, pH 7.5) at 4ºC overnight. Primary antibodies to specific proteins were diluted in 5% non-fat dry milk in TBS/T. Blots were washed in TBS/T and incubated with the primary antibodies for one hour at room temperature. Primary antibodies were removed by washing the blots three times, for ten minutes each with TBS/T. The blots were then incubated with HRP-conjugated secondary antibodies (Santa Cruz) diluted in 5% fat free powdered milk in TBS/T for one hour, followed by three ten minute washes in TBS/T. All incubations and washes were done with rocking. Immunoreactive bands were detected using SuperSignal West Pico enhanced chemiluminescence reagent (ECL, pierce) according to manufacturer's instructions. Exposure to Fujifilm (Kodak) was used to measure chemiluminescence, and exposure time was varied depending on the strength of the signal.

2.4.7 Removal of Primary and secondary antibodies from a Western blot

The membrane was incubated with 10% glacial acetic acid (v/v) four times for 15

minutes each. After washing in PBS for 6 times, each of 10 minutes, the membrane was incubated with primary and secondary antibodies as described in section 2.4.6.

2.5 Two dimensional electrophoresis

All chemicals and reagents used in two dimensional electrophoresis are of electrophoresis grade and obtained from Amersham-Pharmacia-Biotech. All gels and electrophoresis instruments used in two dimensional electrophoresis studies were from Amersham-Pharmacia-Biotech as well.

2.5.1 Preparation of whole-cortex lysate

Wild type and transgenic mice cortices were kindly provided by Prof. Shidu Yan (College of Physicians and Surgeons, Columbia University). These cortices were sent on dry ice and immediately stored at -80°C upon arrival. To prepare cortex lysates for two dimensional electrophoresis, mice cortices were minced in lysis buffer, sonicated on ice six times for 30 seconds each, with at least 30 second-intervals in between, and left to stand on ice for a further 15 minutes. Two different lysis buffers were used. One is lysis buffer 1 which contains 8 M Urea, 2 M Thio-Urea, 4% chaps, 1% IPG buffer (pH 3-10), 40 mM Tris base and 100 μl sigma protease inhibitor. The other is lysis buffer 2 which contains 8 M Urea, 4.5% chaps, 1% DTT, 2% IPG buffer (pH 3-10), 10 μl of nucleic acid inhibitor, 10 μl PMSF and 40 μl Roche protease inhibitor cocktail. The lysates were then subjected to centrifugation at 13,000g, 4°C for 45 minutes. The supernatants were transferred into clean microcentrifuge tubes and flash frozen in liquid nitrogen for equalization

of protein content and two dimensional electrophoresis.

2.5.2 Equalization of protein loading

To ensure that equal protein amounts were loaded onto first dimensional isoelectric focusing (IEF) gels, the samples were pre-run on one-dimensional Bis-Tris 4-12% polyacrylamide mini-gels and visualized by staining with Coomassie. The concentrations of proteins were assessed visually and adjusted accordingly. This method was found to be more reliable than using Bradford assay to determine protein concentration.

2.5.3 First dimensional electrophoresis-Isoelectric focusing

The first dimensional electrophoresis, isoelectric focusing (IEF), was performed on either a Multiphor II apparatus or an Etttan™ IPGphor II Isoelectric Focusing Unit. Immobiline™ DryStrip gels contain a preformed pH gradient immobilized in homogenous polyacrylamide (IPG) gels. 18 cm IPG gels with pH gradient 3-10 and 24 cm IPG strips with pH 3-10, 4-7 and 6-9 were used for IEF. The gels are cast on plastic backing and delivered dried. Prior to IEF, they were rehydrated with Destreak ™ Rehydration Solution.

For IPG strips with pH intervals 3-10 and 4-7, cortex sample was applied by in-gel rehydration and for basic IPG gels (pH 6-9), paper bridge loading was used.

2% IPG buffer was added corresponding to the pH range of Immobiline™ DryStrips to Destreak ™ Rehydration Solution. Add 1 mg of protein sample (if protein sample was loaded with in-gel rehydration) in destreak rehydration solution

to a final volume of 450 µl, and pipette the solution along the entire length of an Immobiline Drystrip Rehydration Tray. Place the IPG strips in the reswelling tray channel gel side down and distribute the rehydration solution evenly by gently sliding strip over solution. Overlay each strip with a sufficient amount Immobiline DryStrip Cover Fluid (2 to 3 ml) to completely cover the strip. Allow strips to rehydrate at room temperature for 20-24 hours.

18 cm IPG strips were focused on a Multiphor II electrophoresis system using a MultiTemp III Thermostatic Circulator maintaining a constant temperature at 20°C. The Immobiline DryStrip tray and Immobiline DryStrip aligner were placed onto the Multiphor II unit and individual rehydrated IPG strips (acidic/pointed end up) were placed into wells of the DryStrip tray and then the IEF started. Running conditions are shown in Table 2.1.

Step	Voltage (V)	Time (hour: minute)
Step 1- Gradient	500 V	0:10 or 2 hours
Step 2- Step and Hold	500 V	2:00 or 4 hours
Step 3- Gradient	3500 V	3 hours
Step 4- Step	3500 V	24 or 14-18 hours

Table 2.1 Standard protocols for isoelectric focusing of 18 cm Immobiline DryStrip gels (pH 3-10) on Multiphor II electrophoresis system. Running conditions: Temperature 20 °C; current 50 µA per strip.

24 cm IPG strips were focused using an Ettan™ IPGphor II electrophoresis unit. An Ettan™ IPGphor II Manifold was placed onto Ettan™ IPGphor II unit and the IPG strips were transferred into the Manifold. Moistened electrode pads were placed onto the ends of the strips. The electrode assembly was positioned over the top of all the electrode pads. For basic IPG strip, a paper bridge was soaked in the sample (up to 400 µl) and was placed between the anode electrode pad and the Immobiline DryStrip. Running conditions were dependent on the pH gradient and the lengths of the IPG gel strips used (Table 2.2).

pH intervals	**Step voltage (mode)**	**Voltage (V)**	**Time (hour: minute)**
pH 3-10	1 Step and hold	500	01:00
	2 Gradient	1000	08:00
	3 Gradient	8000	03:00
	4 Step and hold	8000	2:30-3:45
pH 4-7	1 Step and hold	500	01:00
	2 Gradient	1000	07:00
	3 Gradient	8000	03:00
	4 Step and hold	8000	3:45-5:36
pH 6-9	1 Step and hold	500	01:00
	2 Gradient	1000	05:00
	3 Gradient	8000	03:00
	4 Step and hold	8000	5:36-8:45

Table 2.2 Protocols for running 24 cm Immobiline DryStrip gels with different pH gradients on Ettan IPGphor II Isoelectric Focusing Unit. Running conditions: Temperature 20 °C; current 50 µA per strip.

Focused IEF strips were used immediately or stored at −80°C until further use. Prior to second dimensional electrophoresis, each strip was equilibrated in 15 ml equilibration buffer containing 50 mM Tris-HCl, pH 8.8, 30% glycerol, 2% SDS, and 6 M urea with 1% DTT for 15 minutes at room temperature. This is followed by a second equilibration for 15 minutes using the same buffer, except that DTT was replaced with 2.5% iodoacetamide to prevent thiol reoxidation.

2.5.4 Second dimensional electrophoresis-SDS PAGE

Second dimensional electrophoresis was performed with either a Hoefer-DALT apparatus or an Ettan DALT six electrophoresis unit.

For Hoefer-DALT system, 10% SDS polyacrylamide gels (22 × 25cm) [10% , 0.4 M Tris, pH 8.8, 0.1% SDS, 0.1% ammonium persulphate and 0.01% *N*,*N*,*N*_,*N*_-tetramethylethylenediamine (TEMED)] were used. Gel solution was prepared in a vacuum flask, omitting the TEMED and ammonium persulfate. After degassing for 30 minutes, the TEMED and ammonium persulfate were added and the solution gently swirled to mix, immediately the gels were cast. The gel cassette was filled to 3 to 10 mm below the top. Each gel was overlayed with a layer of water immediately after pouring to minimize gel exposure to oxygen and to create a flat gel surface. The gels were left to set for a minimum of two hours. The equilibrated IPG strips were rinsed and blotted to remove excess equilibration buffer and then applied onto SDS gels. A low-molecular-weight electrophoresis calibration kit was used for protein molecular mass (daltons) reference standards (phosphorylase b,

94,000; bovine serum albumin, 67,000; ovalbumin, 43,000; carbonic anhydrase, 30,000; soybean trypsin inhibitor, 20,100; and α-lactalbumin, 14,400). The markers were applied to a paper IEF sample application piece in a volume of 15-20 µl. The application piece was picked up with forceps and applied to the top surface of the gel next to one end of the IPG strip. 2% low melting point agarose in running buffer was melted and trace bromphenol was added. The IPG strip was sealed in place using this solution. The tank was filled with 1X Laemmli SDS electrophoresis buffer (25 mM Tris base, 192 mM glycine, 0.1% SDS) and the MultiTemp III temperature controller was adjusted to 15°C. The protein gels were separated at 200V and 20 mA/gel for 16-20 hours.

For the Ettan DALT electrophoresis system, DALT Gel 12.5 gel, a precast 12% polyacrylamide gel, was used for the second dimensional electrophoresis. The gel was inserted into a cassette that allowed it to be run in a vertical mode with liquid buffers. The gel was used together with the DALT Buffer Kit which contained concentrated buffers for running the gel, gel buffer for seating the gel in the DALT Precast Gel Cassette, and sealing solution for attaching the IPG strip to the top of the slab gel. The anode assembly was inserted into the tank. One bottle of 10X cathodic buffer was diluted in 800 ml MQ. 37.5 ml of the bottle content 100X Anode buffer included in the DALT Buffer Kit was added to the tank. After which, the electrophoresis unit was filled with 4.5 liter of MQ. The MultiTemp III temperature controller was adjusted to 4°C. A DALT Gel 12.5 was inserted into the precast gel cassette. The equilibrated IPG strips were rinsed in the diluted cathodic

buffer and applied onto DALT gels. Molecular weight marker proteins were applied along with the IPG gel. For each strip, 2 ml of sealing solution from the buffer kit was used to seal the IPG strip in place. The cassettes were now placed into the tank. The upper chamber was filled with 1X cathodic buffer. The gels were separated at 10 V/gel, 2 mA/gel for one hour and then at 15 V/gel, 5 mA/gel for 16-20 hours.

After electrophoresis, the gels were removed from between the glass plates and visualized by silver staining using PlusOne^{TM} silver staining kit following the protocols detailed in Table 3. All staining steps were done at room temperature using high quality (18 megaohm) MQ. Gels were stained in ion staining boxes, with constant shaking on orbital shaker.

Step	Solutions (per gel)	Amount	Time
Fixation	Ethanol	200ml	2X60 minutes
	Glacial acetic acid	50ml	
	Ethanol	75ml	
	Glutardialdehyde (25% w/v)	1.25ml	
Sensitizing	Sodium thiosulphate (5% w/v)	10ml	60 minutes
	Sodium acetate	17g	
	Make up to 250ml MQ		
Washing	MQ		5X 8minutes
Silver reaction	Silver nitrate solution (2.5%w/v)	25ml	
	Formaldehyde (37% w/v)	0.1ml	60 minute
	Make up to 250ml with MQ		
Washing	MQ		4X1 minute
Developing	Sodium carbonate	6.25g	
	Formaldehyde (37% w/v)	200µl	2-3 minutes
	Make up to 250ml MQ		
Stopping	EDTA-Na.2H2O	3.65g	2X45 minutes
	Make up to 250ml with MQ		
Preserving solution	20% Ethanol		

Table 2.3 Protocol for silver staining of two dimensional electrophoresis gels using PlusOne^{TM} silver staining kit. Gels were developed in developing solution until desired intensity was reached. Gels were stored at 4^{o}C in plastic boxes with preserving solution until further use.

2.5.5 Image analysis and protein identification

The images of the silver stained 10% SDS-polyacrylamide gels were captured using a Typhoon 8,600 fluorescence scanner and were printed onto laser transparent papers after processing with Adobe Photoshop. Differential protein expression between different genotypes of mice cortex was analyzed by eye using these gel images. The protein spots were only identified when the expression levels in all three gels of the same genotype were different from that in all three gels of another genotype.

Images of silver stained precast DALT 12.5 gels were captured and digitalized at a resolution of 600 DPI using a Typhoon 9,200 laser scanner. Protein quantification on all two dimensional gels was performed using ImageMaster 2D software (Amersham-Pharmacia-Biotech). Spot features were detected using default and altered settings. Since some real spots were missed and many extraneous spots were detected, spots were manually edited. After spot detection, three to five spots common to all gels and scattered across the area of the gel image were selected as landmarks for gel-to-gel alignment. The two dimensional gel containing the highest number of observed protein spots was selected as the reference gel for the experiment. The remaining 2D gels were matched to the reference gel for spot identification. On average, >80% of all protein spots on each two dimensional gel was successfully matched to their respective protein spots on the reference gel. Spot pairing was manually checked for missed pairs and mismatched spots and was edited. All *de novo* protein spots on non-reference gels were added to the reference

gel image during the matching process. For each protein spot in the reference gel, a molecular weight (mol wt) was assigned using mol wt standard markers.

Spot quantity was expressed in vol% (volume of a spot / total volume of all the spots in a gel) to minimize variations caused by staining and destaining procedures. In this study, for each condition three gels were used for image analysis. The gap values for each spot, which represents the difference between the lowest spot volume of three gels in one condition and the highest spot volume from all three gels in another condition, were calculated by ImageMaster software. If the gap value is positive, it means that the volumes of the protein spots in these two groups of gels do not overlap. The protein spots identified with positive gap values were further analyzed by a two-tailed t test to determine if they were statistically different using a significance level of 5% (P values<0.05). Differences in protein densities between two conditions were then visually reconfirmed with ImageMaster 2D software that provided a simultaneous and enlarged display of the protein spot as it appeared within all two dimensional gels. Identified spots were then excised and sent for MALDI-TOF analysis in Mass Spectrometry service center at University of St Andrews.

Chapter 3: Increased expression of Endophilin 1 leads to increased activation of JNK

Chapter 3: Increased expression of Endophilin 1 leads to increased activation of JNK

3.1 Introduction

In order to study the underlying biochemical events leading to accelerated/enhanced cognitive dysfunction and mitochondrial defects in Tg mAPP/ABAD mice (Section 1.3.2.2), Dr Jim Aiton and Margaret Taylor from our laboratory previously performed two dimensional electrophoresis analysis on four different genotypes of mice brains (Non-Tg, Tg mAPP, Tg ABAD, Tg mAPP/ABAD). They studied differential protein expression between the brains of these four genotypes and found that the antioxidant protein, Peroxiredoxin II protein was consistently up-regulated in Tg mAPP and Tg mAPP/ABAD mice brains as compared to non-Tg and Tg ABAD mice brains (Yao *et al.* 2007). As part of these studies, a second protein was also found to be upregulated in the Tg mAPP and Tg mAPP/ABAD mice brains as compared to non-Tg and Tg ABAD mice brains (Figure 3. 1.). This 42 kDa protein was identified by MALDI-TOF analysis to be endophilin 1 (gene: SH3GL2) (Swiss Prot Accession No Q62420) which has a predicted molecular weight and isoelectric point (pI) of 42,000 Da and 5.4 respectively.

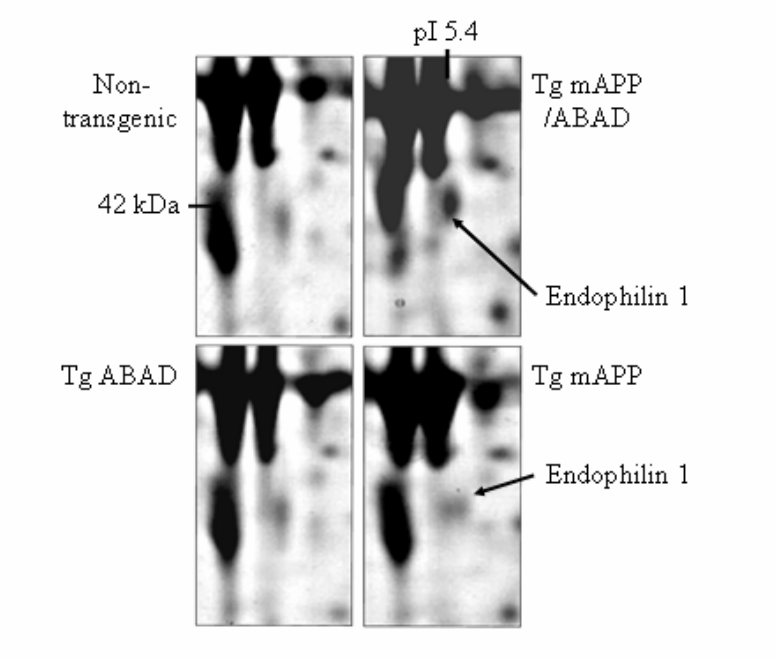

Figure 3.1 Two dimensional gel images of endophilin 1 showing increased level of protein expression in Tg mAPP and Tg mAPP/ABAD mice brains as compared to non-Tg and Tg ABAD mice brains (Figure from Dr Peter Coote, Centre for Biomolecular Science, University of St Andrews).

To confirm the findings from proteomic analysis that endophilin 1 is upregulated in Tg mAPP and Tg mAPP/ABAD mice brains, Margaret Taylor and Prof ShiDu Yan's group (College of Physicians and Surgeons, Columbia University) performed western blot analysis with an endophilin 1 monoclonal antibody. The intensities of the immunoblot bands for endophilin 1 were normalized to β-actin signals. A consistent upregulation of endophilin1 in both the cerebral cortex and hippocampus of Tg mAPP and Tg mAPP/ABAD mice was found compared with non-Tg mice (Figure 3.2A and B). Immunocytochemistry confirmed that the expression level of endophilin 1 was indeed increased in the Tg mAPP/ABAD transgenic animals as compared to the non-Tg (Figure 3.2C). To assess whether the observed increase in endophilin 1 expression was relevant in AD, they next screened human brain tissues.

By western blot analysis (Figure 3.3A) and immunocytochemistry (Figure 3.3B) again a consistent increase in endophilin 1 expression was observed in the temporal cortex of AD patients as compared to non-demented age matched controls.

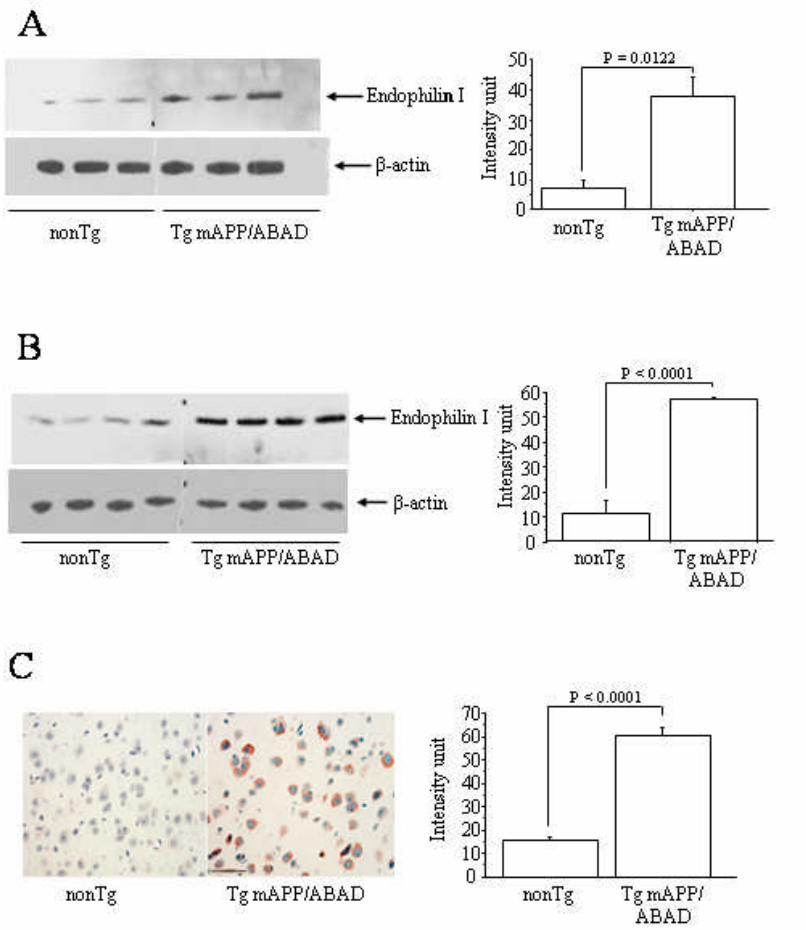

Figure 3.2 Confirmation that endophilin 1 is increased in Tg mAPP/ABAD mice. Western blot analysis of endophilin 1 and β-actin from hippocampus (A) and temporal cortex (B) of Tg mAPP/ABAD animals and non-Tg controls. Right panels of A and B denote the quantification of intensity of all immunoreative bands for endophilin 1 using NIH image program. N = 3-4 mice per group. (C) Immunocytochemistry expression of endophilin 1 in cerebral cortex from indicated transgenic mice. Right panel of C showed intensities of immunostaining for endophilin 1 by quantification with Universal image program (Figure supplied by Prof Shi Du Yan, College of Physicians and Surgeons, Columbia University).

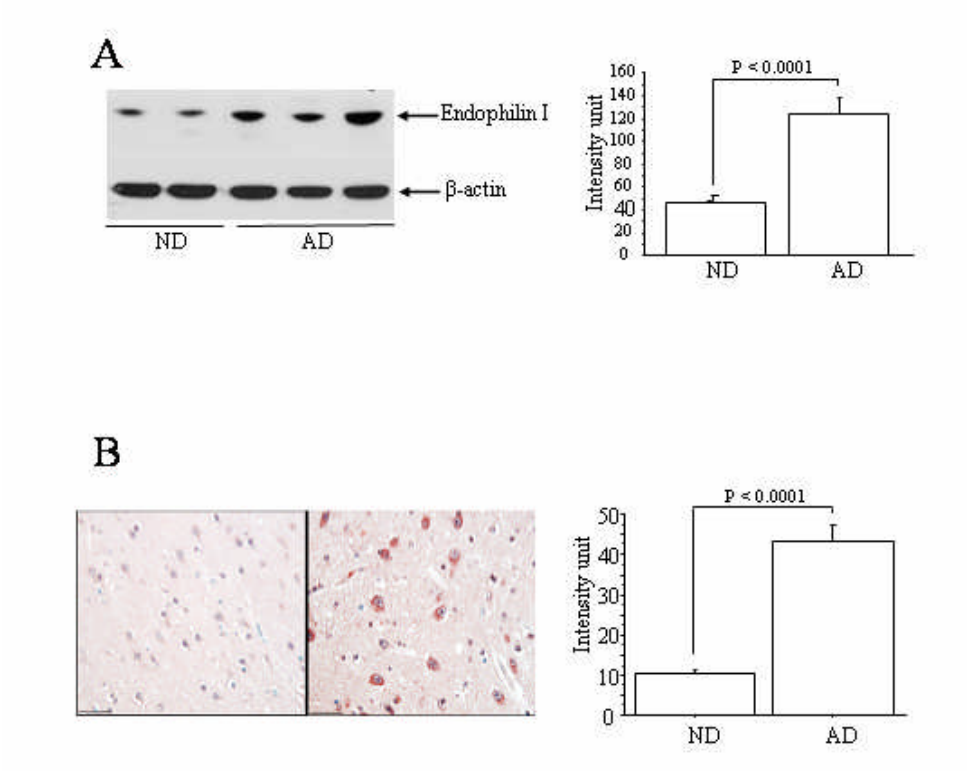

Figure 3.3 Confirmation that endophilin 1 is increased in the brains of AD patients. (A) Western blot analysis of endophilin 1 and β-actin from hippocampus and temporal cortex of Alzheimer's patients and non-demented age matched controls. Right panel indicates quantification of the intensity of immunoreactive bands for endophilin 1 by NIH image program. N = 5 per group. (B) Immunocytochemistry of endophilin I from hippocampus and temporal cortex of Alzheimer's patient and non-demented age matched control. Quantification of the intensity of immunostaining for endophilin I was performed by Universal image program. (Figure supplied by Prof Shi Du Yan, College of Physicians and Surgeons, Columbia University).

3.2 Aims of chapter

Our own and collaborators' work had indicated that endophilin 1 is up-regulated in its expression in the AD brain. Increased expression of endophilin 1 has never been associated with a disease but has been associated with an increase in JNK activity (Ramjaun *et al*. 2001). JNK activity itself has been associated with AD (Okazawa and Estus 2002). Therefore in this chapter, the role of endophilin 1 and JNK activity in both cell-lines and primary neuronal cultures was explored

3.3 Results

3.3.1 Endophilin 1 regulates GLK mediated JNK activation in HEK293 cells

Initially the experiments performed by Ramjaun *et al*. 2001 which demonstrated that endophilin 1 regulates GLK induced JNK activation in HEK293 cells were repeated (Ramjaun *et al*. 2001). The level of activated JNK was monitored with an anti-phospho-JNK antibody.

Plasmids expressing FLAG-GLK, FLAG-JNK, Endophilin 1 full length, Delta SH3 and GFP-SH3 were kindly provided by Prof McPherson (Department of Neurology and Neurosurgery, McGill University). The FLAG epitope, which is an eight amino acid peptide (AspTyrLysAspAspAspAspLys), is tagged to the N-terminus of GLK and JNK respectively for protein expression verification. Since the molecular weight of FLAG-GLK and FLAG-JNK is 100 kDa and 45 kDa respectively, using anti-FLAG antibody (Sigma), the expression of both FLAG-GLK and FLAG-JNK

can be identified. The plasmids expressing endophilin 1 full length and delta SH3 are expressed on a pCDNA3 vector background whilst the GFP-SH3 fusion protein is expressed on a pEGFPN2 vector background (Figure 3.4 and Figure 3.5). pEGFPN2 and pEGFPN3 are two plasmids from clontech which encode a red-shifted variant of wild-type GFP (EGFP) which has been optimized for brighter fluorescence and higher expression in mammalian cells. (Excitation maximum = 488 nm; emission maximum = 507 nm.). The only difference between these two plasmids is that in the region of multiple cloning sites immediately before EGFP sequence, pEGFPN3 has a Xcm 1 site whereas pEGFPN2 contains a Eag 1 site.

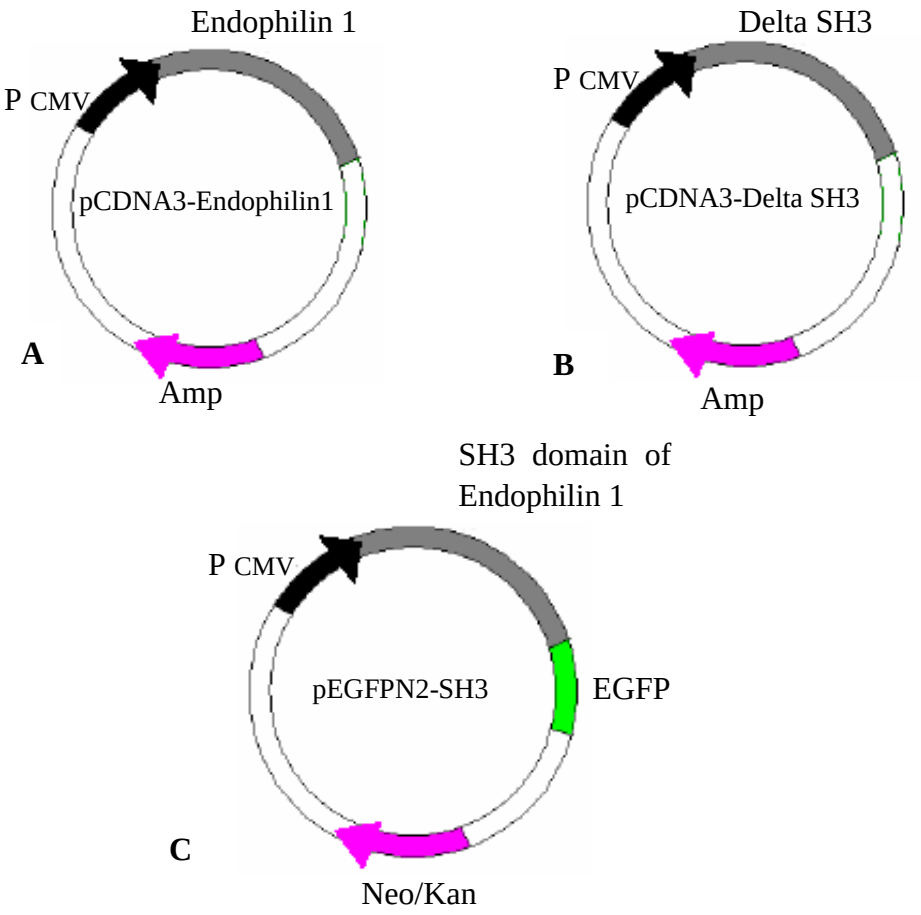

Figure 3.4 The plasmids expressing endophilin 1 full length (A) delta SH3 domain of endophilin 1 (B) are expressed on a pCDNA3 vector background whilst the GFP-SH3 fusion protein is expressed on a pEGFPN2 vector background (C).

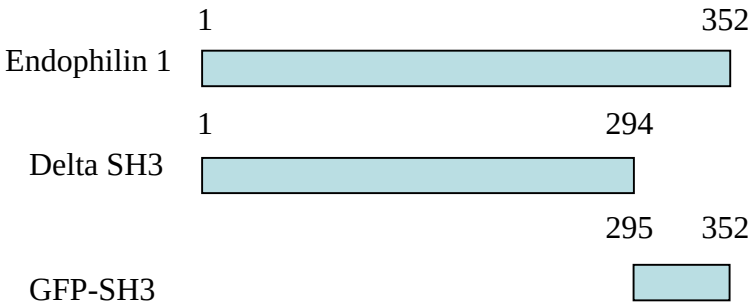

Figure 3.5 Endophilin 1 constructs used in the experiments, showing full-length and truncated versions of endophilin 1.

HEK293 cells were seeded onto 60 mm petri dishes and cultured until reaching 60-80% confluency. The cells were then transfected using the lipofectamine method (section 2.2.5) with the following combinations of plasmids: 2 μg pEGFPN3 control vector; 2 μg FLAG-GLK + 2 μg FLAG-JNK; 2 μg FLAG-GLK + 2 μg FLAG-JNK + 2 μg Endophilin 1; 2 μg FLAG-GLK + 2 μg FLAG-JNK + 2 μg GFP-SH3 (plasmid encoding for EGFP tagged SH3 domain of endophilin 1). After 48 hours, the cells were lysed in 2X SDS sample buffer. After sonication and boiling, proteins were separated on a mini 4-12% Bis-Tris gel. The separated proteins were transferred to a nitrocellulose membrane. The membrane was blocked with 5% fat-free dry milk in TBS/T overnight and washed in TBS/T for ten minutes. The nitrocellulose blot was incubated with phospho-JNK (Thr183/Tyr185) antibodies in TBS/T+5% fat-free milk for one hour. After three five-minute washes in TBS/T, the blot was incubated with an HRP-conjugated anti-mouse secondary antibody raised in goat for one hour. The immunoreactive bands were then detected with ECL detection reagents and quickly exposed to an autoradiography film. The membrane was stripped and reprobed with β-actin antibody to control for equal loading. To confirm similar expression levels of FLAG-JNK, the blot was also stripped and reprobed again with anti-FLAG antibody. The results shown in Figure 3.6 were consistent with previous published results: overexpression of GLK and JNK induced activation of the 46 kDa isoform of JNK and overexpression of endophilin 1 with GLK and JNK led to a further increase of the activation of 46 kDa JNK. In contrast, overexpression of GFP-SH3 along with GLK and JNK suppressed

activation of 46 kDa JNK.

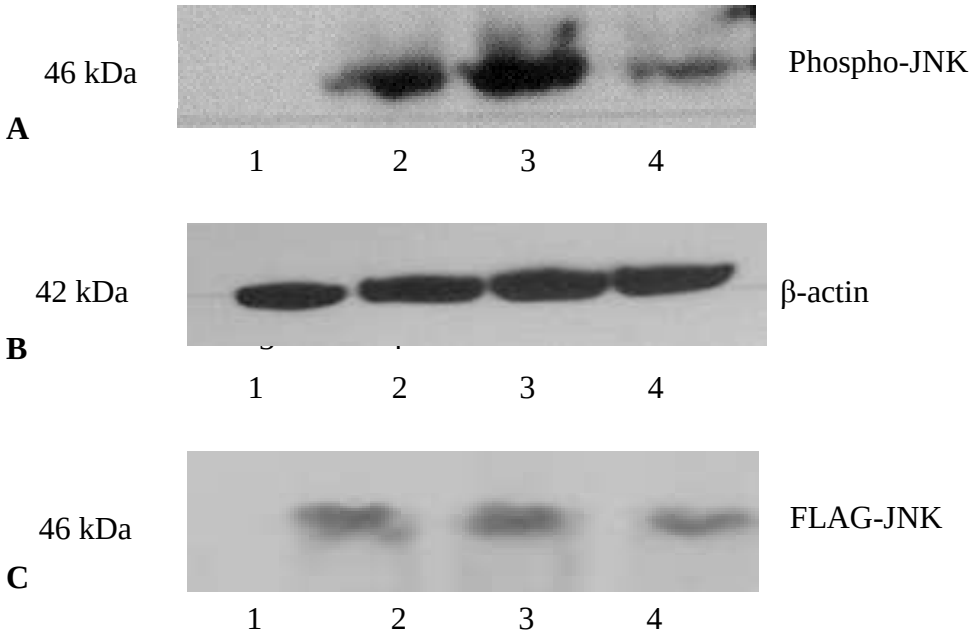

Figure 3.6 Endophilin 1 regulates GLK mediated JNK activation. JNK activity was examined by western blotting using an antibody that recognizes phosphorylated JNK. HEK293 cells were transfected with 2 μg pEGFPN3 control vector (Lane 1), 2 μg FLAG-GLK + 2 μg FLAG-JNK (Lane 2), 2 μg FLAG-GLK + 2 μg FLAG-JNK + 2 μg Endophilin 1 (Lane 3), and 2 μg FLAG-GLK + 2 μg FLAG-JNK + 2 μg GFP-SH3 (Lane 4). 48 hours following transfections, the cells were harvested and processed for Western blot analysis. The subsequent blot was probed with anti-phospho-JNK 1:2000 and secondary anti-mouse-HRP 1:5000 (A) and then stripped and reprobed for β-actin 1:5000 and secondary anti-mouse-HRP 1:5000 (B) to control for equal protein loading. To control for similar expression levels of FLAG-JNK, the blot was stripped and reprobed again with anti-FLAG antibody1:5000 and secondary anti-mouse-HRP 1:5000 (C). Transfection efficiency is approximately 70–80% in this study. The experiments were repeated twice.

3.3.2 Involvement of endophilin 1 in oxidative stress induced JNK activation

Previously Marques *et al*. 2003 used a stable PC12 cell line overexpressing APP containing the Swedish mutation (APPsw PC12) as an in vitro model for AD. APPsw PC12 cells exhibited a moderate expression of human APP leading to

increased levels of Aβ production (90pg/ml) which is close to the situation in vivo (Marques *et al*. 2003). After exposure to H_2O_2, APPsw PC12 cells displayed an increase in 46 kDa JNK activation as compared to PC12cells transfected with a control vector. H_2O_2 treatment of APPsw PC12 cells evoked phosphorylation of the 46 kDa JNK within two hours and the highest level of phosphorylated JNK was detected after four hours (Marques *et al.* 2003). These data collectively indicated that overexpression of APPsw rendered PC12 cells more sensitive to activation of the 46 kDa isoform of JNK after exposure to an oxidative stress.

A SH-SY-5Y stable cell line overexpressing APP-Swedish mutation (APPsw SH-SY-5Y) was a kind gift from Dr Richard Killick (Institute of Psychiatry, King's College London). Firstly, it was examined if, as with APPsw PC12 cells, that after H_2O_2 treatment, APPsw SH-SY-5Y cells also display a higher expression level of activated JNK as compared to SH-SY-5Y cells transfected with a control vector (pEGFPN3).

Following this, the role of endophilin 1 in JNK activation induced by oxidative stress in APPsw SH-SY-5Y cells was to be studied by transfecting dominant negative forms of endophilin 1 (DN-endophilin1) including the SH3 domain deleted form of endophilin 1 (delta SH3) and GFP-SH3 into APPsw SH-SY-5Y cells.

3.3.2.1 H_2O_2 treatment induces increased JNK activation in APPsw SH-SY-5Y cells

Initially, the effects of H_2O_2 on the JNK activation pathway in APPsw SH-SY-5Y cells were studied. SH-SY-5Y cells were transfected with the pEGFPN3 empty

vector. Transfected SH-SY-5Y cells and untransfected APPsw SH-SY-5Y cells were seeded onto petri dishes at a density of $2x10^6$ cells/culture dish (60 mm). 48 hours after transfection, cells were treated with H_2O_2 (freshly prepared solution; 250 μM). Marques *et al.* 2003 demonstrated that maximal JNK activation was detected after 4 hours exposure to H_2O_2 in APPsw PC12 cells, so it was decided to harvest cells after 4 hours treatment with H_2O_2. The cells were lysed in 2X SDS sample buffer and loaded onto a 4-12% mini polyacrylamide gel for electrophoresis followed by protein transfer to a nitrocellulose membrane. Proteins were visualized with anti-phospho-JNK antibody as described in section 3.3.1. The membrane was stripped and reprobed with an antibody to β-actin as an internal loading control. Similar to the data shown previously, APPsw SH-SY-5Y cells, after 4 hours exposure to H_2O_2, exhibited enhanced expression level of activated 46 kDa JNK as compared to control vector transfected SH-SY-5Y cells (Figure 3.7).

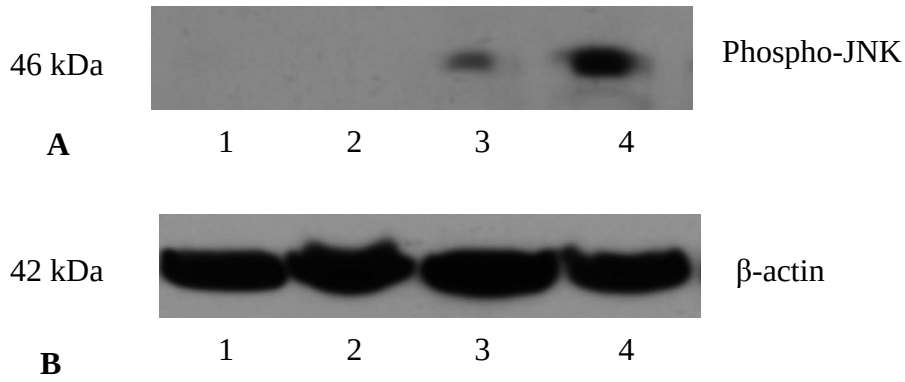

Figure 3.7 4 hours treatment of H_2O_2 led to an enhanced activation of 46 kDa JNK in APPsw SH-SY-5Y cells. SH-SY-5Y cells were transfected with 2 μg pEGFPN3 empty vector (Lane 1 and Lane 3). 48 hours following transfections, SH-SY-5Y cells (Lane 3) and APPsw SH-SH-5Y cells (Lane 4) were treated with 250 μM H_2O_2 for 4 hours. Lane 2 denotes APPsw SH-SY-5Y cells without treatment. The cells were then harvested in 2X SDS sample buffer and processed for Western blot. The blot was probed with anti-phospho-JNK 1:2000 and secondary anti-mouse-HRP 1:5000 (A) and stripped and reprobed for β-actin 1:5000 and secondary anti-mouse-HRP 1:5000 (B) to control for equal protein loading. Transfection efficiency is approximately 40–50% in this study. The experiments were repeated twice.

3.3.2.2 Expression of DN-endophilin1 has no effects on JNK activation

Next, the role of endophilin 1 in oxidative stress induced JNK activation was studied. If endophilin 1 contributes to the increased JNK activation in APPsw SH-SY-5Y cells under oxidative stress condition, then expression of DN-endophilin 1 would attenuate JNK activation.

APPsw SH-SY-5Y cells were transfected either with the pEGFPN3 vector or with GFP-SH3 using the Amaxa nucleofector system according to the protocol detailed in section 2.2.5. Transfected APPsw SH-SY-5Y cells were cultured for 24 hours and then subjected to treatment of 250 μM H_2O_2. 4 hours later, the cells were

harvested in 2X SDS buffer and loaded onto a 4-12% mini Bis-Tris gel for electrophoresis and transfer. The blot was subjected to immunodetection of phosphorylated JNK expression (section 3.3.1). The membrane was striped and reprobed with β-actin antibody as a control for equal loading. To verify that GFP-SH3 was transfected and expressed, the blot was stripped again and reprobed with an anti-GFP antibody. As shown in Figure 3.8, equal amounts of protein were loaded onto the protein gel. A protein band around 45 kDa corresponding to the molecular weight of GFP-SH3 was observed in APPsw SH-SY-5Y cells transfected with GFP-SH3. In two other lanes, as expected, no immunoblot bands around 45 kDa were detected. APPsw SH-SY-5Y showed an increased expression of activated 46 kDa JNK. However, the expression level of activated 46 kDa JNK in GFP-SH3 transfected APPsw SH-SY-5Y cells was comparable with that seen in APPsw SH-SY-5Y cells transfected with a pEGFPN3 empty vector. Therefore, expression of GFP-SH3 did not appear to affect the activation of the 46 kDa isoform of JNK in response to H_2O_2 treatment (Figure 3.8).

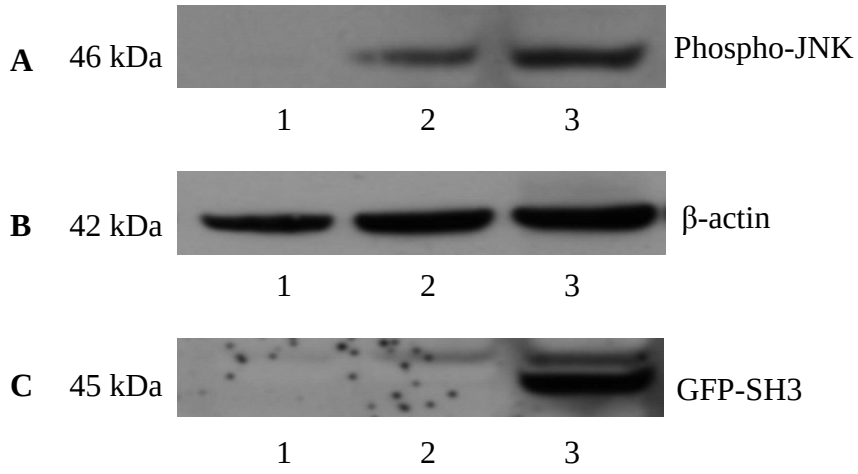

Figure 3.8 Expression of GFP-SH3 did not attenuate H_2O_2 induced activation of the 46 kDa isoform of JNK. APPsw SH-SY-5Y cells were transfected with 2 μg pEGFPN3 empty vector (Lane 1 and Lane 2) or GFP-SH3 (Lane 3). 48 hours following transfections, APPsw SH-SH-5Y cells (Lane 2 and Lane 3) were treated with 250 μM H_2O_2 for 4 hours. The cells were then harvested in 2X SDS sample buffer and processed for Western blot. The blot was probed with anti-phospho-JNK 1:2000 and secondary anti-mouse-HRP 1:5000 (A) and stripped and reprobed for β-actin 1:5000 and secondary anti-mouse-HRP 1:5000 (B) to control for equal protein loading. To verify the expression of GFP-SH3, the blot was stripped and reprobed again with anti-GFP antibody 1:5000 and secondary anti-mouse-HRP 1:5000 (C). Transfection efficiency is approximately 40–50% in this study. The experiments were repeated twice.

This result indicated that endophilin1 is not involved in the elevated JNK activation in APPsw SH-SY-5Y cells under oxidative stress condition. However, endophilin 1 expression had previously been linked to JNK activation via GLK mediated process (Ramjaun *et al.* 2001). Expression of GLK has been detected in a variety of tissues such as heart, kidney and brain. Also, GLK expression has been observed in several cell lines such as HEK293 and HeLa cell lines (Diener *et al.* 1997). Expression of GLK in SH-SY-5Y cells, however, has not been studied yet. Therefore, the reason why expression of GFP-SH3 had no effects on H_2O_2 induced JNK activation could

be because of low or no expression of GLK in SH-SY-5Y cells.

3.3.3 Endophilin 1 regulates Aβ induced JNK activation in cortical neurons

Extracellular Aβ has been reported to induce an enhanced activation of the 46kDa isoform of JNK in primary cortical neurons. The highest level of JNK activity was detected after exposure to Aβ for 8 hours (Morishima *et al.* 2001). Given these findings, and that GLK is expressed in the brain (Diener *et al.* 1997), primary cortical neuronal cultures were used to study if endophilin 1 contributes to extracellular Aβ induced JNK activation.

3.3.3.1 Aβ peptides induces JNK activation in cortical neurons

Initially, the experiments which showed that treatment of cortical neurons with Aβ induced an increased activation of 46 kDa JNK were repeated (Morishima *et al.* 2001). Primary neuronal cultures of embryonic age 14 days (E14) CD1 wild-type mice were generated following the protocols described in section 2.2.3. E14 cortical neurons were seeded onto 35 mm petri dishes pre-coated with poly D-lysine at a density of 500,000 cells per well. 24 hours later, the culture medium was replaced by serum free medium with B27 supplement. Following a further 72 hours, aged Aβ25-35 peptides (50 μM), which were prepared according to the protocol described in section 2.2.4, were added to experimental wells. Since Morishima *et al.* 2001 showed that maximum JNK activation was detected 8 hours after exposure to Aβ peptides, neurons were harvested in kinase buffer at 8 hours time point

following the protocol detailed in section 2.4.1. Protein extracts were quantified using Bradford method as described in section 2.4.3. Equal amounts of proteins were loaded onto a 4-12% SDS-PAGE mini gel for electrophoresis. The proteins were subsequently transferred to a nitrocellulose membrane. The membrane was then subjected to immunoblot detection of anti-phospho-JNK. To control for equal loading, the blot was stripped and reprobed again with β-actin antibody. In the control condition, a 46 kDa phospho-JNK immunoblot band was detected, demonstrating a basal level of JNK activation. However, in cells treated with Aβ, a higher expression level of 46 kDa phospho-JNK was observed. Consistent with the published data, 50 μM of pre-aggregated Aβ resulted in an enhanced activation of the 46 kDa isoform of JNK at 8 hours time point (Figure 3.9).

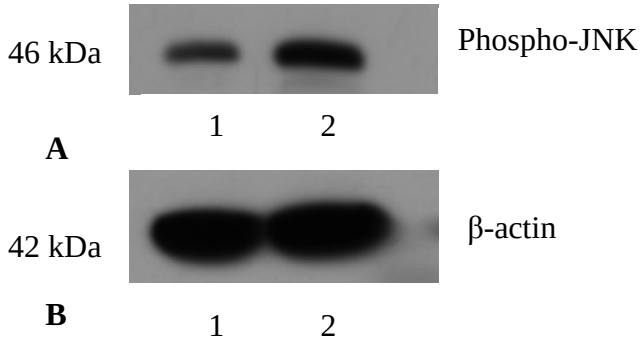

Figure 3.9 Aβ induced elevated JNK activation (46 kDa) in cortical neurons. Untreated cortical neurons (Lane 1) and cortical neurons (Lane 2) which were exposed to pre-aggregated Aβ25-35 (50 μM) for 8 hours, were harvested in kinase buffer. The proteins were loaded onto a mini 4-12% Bis-Tris gel and transferred to a nitrocellulose membrane. The membrane was probed with anti-phospho-JNK 1:2000 and secondary anti-mouse-HRP 1:5000 (A) and stripped and reprobed for β-actin 1:5000 and secondary anti-mouse-HRP 1:5000 (B) to control for equal protein loading. Transfection efficiency is approximately 30–40% in this study. The experiments were repeated for five times.

3.3.3.2 The role of endophilin 1 in Aβ induced JNK activation

Having successfully demonstrated that Aβ induced increased JNK activation in primary cortical neurons, the next question was: is endophilin 1 involved in the JNK activation pathway induced by Aβ? To answer this question, the effects of overexpression of endophilin 1 and two forms of DN-endophilin 1 (the GFP-SH3 and delta SH3 constructs) on Aβ induced JNK activation were studied. If, as in HEK293 cells, endophilin 1 plays a regulating role in JNK activation, then in cortical neurons, overexpression of endophilin 1 will lead to an increase in the level of activated JNK, whereas expression of DN-endophilin 1 will attenuate Aβ induced JNK activation. In this study, using the immunoblotting method, the level of activated JNK was monitored with anti-phospho-JNK antibody whilst the total expression level of JNK was evaluated using an anti-JNK monoclonal antibody. Since endophilin 1 and delta SH3 are expressed in pCDNA3 vector and GFPSH3 is expressed in pEGFPN2 vector, cortical neurons were transfected with pCDNA3 and pEGFPN3 empty vectors as controls. To investigate the function of endophilin 1 in Aβ induced JNK activation, E14 neuronal cultures were transfected with endophilin 1 or the two forms of DN-endophilin 1, GFP-SH3 and delta SH3.

$4X10^6$ neurons were nucleofected with 2 μg DNA (pEGFPN3, pCDNA3, endophilin 1 full length, delta SH3, GFP-SH3) using the Amaxa mouse neuron nucleofector kit according to the protocol described in section 2.2.5. Transfected neurons were then seeded onto 35 mm poly D-lysine coated petri dishes at a density of $1X10^6$ neurons per well. 24 hours later, culture medium was replaced by serum

free medium with B27 supplement. Following a further 72 hours, aged Aβ peptides were added to experimental wells at a concentration of 50 μM. 8 hours after Aβ treatment, neurons were harvested in kinase buffer (section 2.4.1.), sonicated for four times, five seconds each and then centrifuged for 15 minutes at 13,000 rpm, 4°C. The protein concentrations of the supernatants were determined using Bradford assay (Section 2.4.3). Equal amounts of lysate proteins were run on a 4-12% precast Bis-Tris gel and transferred to a nitrocellulose membrane. The nitrocellulose blot was blocked with 3% BSA in TBS/T for one hour and then incubated with primary antibody anti-phospho-specific-JNK in TBS/T containing 3% BSA at 4°C overnight. After three five-minute washes in TBS/T, the blot was incubated with secondary antibody anti-mouse HRP for one hour. The blot was then washed in TBS/T for three times, five minutes of each, and subjected to ECL reagents for immune-reactivity detection. The membrane was stripped and reprobed with anti-JNK antibody following the same protocol for phospho-JNK antibody apart from that secondary antibody anti-rabbit HRP was used instead of anti-mouse HRP (Figure 3.10).

Each experiment was repeated three times using different animal tissues. The intensities of the immunoblot bands for all three experiments were quantified using ImageJ software. To control for internal variation, the levels of the phospho-JNK bands were normalized to corresponding total 46 kDa JNK expression levels. The results of the normalized expression of phospho-JNK under different conditions are expressed as means ± S.E.M. from three independent experiments and summarized

in Table 3.1. Statistical test was performed using student's t test. A significance level at $p<0.05$ was used. The P values for each comparison between different conditions are displayed in Table 3.2.

In the absence of Aβ, cortical neurons overexpressing endophilin 1 exhibited a significant increase in the activation of the 46 kDa JNK as assessed by normalized expression of phospho-JNK compared to neurons transfected with a pEGFPN3 empty vector or a pCDNA3 empty vector. 8 hours of Aβ treatment caused an elevated activation of the 46 kDa isoform of JNK in neurons transfected with pEGFPN3 empty vector or pCDNA3 empty vector. After Aβ treatment, JNK activation in cells transfected with endophilin 1 was also significantly increased compared to neurons transfected with pEGFPN3 empty vector or pCDNA3 empty vector without Aβ treatment. However, in the presence of Aβ, the level of activated 46 kDa JNK in neurons transfected with endophilin 1 was comparable with that in cells transfected with pEGFPN3 or pCDNA3 vectors. In contrast, expression of GFP-SH3 and delta SH3 markedly abolished JNK activation (46 kDa) in cortical neurons (Figure 3.10).

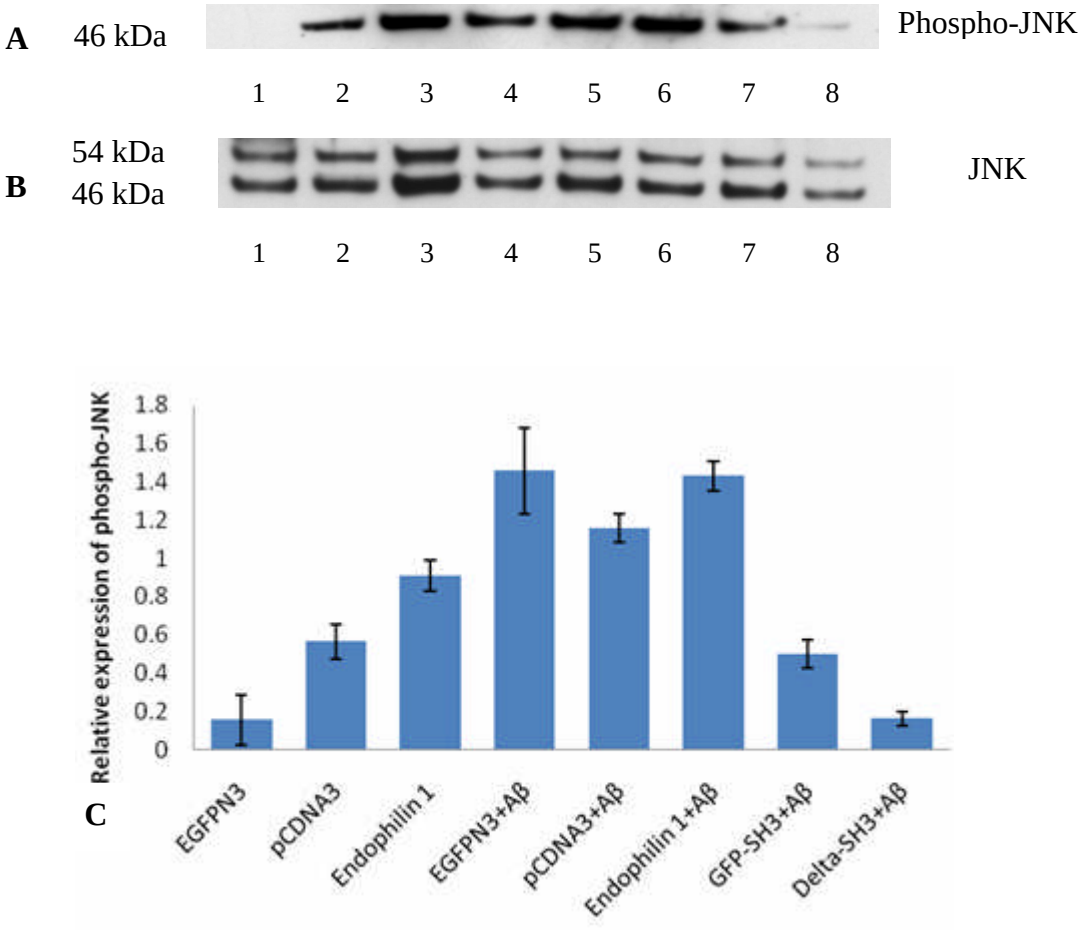

Figure 3.10 The role of endophilin 1 in Aβ induced JNK activation in cortical neurons. Western blotting analysis was performed using anti-phospho-JNK and anti-JNK antibodies for the analysis of activated JNK and total JNK expression. Cortical neurons were transfected with pEGFPN3 (Lane 1 and Lane 4), pCDNA3 (Lane 2 and Lane 5), endophilin 1 (Lane 3 and Lane 6), GFP-SH3 (Lane 7), and delta SH3 (Lane 8). 4 days after transfection, neurons were treated with 50 μM pre-aggregated Aβ for 8 hours (Lane 4, 5, 6, 7, and 8). The cells were then harvested in kinase buffer. Equal amounts of proteins for each sample were loaded onto a 4-12% Bis-Tris mini gel for electrophoresis and immunoblotting. The blot was subjected to immunodetecton with anti-phospho-JNK (A). The blot was stripped and reprobed with anti-JNK to assess total JNK expression level (B). Representative Western blotting images are shown from three independent observations. (C) Immunoblott bands were quantified using ImageJ software. Normalized expression of phosphor-JNK was compared between different conditions. Results are expressed as means ± S.E.M. Without Aβ, neurons transfected with endophilin 1 exhibited an enhanced expression level of phospho-JNK compared to EGFPN3 and pCDNA3 transfected cells. Aβ evoked an enhanced expression of activated JNK in neurons transfected with EGFPN3 or pCDNA3. After Aβ treatment, overexpression of endophilin 1 also displayed a

significant increase in JNK activation compared to cells transfected with EGFPN3 vector or pCDNA3 vector without Aβ treatment. However, after Aβ treatment, the expression of activated JNK in neurons transfected with endophilin 1, neurons transfected with EGFPN3 and neurons transfected with pCDNA3 was comparable. In contrast, the expression of phospho-JNK was markedly reduced in neurons transfected with GFP-SH3 or delta SH3. Transfection efficiency is approximately 30–40% in this study.

	Relative expression of phospho-JNK
EGFPN3	0.16 ± 0.13
pCDNA3	0.56 ± 0.09
Endophilin 1	0.90 ± 0.08
EGFPN3+Aβ	1.46 ± 0.22
pCDNA3+Aβ	1.15 ± 0.08
Endophilin 1+Aβ	1.43 ± 0.08
GFP-SH3+Aβ	0.50 ± 0.08
Delta-SH3+ Aβ	0.16 ± 0.04

Table 3.1 Immunoblot bands were quantified using ImageJ software. Results are expressed as normalized expression of phospho-JNK. Values displayed are means ± S.E.M.

	Endophilin 1	EGFPN3+Aβ	pCDNA3+Aβ	Endophilin1+Aβ
EGFPN3	P=0.025	P=0.0031		P=0.00059
pCDNA3	P=0.04		P=0.0036	P=0.001
GFP-SH3+Aβ		P=0.003		P=0.0002
Delta-SH3+Aβ			P<0.0001	P<0.0001

Table 3.2 Student's t test was used to analyze statistical significance between two different conditions. The P values for all comparisons are summarized in Table 3.2.

3.3.3.3 The involvement of endophilin 1 in Aβ induced apoptosis

Increased JNK activation triggered by Aβ has been associated with cell death. Overexpression of several dominant negative forms of JNK has been reported to increase cell viability significantly (Marques *et al.* 2003; Morishima *et al.* 2001). Data in section 3.3.3.2 showed that expression of endophilin 1 caused an increase in JNK activation whereas overexpression of two dominant negative forms of endophilin 1 significantly reduced Aβ induced JNK activation. Based on these data, it was proposed that overexpression of endophilin 1 can cause JNK activation, which in turn results in increased cell death. In contrast, expression of two forms of DN-endophilin 1 can attenuate JNK activation and thus increase cell viability. To test this hypothesis, in collaboration with Dr Fleur Davey from our group, cell survival assays were performed to study if endophilin 1 is involved in Aβ induced cell death.

E14 cortical neurons were transfected with 2 μg each of pEGFPN3, pCDNA3, endophilin 1, GFP-SH3 or delta SH3 constructs respectively. Transfected cells were then seeded onto poly-D-lysine coated 96 well plates at a density of 200 cells per well. After 24 hours, cell medium was replaced with serum free medium. The neurons were serum starved for 72 hours, upon which time points, 50 μM of pre-aggregated Aβ25-35 peptides were applied. 24 hours after Aβ treatment, cells were fixed and DAPI stained. The total number of live cells (as assessed by DAPI staining) per well at the completion of the trial, was counted. Each experiment was performed three times. In each experiment, control and Aβ treated cultures were set up in triplicate.

The numbers of viable cells under different conditions are summarized in Table 3.3. Results are expressed as means ± S.E.M. from three independent experiments. Statistical significance was analyzed using student's t test. The P values for each comparison made between different conditions are shown in Table 3.4. Overexpression of endophilin 1 in cortical neurons significantly reduced cell viability as compared with neurons transfected with control vectors (pEGFPN3 or pCDNA3). After 24 hours treatment of Aβ, neurons transfected with endophilin 1, pEGFPN3, or pCDNA3 all exhibited a marked decrease of cell viability compared to cells transfected with pEGFPN3 or pCDNA3 without Aβ treatment. However, after Aβ treatment, no significant difference in cell viability between neurons transfected with endophilin 1, EGFPN3, or pCDNA3 was detected. In contrast, after exposure to Aβ for 24 hours, neurons expressing GFP-SH3 or delta SH3

displayed a significantly enhanced cell number as compared with cells transfected with endophilin 1, pEGFPN3, or pCDNA3 (Figure 3.11).

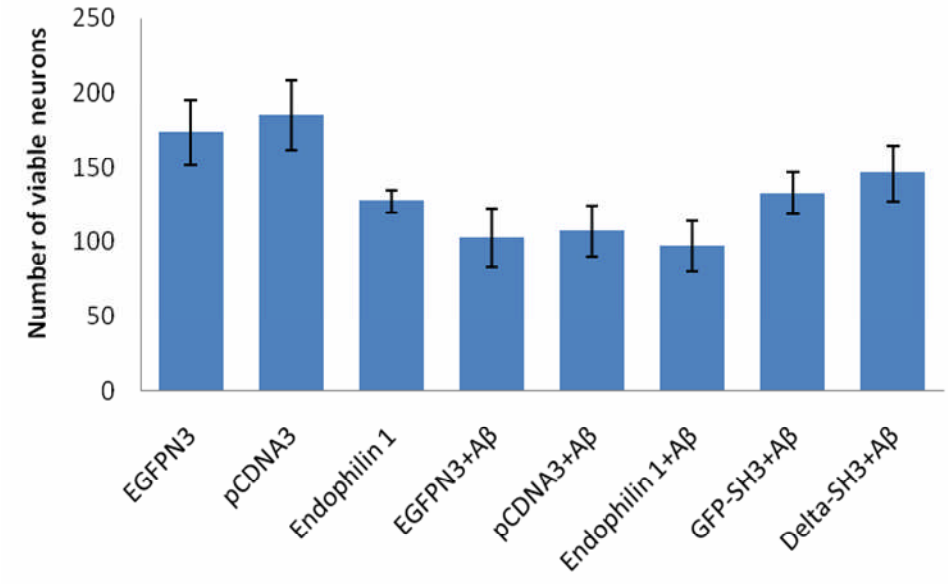

Figure 3.11 The role of endophilin 1 in Aβ induced neuron death. Cortical neurons were transfected with pEGFPN3, pCDNA3, endophilin 1, GFP-SH3 or delta SH3. 4 days after transfection, neurons were treated with 50 μM pre-aggregated Aβ for 24 hours. Total number of live neurons counted by DAPI-stained nuclei is expressed as means ± S.E.M. and analyzed using student's t test. Significance level was set at $p<0.05$. Overexpression of endophilin 1 without Aβ induced decreased viable neuron numbers. For neurons transfected with pEGFPN3, pCDNA3 and endophilin 1, 24 hours treatment of Aβ led to a significant decrease of neuron viability. In contrast, expression of GFP-SH3 or delta SH3 protected neurons from Aβ induced cell death. Transfection efficiency is approximately 30–40% in this study.

	Number of viable neurons per well
pEGFPN3	174 ± 22
pCDNA3	185 ± 24
Endophilin 1	127 ± 8
pEGFPN3+Aβ	103 ± 20
pCDNA3+Aβ	107 ± 18
Endophilin 1+Aβ	97 ± 17
GFP-SH3+Aβ	133 ± 14
Delta-SH3+Aβ	146 ± 19

Table 3.3 The numbers of viable neurons under different conditions. Values are expressed as means ± S.E.M.

	Endophilin 1	EGFPN3+Aβ	pCDNA3+Aβ	Endophilin 1+Aβ
pEGFPN3	P=0.007	P=0.0004		P=0.0001
pCDNA3	P=0.003		P=0.0001	P<0.0001
GFP-SH3+Aβ		P=0.024		P=0.006
Delta-SH3+Aβ			P=0.009	P=0.002

Table 3.4 The statistical difference between different conditions was analyzed using student's t test. The P values for each comparison are summarized in Table 3.4.

3.4 Discussion

3.4.1 ABAD-Aβ interaction causes an increase in the expression of endophilin 1

Two dimensional electrophoresis analysis of cortex from different genotypes of mice revealed that endophilin 1 was upregulated in Tg mAPP and Tg mAPP/ABAD mice as compared to non-Tg littermates and Tg ABAD mice. Using Western blotting, the proteomic results were confirmed. Furthermore, expression of endophilin 1 was also found to be increased in the brains of AD patients as compared to age matched non-demented control brain tissues.

3.4.2 Endophilin 1 is involved in Aβ induced JNK activation pathway

Endophilin 1 has been reported to regulate GLK mediated JNK activation (Ramjaun *et al.* 2001). To examine if endophilin 1 induced JNK activation cascade is involved in the pathogenesis of AD, two in vitro models of AD were used.

The first model was a stable SH-SY-5Y cell line overexpressing APP Swedish mutation (APPsw SH-SY-5Y). Oxidative stress induced an increased expression of activated 46 kDa JNK in APPsw SH-SY-5Y cells compared to SH-SY-5Y cells transfected with a control vector (Figure 3.7). To examine if endophilin 1 contributes to the increased JNK activation in APPsw SH-SY-5Y cells under oxidative stress condition, APPsw SH-SY-5Y cells were transfected with GFP-SH3, a dominant negative form of endophilin 1. There were no differences in the expression level of activated JNK between APPsw SH-SY-5Y cells transfected with GFP-SH3 and APPsw SH-SY-5Y cells transfected with a pEGFPN3 control vector

after H_2O_2 treatment (Figure 3.8). Therefore, expression of GFP-SH3 did not affect H_2O_2 induced JNK activation in APPsw SH-SY-5Y cells. It is possible that none or very low level of GLK expression in SH-SY-5Y cells is responsible for this result. GLK expression has been detected in brain tissue (Diener *et al.* 1997). Moreover, extracellular Aβ has been shown to cause elevated JNK activation in primary cortical neurons (Morishima *et al.* 2001). Therefore, E14 mice cortical neuronal cultures were used as the second in vitro model. Application of aggregated Aβ induced elevated 46kDa JNK activation and cell death in primary mouse cortical neurons. In the absence of Aβ treatment, there was an increase in the expression level of phospho-JNK in mouse cortical neurons transfected with endophilin 1 compared to cortical neurons transfected with control vectors. Expression of DN-endophilin 1, including delta SH3 and GFP-SH3, however, led to a significant reduction of Aβ induced JNK activation (Figure 3.10). Cortical neurons overexpressing endophilin 1 showed exaggerated cell death as compared to cortical neurons transfected with control vectors. In contrast, expression of GFP-SH3 and delta SH3 in cortical neurons protected neurons from Aβ induced cell death (Figure 3.11).

These results suggested that endophilin 1 expression can regulate the JNK cascade and thus contribute to the increased JNK activation and cell death in cortical neurons after Aβ treatment. Thus, the increased expression of endophilin 1 may be partially responsible for the increased JNK activation and neuron death in AD.

The exact isoform of JNK responsible for the increased activation after exposure to

Aβ peptides remains to be established. Aβ induced increased activation of the 46 kDa isoform of JNK in cortical neuronal culture whereas in AD, both 46 kDa and 54 kDa isoforms of JNK were increased as compared to non-demented controls (Zhu *et al.* 2001). One study showed that JNK3 null mice displayed a significant reduction of Aβ induced apoptosis in cortical neurons. However, the Aβ induced neurotoxicity was not completely abolished in cortical neurons indicating that JNK1 and JNK2 may also be involved (Morishima *et al.* 2001).

3.4.3 Multiple functions of Endophilin 1

This is the first report demonstrating that endophilin 1 is associated with Alzheimer's disease. Endophilin 1 is a multifunctional protein. It is involved in synaptic vesicle formation by binding to other endocytic proteins such as synaptojanin and dynamin through its SH3 domains (Reutens and Begley 2002). Endophilin 1 can also affect intracellular biochemical events via complexing with signaling molecules such as CIN85 and G-protein-coupled β1-adrenergic receptor (section 1.4.1).

Endophilin 1 has been reported to regulate GLK-mediated JNK activation (Ramjaun *et al.* 2001). In this study, endophilin 1 induced JNK activation signalling cascade was shown to be involved in the pathogenesis of AD. Several of the other functions of endophilin 1 may also be involved in the pathogenesis of AD. For example, endophilin 1 can bind to SH3-domain GRB2-like (endophilin) interacting protein 1, which has been identified as a neuronal protein that regulates energy

balance (Trevaskis *et al.* 2005). A change in the overall energy balance is known to be an important factor in the pathogenesis of Tg mAPP/ABAD animals and also in patients with Alzheimer's disease (Takuma *et al.* 2005). Furthermore, endophilin 1 has been reported to increase the production of Aβ (Schobel *et al.* 2006).

3.4.4 Blocking the interaction of Aβ with ABAD can reverse the expression level of endophilin 1

Structural studies of ABAD indicated that residues 94-114 of ABAD interact with Aβ (Powell *et al.* 2000). A peptide spanning this region of ABAD inhibited ABAD-Aβ interaction *in vitro* and protected primary neuronal cultures from Aβ-induced cytotoxicity. This peptide had been modified further by the addition of the cell membrane transduction domain of the human immunodeficiency virus-type 1 Tat protein fused with a mitochondrial matrix protein targeting sequence to produce Tat-mito-ABAD-DP (Lustbader *et al.* 2004). This chimeric peptide was then used in living animals by intra-peritoneal injection which leads to a subsequent improvement in the transgenic animals learning and memory (Yao *et al.* 2007). Therefore, in a subsequent experiment to determine whether endophilin 1 expression is directly due to Aβ-ABAD interaction, Prof ShiDu Yan's group (College of Physicians and Surgeons, Columbia University) injected intra-peritoneally either the forward (Tat-mito-ABAD-DP) or the reverse peptides (Tat-mito-ABAD-RP) into Tg mAPP/ABAD animals. Western blot analysis of the proteins from hippocampus of Tg mAPP/ABAD animals of 6 months of age,

showed a significant increase in the expression level of endophilin 1 as compared to non-Tg animals using β-actin as control. Tg mAPP/ABAD animals treated with the reverse peptide (Tat-mito-ABAD-RP) also showed an elevated level of endophilin 1. However, in those animals that were treated with Tat-mito-ABAD-DP, the expression of endophilin 1 was significantly decreased (Figure 3.12). These data indicated that the increased expression of endophilin 1 is a result of the interaction of Aβ and ABAD.

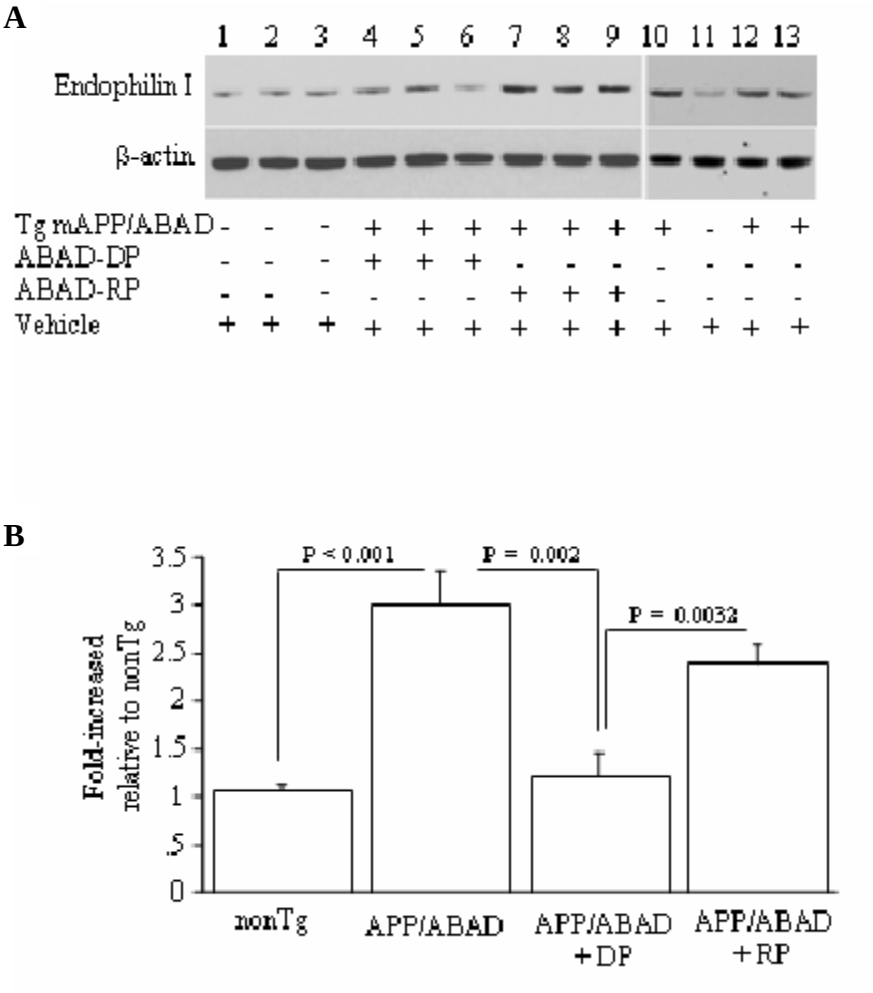

Figure 3.12 (A) The increased expression of endophilin 1 can be reversed by the intra-peritoneal injection in Tg mAPP/ABAD animals of a Tat-mito-ABAD peptide (Tat-mito-ABAD-DP) but not a reverse peptide (Tat-mito-ABAD-RP). Tg mAPP /ABAD mice and non-Tg at the age of 6 months daily received either Tat-mito-ABAD-DP (80 µg) or Tat-mito-ABAD-RP (80 µg) via intra-peritoneal injection for two weeks. The treated mice were then sacrificed and rapidly removed the brains. The hippocampus was subjected to Western blot analysis. (B) Quantification of the reversal of endophilin 1 of several experiments (n = 3-5) showing that the administration of ABAD-DP reduces expression level of endophilin 1 back to normal levels. The statistical test was analyzed by ANOVA using STATVIEW program (Figure supplied by Prof Shi Du Yan, College of Physicians and Surgeons, Columbia University).

3.5 Conclusion

Elucidating the signaling pathways that underlie neuronal responses to Aβ can help developing novel neuroprotective therapeutic strategies. The above study demonstrated that ABAD-Aβ interaction can lead to an increase of the expression of endophilin 1 in the CNS, which then stimulates GLK mediated JNK activation (Figure 3.13). An increased activation of the JNK cascade has been observed in brains of patients with AD. Enhanced JNK activation in AD has been proposed to lead to neuron death and tau phosphorylation (section 1.4.4.2 and 1.4.4.3). Therefore, pharmacological inhibitors of endophilin 1 may offer neuroprotection in Alzheimer's disease.

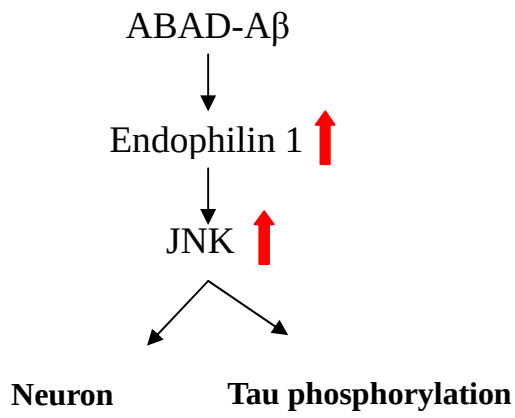

Figure 3.13 A hypothetical sequence of signaling events in AD. In an Aβ rich environment, The ABAD-Aβ interaction causes an increased expression of endophilin 1, which stimulates JNK activation. Increased JNK activation then leads to neuron death and tau phosphorylation.

Chapter 4: ABAD interacts with Cyclophilin D in the mitochondria

Chapter 4: ABAD interacts with Cyclophilin D in the mitochondria

4.1 Introduction

4.1.1 Interaction of ABAD and Cyclophilin D

ABAD is a member of the short chain dehydrogenase/reductase family with broad substrate specificity. Several lines of evidences suggested that ABAD contributes to the maintenance of metabolic homeostasis and confers protection under metabolic stress conditions (Yan *et al.* 2000). In contrast, in an Aβ-rich environment as occurs in AD, ABAD was reported to potentiate cell stress and cytotoxicity (Takuma *et al.* 2005).

CypD is a mitochondrial isoform of cyclophilin which contains an N-terminal targeting sequence that directs the translated proteins to the mitochondria (Connern and Halestrap 1992). CypD is mainly found in the matrix and inner membrane of mitochondria and has been proposed to be an essential component of MPTP. Recruitment of CypD to the ANT on the inner mitochondrial membrane can elicit MPT (Norenberg and Rao 2007).

It was previously demonstrated that CysA blocks MPTP formation by interacting with CypD (Schinzel *et al.* 2005). Application of CysA significantly reduced mitochondrial dysfunction and cell death in cortical neurons from Tg mAPP/ABAD mice (Takuma *et al.* 2005). These data implicated the involvement of MPTP in

neuron toxicity induced by ABAD-Aβ interaction. Indeed, Yan and Stern observed that CypD binds ABAD (Yan and Stern, 2004, unpublished data). Therefore, they proposed that ABAD binds to CypD and sequestrates it in the mitochondria matrix, thus preventing the translocation of CypD to the inner mitochondria membrane and bind to ANT. In contrast, in an Aβ rich environment, ABAD-Aβ interaction displaces ABAD-CypD interaction and results in the translocation of CypD to the inner mitochondrial membrane, which then leads to MPT and ultimately cell death (Yan and Stern 2004).

4.1.2 FRET analysis method

Confocal light microscopy can reveal subcellular distribution and colocalization of labeled or fluorophore tagged proteins. However, there is no indication if these two proteins interact with one another because the order of the resolution of light microscope is 100 nm.

In contrast, FRET is a phenomenon that occurs when two fluorophores are within a distance of 1-10 nm and an appropriate relative orientation such that an excited fluorophore (donor) can transfer its energy to a second, longer-wavelength fluorophore (acceptor) in a nonradiative manner (Kenworthy 2001). Thus, excitation of the donor can produce light emission from the acceptor, with corresponding loss of emission from the donor. There are three requisites for FRET to occur (Schaufele *et al.* 2005):

1) there needs to be sufficient separation in excitation spectra between the donor

and acceptor fluorophore to allow the donor to be stimulated independently.

2) there needs to be an overlap between the emission spectrum of the donor and the excitation spectrum of the acceptor to obtain efficient energy transfer (Figure 4.1).

3) there needs to be reasonable separation in emission spectra between donor and acceptor fluorophore to allow the fluorescence of each fluorophore to be collected separately.

Therefore, by attaching a pair of proteins to be investigated with donor and acceptor fluorophores, FRET can be used as an ideal technique to determine protein-protein interaction in cells. Two variants of green fluorescent protein (GFP) including enhanced cyan fluorescent protein (ECFP) and enhanced yellow fluorescent protein (EYFP) is a well characterized pair of fluoroproteins for FRET analysis (Figure 4.2). ECFP has two excitation peaks: a major peak at 434 nm and a minor peak at 453 nm. EYFP exhibits single excitation maxima at 514 nm. The emission spectrum of ECFP (460-520 nm) overlaps significantly with the excitation spectrum of EYFP (450-565 nm). The emission spectrum of EYFP is from 495 nm to 615 nm. The emission spectrum of ECFP exhibits two maxima (475 nm and 501 nm), whereas EYFP shows only a single peak (527 nm) (Figure 4.1). A pair of proteins of interest is fused with ECFP and EYFP respectively. If the two proteins interact with each other, when ECFP fused protein is excited at 458 nm wavelength, a large proportion of the energy from ECFP will be transferred to EYFP fused protein and result in an EYFP emission peak (Figure 4.2).

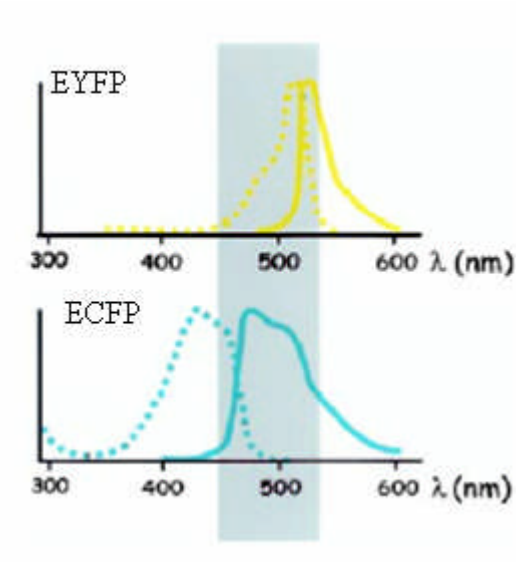

Figure 4.1 Illustration of the excitation and emission spectrum of EYFP and ECFP. The overlapping region of the emission spectrum of the donor and the excitation spectrum of the acceptor is shown as a gray region. Dotted lines indicate the excitation spectrum of ECFP and EYFP. Plain lines indicate emission spectrum of ECFP and EYFP.
From: Zaccolo *et al.* (2007) *Circ. Res.* **94,** 866–873.

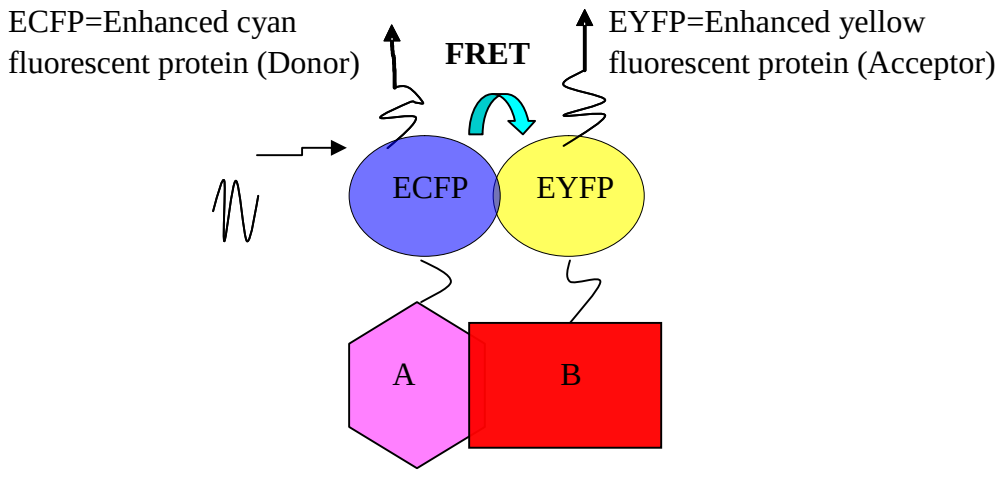

Figure 4.2 Illustration of the occurrence of FRET between ECFP attached protein (A) and EYFP attached protein (B). Excitation of ECFP leads to an increase in EYFP emission.

Two different approaches are generally used to measure FRET (Schaufele *et al.* 2005):

1) Emission measurement. After excitation of the donor, both the donor and acceptor emission in the presence of the other fluorophore were detected. When FRET occurs, there is quenching of the donor fluorescence and an increase of the acceptor fluorescence since energy is transferred from the excited donor to the acceptor. As described previously, overlapping of the donor emission and acceptor absorption spectra is required for the efficient transfer of energy. This spectral overlap, however, causes a significant spectral bleed-through (SBT) background to the FRET signal. Therefore, to characterize FRET efficiency, image processing to remove the SBT background based on reference images acquired from separate control cells is commonly used (Wallrabe and Periasamy 2005).

2) Acceptor photobleaching. Acceptor photobleaching method is based on the principle that the acceptor is destroyed irreversibly by extensive illumination from excitation light. After bleaching of the acceptor fluorophore, FRET is stopped. Therefore, the donor shows an increase in fluorescence intensity after the acceptor photobleaching. Compared to measurement of sensitized emission, this method has the advantage that separate measurements from reference cells are not required since each cell serves as its own control (Berney and Danuser. 2003). Therefore, in this study, I used acceptor photobleaching method to study the interaction of ABAD and CypD in the mitochondria.

4.2 Aims of chapter

MPTP has been associated with the pathogenesis of AD (Norenberg and Rao 2007). Yan and Stern 2004 proposed that under physiological conditions, ABAD binds CypD and sequestrate it in the matrix of the mitochondria, whereas, in an Aβ rich environment, such as in AD, ABAD-Aβ interaction displaces CypD. CypD then translocates to the inner membrane of mitochondria and binds ANT, which induces MPTP and eventually neuron death (Yan and Stern 2004). To study if ABAD interacts with CypD in the mitochondria, ABAD proteins were fused with the EYFP acceptor fluorophore whereas CypD proteins were fused with the ECFP donor fluorophore, and the acceptor photobleaching FRET method was used.

4.3 Results

4.3.1 Construction of the pMito-ABAD-EYFP plasmid

To study the interaction of ABAD and CypD in the mitochondria, I firstly developed a YFP tagged, mitochondria targeted ABAD plasmid construct (pMito-ABAD-EYFP). A schematic outline of the cloning procedure is illustrated in Figure 4.3.

Previously, a mitochondrial targeted, and GFP tagged ABAD plasmid construct (pMito-ABAD-GFP) has been produced in the laboratory by Margaret Taylor. The mitochondria targeting sequence of pMito-ABAD-GFP was derived from the

pDsRed2-Mito vector (Clonetech). The most convenient cloning sites in the pMito-ABAD-GFP vector were Not 1 and BamH 1. However, there was a single BamH I site between the mitochondria targeting sequence and ABAD sequence. Therefore, a two-step cloning strategy was devised. First, pMito-ABAD-GFP was digested with the restriction enzyme BamH 1, releasing a 786 bp fragment of ABAD. Then, using pGT-EYFP as a template, EYFP was cloned by PCR using the forward oligonucleotide, CGGGATCCATGGTGAGCAAGGGCGAGGAG, which encodes a BamH1 site and the reverse oligonucleotide, TTTTGCGGCCGCTTACTTGTACAGCTCGTCCATGCC, which encodes a Not 1 site. The PCR product containing the 720 bp of EYFP was subsequently digested with the restriction enzymes Not 1and BamH 1. The pMito-ABAD-GFP vector was also digested with Not 1 and BamH 1, and the digested PCR product containing EYFP was ligated with it. The ligation mixture was transformed into *E. coli* (DH5α) and prepared with Qiagen's Miniprep Kit as described in section 2.1.8. Restriction digest analysis showed that the ligated plasmid was present. This plasmid was then digested with BamH 1, and the 786 bp of ABAD containing fragment was ligated with it. As two orientations for this insert were possible, several digests were performed to test both the presence and direction of the insert, and the complete plasmid was further confirmed by sequencing.

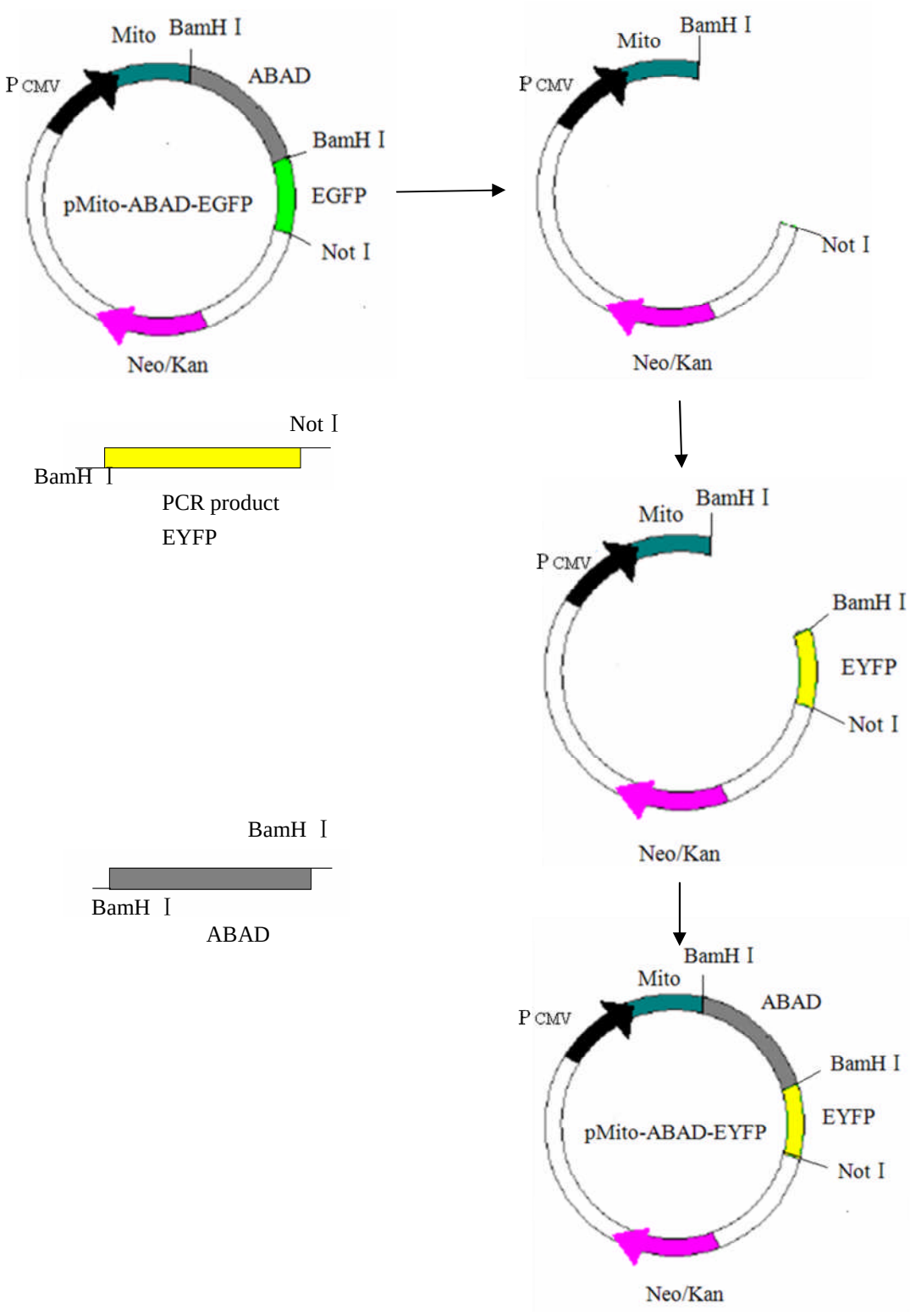

Figure 4.3 Two-step cloning strategy for pMito-ABAD-EYFP. pMito-ABAD-EGFP plasmid was digested with BamH I and Not I. pGT-EYFP was used as the template for PCR of EYFP. Both the PCR products containing EYFP and the fragment digested from pMito-ABAD-EGFP which contains ABAD were then sequentially ligated into the vector digested from pMito-ABAD-EGFP plasmid.

The plasmid pCypD-ECFP was a kind gift from Dr Anne Murphy (Department of Pharmacology, University of California, San Diego). In this DNA construct, CypD was cloned from human heart mRNA and ligated into the expression vector pECFP-N1 resulting in a CypD-ECFP fusion protein.

4.3.2 Colocalization of pMito-ABAD-YFP, pCypD-ECFP, and pDsRed2-Mito

pDsRed2-Mito (clontech) is a mammalian expression vector that encodes a fusion of *Discosoma sp.* red fluorescent protein (DsRed2) and the mitochondrial targeting sequence from subunit VIII of human cytochrome c oxidase (Mito). The Mito sequence targets the Mito-DsRed2 fusion protein to the cell mitochondria, and as such, pDsRed2-Mito has been widely used as a marker of mitochondrial matrix (Karbowski *et al.* 2002; Karbowski *et al.* 2004; Cordell *et al.* 2004).

To verify that Mito-ABAD-EYFP and CypD-ECFP are expressed in the mitochondria, a colocalization study of DsRed2-Mito with Mito-ABAD-EYFP or CypD-ECFP was performed. SK-N-SH cells were transfected with pDsRed2-Mito, pCypD-ECFP, pMito-ABAD-EYFP alone or a combination of two of them using Amaxa Cell line nucleofector Solution V according to the protocol described in section 2.2.5. Transfected cells were seeded onto coverslips containing 35 mm petri dishes at a density of $1X10^6$ cells per dish. After 24 hours, cells were fixed in 4% PFA and mounted with Moviol+Dapi solution. The fluorescent images were then examined using a Leica TCS-SP confocal microscope equipped with 40X, and 63X oil immersion objectives. Mito-ABAD-EYFP showed a mitochondrial distribution

(4.4A, B and C) and the merged image clearly showed that it colocalized well with DsRed2-Mito (Figure 4.5). CypD-ECFP also displayed a mitochondrial distribution (4.4D, E and F). But, notably, the expression of CypD-ECFP was partially colocalized with that of DsRed2-Mito (Figure 4.6).

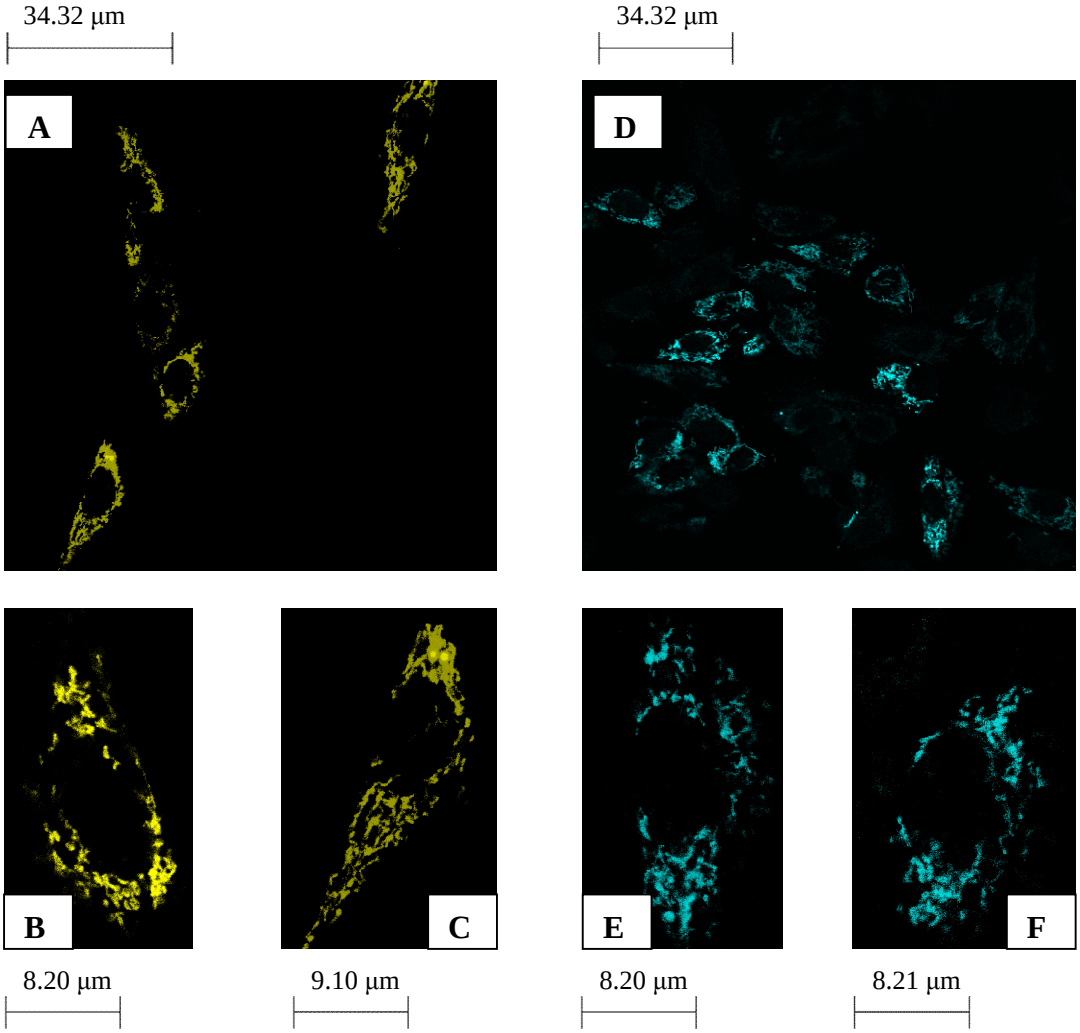

Figure 4.4 Expression distributions of Mito-ABAD-EYFP and CypD-ECFP. SK-N-SH cells were transfected with pMito-ABAD-EYFP and pCypD-ECFP. Mito-ABAD-EYFP exhibited a mitochondrial distribution in the cells (A, B and C). CypD-ECFP proteins were also localized to the mitochondria (D, E and F). Transfection efficiency is approximately 40–50% in this study

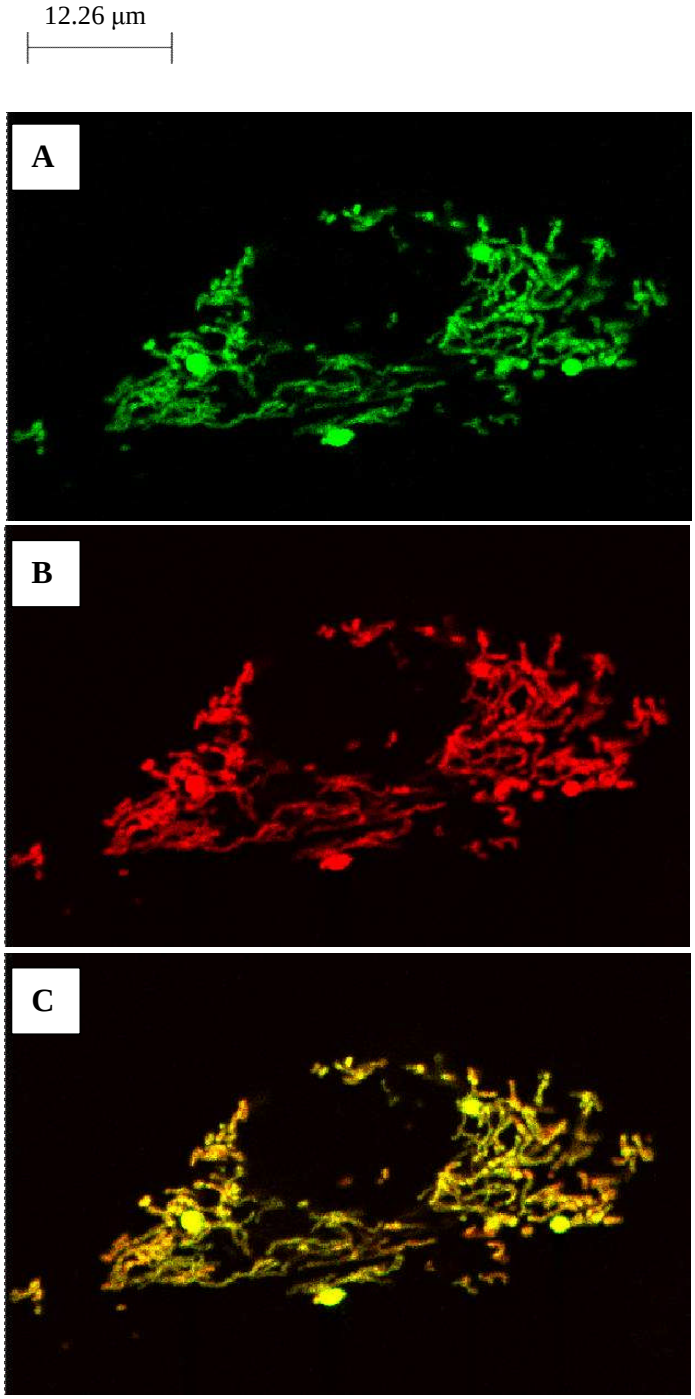

Figure 4.5 Colocalization of Mito-ABAD-EYFP and DsRed2-Mito in SK-N-SH cells. SK-N-SH cells cotransfected with pMito-ABAD-EYFP and pDsREd2-Mito were fixed and mounted for microscopic observation. Mito-ABAD-EYFP exhibited mitochondrial distribution (A). pDsRed2-Mito has been widely used as a marker of the mitochondrial matrix (B). Merged image demonstrated that Mito-ABAD-EYFP colocalized well with DsREd2-Mito (C).

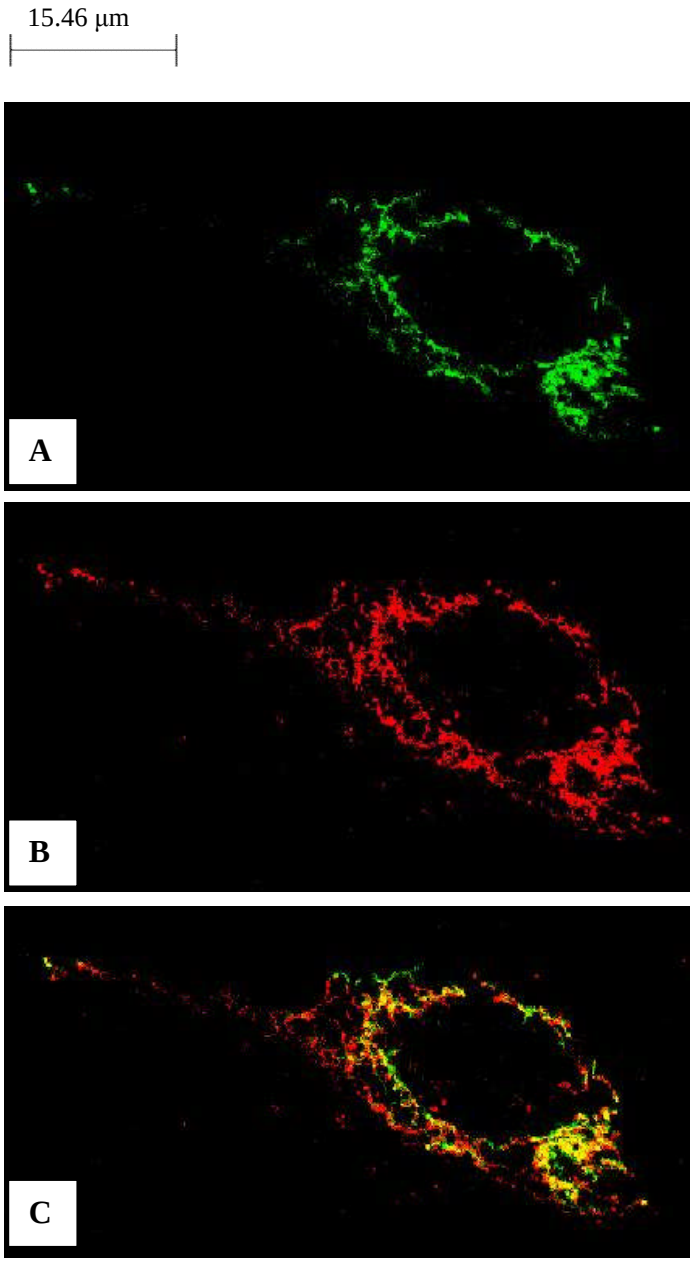

Figure 4.6 Colocalization of CypD-ECFP and DsRed2-Mito in SK-N-SH cells. SK-N-SH cells cotransfected with pCypD-ECFP and pDsREd2-Mito were fixed and mounted for microscopic observation. CypD-ECFP exhibited mitochondrial distribution (A). pDsRed2-Mito has been widely used as a mitochondrial marker (B). Merged image demonstrated that CypD-ECFP colocalized partially with DsRed2-Mito (C).

Furthermore, in accordance with the above results, a colocalization study of Mito-ABAD-EYFP and CypD-ECFP revealed that the expression of Mito-ABAD-EYFP only partially overlaps with the expression of CypD-ECFP in the mitochondria of the cells (Figure 4.7).

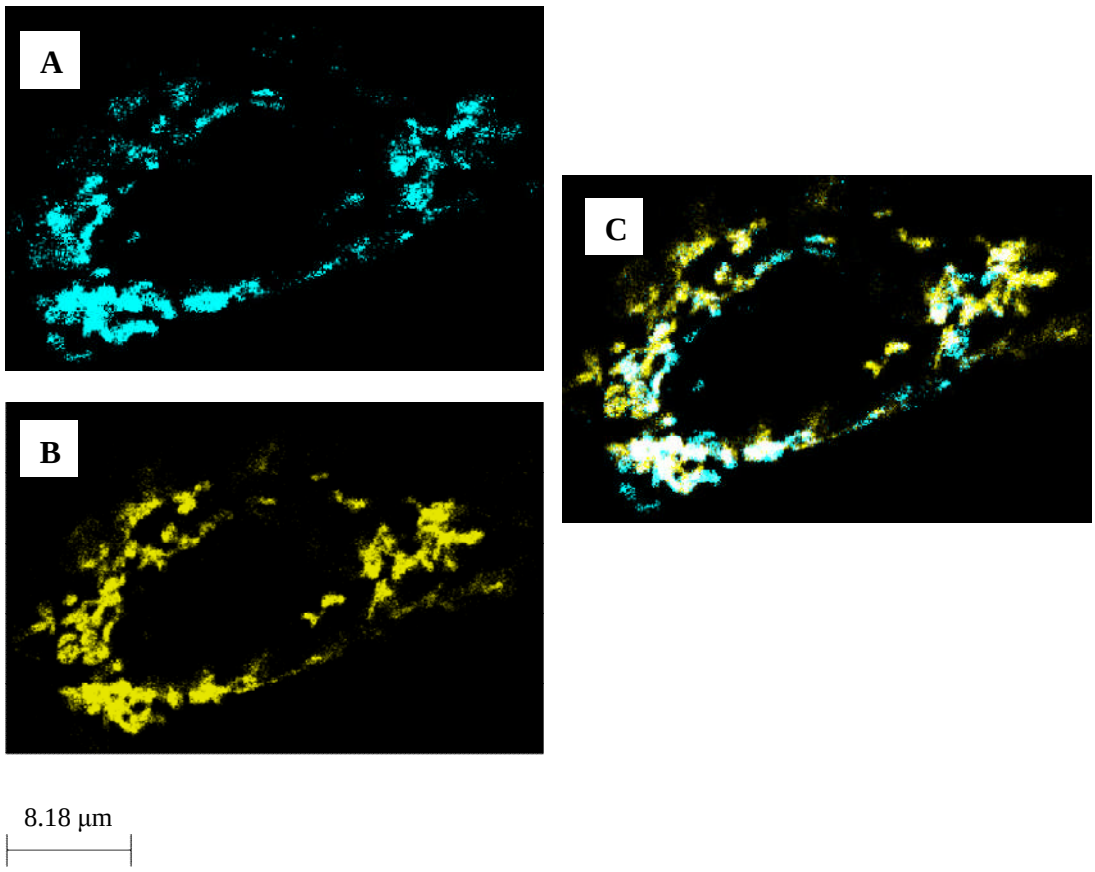

Figure 4.7 Colocalization of CypD-ECFP and Mito-ABAD-EYFP in SK-N-SH cells. SK-N-SH cells cotransfected with pCypD-ECFP and pMito-ABAD-EYFP were fixed and mounted for microscopic observation. Both CypD-ECFP (A) and Mito-ABAD-EYFP (B) exhibited mitochondrial distribution. Merged image demonstrated that CypD-ECFP colocalized partially with Mito-ABAD-EYFP (C).

pMito-ABAD-EYFP and pDsRed2-Mito contain the same mitochondria targeting sequence. This targeting sequence was reported to target proteins to the mitochondrial matrix (Karbowski *et al.* 2002; Karbowski *et al.* 2004; Cordell *et al.* 2004). However, pCypD-ECFP has its own intrinsic N terminal mitochondria targeting sequence of approximately 13 amino acids (Connern and Halestrap 1992). CypD has been reported to be expressed in both the mitochondrial inner membrane and mitochondrial matrix (Schinzel e*t al.* 2005). These data might explain the differential distribution in the mitochondria of the cells between Mito-ABAD-EYFP proteins and CypD-ECFP proteins.

4.3.3 FRET analysis of ABAD-CypD interaction using acceptor photobleaching method

Given that there are areas of colocalization between the tagged ABAD and CypD proteins, acceptor photobleaching measurements were used to investigate if ABAD interacts with CypD in mitochondria. In cells expressing EYFP tagged protein acceptor fluorophore was photobleached. Interaction between two fluorophore-tagged proteins permits energy transfer between the fluorophores, which results in an unquenching of the fluorescence intensity of ECFP tagged protein (donor fluorophore). FRET between the donor and the acceptor (D–A) can be characterized by the efficiency of energy transfer ($FRET_{Eff}$), which is measured as the relative variation of fluorescence intensity of ECFP pre and post bleaching ($FRET_{Eff} = D_{post}\text{-}D_{pre}/D_{pre}$).

In this study, SK-N-SH cells were cotransfected with pMito-ABAD-EYFP and pCypD-ECFP to study the FRET between Mito-ABAD-EYFP and CypD-ECFP. The detection of FRET has been found to be sensitive to the ratio of the intensities of donor and acceptor fluorophores (Zal *et al.* 2002). Therefore, 2 μg of pMito-ABAD-EYFP plasmid DNA were cotransfected with 2 μg, 4 μg, or 6 μg of pCypD-ECFP plasmid DNA respectively. Cells cotransfected with pMito-ABAD-EYFP and pCypD-ECFP at a ratio of 1:3 showed similar fluorescent intensities of ECFP and EYFP (unpublished observation). Therefore, in this study, plasmid DNA encoding for EYFP fused to protein of interest was cotransfected with plasmid DNA encoding for ECFP fused to protein of interest at a ratio of 1:3. To confirm the occurrence of FRET, two negative controls were set up: 1) SK-N-SH cells transfected with pCypD-ECFP alone and 2) SK-N-SH cells cotransfected with pCypD-ECFP and pEYFP vector. SK-N-SH cells expressing a fusion plasmid, pECFP-DEVD-EYFP (a kind gift from Prof Professor Tavaré, Department of Biochemistry, University of Bristol) was also included to serve as a positive control. ECFP-DEVD-EYFP is a hybrid protein consisting of ECFP and EYFP linked by a spacer containing the amino acid sequence DEVD. It has been demonstrated that in COS7 cells expressing pECFP-DEVD-EYFP, strong FRET signals can be observed (Brophy *et al.* 2002)., Transfection of SK-N-SH cells was performed using Amaxa's nucleofactor system according to the protocol detailed in section 2.2.5. Transfected cells were seeded onto 35 mm coverslips containing petri dishes at a density of $1X10^6$ cells per dish. 48 hours later, the cells were fixed and

mounted in Moviol+Dapi solution. The slides were examined with Leica TCS-SP5 multiphoton confocal microscope equipped with 40X, and 63X oil immersion objectives. The 458 nm and 514 nm argon laser lines were used for activation of ECFP and EYFP respectively. Laser intensity was set at 20% of available power. The emission window was set at 475–500 nm for visualization of ECFP and for visualization of EYFP, the emission window was set at 520–600 nm. The 415 nm laser was used to visualize Dapi stained nuclei to allow the focusing of cells. The Leica FRET wizard in the application module was set up and the acceptor photobleaching module was chosen. For photobleaching, 514 nm laser was set to full power. 4-8 regions of interest (ROIs) within each cell were chosen and photobleached by 514 nm laser until most of the fluorescence intensity was bleached. Pre and post bleach images in both ECFP and EYFP channels were taken. The FRET efficiency was calculated automatically by the Leica FRET wizard software. For internal control of real FRET, 4-8 unbleached ROIs in cells cotransfected with pMito-ABAD-EYFP and pCypD-ECFP were chosen, and the corresponding FRET efficiency was calculated.

4.3.3.1 Characterization of FRET in SK-N-SH cells co-expressing pMito-ABAD-EYFP and pCypD-ECFP

The data from a typical imaging FRET experiment are shown in Figure 4.8. The initial acceptor (Mito-ABAD-EYFP) image represents acceptor fluorescence in the presence of the donor CypD-ECFP (Figure 4.8A). After complete photobleaching

of the acceptor, image of the acceptor was collected (Figure 4.8B). The images of the donor pre and post photobleaching were also collected (Figure 4.8C and 4.8D). As shown in Figure 4.8C and 4.8D, in the bleached regions, the fluorescence of the donor was increased after acceptor photobleaching indicating the occurrence of FRET. The fluorescence intensities of both donor and acceptor pre and post bleaching and the values of FRET efficiency for different ROIs within one cell are displayed in Table 4.1.

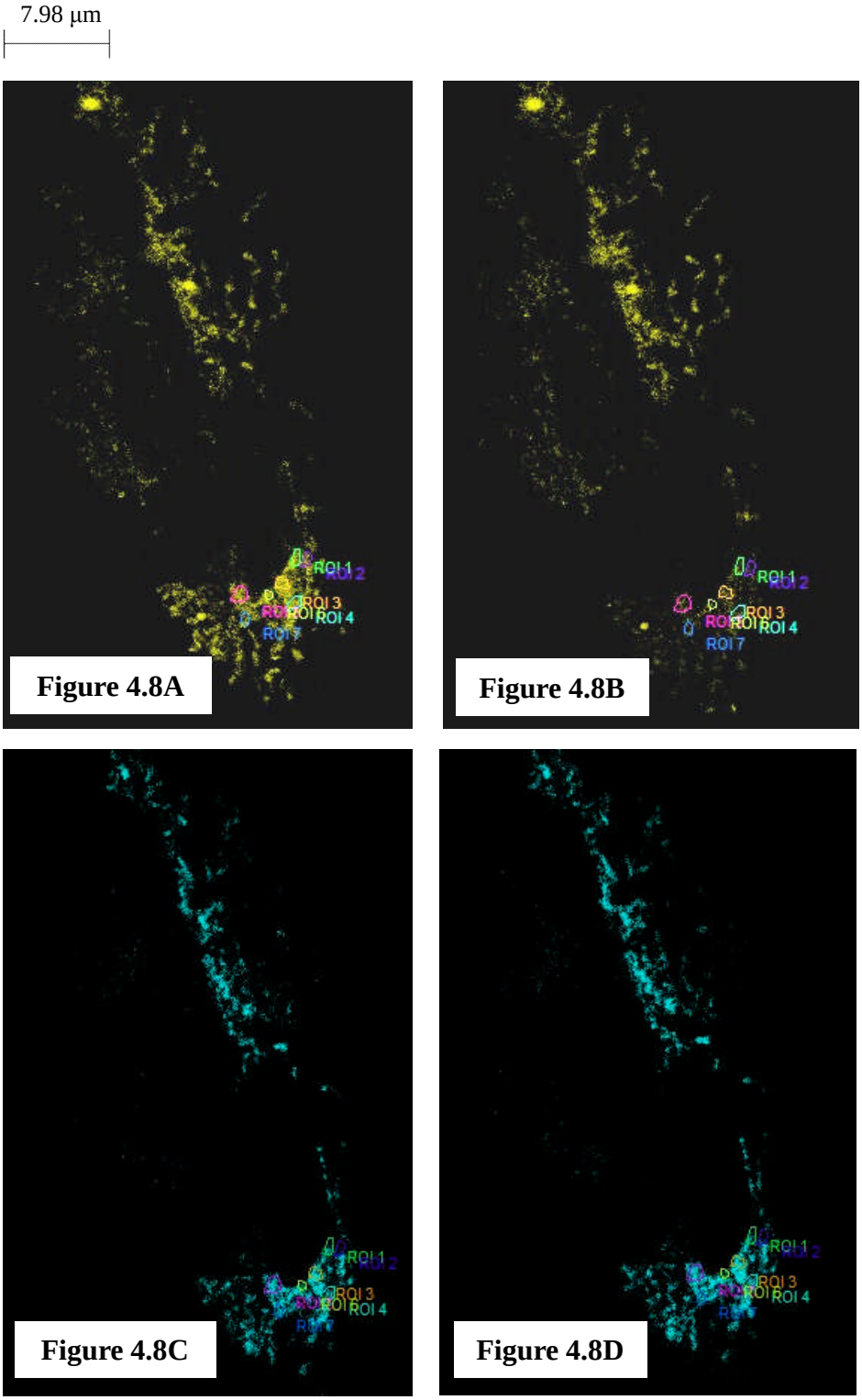

Figure 4.8 Detection of FRET in SK-N-SH cells co-expressing pMito-ABAD-EYFP and pCypD-ECFP by means of the increase in donor fluorescence after acceptor photobleaching. Region of interests (ROIs) as indicated were photobleached by 514 nm laser. (A) Acceptor (Mito-ABAD-EYFP) image before photobleaching of the acceptor; (B) Acceptor (Mito-ABAD-EYFP) image after photobleaching;(C) Donor (CypD-ECFP) image before acceptor photobleaching; and (D) Donor (CypD-ECFP) image after photobleaching.

ROI	ROI_1	ROI_2	ROI_3	ROI_4	ROI_5	ROI_6	ROI_7
D pre	73.78	40.14	193.98	126.82	173.80	105.07	140.58
D post	69.57	49.51	204.47	148.06	190.21	107.52	155.50
A pre	104.67	73.10	132.05	111.00	100.81	105.67	84.97
A post	28.88	16.20	45.18	33.82	29.36	24.15	25.06
FRETeff (%)	0.00	18.92	5.13	14.34	8.63	2.27	9.59

Table 4.1 The fluorescence intensities and FRET efficiency calculated for different ROIs within one cell as indicated. FRETeff = D_{post}-D_{pre}/$D_{post.}$

4.3.3.2 Characterization of FRET in unbleached ROIs in SK-N-SH cells co-expressing pMito-ABAD-EYFP and pCypD-ECFP

As an internal control for real occurrence of FRET, within the same cell, 4-8 ROIs in the unbleached regions were chosen as well. Pre and post bleaching images of Mito-ABAD-EYFP and CypD-ECFP were captured. The fluorescence intensities of Mito-ABAD-EYFP and CypD-ECFP in the unbleached ROIs were measured and the corresponding FRET efficiency was calculated.

Representative FRET images of the unbleached regions in SK-N-SH cells co-expressing pMito-ABAD-EYFP and pCypD-ECFP are shown in Figure 4.9. Table 4.2 demonstrates the values of the FRET efficiency in the unbleached ROIs.

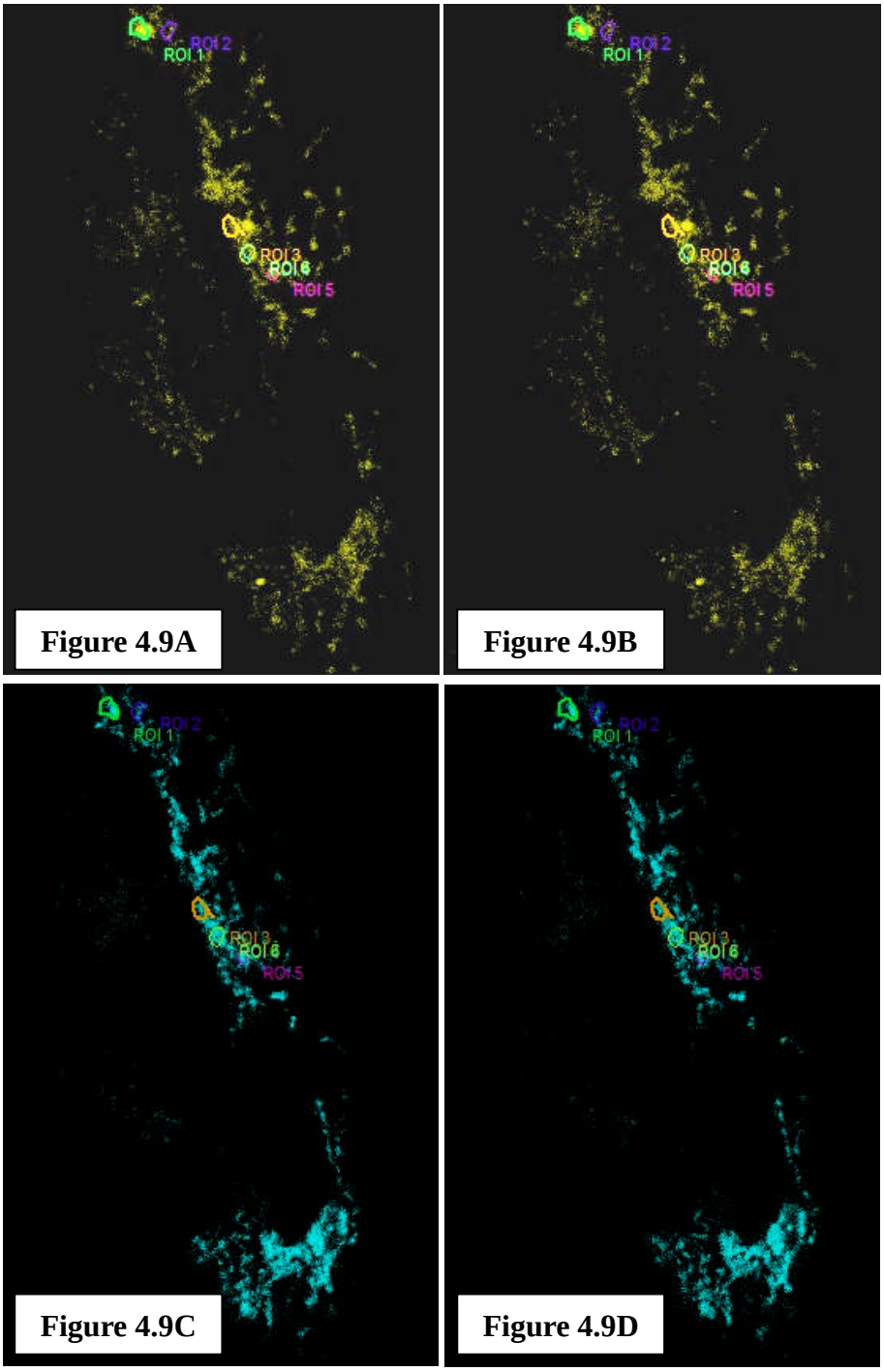

Figure 4.9 Characterization of the FRET efficiency of in the unbleached ROIs of SK-N-SH cells co-expressing pMito-ABAD-EYFP and pCypD-ECFP. (A) Acceptor (Mito-ABAD-EYFP) image before photobleaching of the acceptor; (B) Acceptor (Mito-ABAD-EYFP) image after photobleaching;(C) Donor (CypD-ECFP) image before acceptor photobleaching; and (D) Donor (CypD-ECFP) image after photobleaching.

ROI	ROI_1	ROI_2	ROI_3	ROI_4	ROI_5	ROI_6
D pre	129.79	102.94	140.27	206.38	224.06	186.83
D post	120.93	91.60	124.22	203.67	219.00	183.08
A pre	126.49	36.45	55.44	94.88	106.97	89.48
A post	125.95	44.48	47.99	88.42	101.30	82.23
FRETeff (%)	0.00	0.00	0.00	0.00	0.00	0.00

Table 4.2 Values of the fluorescence intensities and FRET efficiency for different ROIs as indicated in unbleached regions within one cell. FRETeff = D_{post}-D_{pre}/D_{post}

4.3.3.3 Characterization of FRET in SK-N-SH cells expressing pCypD-ECFP

In this study, I also analyzed FRET of two negative controls including SK-N-SH cells expressing pCypD-ECFP alone and SK-N-SH cells co-expressing pEYFP and pCypD-ECFP. Representative FRET images of SK-N-SH cells transfected with pCypD-ECFP alone are shown in Figure 4.10. Hardly any fluorescence was detected in the EYFP channel. There was no increase in the fluorescence intensities of the ROIs in the ECFP channel after photobleaching (Figure 4.10 C and D). Table 4.3 displays the values of the FRET efficiency in ROIs of cells expressing pCypD-ECFP alone.

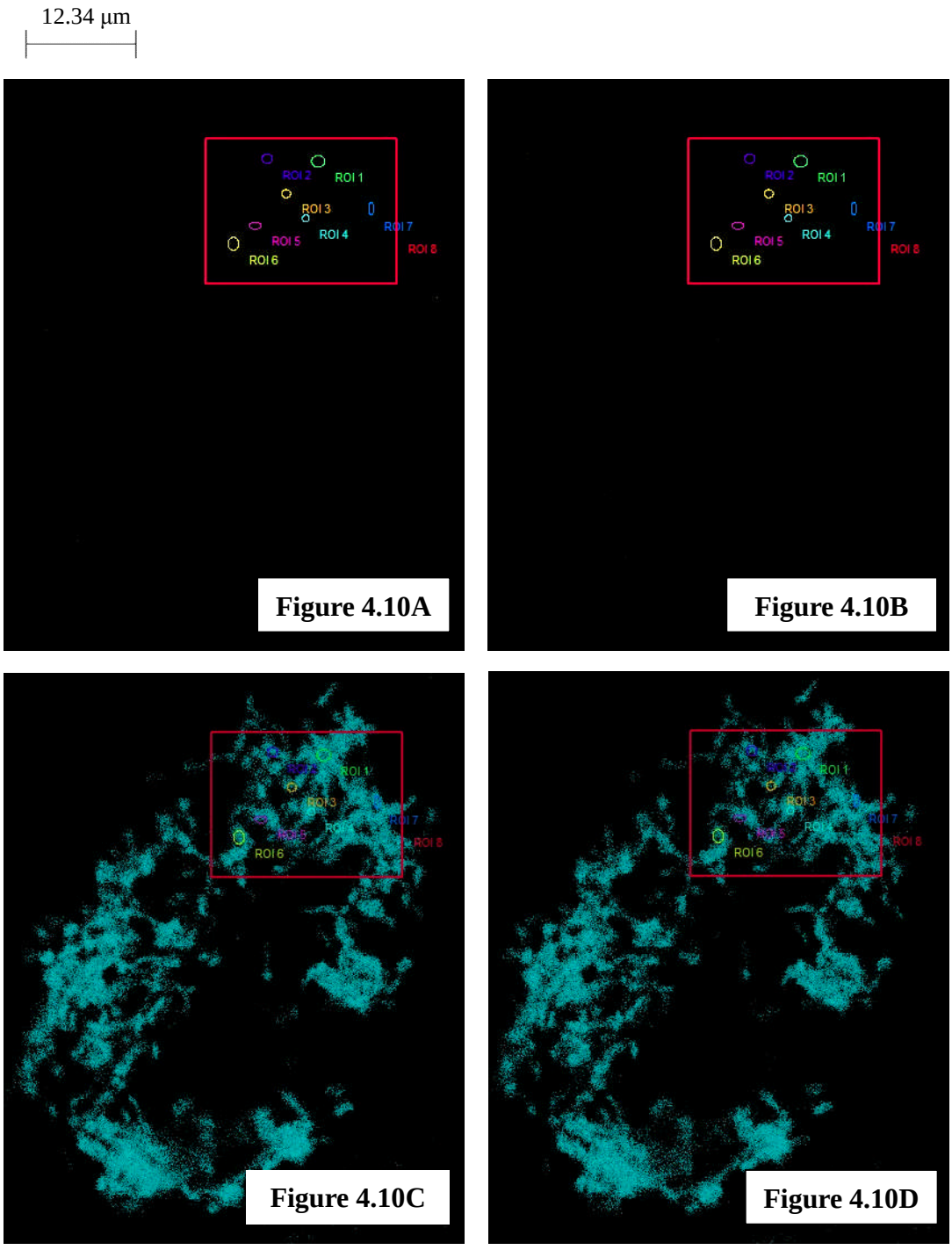

Figure 4.10 Characterization of FRET in SK-N-SH cells expressing pCypD-ECFP alone. (A) Image captured in the EYFP channel before photobleaching of the acceptor; (B) Image captured in the EYFP channel after photobleaching; (C) Donor (CypD-ECFP) image before acceptor photobleaching; and (D) Donor (CypD-ECFP) image after photobleaching.

ROI	ROI_1	ROI_2	ROI_3	ROI_4	ROI_5	ROI_6	ROI_7	ROI_8
D pre	162.56	125.20	101.64	180.63	97.45	143.66	162.15	65.46
D post	162.12	104.26	95.44	168.37	91.10	120.61	168.78	58.66
A pre	0.03	0.00	0.00	0.00	0.24	0.08	0.00	0.04
A post	0.00	0.00	0.00	0.00	0.00	0.01	0.15	0.02
FRETeff (%)	0.00	0.00	0.00	0.00	0.00	0.00	3.93	0.00

Table 4.3 Values of the fluorescence intensities and FRET efficiency for different ROIs as indicated within one cell. FRETeff = D_{post}-D_{pre}/D_{post}

4.3.3.4 Characterization of FRET in unbleached ROIs of SK-N-SH cells co-expressing pEYFP and pCypD-ECFP

SK-N-SH cells co-expressing pEYFP vector and pCypD-ECFP were also employed as a negative control. In the EYFP channel, yellow fluorescence was distributed diffusely in the cell. CypD-ECFP still showed a mitochondrial distribution. Representative FRET images are shown in Figure 4.11. After photobleaching of the acceptor (EYFP), there was no obvious increase in the fluorescence intensities of CypD-ECFP. Table 4.4 demonstrates the values of the FRET efficiency in ROIs of cells co-expressing pCypD-ECFP and pEYFP.

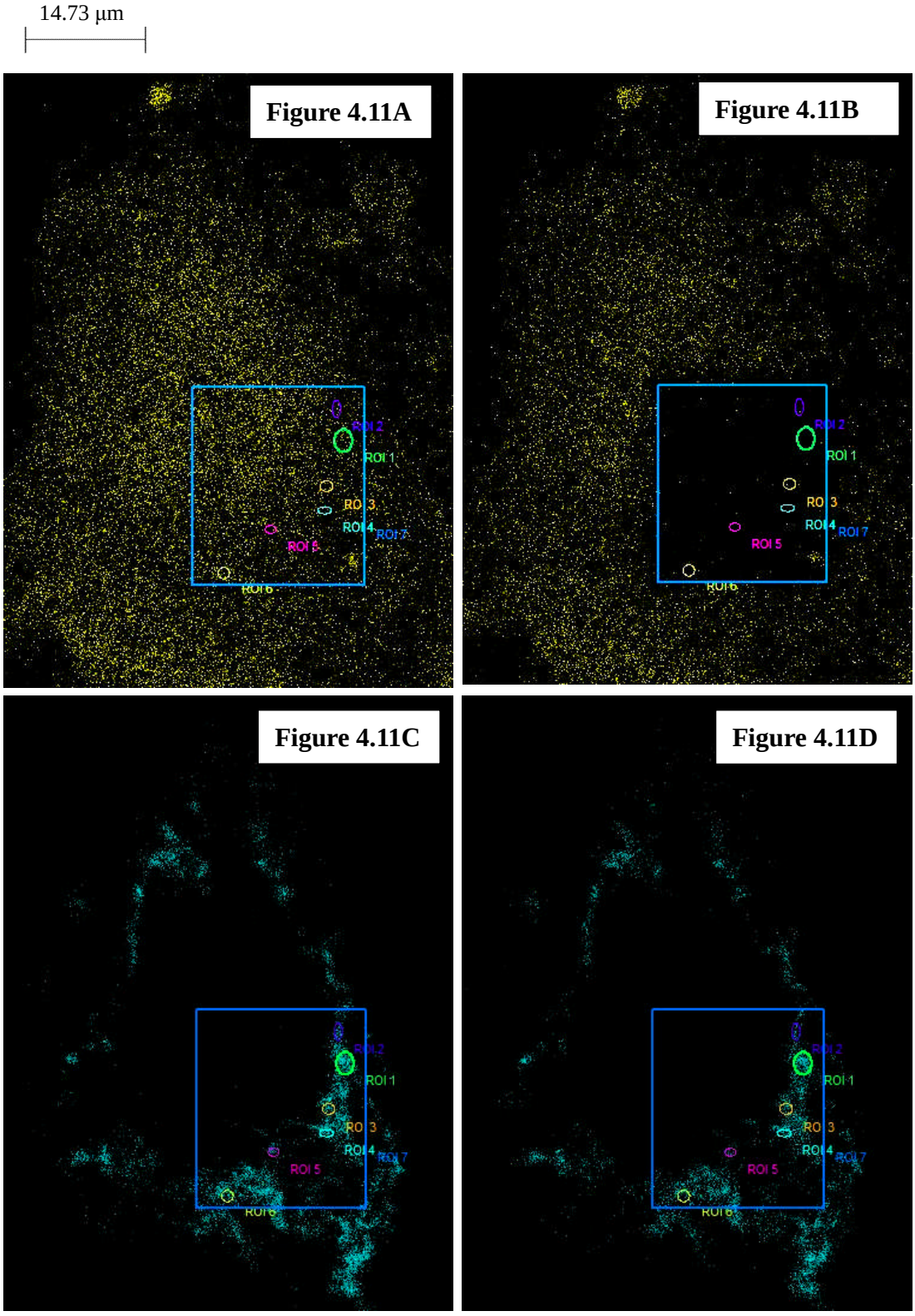

Figure 4.11 Characterization of FRET in SK-N-SH cells co-expressing pEYFP and pCypD-ECFP. (A) Acceptor (EYFP) image before photobleaching of the acceptor; (B) Acceptor (EYFP) image after photobleaching;(C) Donor (CypD-ECFP) image before acceptor photobleaching; and (D) Donor (CypD-ECFP) image after photobleaching.

ROI	ROI_1	ROI_2	ROI_3	ROI_4	ROI_5	ROI_6	ROI_7
D pre	102.51	74.42	83.37	86.06	59.63	63.29	15.98
D post	96.41	47.12	60.42	57.98	36.17	48.29	11.94
A pre	23.10	20.01	21.11	24.76	22.98	30.33	26.45
A post	1.04	2.88	4.06	1.24	0.43	1.03	1.47
FRETeff (%)	0.00	0.00	0.00	0.00	0.00	0.00	0.00

Table 4.4 Values of the fluorescence intensities and FRET efficiency in different ROIs as indicated within one cell. FRETeff = D_{post}-D_{pre}⁄D_{post}

4.3.3.5 Characterization of FRET in ROIs of SK-N-SH cells expressing pEYFP-DEVD-ECFP

To further verify that the FRET observed in bleached ROIs of SK-N-SH cells cotransfected with pMito-ABAD-EYFP and pCypD-ECFP are true, a positive control was used. SK-N-SH cells were transfected with a pEYFP-DEVD-ECFP fusion plasmid. Both the yellow and blue fluorescence were distributed diffusely throughout the cell. The 514 nm laser was used to bleach ROIs in the cells and a significant increase of the fluorescence intensity of pCypD-ECFP was observed after photobleaching. Representative FRET images are shown in Figure 4.12. Table 4.5 demonstrates the values of the FRET efficiency in ROIs of SK-N-SH cells expressing an EYFP-DEVD-ECFP fusion protein.

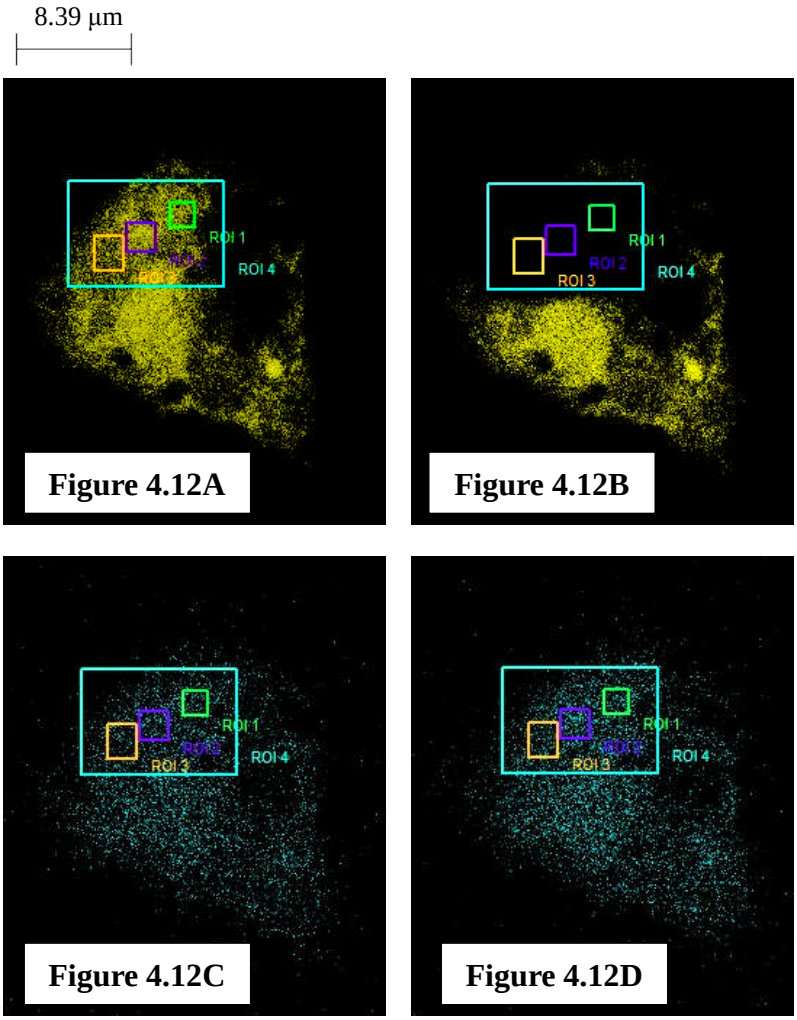

Figure 4.12 Detection of FRET signals in SK-N-SH cells expressing pECFP-DEVD-EYFP by means of the increase in donor fluorescence after acceptor photobleaching. Region of interests (ROIs) as indicated were photobleached by 514 nm laser. (A) Acceptor image before photobleaching of the acceptor; (B) Acceptor image after photobleaching;(C) Donor image before acceptor photobleaching; and (D) Donor image after photobleaching.

ROI	ROI_1	ROI_2	ROI_3	ROI_4
D pre	29.34	32.85	26.38	21.33
D post	38.52	51.70	34.38	28.88
A pre	108.94	138.73	97.75	82.00
A post	0.06	0.09	0.03	0.16
FRETeff (%)	23.84	36.47	23.27	26.13

Table 4.5 Values of the fluorescence intensities and FRET efficiency for different ROIs as indicated within one cell. FRETeff = D_{post}-D_{pre}/ D_{post}

4.3.4 Quantitative analysis of FRET efficiency

14 cells co-expressing pMito-ABAD-EYFP and pCypD-ECFP, 11 cells expressing pCypD-ECFP alone, 12 cells co-expressing pCypD-ECFP and pEYFP vector, and 12 cells expressing pECFP-DEVD-EYFP were quantitatively analyzed for detection of FRET. For FRET analysis, 4-8 regions within each cell were chosen and the corresponding FRET efficiency was calculated. Statistical significance was performed using student's t test. Significance level was expressed at 0.05% level.

The FRET efficiency data are expressed as means ± S.E.M. SK-N-SH cells co-expressing pMito-ABAD-YFP and pCypD-ECFP displayed a FRET efficiency of 11.46±1.17 (n=14cells). It is significantly higher than the FRET efficiency of the SK-N-SH cells expressing pCypD-ECFP alone (3.70±1.15, n=11cells) or SK-N-SH cells co-expressing pCypD-ECFP and pEYFP vector (2.53±0.5, n=12 cells). The unbleached regions of SK-N-SH cells co-expressing both pMito-ABAD-EYFP and

pCypD-ECFP exhibited a FRET efficiency of 2.03±0.64 (n=14 cells). Serving as a positive control, SK-N-SH cells expressing a pECFP-DEVED-EYFP fusion plasmid showed a FRET efficiency of 16.12± 2.74 (n=12 cells) (Figure 4.13).

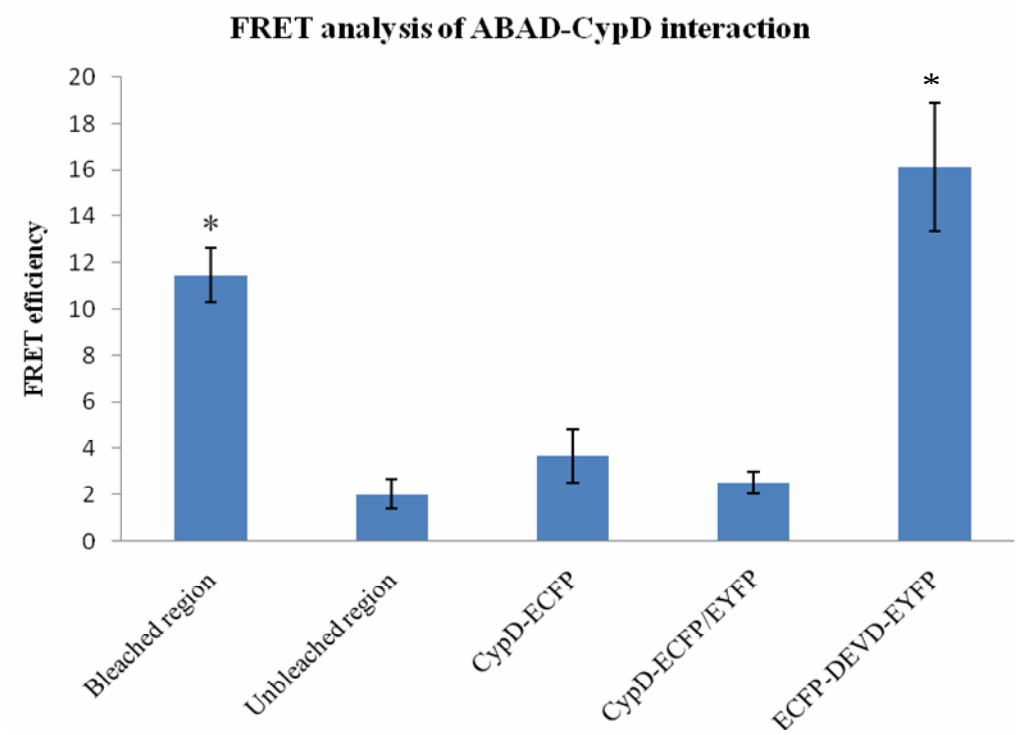

Figure 4.13 Quantitative analysis of FRET efficiency. The results are expressed as means ± S.E.M. SK-N-SH cells co-expressing pMito-ABAD-EYFP and pCypD-ECFP exhibited a FRET efficiency of 11.46±1.17 (n=14) in the phototobleached ROIs. In contrast, the unbleached ROIs showed a markedly reduced level of FRET efficiency (2.03±0.64, n=14). Two negative controls including SK-N-SH cells expressing pCypD-ECFP alone and SK-N-SH cells co-expressing pCypD-ECFP and pEYFP vector, however, displayed FRET efficiency of 3.70±1.15 (n=11cells) and 2.53±0.5, (n=12 cells) respectively. SK-N-SH cells expressing an ECFP-DEVD-EYFP fusion protein showed a FRET efficiency of 16.12±2.74 (n=12 cells). * indicates a significance level of 0.05%.

Quantitative analysis of the values of FRET efficiency indicated high FRET signals between Mito-ABAD-EYFP and CypD-ECFP. Cells expressing an ECFP-DEVD-EYFP fusion protein also exhibited high level of FRET efficiency. In contrast, cells transfected with pCypD-ECFP alone or both pCypD-ECFP and pEYFP displayed very low FRET signals. Taken together, these data demonstrated that there is a tight intermolecular association between Mito-ABAD-EYFP and CypD-ECFP in the mitochondria. In general, strong FRET signals imply that the fluorophores are within 10 nm distance. Thus, these FRET results substantially indicated a close association between Mito-ABAD-EYFP and CypD-ECFP in the mitochondrial compartment of cells.

4.4 Discussion

Accumulating evidences suggested that high cytosolic levels of Ca^{2+} and oxidative stress are two major factors for the induction of the MPTP (Hale strap *et al.* 1999); Kwiatkowski *et al.* 2001). Opening of the MPTP led to dissipation of the mitochondrial inner membrane potential, which then caused uncoupling of oxidative phosphorylation and ATP synthesis deficiency. Also, such dysfunction of the electron transport chain in the mitochondria resulted in ROS production (Votyakova and Reynolds, 2005). Thus, while oxidative stress is a major cause of the MPT, it can also be a consequence of the MPT. Moreover, MPT is involved in the apoptotic cell death pathway by releasing of cytochrome c. Once released from

the mitochondria, cytochrome c activated procaspase 9 to stimulate downstream events related to apoptosis (Jemmerson *et al.* 2005).

It is well recognized that oxidative stress plays an important role in the pathogenesis of AD (Butterfield *et al.* 2006). Furthermore, aggregated Aβ was reported to lead to a dysregulation of Ca^{2+} homeostasis (Mattson *et al.* 1992). Together, these results implicated the involvement of MPTP in the pathogenesis of AD. However, the precise mechanisms by which high cytosolic levels of Ca^{2+} and oxidative stress elicit the MPT remain to be established.

Yan and Stern 2004 proposed a novel signaling pathway which may contribute to the MPTP formation in AD. Under physiological conditions, ABAD binds CypD, whereas in AD, Aβ binds ABAD and disturbs the interaction of ABAD and CypD. CypD is then recruited to ANT on the inner membrane of mitochondria and induce MPT (Yan and Stern 2004).

In this study, using the acceptor photobleaching method, strong FRET signals were detected in SK-N-SH cells co-expressing pMito-ABAD-EYFP and pCypD-ECFP. In contrast, three negative controls including unbleached ROIs of SK-N-SH cells co-expressing pMito-ABAD-EYFP and pCypD-ECFP, SK-N-SH cells expressing pCypD-ECFP alone and SK-N-SH cells co-expressing pEYFP and pCypD-ECFP, all exhibited low FRET signals. Moreover, as a positive control, SK-N-SH cells expressing an ECFP-DEVD-EYFP fusion protein displayed strong FRET signals. These data indicated that, ABAD may interact with CypD in the mitochondria of SK-N-SH cells.

Also of interest is that in SK-N-SH cells expressing an ECFP-DEVD-EYFP fusion protein (positive control), strong FRET signals were detected in all bleached ROIs. However, in SK-N-SH cells co-expressing pMito-ABAD-EYFP and pCypD-ECFP, there were a small percentage of bleached ROIs which displayed very low FRET signals. These data indicated that the interaction of ABAD and CypD may not be global. It may only occur in some parts of the mitochondria of the cells. Apart from the spatial context, ABAD-CypD interaction may also vary across different time scales. Therefore, in future studies, FRET analysis of live cells should be performed to study the dynamic relationship between ABAD and CypD in cell mitochondria. Moreover, an Aβ rich environment can be set up by applying extracellular aggregated Aβ to cells or transfecting mAPP into cells. Thus, the hypothesis that, in an Aβ rich environment, ABAD-Aβ interaction displaces CypD which then results in MPT and neuron death can be tested.

Despite the power of these FRET-based approaches, it is important to note that, positive FRET results by themselves can not prove the direct interaction of the labeled proteins. Other techniques, such as co-immunoprecipitation, epitope-tagged protein pull-down, and two-hybrid assays are required to substantiate the direct protein-protein interactions. However, it needs to be pointed out that the application of these approaches is also limited due to the nonphysiological conditions of protein extraction and analysis (Voss *et al.* 2005).

Chapter 5: Two dimensional electrophoresis analysis of RAGE knock out mice

Chapter 5: Two dimensional electrophoresis analysis of RAGE knock out mice

5.1 Introduction

Receptor for advanced glycation end products (RAGE) is a cell surface receptor, which binds to Aβ, AGEs, S100/Calgranulins and amphoterin (Lue *et al.* 2005). Tg mice overexpressing neuron targeted RAGE in an Aβ rich environment (Tg mAPP/RAGE) displayed accelerated/exaggerated spatial memory and learning impairment and loss of density of cholinergic fibers and synapses at an early stage compared to Tg mAPP, Tg RAGE and non-Tg littermates. In contrast, Tg mAPP/DN-RAGE mice exhibited a preservation of cognitive function at an early stage and the decrease in AChE-positive neurites in the subiculum, were virtually completely prevented in Tg mAPP/DN-RAGE mice (Arancio *et al.* 2004). These data collectively suggested that RAGE may accelerate Aβ induced cytotoxicity at an early stage of AD and blocking of this interaction can rescue cognitive dysfunction.

Prof ShiDu Yan (College of Physicians and Surgeons, Columbia University), our collaborators in the United States, provided us with mice cortex of four different genotypes including non-Tg littermates, Tg mAPP, Tg DN-RAGE and Tg mAPP/DN-RAGE. A two dimensional electrophoresis method was employed to study differential protein expression between different genotypes of mice brain. The

results of the analysis could provide insights into the cognitive rescuing mechanisms in Tg mAPP/DN-RAGE mice. Furthermore, the results could also be important for finding potential therapeutic targets in the treatment of AD.

5.2 Two dimensional electrophoresis analysis using Hoefer-DALT system

5.2.1 Identification of glyoxalase 1

Mice cortices (8-9 months old) from four different genotypes of animals including non-Tg littermates, Tg mAPP, Tg DN-RAGE and Tg mAPP/DN-RAGE were sent to us on dry ice by Prof ShiDu Yan (College of Physicians and Surgeons, Columbia University). Sample preparation of mice cortex and the subsequent two dimensional electrophoresis were performed as described in section 2.4.3. Mice cortices from three different animals for each of the four genotypes were lysed in lysis buffer 1 [8 M Urea, 2 M Thio-Urea, 4% chaps, 1% IPG buffer (pH 3-10), 40 mM Tris base and 100 μl sigma protease inhibitor]. In the first dimension, mice cortex proteins were separated by applying 1 mg of protein of each sample onto 18 cm IPG drystrips with a pH interval of 3-10. After isoelectric focusing, the IPG drystrips were loaded onto premade 10% SDS polyacrylamide gels for second dimensional separation. Electrophoresis of 12 gels was carried out in Hoefer-Dalt system at 15°C for 16-20 hours. The SDS polyacrylamide gels were silver stained. Images of the gels were captured using a Typhoon 9200 laser scanner and printed onto laser transparent

papers after processing with Adobe Photoshop. Representative two dimensional gel images are shown in Figure 5.1. Differential protein expression between different genotypes of mice brain was analyzed by eye using these gel images. Only the protein spots, which displayed a difference in the levels of expression in all three gels of the same genotype as compared to that in all three gels of another genotype, were selected. A protein was found consistently upregulated in Tg DN-RAGE and Tg mAPP/DN-RAGE animals compared to Tg mAPP and non-Tg mice (Figure 5.2). This protein spot was then excised from the gels and stored in 1 ml MQ at 4°C. Using MALDI-TOF mass spectrometry, this protein was identified as glyoxalase 1 (GLO1).

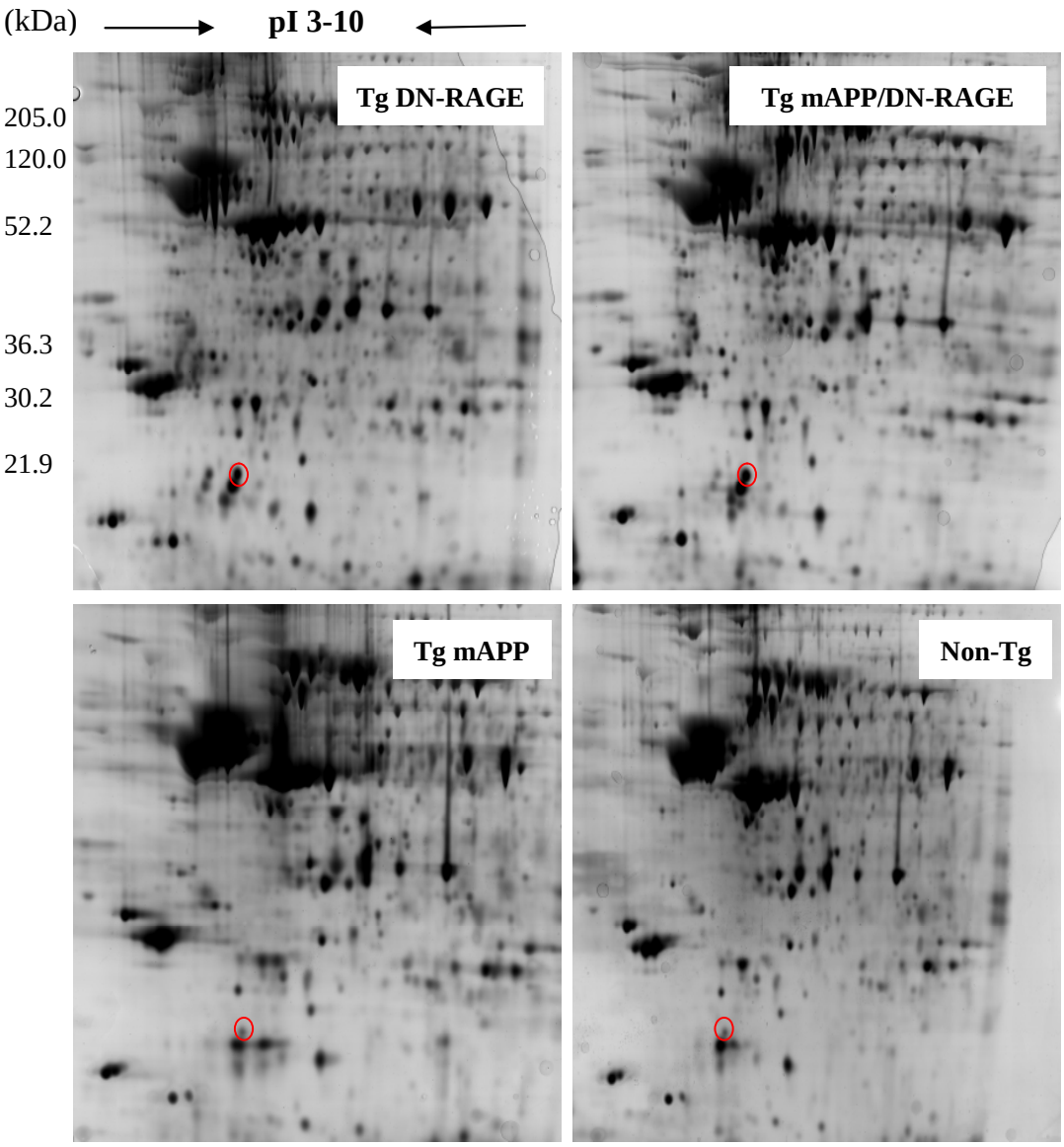

Figure 5.1 Representative images of silver stained two dimensional gels. 1 mg of protein sample from each genotype was loaded onto 18 cm IPG strips containing a pH interval of 3-10. The focused IPG strips were loaded onto 10% SDS polyacrylammide gels and the electrophoresis was carried out in Hoefer-Dalt system. Two dimensional gels were then silver stained and images of the gels were captured with an image scanner and processed with Adobe Photoshop. After comparison studies by eye, one protein spot (indicated by red circles), latterly identified as GLO1, was found to be increased in Tg DN-RAGE and Tg mAPP/DN-RAGE mice brains compared to Tg mAPP and non-Tg mice brains.

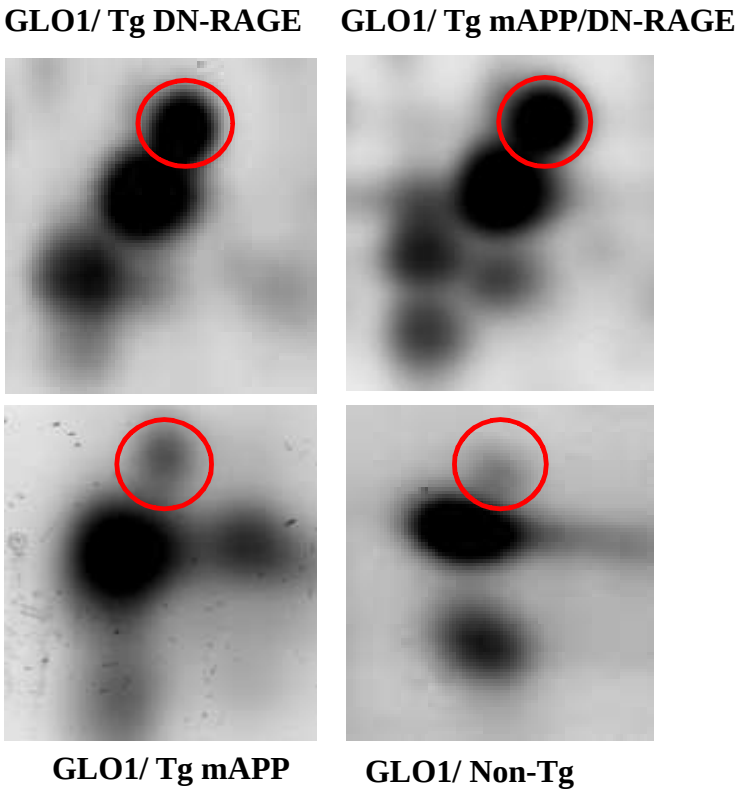

Figure 5.2 Partial images of two dimensional gels. The expression level of GLO1 (indicated by red circles) in Tg DN-RAGE and Tg mAPP/DN-RAGE mice was significantly higher than in Tg mAPP and non-Tg animals.

5.2.2 mRNA expression of GLO1

The mRNA expression of GLO1 was studied by Prof ShiDu Yan's group (College of Physicians and Surgeons, Columbia University) using RT-PCR to confirm the differential expression of GLO1 between different genotypes of mice brain. Tg mAPP/DN-RAGE exhibited a 1.5 fold increase of the mRNA expression level of GLO1 compared to non-Tg animals. However, unlike the results obtained by two dimensional electrophoresis studies, the mRNA expression level of GLO1 in Tg DN-RAGE mice was comparable with that in non-Tg and Tg mAPP animals (Figure 5.3).

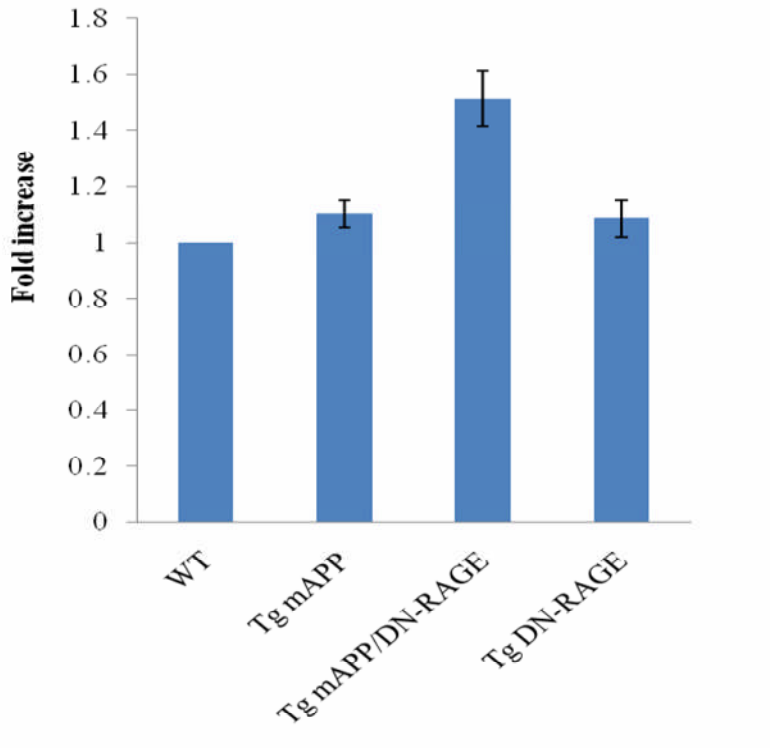

Figure 5.3 The mRNA expression level of GLO1 in non-Tg, Tg mAPP, Tg DN-RAGE and Tg mAPP/DN-RAGE was assessed by real-time RT-PCR. Data are presented as fold increase over non-Tg animals for each type of transgenic animals. There was a significant increase of the expression level of GLO1 in Tg mAPP/DN-RAGE animals as compared to non-Tg, Tg mAPP and Tg DN-RAGE animals (Figure supplied by Prof Shi Du Yan, College of Physicians and Surgeons, Columbia University).

5.2.3 Protein expression level of GLO1 in Tg mAPP and Tg mAPP/DN-RAGE mice cortex

To confirm the RT-PCR results, protein expression level of GLO1 in Tg mAPP/DN-RAGE and Tg mAPP animals was examined using immunoblotting method. Mice cortices from three of each of Tg mAPP/DN-RAGE and Tg mAPP animals were minced and lysed with RIPA buffer as described in section 2.4.1. Protein concentrations were quantified using Bradford's reagent. Equal amount of proteins were loaded onto a 4-12% mini Bis-Tris gel for electrophoresis. Proteins

were then transferred to a polyvinylidene fluoride (PVDF) transfer membrane. After blocking overnight in 5% milk + TBS/T, the membrane was incubated with an anti-GLO1 antibody (From Dr Carol Brown, Department of Pharmacology, University of California, San Diego) at a dilution of 1:2000 overnight. After three five minutes washes in TBS/T, the blot was incubated with HRP conjugated goat anti-rabbit secondary antibody at a dilution of 1:5000 for one hour. The membrane was washed in TBS/T for three times of ten minutes each and then subjected to ECL detection. To control for equal loading of protein samples, after five ten minutes washes, the blot was stripped and reprobed with β-actin antibody. Tg mAPP mice displayed highly varied expression of GLO1 as shown in Figure 5.4A. The immunoblot bands were quantified using ImageJ software. The intensities of the GLO1 bands were normalized to β-actin signals. The relative expression of GLO1 is expressed as means ± S.E.M. Statistical analysis was performed using student's t test. No significant difference in the expression level of GLO1 between Tg mAPP and Tg mAPP/DN-RAGE was observed (Figure 5.4B.).

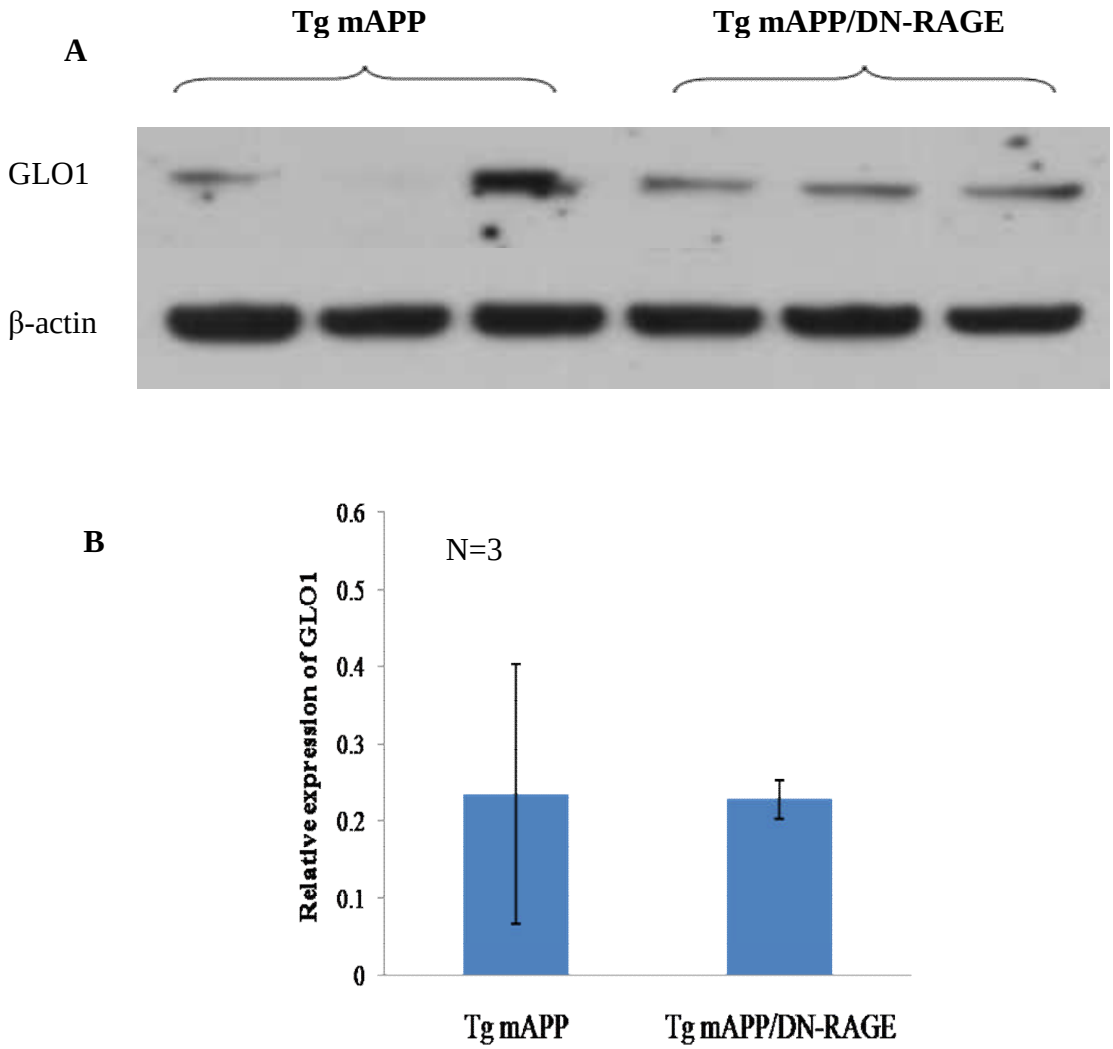

Figure 5.4 (A) Immunoblotting study of GLO1 expression in Tg mAPP and Tg mAPP/DN-RAGE animals. The blot was reprobed with β-actin antibody as indicated to control for equal loading. (B) The immunoblot bands were quantified using ImageJ software. The GLO1 expression levels were normalized to actin levels. Results of the relative expression of GLO1 are expressed as means ± S.E.M. There was no significant difference in the expression level of GLO1 between Tg mAPP and Tg mAPP/DN-RAGE animals.

5.3 Two dimensional electrophoresis using Ettan-Dalt system

With a new set of 8-9 months mice cortices from four different genotypes including non-Tg, Tg mAPP, Tg DN-RAGE and Tg mAPP/DN-RAGE, which were kindly provided by Prof ShiDu Yan (College of Physicians and Surgeons, Columbia University) and our new Ettan-Dalt two dimensional electrophoresis system, a more thorough screening analysis for differential protein expression between different genotypes of mice brain was then able to be performed.

Longer IPG strips provide high resolution and protein loading capacity which would allow the detection of more spots and facilitate the identification of proteins in the spots. 18 cm IPG gels were used in the first dimension in the above experiments. In the following two dimensional electrophoresis studies, 24 cm IPG gels were used to achieve better resolution.

Beside the length of IPG gels, the pH intervals of IPG gels are also important. Narrow pH range delivers high resolution and protein loading capacity. In the following studies, IPG strips with a linear gradient pH 3–10 were used for an overview of total protein distribution. IPG strips with pH 4–7 and pH 6–9 were combined to obtain a more detailed study of protein distribution.

5.3.1 Two dimensional electrophoresis studies using IPG strips containing a linear gradient pH 3–10

5.3.1.1 Differential protein expression between wild type and Tg DN-RAGE mice

Sample preparation of mice cortex and the subsequent two dimensional electrophoresis were performed following the protocol described in section 2.4.3. Mice cortices from three different animals for each of the four genotypes including non-Tg, Tg mAPP, Tg DN-RAGE and Tg mAPP/DN-RAGE were lysed in lysis buffer 2 [8 M Urea, 4.5% chaps, 1% DTT, 2% IPG buffer (pH 3-10), 10 µl nucleic acid inhibitor, 10 µl PMSF and 40 µl Roche protease inhibitor cocktail]. In the first dimension, 1 mg of proteins of each sample was applied onto 24 cm IPG gels with a pH interval of 3-10. After isoelectric focusing, the IPG gels were loaded onto precast DALT Gel 12.5 gels for second dimensional separation. In total, six gels were run in an Ettan-Dalt two dimensional electrophoresis system at 4°C for 16-20 hours. The proteins on the gels were visualized by silver staining. Gel images were captured with a Typhoon 9,200 laser scanner and analyzed using ImageMaster software as described in section 2.5.5. For each genotype of mice, three two dimensional gels were used for analysis. Data of the relative spot volumes (volume of a spot / total volume of all the spots in a gel) are expressed as means ± S.E.M. Statistical significance was studied using student's t test ($p<0.05$). Gap values for each spot between two different genotypes were calculated automatically by ImageMaster software. Only the spots that exhibited both positive gap values and a statistical significance ($p<0.05$) were selected. Three proteins were found to be

differentially expressed between Tg DN-RAGE mice and non-Tg littermates. However, no protein spots were identified to be differentially expressed between Tg mAPP mice and Tg mAPP/DN-RAGE mice. The three spots identified were then excised from the gels and subjected to MALDI-TOF mass spectrometry analysis. These proteins were identified as translation initiation factor eIF-5A (eIF-5A), glia maturation factor beta (GMFB), and fatty acid-binding protein, epidermal (E-FABP). The relative spot volume of E-FABP in Tg DN-RAGE mice (0.99±0.16) was significantly higher than in non-Tg littermates (0.6±0.15). In contrast, the relative spot volumes of eIF-5A and GMFB were decreased from 0.8±0.16 and 0.86±0.18 in non-Tg littermates to 0.52±0.05 and 0.47±0.01 in Tg DN-RAGE mice, respectively.

Representative two dimensional gels of Tg DN-RAGE mice and non-Tg littermates are shown in Figure 5.5. The spots indicated by red circles are proteins identified to be differentially expressed between Tg DN-RAGE animals and non-Tg littermates. The identified proteins including eIF-5A, GMFB, and E-FABP are also shown in enlarged partial images of two dimensional gels (Figure 5.6).

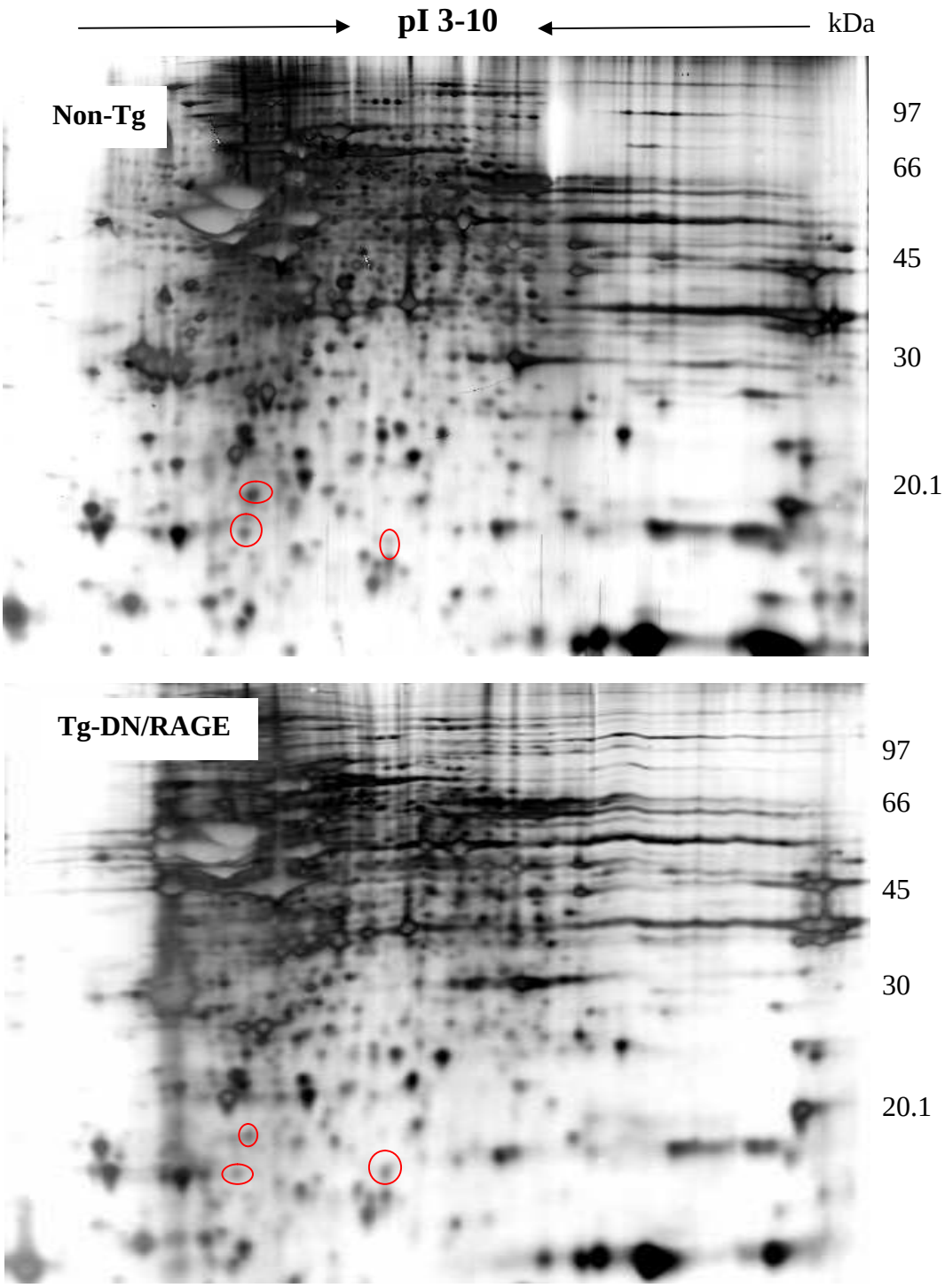

Figure 5.5 Representative two dimensional gel images of mice cortex from Tg DN-RAGE mice and non-Tg littermates. 1 mg of proteins of each sample was applied onto 24 cm IPG gels. After isoelectric focusing, the IPG strips were loaded onto precast DALT gel 12.5 gels and run in an Ettan-Dalt system. After silver staining, the gel images were captured with image scanner and analyzed with ImageMaster software. Three proteins were found to be differentially expressed (as indicated by red circles) between Tg DN-RAGE mice and non-Tg littermates.

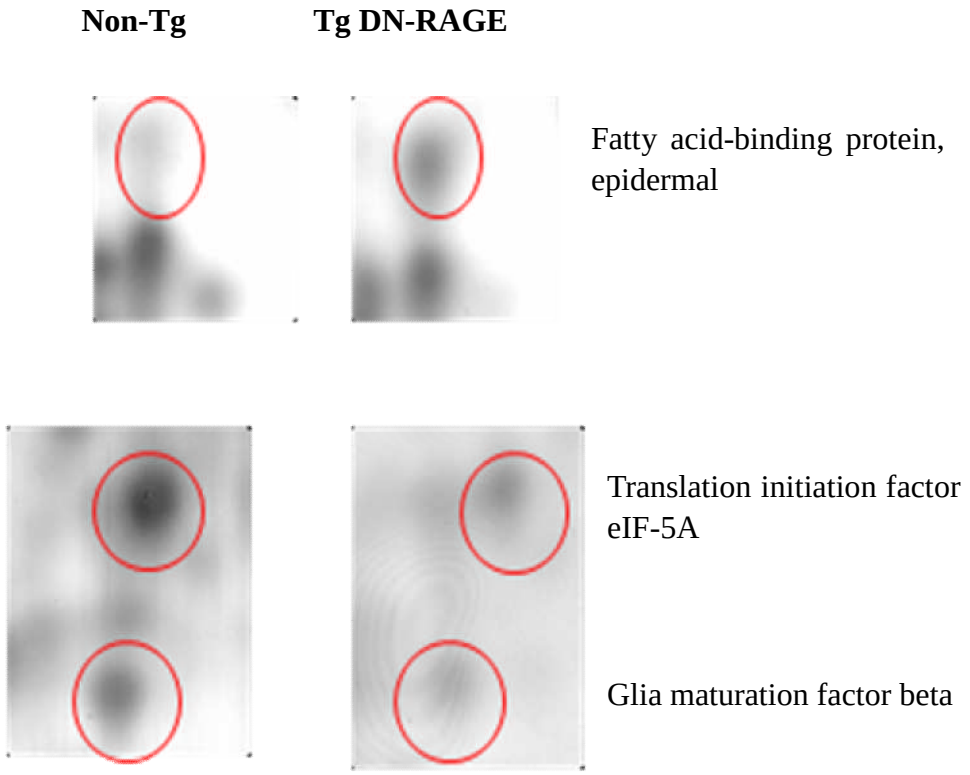

Figure 5.6 Partial images of two dimensional gels showing that three proteins including translation initiation factor eIF-5A, glia maturation factor beta, and fatty acid-binding protein, epidermal were differentially expressed between non-Tg littermates and Tg DN-RAGE mice. Fatty acid-binding protein (epidermal) (indicated by red circles) was found to be upregulated in Tg DN-RAGE animals compared to non-Tg littermates, whereas eIF-5A and GMFB (indicated by red circles) were downregulated.

5.3.1.2 Confirmation of differential protein expression between non-Tg and Tg DN-RAGE using RT-PCR

The mRNA expression levels of eIF-5A, GMFB, and E-FABP were studied using RT-PCR method by Prof ShiDu Yan's group (College of Physicians and Surgeons, Columbia University). On the contrary to the results obtained from the two dimensional electrophoresis studies, Tg DN-RAGE exhibited a 0.8 fold decrease of the mRNA expression level of E-FABP as compared to non-Tg animals. The mRNA expression levels of eIF-5A, GMFB in Tg DN-RAGE mice were increased 1.3 and

1.1 fold, respectively, compared to non-Tg animals (Figure 5.7).

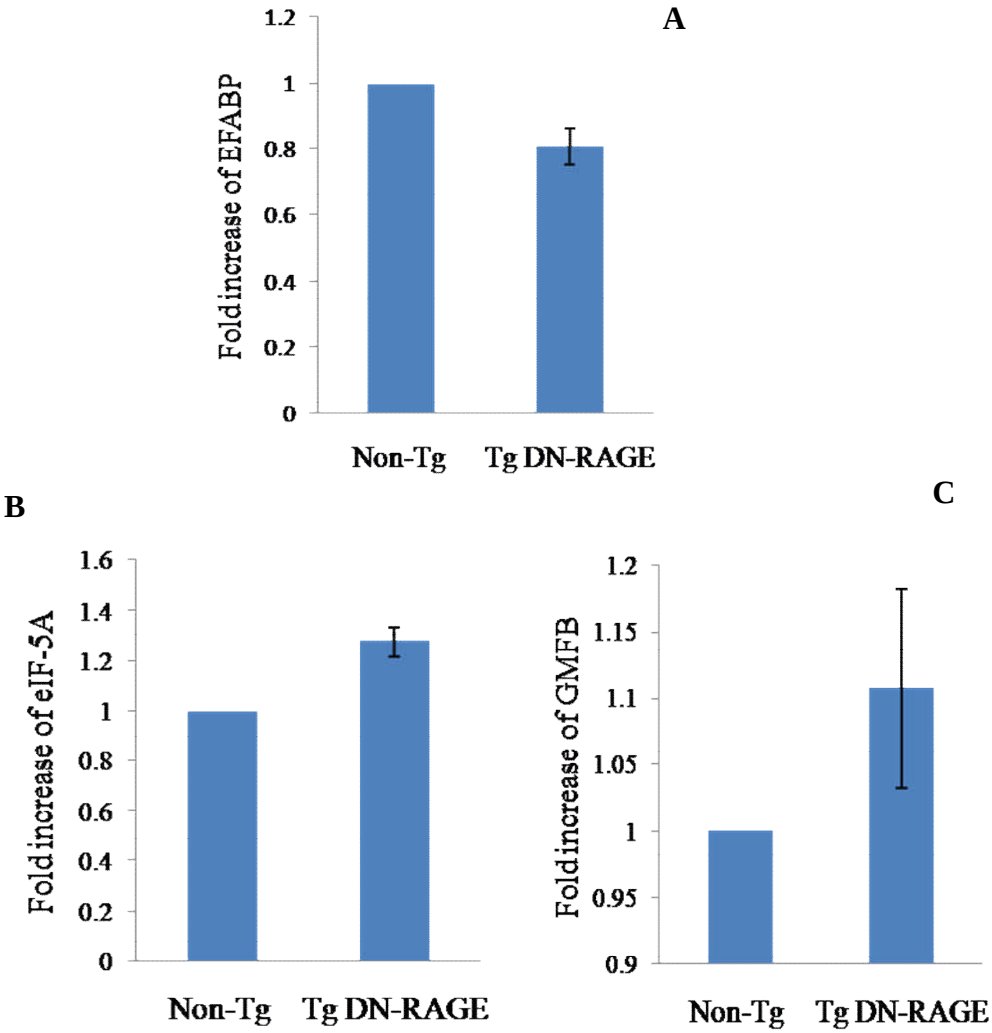

Figure 5.7 The mRNA expression levels of eIF-5A, GMFB, and E-FABP in non-Tg and Tg DN-RAGE animals were assessed by real-time RT-PCR. Data are presented as fold increase over non-Tg mice for Tg DN-RAGE mice. There was a decrease of the expression level of E-FABP in Tg DN-RAGE animals compared to non-Tg animals (A). The mRNA levels of eIF-5A (B) and GMFB (C) were increased in Tg DN-RAGE mice brains compared to non-Tg mice brains (Figure supplied by Prof Shi Du Yan, College of Physicians and Surgeons, Columbia University).

5.3.2 Two dimensional electrophoresis analysis using IPG strips containing a linear gradient pH 4–7 or pH 6-9

Using IPG strips with pH 3-10, two dimensional electrophoresis studies had successfully identified three proteins which were differentially expressed between non-Tg littermates and Tg DN-RAGE mice. However, no protein spots were found to be significantly differentially expressed between Tg mAPP and Tg mAPP/DN-RAGE mice. In order to obtain a more detailed screening analysis of differential protein expression between different genotypes of mice cortex, IPG strips with pH 4-7 were combinely used with IPG strips with pH 6-9.

Mice cortex sample preparation and two dimensional electrophoresis were again performed following the protocols described in section 2.5. Mice cortices from four genotypes of mice including non-Tg littermates, Tg mAPP, Tg DN-RAGE and Tg mAPP/DN-RAGE were lysed in lysis buffer 2. For each genotype of animals, mice cortices from three different animals were used. 1 mg of proteins from each sample was applied onto 24cm IPG gels with pH 4-7 and pH 6-9. Focused IPG strips were then loaded onto precast DALT 12.5 gels. Electrophoresis of gels was carried out in an Ettan-Dalt system. The proteins on the gels were visualized by silver staining. Gel images were captured using a Typhoon 9200 scanner and analyzed with ImageMaster software as described in 5.3.1.

5.3.3 Differential protein expression between Tg mAPP and Tg mAPP/DN-RAGE using IPG strips with pH 4-7

Three proteins were found to be differentially expressed between Tg mAPP mice and Tg mAPP/DN-RAGE mice. The identified protein spots were excised from two dimensional gels and sent for mass spectrometry analysis. These three proteins were identified as NDUFV2 (NADH ubiquinone oxidoreductase flavoprotein 2), PSMB4 (Proteasome subunit beta type 4), and Nit protein 2 (Nitrilase family, member 2). In comparison with Tg mAPP mice, NDUFV2 and PSMB4 were upregulated in Tg mAPP/DN-RAGE mice whereas Nit protein 2 was down regulated. The relative volumes of identified protein spots are expressed as means ± SD. The relative spot volumes of NDUFV2 and PSMB4 were significantly increased from 0.09±0.06 and 0.18±0.02 in Tg mAPP mice to 0.3±0.08 and 0.26±0.01 in Tg mAPP/DN-RAGE mice, respectively. In contrast, the relative spot volume of Nit protein 2 was decreased from 0.08±0.01 in Tg mAPP mice to 0.054±0.005 in Tg mAPP/DN-RAGE mice. Representative two dimensional gel images of Tg mAPP/DN-RAGE and Tg mAPP using IPG strips with pH 4-7 are shown in Figure 5.8. The proteins which were identified to be differentially expressed between Tg mAPP/DN-RAGE and Tg mAPP are indicated by red circles. The identified proteins including NDUFV2, PSMB4 and Nit protein 2 are also shown in enlarged partial images of two dimensional gels (Figure 5.9).

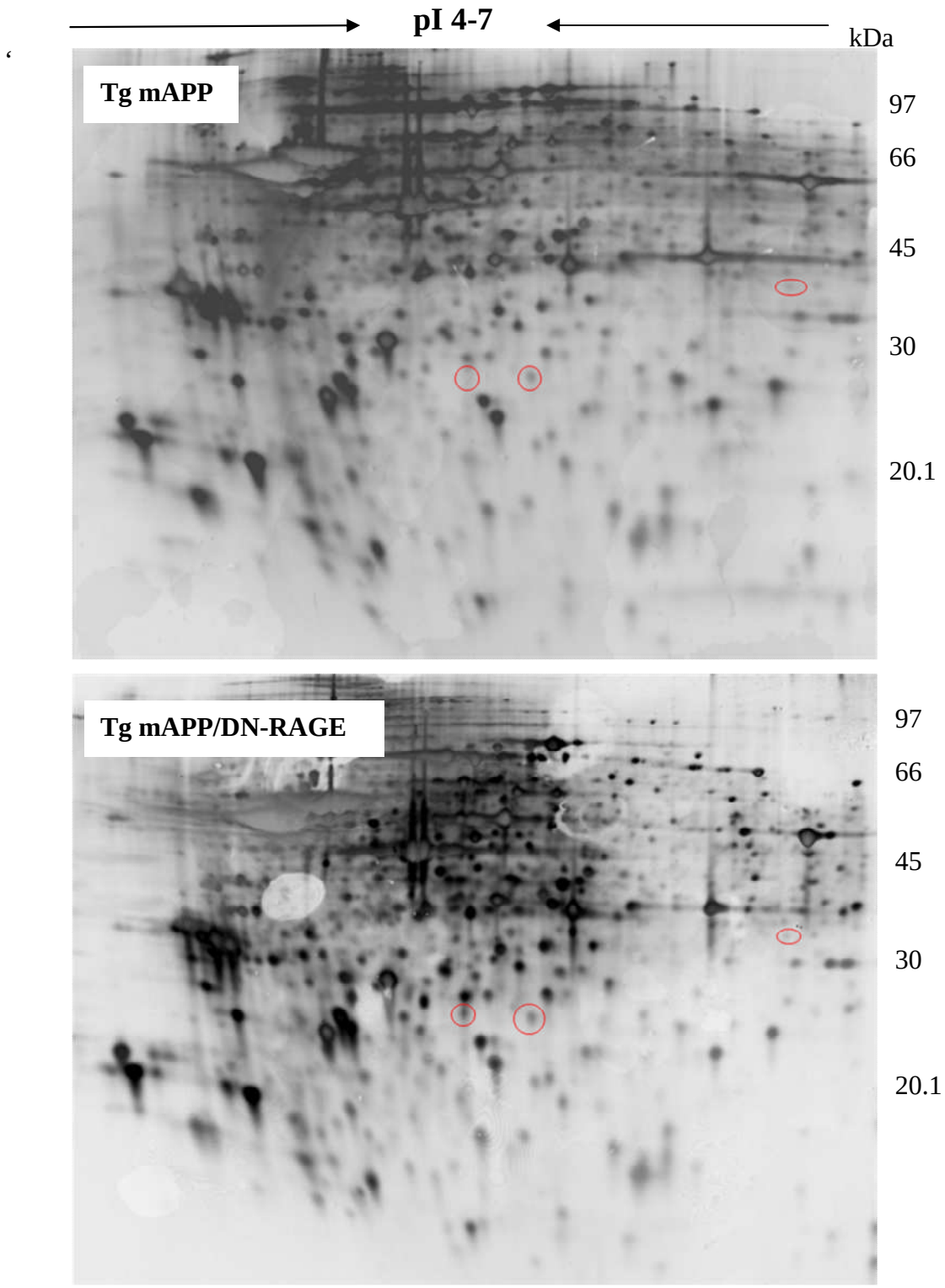

Figure 5.8 Representative two dimensional gel images of Tg mAPP/DN-RAGE and Tg mAPP mice cortex using IPG strips (pH 4-7). 1 mg of proteins of Tg mAPP or Tg mAPP/DN-RAGE mice cortex was separated in the first dimension using IPG strip (pH 4-7). In the second dimension, the proteins were separated on precast DALT 12.5 gels. After silver staining, gels images were captured with an image scanner and analyzed using ImageMaster software. Three proteins (indicated by red circles) were identified to be differentially expressed between Tg mAPP and Tg mAPP/DN-RAGE mice cortex.

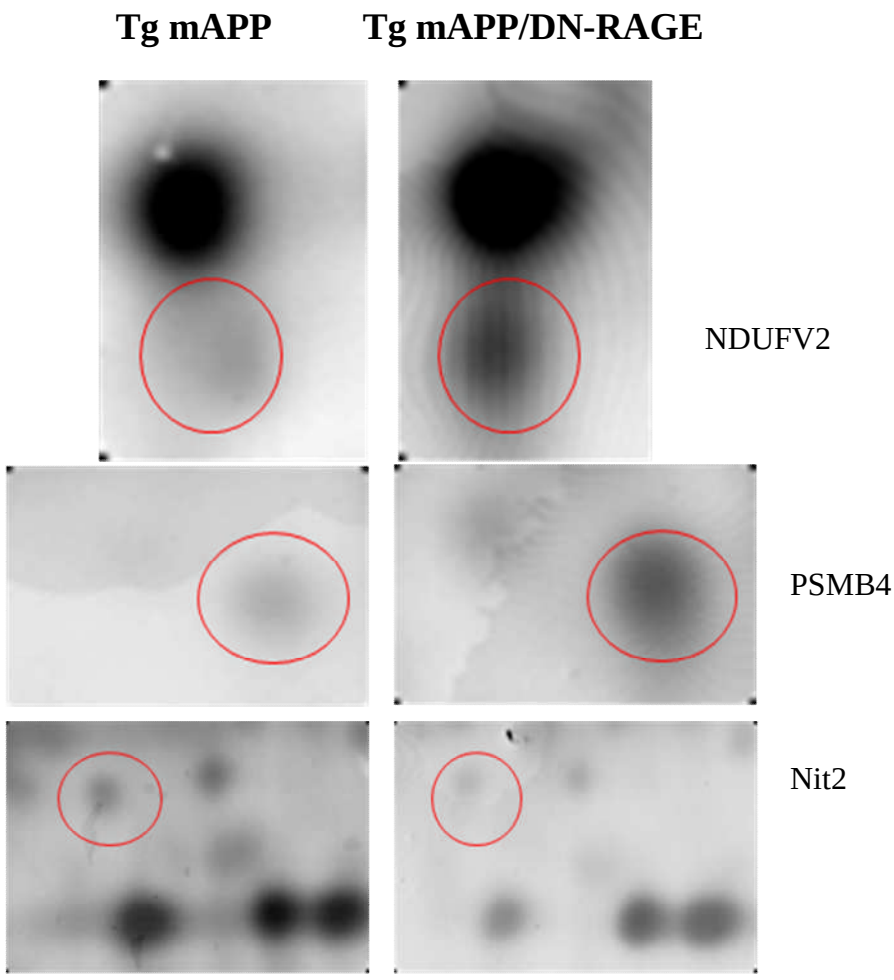

Figure 5.9 Partial images of two dimensional gels indicating the differential expression of three proteins between Tg mAPP and Tg mAPP/DN-RAGE mice cortex. The expression levels of NDUFV2 and PSMB4 were increased in Tg mAPP/DN-RAGE mice compared to Tg mAPP mice. In contrast, the expression level of Nit protein 2 was decreased in Tg mAPP/DN-RAGE mice compared to Tg mAPP animals.

5.3.3.1 Study of protein expression levels of PSMB4 and NDUFV2 in Tg mAPP and Tg mAPP/DN-RAGE mice cortex using immunoblotting method

Two dimensional electrophoresis studies had found that three proteins including PSMB4, NDUFV2 and Nit protein 2 were differentially expressed between Tg mAPP and Tg mAPP/DN-RAGE mice cortex. To confirm the results of the two

dimensional electrophoresis, immunoblotting method was used. A monoclonal antibody for PSMB4 was obtained from Biomol international and monoclonal anti-NDUFV2 was a kind gift from Dr Ian M. Fearnley (MRC Dunn Human Nutrition Unit, Wellcome Trust / MRC Building, Cambridge). However, no commercial or home made antibodies for Nit protein 2 were available.

Tg mAPP and Tg mAPP/DN-RAGE mice cortices were lysed in RIPA buffer as described in section 2.4.1. Cortices from three different animals of each genotype were used. The protein lysates were quantified using Bradford's reagent. Equal amounts of proteins were loaded onto 4-12% Bis-Tris mini gels. After electrophoresis, the proteins were transferred to nitrocellulose membranes. The membranes were blocked in TBS/T + 5% milk overnight at 4°C. Monoclonal anti-PSMB4 (1:2000) or monoclonal anti-NDUFV2 (1:5000) was incubated with membranes for one hour. After three five minutes washes in TBS/T, the membranes were incubated with HRP conjugated goat-anti-rabbit (1:5000) or goat-anti-mice (1:5000) for an hour. The membranes were washed again in TBS/T for three times, five minutes of each and then subjected to ECL detection. To control for equal protein loading, the membranes were stripped and reprobed with β-actin antibody. The immunoblot bands were quantified using ImageJ software. The intensities of the protein bands of PSMB4 and NDUFV2 were normalized to those of β-actin bands. The relative expression levels of PSMB4 and NDUFV2 are expressed as means ± S.E.M. Statistical difference was analyzed by student's t test ($p<0.05$).

5.3.3.2 Protein expression level of NDUFV2 in Tg mAPP and Tg mAPP/DN-RAGE mice cortex

A western blot image of detection of NDUFV2 in Tg mAPP and Tg mAPP/DN-RAGE mice cortex is shown in Figure 5.10. The blot was stripped and reprobed with β-actin as indicated. Both Tg mAPP and Tg mAPP/DN-RAGE mice cortex exhibited varied expression level of NDUFV2. Quantitative analysis found that there is no significant difference in the relative expression level of NDUFV2 between Tg mAPP and Tg mAPP/DN-RAGE mice cortex (Figure 5.11).

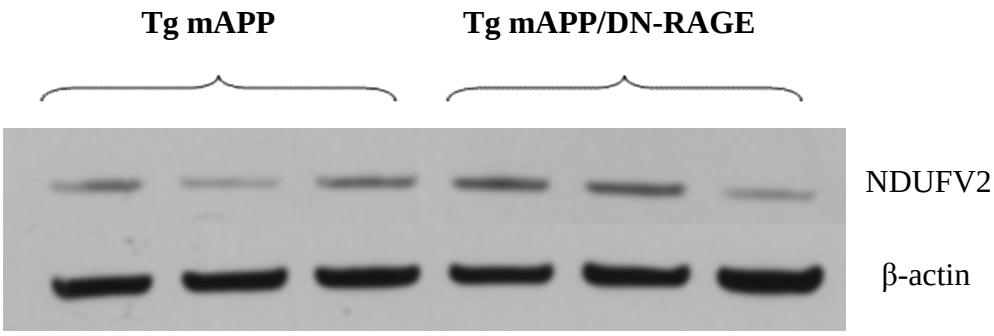

Figure 5.10 A western blot image of protein extracts of Tg mAPP and Tg mAPP/DN-RAGE mice cortex probed with monoclonal anti-NDUFV2. The blot was stripped and reprobed with β-actin antibody. Varied expression level of NDUFV2 was observed in both Tg mAPP and Tg mAPP/DN-RAGE mice cortex.

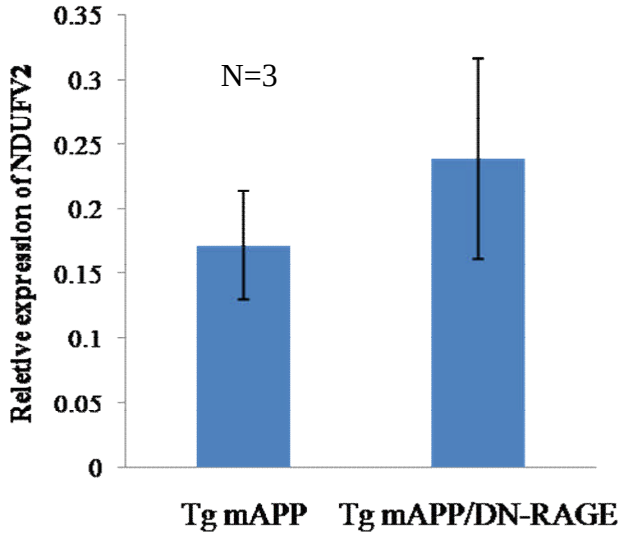

Figure 5.11 Quantitative analysis of the relative expression of NDUFV2 in Tg mAPP and Tg mAPP/DN-RAGE mice cortex. The immunoblot bands were quantified using ImageJ software. The expression level of NDUFV2 was normalized to that of actin. Data of the relative expression of NDUFV2 are expressed as means ± S.E.M. There was no significant difference in the relative expression level of NDUFV2 between Tg mAPP and Tg mAPP/DN-RAGE mice.

5.3.3.3 Protein expression level of PSMB4 in Tg mAPP and Tg mAPP/DN-RAGE mice cortex

A western blot image of Tg mAPP and Tg mAPP/DN-RAGE probed with monoclonal anti-PSMB4 is displayed in Figure 5.12. To control for equal loading, the membrane was stripped and reprobed again with β-actin antibody. Quantitative analysis revealed that the relative expression level of PSMB4 was significantly increased from 0.068±0.04 in Tg mAPP mice cortex to 0.36±0.11 in Tg mAPP/DN-RAGE cortex (Figure 5.13.).

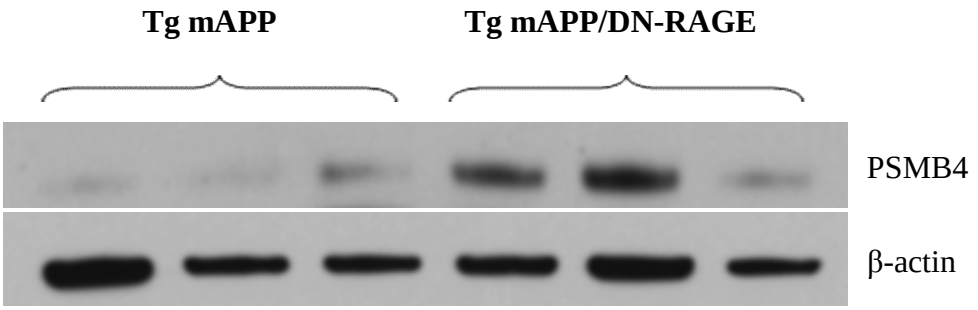

Figure 5.12 A western blot image of Tg mAPP and Tg mAPP/DN-RAGE mice cortex probed with monoclonal anti-PSMB4. The blot was stripped and reprobed with β-actin antibody. The expression level of PSMB4 was significantly increased in Tg mAPP/DN-RAGE mice cortex compared to Tg mAPP mice cortex.

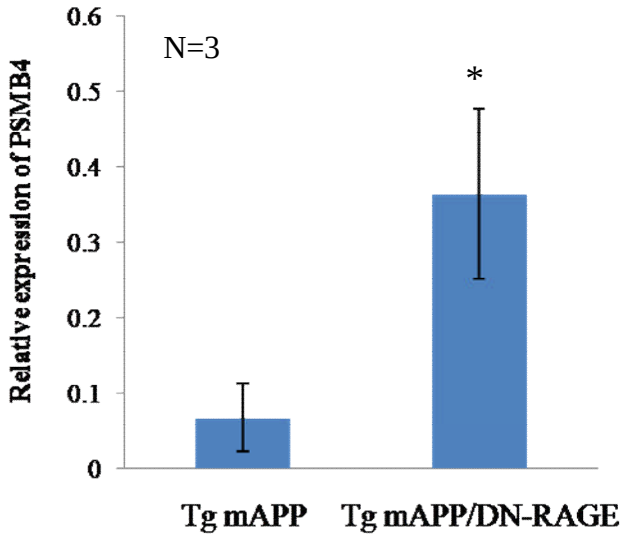

Figure 5.13 Quantitative analysis of the relative expression level of PSMB4 in Tg mAPP and Tg mAPP/DN-RAGE mice cortex. The immunoblot bands were quantified using ImageJ software. The expression level of PSMB4 was normalized to that of actin. The results of the relative expression of PSMB4 are expressed as means ± S.E.M. Tg mAPP/DN-RAGE mice cortex displayed a significantly enhanced level of PSMB4 expression compared to Tg mAPP mice cortex. * indicates a significance level of 0.05.

5.3.4 Differential protein expression between Non-Tg and Tg DN-RAGE mice cortex using IPG strips with pH 4-7

Three proteins were identified to be differentially expressed between non-Tg and Tg DN-RAGE mice cortex. These protein spots were then excised from the gels and sent for mass spectrometry analysis. The selected proteins were identified as alpha enolase, sepiapterin reductase and triose-phosphate isomerase. All three proteins were found to be upregulated in Tg DN-RAGE mice compared to non-Tg littermates. The relative volumes of identified protein spots are expressed as means ± SD. The relative spot volumes of alpha enolase, sepiapterin reductase and triose-phosphate isomerase were significantly increased from 0.09±0.03, 0.11±0.01, 0.13±0.04 in non-Tg mice to 0.18±0.02, 0.19±0.01, 0.24±0.03 in Tg DN-RAGE mice, respectively. Representative images of two dimensional gels of Tg mAPP/DN-RAGE and Tg mAPP mice cortex using IPG strips (pH 4-7) are shown in Figure 5.14. The proteins that were identified to be differentially expressed between Tg DN-RAGE mice and non-Tg littermates are indicated by red circles. The identified proteins including alpha enolase, sepiapterin reductase and triose-phosphate isomerase are also displayed in enlarged partial images of two dimensional gels (Figure 5.15).

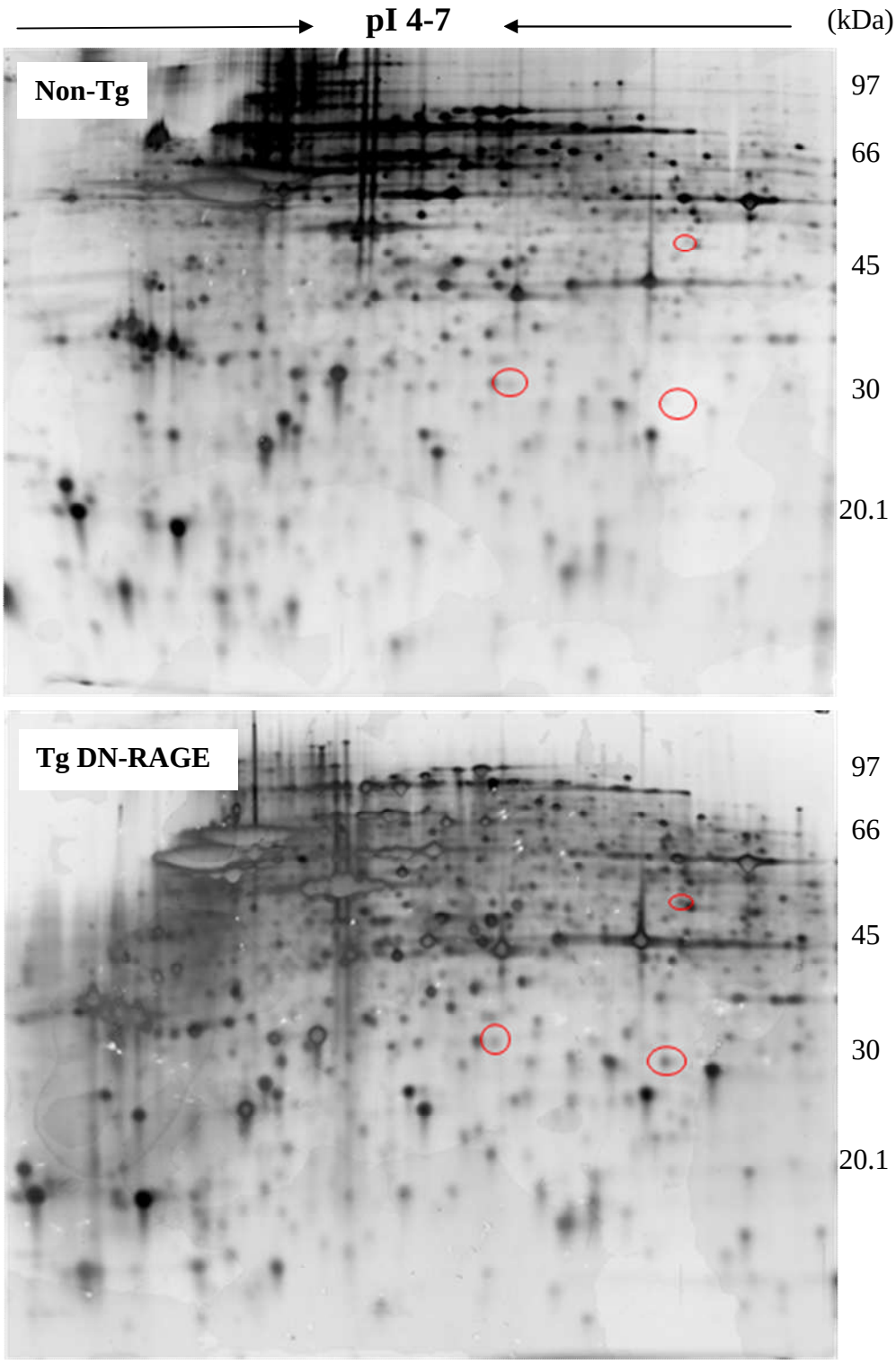

Figure 5.14 Representative two dimensional gel images of mice cortex from Tg DN-RAGE and non-Tg. 1 mg of proteins of each sample was applied onto 24 cm IPG gels (pH 4-7). After isoelectric focusing, the IPG strips were loaded onto precast DALT gel 12.5 gels and run in an Ettan-Dalt system. After silver staining, the gel images were captured with image scanner and analyzed using ImageMaster software. Three proteins were found to be upregulated (as indicated by red circles) in Tg DN-RAGE mice cortex compared to non-Tg mice cortex.

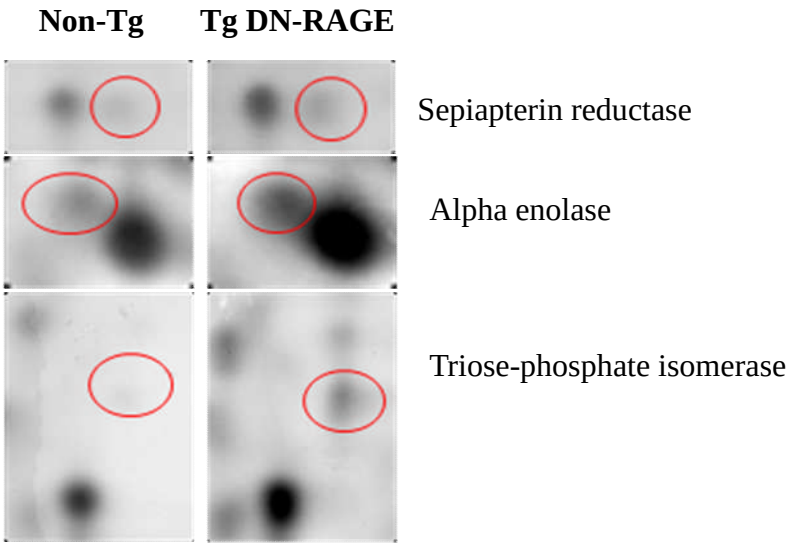

Figure 5.15 Partial images of two dimensional gels showing that three proteins (indicated by red circles) were differentially expressed between non-Tg littermates and Tg DN-RAGE animals. Alpha enolase, sepiapterin reductase and triose-phosphate isomerase were all upregulated in Tg DN-RAGE mice cortex compared to non-Tg mice cortex.

5.3.5 Two dimensional electrophoresis analysis using IPG strips containing a 6-9 pH gradient

With IPG strips (pH 6-9), a more detailed protein distribution in the alkaline pI range was obtained. There were three two dimensional gels for each of the four genotypes including non-Tg, Tg mAPP, Tg DN-RAGE and Tg mAPP/DN-RAGE. The 12 gels were analyzed using ImageMaster software. No protein spots were found to be differentially expressed between non-Tg mice cortex and Tg DN-RAGE mice cortex. Quantitative comparisons of the protein spots between Tg mAPP and Tg mAPP/DN-RAGE mice cortex revealed no significant differences as well. A representative image of a two dimensional gel using IPG strip (pH 6-9) is shown in Figure 5.16.

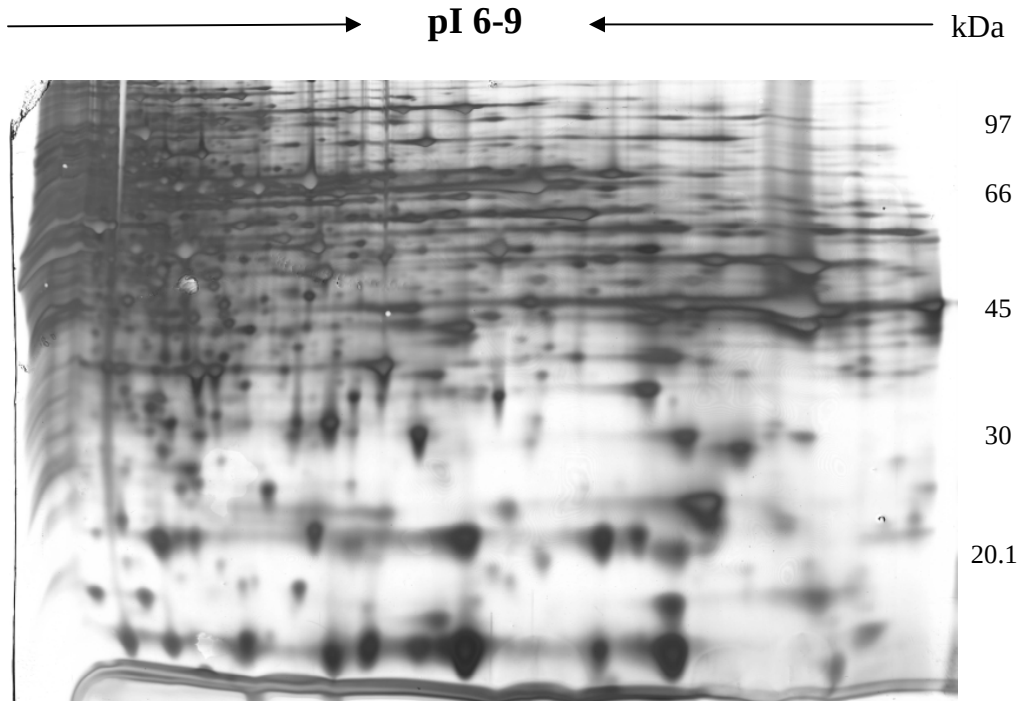

Figure 5.16 A representative image of two dimensional gel using IPG strip (pH 6-9). 1 mg protein of mice cortex was applied onto IPG strip (pH 6-9). The focused strip was then loaded onto a precast DALT 12.5 gel. After completion of electrophoresis, the gel was silver stained.

All the proteins that had been identified with altered expression levels between different genotypes of mice are summarized in Table 5.1. The molecular weight and pI of theses proteins are displayed. Also, the number of matched peptides and sequences coverage for the mass spectrometry analysis are shown.

Protein name	Accession Number Swiss-Prot	Molecular mass (kDa)	pI	Number of matched peptides	Sequence coverage (%)
GLO 1	Q09751	20.774	5.08	16	30
NDUFV2	Q8K2L0	27.61	7	6	33
PSB4	Q5IST4	24.83	5.5	3	14
Nit 2	Q9JHW2	30.825	6.44	22	40
eIF-5A	Q5NCX0	17.049	5.08	16	51
GMFB	Q9CQI3	16.752	5.07	6	16
EFABP	Q05816	15.338	6.18	9	25
Alpha enolase	Q5FW97	47.322	6.36	14	21
Triosephosphate isomerase	AAH46761	26.907	7.08	12	41
Sepiapterin reductase	Q91XH5	27.947	5.97	8	25

Table 5.1 List of characteristics of all identified proteins that were differentially expressed between Tg mAPP and Tg mAPP/DN-RAGE mice, or non-Tg and Tg DN-RAGE animals.

5.4 Discussion

5.4.1 Altered expression of GLO1, PSMB4, NDUFV2 and Nit 2 between Tg mAPP/DN-RAGE mice brain and Tg mAPP mice brain

Transgenic mice overexpressing neuronal targeted RAGE in an Aβ rich environment displayed accelerated cognitive impairment whereas Tg mAPP/ DN-RAGE exhibited preserved cognitive function as compared to Tg mAPP (Arancio *et al.* 2004). These data indicated a role of RAGE in the early stages of Alzheimer's disease. To elucidate the signaling mechanisms underlying the involvement of RAGE in AD, a two dimensional electrophoresis method was used to identify differential protein expression between Tg mAPP and Tg mAPP/DN-RAGE mice cortex. This involved separating proteins with respect to their pI by isoelectric focusing in the first dimension and according to size by SDS-PAGE in the second dimension.

Four proteins, GLO1, PSMB4, NDUFV2 and Nit protein 2 were identified by two dimensional electrophoresis to be differentially expressed between Tg mAPP and Tg mAPP/DN-RAGE mice brains. These results were further tested using western blotting and RT-PCR. Due to limited resources, we were not able to perform RT-PCR analysis in our laboratory. All RT-PCR results were obtained from Prof ShiDu Yan (College of Physicians and Surgeons, Columbia University). Therefore, the mRNA expression levels of identified proteins were not all analyzed with RT-PCR In the following sections, their known function and their possible

involvement in the early stages of AD will be discussed.

5.4.1.1 AGEs, GLO1 and AD

AGEs are predominantly formed by the non-enzymatic and irreversible reaction of the amino groups of proteins with reactive dicarbonyl compounds, such as 3-deoxyglycosone, glyoxal or MG. This process involves a complex sequence of reactions, including intramolecular rearrangements, dehydration and oxididation/reduction reactions. AGE modified proteins are less soluble and more resistant to enzymatic hydrolysis (Kalousova *et al.* 2005).

It was previously demonstrated that intracellular AGE deposits increase in brains of Alzheimer's patients compared to age-matched, non-demented controls. Histochemical analysis revealed the localization of AGEs in neuritic plaques and neurofibrillary tangles in AD. Moreover, during the advancement of the disease, there was a continuous increase in the immunoreactivity of AGEs (Staniszewska *et al.* 2005; Takeuchi *et al.* 2004; Sasaki *et al.* 1998). These data suggested that increased AGEs may contribute to the pathogenesis of AD. Further support of this hypothesis came from an in vitro study which showed that AGEs can induce cell toxicity in cortical neuronal cultures (Kikuchi *et al.* 1999).

Several AGEs related signaling mechanisms were proposed to be involved in AD. Firstly, the polymerization of Aβ peptide was found to be accelerated by crosslinking through AGEs in vitro studies (Smith *et al.* 1994; Sasaki *et al.* 1998). This indicated that AGEs may be the driving force in the accelerated formation of

insoluble Aβ plaques. Also, the main constituent of neurofibrillary tangles, tau protein is enriched in lysine which is prone to AGE formation (Kuhla *et al.* 2007b). Furthermore, protein AGEs can bind several receptors and lead to intracellular responses (Schmidt *et al.* 1996; Bierhaus *et al.* 1998). In addition, compared to normal proteins, AGE modified proteins were reported to increase the rate of free radical production. This oxidative stress may contribute to DNA damage, lipid peroxidation, protein oxidation in AD (Kikuchi *et al.* 1999).

The glyoxalase system is an efficient enzymatic detoxification system suppressing the formation of methylglyoxal and glyoxal-derived AGEs. It consists of GLO1 and glyoxalase 2 (GLO2), together with the cofactor glutathione. The glyoxalase system detoxifies glyoxal and methylglyoxal, thereby preventing the formation of AGEs (Kuhla *et al.* 2006). *In situ* hybridization analysis showed that GLO1 is expressed in neurons and glial cells throughout the brain (Chen *et al.* 2004).

In healthy human brains, GLO1 RNA, protein and activities were diminished in old age. However, in brains of AD sufferers, GLO1 was found to be generally up-regulated at the beginning of the disease, and continuously decreased with advancing stage of AD (Kuhla *et al.* 2007a).

In early and middle stages of AD, co-localization of AGEs and GLO1 was observed, whereas in late stages of AD, immunoreactivity for GLO1 was diminished and AGE deposits clearly dominated (Kuhla *et al.* 2007a). These immunohistochemical results suggested that reduced GLO1 protein amounts may be the cause for accumulating AGE deposits.

In accordance with these data, several lines of evidence demonstrated a possible causal relationship between low GLO1 levels and increased formation of AGEs. Firstly, overexpression of GLO1 in endothelial cells was shown to prevent hyperglycemia-induced AGE formation (Shinohara *et al.* 1998). Moreover, a hemodialysis patient exhibited unusual high levels of AGEs and a very low activity of GLO1 (Miyata *et al.* 2001).

However, the exact mechanisms regulating synthesis and enzymatic activation of GLO1 are not understood yet. It was proposed that, in AD, GLO1 may be upregulated to reduce levels of MG and to decrease AGE formation. Alternatively, it may be up-regulated as a general stress response, independent of the levels of MG (Chen *et al.* 2004). The decrease of GLO1 protein with advancing stage of AD may be caused by post-translational downregulating influences.

In this study, by using two dimensional electrophoresis method, GLO1 was found to be increased in Tg DN-RAGE and Tg mAPP/DN-RAGE mice brain as compared to non-Tg and Tg mAPP animals. Using RT-PCR method, Prof ShiDu Yan's group (College of Physicians and Surgeons, Columbia University) found that the mRNA expression of GLO1 was increased in Tg mAPP/DN-RAGE mice as compared to Tg mAPP mice. However, further studies with western blot found no significant difference of the protein expression level of GLO1 between Tg mAPP/DN-RAGE and Tg mAPP mice cortex. This could be due to the small sample size for western blotting and the high variation of the protein expression level of GLO1 within the same genotype (Figure 5.4A). These data indicated that RAGE signaling may

contribute to GLO1 expression reduction in AD. Both Aβ and AGEs bind RAGE and trigger intracellular signaling events (Schmidt *et al.* 1996; Yan *et al.* 1998). With the advancement of AD, both Aβ and AGEs were found to be continuously increased in the brain (Staniszewska *et al.* 2005; Takeuchi *et al.* 2004). RAGE ligands accumulation leads to an ascending spiral of the receptor-induced intracellular responses which may account for the continuous decrease of GLO1 expression during the advancement of AD. The signaling events linking RAGE activation to GLO1 expression remain to be established.

5.4.1.2 PSMB4 and AD

The pathogenesis of Alzheimer's disease is characterized by protein misfolding and aggregate formation. In the human body, these misfolded proteins are generally degraded by the ubiquitin proteasome system in two successive steps: (i) covalent attachment of multiple ubiquitin molecules to the protein substrate, and (ii) degradation of the targeted protein by the 26S proteasome (Ciechanover and Schwatz 1998). The 26S proteasome complex is a symmetric structure composed of a core catalytic unit, a barrel-shaped catalytic 20S proteasome complex, which is capped at both poles by a 19S regulatory ATPase complex (19S-20S-19S). The proteasome complex is arranged as a stack of four rings, each containing seven distinct subunits, α1–7, β1–7, β1–7, α1–7. The active sites reside in three β subunits, β1, β2, and β5 (Wojcik and Di Napol 2004).

Accumulating evidences indicated that functional impairment of the proteasome is

associated with Alzheimer's disease (Keller *et al.* 2000). It was shown that overexpression of mutant amyloid precursor protein significantly inhibits proteasome chymotryptic activity in transgenic mice brains and in cultured cortical neurons and blocking of Aβ production by a γ-secretase inhibitor restores proteasome activity to levels of wild-type neurons (Fretta *et al.* 2005; Almeida *et al.* 2006). Furthermore, recombinant Aβ peptides or paired helical filament tau led to a significant reduction of the chymotryptic activity of the isolated human 20S proteasome (Keck *et al.* 2003; Oh *et al.* 2005). In addition, the expression levels of several isoforms of proteasome subunits including α4, α7, β2 and β7 were found to differ between AD and non-demented controls (Gillardon *et al.* 2007). These findings collectively suggested that in AD, misfolded proteins, including aggregated Aβ and tau, directly affects function and expression of proteasome which again favors protein misfolding and aggregation.

Several lines of evidence indicated that β7 subunit of proteasome (PSMB4) serves as an interaction partner for several proteins, such as SNEV (senescence evasion factor), a multifaceted protein that is involved in DNA doublestrand break repair and splicing. Signaling of the transforming growth factor β superfamily was also influenced by binding of Smad1 to PSMB4 (Loscher *et al.* 2005). Given these data, it was suggested that PSMB4 might be a major site for proteasome regulation, where signals from the outside might be transduced to the protease activities inside.

In the study here, by using two dimensional electrophoresis, the protein expression level of PSMB4 was found to be significantly increased in Tg mAPP/DN-RAGE

mice brain as compared to Tg mAPP mice brain. Further studies using immunoblotting method confirmed this finding (Figure 5.12). This result indicated that RAGE signaling may be involved in the regulation of PSMB4 expression. The signaling pathways between RAGE activation and PSMB4 expression remain to be elucidated. However, it was found that, in muscle cells, NF-κB functions as a negative regulator of the transcription of proteasome subunit, α type 2 (PSMA2) (Du *et al.* 2000). Since PSMB4 gene also contains potential NF-κB binding sites in its promoter regions, NF-κB may regulate the transcription of PSMB4 in the same way. Both in vivo and in vitro studies showed that, in an Aβ rich environment, overexpression of RAGE leads to an increased NF-κB activation (Yan *et al.* 1996; Arancio *et al.* 2004). Therefore, it is possible to speculate that, after binding to ligands such as Aβ or AGEs, activated RAGE triggers activation of NF-κB, which then suppresses transcription of PSMB4.

5.4.1.3 NDUFV2 and AD

NADH: ubiquinone oxidoreductase (complex I) is one of the energy metabolism enzymes catalyzing the transport of electrons from NADH to ubiquinone for ATP synthesis. Complex I comprise 41 subunits of which 7 are encoded in the mitochondrial DNA (mtDNA) and 34 are encoded in nuclear DNA (nDNA) (Smeitink and van den Heuvel 1999). By using chaotropic agents, complex I can be separated into 3 different fractions, flavoprotein (FP) fraction including 24-kDa subunit, iron-sulfur protein (IP) fraction including 75-kDa subunit and hydrophobic protein (HP) fraction (Smeitink *et al.* 1998; Smeitink *et al.* 2004).

Complex I deficiency was associated with the pathogenesis of Alzheimer's disease. Biochemical findings demonstrated that in Alzheimer's disease (AD) brain mitochondria, there is a generalized depression of activity of all electron transport chain complexes (complex I, II, III and IV) (Parker *et al.* 1994; Zhu *et al.* 2004). Moreover, it was observed that the protein levels of NDUFV2 and 75-kDa subunit of complex I were significantly decreased in Down's syndrome and AD as compared to controls (Kim *et al.* 2001).

Here two dimensional electrophoresis analysis revealed that NDUFV2 was significantly increased in Tg mAPP/DN-RAGE mice brain as compared to Tg mAPP mice brain indicating that ligand activated RAGE signaling events may be involved in the regulation of NDUFV2 expression. However, when using western blot with a monoclonal anti-NDUFV2 antibody, no significant difference of the protein expression level of NDUFV2 between Tg mAPP/DN-RAGE and Tg mAPP mice cortex was observed. This could be due to the small sample size for western blotting and the high variation of the protein expression level of NDUFV2 within the same genotype (Figure 5.10A). The biochemical events linking RAGE activation and altered expression of NDUFV2 are still unknown. One possibility is that after ligand binding, activated RAGE induces oxidative stress which would then affect NFDUFV2 expression.

5.4.1.4 Nit2 and AD

In this study, Nit2 was found to be significantly decreased in Tg mAPP/DN-RAGE animals compared to Tg mAPP animals. As no commercial or home made

antibodies were available for this protein, immunoblotting confirmation of the altered expression of Nit2 was not able to be performed. Nit2, a member of the nitrilase superfamily, is ubiquitously expressed in multiple tissues. It was demonstrated that Nit2 plays an important role in cell growth inhibition. Nit2 was also linked to malignancies, indicating a potential as tumor suppressor (Lin *et al.* 2007). Although Nit2 has not been associated with AD, it was found to be significantly reduced in fetal Down's syndrome brain (Myung *et al.* 2003).

5.4.2 Differentially expressed proteins between non-Tg mice brain and Tg DN-RAGE mice brain

Using two dimensional electrophoresis, I also analyzed differential protein expression between non-Tg mice and Tg DN-RAGE mice cortex. These data would provide further insights into the functions of RAGE.

Two dimensional electrophoresis studies had revealed that four proteins, including E-FABP, sepiapterin reductase, alpha enolase and triose-phosphate isomerase, were upregulated in Tg DN-RAGE mice brain as compared to non-Tg mice brain. Two proteins, including eIF-5A and GMFB were downregulated in Tg DN-RAGE mice brain as compared to non-Tg mice brain.

Using RT-PCR, Prof ShiDu Yan's group (College of Physicians and Surgeons, Columbia University) found that, contradictory to the results from my two dimensional electrophoresis analysis, mRNA expression level of EFABP was decreased in Tg DN-RAGE mice brain whereas mRNA expression levels of eIF-5A

and GMFB were increased in Tg DN-RAGE mice brain as compared to non-Tg mice brain. The reason why the two dimensional electrophoresis results were opposite to the RT-PCR results could be because of the small sample size used for analysis and high variation of mRNA expression among different animals with the same genotype. Due to limited resources, we were not able to perform RT-PCR analysis in our laboratory. All RT-PCR results were obtained from Prof ShiDu Yan. Therefore, the mRNA expression levels of identified proteins were not all analyzed using RT-PCR method. However for reasons explained below these proteins require further analysis.

5.4.2.1 RAGE and E-FABP, eIF-5A and GMFB

Intracellular lipid binding proteins called fatty acid binding proteins (FABPs) proteins are small, abundantly expressed cytoplasmic proteins that are involved in fatty acid (FA) uptake, transport, storage, and metabolism. They may modulate FA concentration and in this way influence function of enzymes, membranes, ion channels and receptors, and gene expression and cellular growth and differentiation (Makowski and Hotamisligil 2004). Nine different types of cytoplasmic FABP have been identified up to now. Among which, four types are expressed in the nervous system with a distinct spatial-temporal distribution. Myelin (M)-FABP is only present in the peripheral nerves, brain (B)-FABP and epidermal (E)-FABP mainly localized in glial cells and neurons of pre- and perinatal brain, respectively, and heart (H)-FABP in adult brain (Liu *et al.* 2000; Veerkamp and Zimmerman 2001)

The functional significance of the spatial-temporal pattern of the four FABP types in nervous tissue is still unclear. In PC12 cells, it was demonstrated that E-FABP expression is required for normal neurite outgrowth after nerve growth factor treatment (Allen *et al.* 2000). Furthermore, one study showed that E-FABP is involved in retinal ganglion cell differentiation and axon growth (Allen *et al.* 2001). These results suggested a role of E-FABP in central nervous system during neuronal migration and development. E-FABP is also expressed in adult brain although the level is dramatically lower as compared to perinatal brain (Veerkamp and Zimmerman 2001). The function of E-FABP in adult brain remains to be elucidated.

In all eukaryotic organisms, protein translation is regulated by a variety of translation initiation factors. One of these is Eif-5A. eIF-5A was shown to promote the formation of the first peptide bond between methionine (amino acid of the start codon) and the first amino acid of the coding sequence thereby playing an essential role in initiating translation (Langer *et al.* 2006). It was reported that loss of eIF-5A activity leads to a reversible arrest of the cells in the G1- phase of the cell cycle and inhibits the growth of mammalian cells. Also, eIF-5A was demonstrated to be involved in cell proliferation (Huang *et al.* 2007).

GMFB is expressed predominantly in the brain, especially astrocytes and some neuronal cells (Wang *et al.*1992). It is a protein of 141 amino acids and functions as a growth and differentiation regulator for neurons as well as glia (Lim *et al.* 1989; Hotta *et al.* 2005).

Two dimensional studies suggested a possible linkage between RAGE and E-FABP,

eIF-5A and GMFB. As described above, E-FABP, eIF-5A and GMFB all seem to be involved in growth and differentiation of neurons. RAGE was known to interact with amphoterin and this interaction was proposed to play a prominent role in neurite outgrowth (Sajithlal *et al.* 2002). Therefore, during development, it is possible that E-FABP, eIF-5A and GMFB are subsequent signaling events of RAGE activation. In the adult brain, however, the functions of these proteins are not clear. They were proposed to be involved in neural survival after injury (Allen *et al.* 2001; Hotta *et al.* 2005). In the adult brain, many ligands can bind and activate RAGE, thus inducing multiple intracellular signaling events. Altered expression of E-FABP, eIF-5A and GMFB may be part of these events.

5.4.2.2 RAGE and sepiapterin reductase, alpha enolase and triose-phosphate isomerase

Glycolysis is the pathway which oxidizes glucose and converts it into pyruvate or lactate, resulting in the production of energy. Glycolytic pathway is the main route that provides energy to brain functioning (Magistretti *et al.* 2000). Alpha-enolase and triose-phosphate isomerase are enzymes involved in the glycolytic pathway of metabolism. Alpha-enolase is a metalloenzyme that catalyses the reaction of 2-phopho-D-glycerate to phophoenolpyruvate. Triosephosphate isomerase catalyzes the interconversion of glyceraldehyde phosphate and dihydroxyacetone phosphate in the glycolytic pathway.

Sepiapterin reductase catalyzes the final step of the biosynthetic pathway of tetrahydrobiopterin (BH4). BH4 is an essential cofactor for multiple enzymes such

as all three isoforms of nitric oxide synthase, tyrosine hydroxylase and tryptophan-5-hydroxylase. NO is synthesized by the three forms of nitric oxide synthase and has a variety of physiological roles. Tyrosine hydroxylase and tryptophan-5-hydroxylase are rate-limiting enzymes for the production of the biogenic amine neurotransmitters dopamine, norepinephrine, and serotonin (Friedman *et al.* 2006; Yang *et al.* 2006; Tobina *et al.* 2007).

The results obtained by two dimensional electrophoresis analysis of Tg DN-RAGE and non-Tg mice cortices suggested a potential relationship between RAGE and sepiapterin reductase, alpha enolase and triose-phosphate isomerase. These data indicated that activated RAGE signaling may be involved in the regulation of the glycolytic pathway and BH4 synthesis. However, the underlying mechanisms linking RAGE and altered expression of sepiapterin reductase, alpha enolase and triose-phosphate isomerase remain to be elucidated.

Chapter 6: Conclusion and future perspective

Chapter 6: Conclusion and future perspective

In the late stages of Alzheimer's disease, multiple signaling pathways are impaired and extensive neurodegeneration and neuron loss occur. Therefore, it is of essential importance to identify the initiating events in the pathogenesis of Alzheimer's disease and find potential therapeutic strategy to prevent the disease at an early stage. Our collaborator, Prof ShiDu Yan's group (Department of Surgery, Columbia University) have identified two receptors, ABAD and RAGE, which have been proposed to bind Aβ and mediate Aβ induced neurotoxicity in the early stages of AD (Yan *et al.* 2000).

6.1 The endophilin 1-GLK-JNK pathway in AD

To study the involvement of ABAD in AD, Prof ShiDu Yan's group developed transgenic mice overexpressing neuron targeted ABAD and double transgenic mice overexpressing both ABAD and mAPP (Takuma et al. 2005). Using proteomic analysis, previous work by Dr Jim Aiton and Margaret Taylor had found that endophilin 1 is consistently upregulated in Tg mAPP and Tg ABAD/mAPP mice brains as compared to non-Tg and Tg ABAD mice brains. Studies using immunoblotting further confirmed that endophilin 1 expression is increased in brain tissues of Alzheimer's patients as well (section 3.1). Given the finding that injection of a peptide which can disrupt the interaction between Aβ and ABAD in Tg mAPP/ABAD animals resulted in a reversal of endophilin 1 expression (section

3.4.4), these results collectively suggested that endophilin 1 expression is increased in brains of AD patients and this increased expression is a direct consequence of the Aβ-ABAD interaction.

How Aβ-ABAD interaction can lead to increased expression of endophilin 1 is still unknown. The human endophilin 1 gene promoter is TATA-less, with multiple potential transcription factor binding sites (e.g. Sp1, NF-KB, ATF, c-Jun) (Reutens and Begley 2002). So, it seems possible to speculate that the signaling events after Aβ-ABAD interaction lead to activation of several gene transcription factors for endophilin 1 such as NF-KB, ATF or c-Jun, which then causes increased expression of endophilin 1. In the future, using gel mobility-shift assays, experiments will be performed in our laboratory to study if the Aβ-ABAD interaction can cause an increase of the activity of transcription factors such as NF-KB, ATF or c-Jun in cortical neurons. Moreover, experiments will also be performed to examine the effects of these transcription factors on endophilin 1 expression.

Endophilin 1 is a SH3 domain containing protein which is expressed predominantly in the presynaptic terminals of the brain (Ringstad *et al.* 2001; Micheva *et al.* 1997). Endophilin 1 is a multifunctional protein (Reutens and Begley 2002). It was proposed to participate in synaptic vesicle endocytosis through SH3 domain mediated interactions with synaptojanin and dynamin (Gat *et al.* 2000). Endophilin 1 was also identified to bind a number of diverse cellular proteins (Reutens and Begley 2002). Ramjaun *et al.* 2001 reported that through its SH3 domain, endophilin 1 binds GLK and regulates GLK mediated JNK activation in HEK293 cells. In vitro studies found

that GLK can directly phosphorylate MEKK1 (Diener *et al.* 1997). Previous findings indicated that MEKK1 interacts with inactive MKK4 to form a MEKK1MKK4 complex. Active MEKK1 can phosphorylate and activate MKK4, resulting in its dissociation from the complex. The free and active MKK4 then specifically interacts with JNK. Once activated, JNK is now freed from the MKK4JNK complex and translocated to the cytoplasm or the nucleus to phosphorylate downstream effectors (Chang and Karin 2001).

Since increased JNK activation has long been associated with Alzheimer's disease, I studied the involvement of the endophilin 1-GLK-JNK pathway in AD (Zhu *et al.* 2001). Similar to the previously published observations (Morishima *et al.* 2001), it had been found that JNK activation is increased in cortical neurons after Aβ treatment (section 3.3.3.1). Overexpression of endophilin 1 in mice cortical neurons caused an increase of JNK activation in the absence of Aβ. In contrast, expression of two dominant negative forms of endophilin 1 significantly reduced JNK activation in cortical neurons after treatment of Aβ (section 3.3.3.2).

There are at least three possibilities that increased activation of JNK may be involved in the pathogenesis of AD. Firstly and most notably is that increased JNK activation can lead to neuron death. It was found that extracellular Aβ induces an enhanced JNK activation which then phosphorylates and activates c-Jun. Activated c-Jun led to neuron death via Fas signaling pathway (Morishima *et al.* 2001). Indeed, in this study here, expression of two forms of dominant negative endophilin 1 in cortical neurons protected against Aβ induced neuron death (section 3.3.3.3). Given the finding that

c-Jun activation is increased in brains of AD patients as compared to age-matched controls, these data indicated that endophilin 1 regulated JNK activation may lead to c-Jun activation, thus contributing to neuron loss in AD (Marcus *et al.* 1998).

Another possibility is that activated JNK may be involved in tau hyperphosphorylation. In vitro studies showed that JNK can phosphorylate tau (Sato *et al.* 2002; Okazawa and Estus 2002). By immunocytochemistry, activated JNK was colocalized with tau in brains of AD sufferers (Zhu *et al.* 2001). These observations indicated that increased JNK activation may result in tau hyperphosphorylation and NFT formation, thereby leading to neurodegeneration.

In addition, Aβ was shown to inhibit long-term potentiation (LTP) in the hippocampus. However, pretreatment of the hippocampal slices with JNK inhibitors prevented the Aβ induced LTP inhibition (Wang *et al.* 2004). Synaptic plasticity, especially LTP, is involved in learning and memory mechanisms (Morris *et al.* 2003). Therefore, the increased JNK activation may contribute to the cognitive deficits in AD.

Given the findings from this study and the above evidences, a hypothetical sequence of events that may occur during the pathogenesis of AD was proposed (Figure 6.1). In an Aβ rich environment, as present in AD, Aβ-ABAD interaction leads to increased expression of endophilin 1 which binds and activates GLK. Active GLK phosphorylates and activates MEKK1, which then triggers activation of MKK4. Phosphorylated MKK4 induces JNK activation, thereby leading to the activation of c-Jun, which stimulates Fas signaling, and eventually neuron death.

Increased JNK activation may also lead to abnormal phosphorylation of tau protein, thus participating in NFT formation. In addition, activated JNK may contribute to cognitive impairment in AD patients by inhibition of LTP.

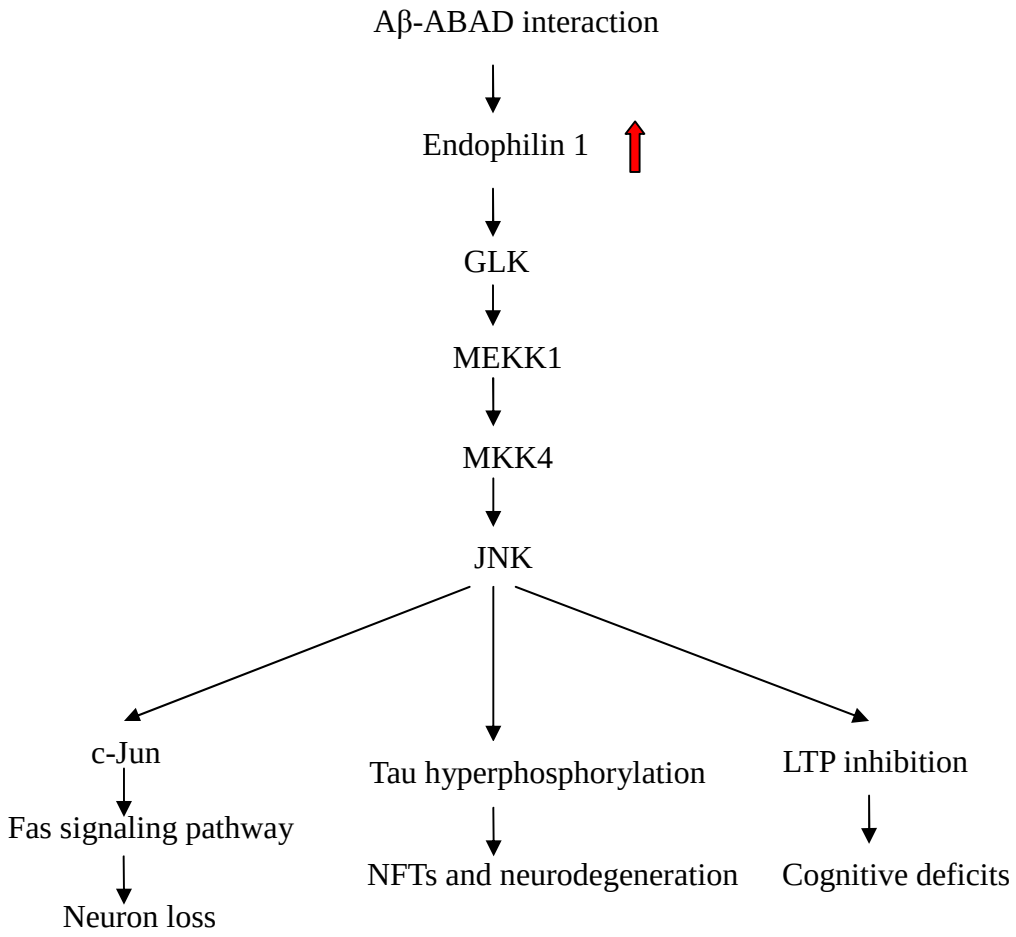

Figure 6.1 A hypothetical sequence of events in AD. Endophilin 1 induces JNK activation through a series of kinases including GLK, MEKK1 and MKK4. Increased JNK activation leads to neurodegeneration, neuron loss and cognitive deficits.

In light of the above mentioned data implicating a role of JNK signaling in AD, inhibition of JNK seems to be a promising therapeutic strategy for AD. Our study indicated that endophilin 1 may act as a regulator of JNK activity in AD. Therefore, inhibition of endophilin 1 may offer neuroprotection to patients with AD. In order to examine if endophilin 1 is indeed a good therapeutic target, more studies need to be done in the future. Firstly, a transgenic animal model overexpressing endophilin 1 in an Aβ rich environment should be developed to study if increased expression of endophilin 1 can cause accelerated/enhanced cognitive deficits and neuron loss. Followed by this study, transgenic mice expressing dominant negative endophilin 1 in an Aβ rich environment should be developed. Characterization of this transgenic animal model will be able to allow us to investigate if inhibition of endophilin 1 can rescue Aβ induced cognitive impairment and neuron death.

6.2 The relationship between activation of RAGE and expression of GLO1 or PSMB4

To study the role of RAGE in AD, Prof ShiDu Yan's group have developed transgenic mice overexpressing RAGE or dominant negative form of RAGE (DN-RAGE) in an Aβ rich environment. They found that Tg mAPP/RAGE mice displayed accelerated/enhanced cognitive impairment whereas Tg mAPP/DN-RAGE showed preserved cognitive function as compared to Tg mAPP mice (Arancio *et al.* 2004). In this study, in order to understand the molecular mechanisms that protect cognitive function in Tg mAPP/DN-RAGE mice brains, two dimensional electrophoresis method was used. Among the four proteins identified to be differentially expressed between Tg mAPP and Tg mAPP/DN-RAGE mice brains, GLO1 and PSMB4 are of particular interest. These two proteins were found to be upregulated in Tg mAPP/DN-RAGE mice brains as compared to Tg mAPP mice brains (section 5.2.1 and 5.3.3).

GLO1 is part of the glyoxalase system which detoxifies dicarbonyl metabolites, such as MG. MG participates in the glycation of proteins and nucleotides, resulting in the formation of advanced glycation end products (AGEs) (Kuhla *et al.* 2007a). The levels of AGEs were increased in the brains of AD patients as compared to non-demented controls (Staniszewska *et al.* 2005; Takeuchi *et al.* 2004; Sasaki *et al.* 1998). In vitro studies showed that AGEs cause neuron toxicity possibly via oxidative stress-related pathways (Kikuchi *et al.* 1999). These results indicated that interference with the AGEs production process may reduce the neuropathologic

changes in AD. Therefore, GLO1 might be a useful therapeutic target for AD. By increasing the expression or activity of GLO1, AGEs levels can be reduced. However, the factors regulating GLO1 expression are still unclear. Several transcription factors including activating protein-1 (AP-1) and NF-κB were proposed to regulate GLO1 gene expression under oxidative stress conditions (Ranganathan *et al.* 1999). Furthermore, IRE (insulin response element) was identified in the promoter region of GLO1gene (Ranganathan *et al.* 1999).

In this study, GLO1 expression was identified to be upregulated in Tg mAPP/DN-RAGE mice brains as compared to Tg mAPP mice brains indicating the effects of RAGE signaling on GLO1 expression (section 5.2.1). The signaling events between RAGE activation and GLO1 expression remain unknown. It is rational to speculate that RAGE ligands bind RAGE and triggers intracellular signaling events which then activate transcription factors such as AP-1, IRE or NF-κB, thereby regulating the expression of GLO1. In the future, experiments will be performed to test this hypothesis. Elucidation of the molecular mechanisms linking RAGE activation and GLO1 expression will not only provide insights into the involvement of RAGE and GLO1 in AD but also help developing novel therapeutic methods for the treatment of AD.

The ubiquitin/proteasome protein degradation pathway is a major cellular proteolytic system. In this pathway, damaged and abnormal proteins are targeted for degradation by the covalent attachment of several ubiquitin moieties to form ubiquitin conjugates. Ubiquitinated proteins are then rapidly degraded by the 26 S

proteasome (Ciechanover and Schwatz 1998). Alzheimer's disease is characterized by abnormal protein aggregation such as amyloid plaques or NFTs (Mott and Hulette 2005). Several studies showed that different forms of tau, including phosphorylated tau (PHF-1) and non-phosphorylated tau (Tau-1) in rat brain cortex extract are degraded by 26S proteasome in an ubiquitin- and ATP-dependent manner (Zhang *et al.* 2004). Furthermore, when using lactacystin, an inhibitor of the 26S proteasome, a marked decrease in Aβ degradation was detected in both astrocytes and neurons (Lopez *et al.* 2003). In addition, in HEK293 cells transfected with FAD-linked PS1, the proteasome was shown to participate in the degradation of FAD-linked PS1, thereby directly influencing the production of Aβ (Marambaud *et al.* 1998).

Given that impairment of proteasome function has been associated with AD, the above findings together suggested that alterations in the Ub–proteasome pathway in AD could affect the normal protealytic removal of Aβ and tau, resulting in an abnormal accumulation of Aβ and tau (Keller *et al.* 2000).

In this study, PSMB4 was found to be significantly increased in Tg mAPP/DN-RAGE mice brains as compared to Tg mAPP mice brains indicating the involvement of RAGE signaling in PSMB4 expression (5.3.3). The factors regulating PSMB4 expression are still unknown. However, NF-κB was identified to be an important negative regulator of the transcription of one component of proteasome, PSMA2 (Du *et al.* 2000). Since PSMB4 contains potential NF-κB -like binding sites in its promoter regions as well, it is possible that RAGE ligands bind

RAGE and induce activation of NF-κB, which then leads to decreased expression of PSMB4 whilst expression of DN-RAGE blocks this pathway.

Therefore, given the above evidences, there are at least two reasons that prove that RAGE is a good therapeutic target. First, blocking of RAGE leads to an increase of GLO1 expression. Increased GLO1 expression may reduce AGEs formation, thereby ameliorating AGEs induced neurotoxicity in AD (Figure 6.2).

Secondly, blocking of RAGE causes an increased expression of PSMB4. Increased PSMB4 may lead to increased proteasome activity which will then result in increased degradation of Aβ and tau. Therefore, by blocking of RAGE, abnormal accumulation of Aβ and tau can be reduced (Figure 6.2).

More studies need to be done to investigate the signaling events between RAGE activation and expression of GLO1 or PSMB4. This may provide help for developing RAGE-targeted therapeutic strategy for the treatment of AD. Also, by elucidating these mechanisms, novel therapeutic targets for treatment of AD may be identified.

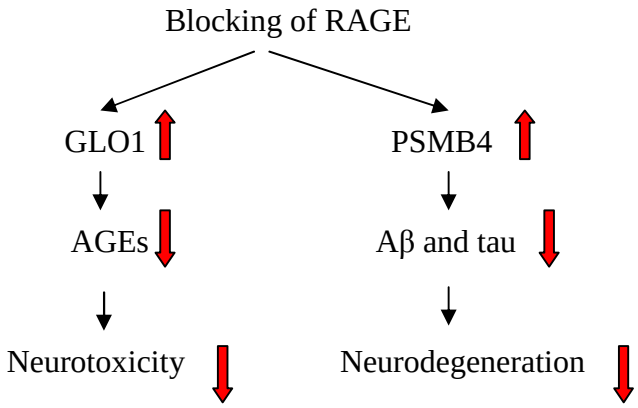

Figure 6.2 A schematic illustration of the possible neuroprotective mechanisms by blocking of RAGE.

Reference List

Aisen P. S. (2002) Anti-inflammatory agents in Alzheimer's disease. *Curr. Neurol. Neurosci. Rep.* **2,** 405-409.

Allen G. W., Liu J. and De Leon M. (2000) Depletion of a fatty acid-binding protein impairs neurite outgrowth in PC12 cells. *Brain Res. Mol. Brain Res.* **76**, 315-324.

Allen G. W., Liu J., Kirby M.A. and De Leon M. (2001) Induction and axonal localization of epithelial/epidermal fatty acid-binding protein in retinal ganglion cells are associated with axon development and regeneration. *J. Neurosci. Res.* **66**, 396-405.

Allinson, T. M., Parkin, E. T., Turner, A. J. and Hooper, N. M. (2003) ADAMs family members as amyloid precursor protein alpha-secretases. *J. Neurosci. Res.* **74**, 342–352.

Almeida C G., Takahashi R. H and Gouras G. (2006) Beta-amyloid accumulation impairs multivesicular body sorting by inhibiting the ubiquitin-proteasome system. *J. Neurosci.* **26**, 4277–4288.

Alzheimer A. (1907) Uber eine eigenartige Erkrankung der Hirnrinde. *Allgemeine Zeitschrift fur Psychiatrie und Psychisch-gerichtliche Medizin*. 64, 146-148.

Anandatheerthavarada H. K., Biswas G., Robin M. A. and Avadhani N. G. (2003) Mitochondrial targeting and a novel transmembrane arrest of Alzheimer's amyloid precursor protein impairs mitochondrial function in neuronal cells. *J. Cell Biol.* **161**, 41–54.

Anandatheerthavarada H. K. and Devi L. (2007) Amyloid precursor protein and mitochondrial dysfunction in Alzheimer's disease. *Neuroscientist.* **13**, 626-638.

Aoki H., Kang P. M., Hampe J., Yoshimura K., Noma T., Matsuzaki M. and Izumo S. (2002) Direct activation of mitochondrial apoptosis machinery by c-Jun N-terminal kinase in adult cardiac myocytes. *J. Biol. Chem.* **277**, 10244-10250.

Arancio O., Zhang H. P., Chen X., Lin C., Trinchese F., Puzzo D., Liu S., Hegde A., Yan S. F., Stern A., Luddy J. S., Lue L. F., Walker D. G., Roher A., Buttini M., Mucke L., Li W., Schmidt A. M., Kindy M., Hyslop P. A., Stern D. M. and Du Yan S. S. (2004) RAGE potentiates Abeta-induced perturbation of neuronal function in transgenic mice. *EMBO J.* **23**, 4096-4105.

Baloyannis S. J. (2006) Mitochondrial alterations in Alzheimer's disease. *J. Alzheimers. Dis.* **9,** 119-126.

Berney C. and Danuser G. (2003) FRET or no FRET: A quantitative comparison. *Biophys. J.* **84**, 3992-4010.

Bierhaus A., Hofmann M. A., Ziegler R. and Nawroth P. P. (1998) AGEs and their interaction with AGE-receptors in vascular disease and diabetes mellitus. I. The AGE concept. *Cardiovasc. Res.* **37**, 586-600.

Billings L. M., Oddo S., Green K. N., McGaugh J. L. and LaFerla F. M. (2005) Intraneuronal Abeta causes the onset of early Alzheimer's disease-related cognitive deficits in transgenic mice. *Neuron* **45**, 675-688.

Bitan G., Vollers S. S. and Teplow D. B. (2003) Elucidation of primary structure elements controlling early amyloid beta-protein oligomerization. *J. Biol. Chem.* **278**, 34882-34889.

Borsello T. and Forloni G. (2007) JNK Signalling: A possible target to prevent neurodegeneration. *Curr. Pharm. Des.* **13**, 1875-1886.

Brecht S., Kirchhof R., Chromik A., Willesen M., Nicolaus T., Raivich G., Wessig J., Waetzig V., Goetz M., Claussen M., Pearse D., Kuan C. Y., Vaudano E., Behrens A., Wagner E., Flavell R. A., Davis R. J. and Herdegen T. (2005) Specific pathophysiological functions of JNK isoforms in the brain. *Eur. J. Neurosci.* **21**, 363-377.

Brookmeyer R., Johnson E., Ziegler-Graham K. and Arrighi H. M. (2007) *Alzheimer's and Dementia*.

Brooks W. M., Lynch P.J., Ingle C. C., Hatton A., Emson' P. C., Faull R. L. and Starkey M. P. (2007) Gene expression profiles of metabolic enzyme transcripts in Alzheimer's disease. *Brain Res.* **1127**, 127-135.

Brophy V. A., Tavare J. M. and Rivett A. J. (2002) Treatment of COS-7 cells with proteasome inhibitors or γ-interferon reduces the increase in caspase 3 activity associated with staurosporine-induced apoptosis. *Arch. Biochem. Biophys.* **397**, 199-205.

Butterfield D. A., Perluigi M. and Sultana R. (2006) Oxidative stress in Alzheimer's disease brain: New insights from redox proteomics. *Eur. J. Phar.* **545**, 39-50.

Cai X. D., Golde T. E. and Younkin S. G. (1993) Release of excess amyloid beta protein from a mutant amyloid beta protein precursor. *Science* **259**, 514-516.

Canevari L., Abramov A. Y. and Duchen M. R. (2004) Toxicity of amyloid beta peptide: tales of calcium, mitochondria, and oxidative stress. *Neurochem. Res.* **29**, 637-650.

Caspersen C., Wang N., Yao J., Sosunov A., Chen X., Lustbader J. W., Xu H. W., Stern D., McKhann G. and Yan S. D. (2005) Mitochondrial Abeta: a potential focal point for neuronal metabolic dysfunction in Alzheimer's disease. *FASEB J.* **19**, 2040-2041.

Caughey B. and P. T. Lansbury Jr. (2003) Protofibrils, pores, fibrils and neurodegeneration: separating the responsible protein aggegates from the innocent bystanders. *Annu. Rev. Neurosci.* **26**, 267-298.

Chang L. and Karin M. (2001) Mammalian MAP kinase signaling cascades. *Nature* **410**, 37-40.

Chen F., Wollmer M. A., Hoerndli F., Munch G.., Kuhla B., Rogaev E. I., Tsolaki M., Papassotiropoulos A. and Gotz J. (2004) Role for glyoxalase I in Alzheimer's disease**.** *Proc. Nati. Acad. Sci. U. S. A.* **101**, 7687 - 7692.

Chen J. X. and Yan S. D. (2007) Pathogenic role of mitochondral amyloid-beta peptide. *Expert. Rev. Neurother.* **7,** 1517-1525.

Ciechanover A. (1998) The ubiquitin-proteasome pathway: on protein death and cell life. *EMBO J.* **17**, 7151-7160.

Citron M., Oltersdorf T., Haass C., McConlogue L., Hung A. Y., Seubert P., Vigo-Pelfrey C., Lieberburg I. and Selkoe D. J. (1992) Mutation of the beta-amyloid precursor protein in familial Alzheimer's disease increases beta-protein production. *Nature* **360**, 672-674.

Comas-Herrera A., Wittenberg R., Pickard L. and Knapp M. (2007) Cognitive impairment in older people: future demand for long-term care services and the associated costs. *Int. J. Ger. Psy.* **22**, 1037-1045.

Connern C. P. and Halestrap A. P. (1992) Purification and N-terminal sequencing of peptidyl-prolyl cis-trans-isomerase from rat liver mitochondrial matrix reveal the existence of a distinct mitochondrial cyclophilin. *Biochem. J.* **284**, 381–385.

Cordell, P. A., Futers T. S., Grant P. J. and Pease R. J. **(**2004) The Human hydroxyacylglutathione hydrolase (HAGH) gene encodes both cytosolic and mitochondrial forms of glyoxalase II. *J. Biol. Chem.* **279**, 28653-28661.

Corder E. H., Lannfelt L., Bogdanovic N., Fratiglioni L. and Mori H. (1998) The role of APOE polymorphisms in late-onset dementias. *Cell Mol. Life Sci.* **54**, 928-934.

Crespo-Beal N., Canudas A. M., Camins A. and Pallas M. (2007) Kainate induces EKT, ERK, cdk5/GSK3β pathway deregulation, phosphorylate tau protein in mouse hippocampus. *Neurochem. Inter.* **50**, 435-442.

Crompton M. (1999) The mitochondrial permeability transition pore and its role in cell death. *Biochem. J.* **341 (Pt 2)**, 233-249.

David D., Layfield C., Serpell R., Narain L., Goedert Y. and Spillantini M. (2002) Proteasomal degradation of tau protein. *J. Neurochem.* **83**, 176–185.

De Strooper B., Annaert W., Cupers P., Saftig P., Craessaerts K., Mumm J. S., Schroeter E. H., Schrijvers V., Wolfe M. S., Ray W. J., Goate A. and Kopan R. (1999) A presenilin-1-dependent gamma-secretase-like protease mediates release of Notch intracellular domain. *Nature* **398**, 518-522.

De Strooper B (2003) Aph-1, Pen-2, and Nicastrin with Presenilin generate an active gamma-Secretase complex. *Neuron* **38**, 9–12.

Devi L., Prabhu B. M., Galati D. F., Avadhani N. G.. and Anandatheerthavarada H. K. (2006). Accumulation of amyloid precursor protein in the mitochondrial import channels of human Alzheimer's disease brain is associated with mitochondrial dysfunction.. *J. Neurosci.* **26**, 9057-9068.

Diener K., Wang X. S., Chen C., Meyer C. F., Keesler G., Zukowski M., Tan T. H. and Yao Z. (1997) Activation of the c-Jun N-terminal kinase pathway by a novel protein kinase related to human germinal center kinase. *Proc. Natl. Acad. Sci. U. S. A.* **94,** 9687-9692.

Ding Q. and Keller J. N. (2005) Splice variants of the receptor for advanced glycosylation end products (RAGE) in human brain. *Neurosci. Lett.* **373,** 67-72.

Dougherty C. J., Kubasiak L. A., Frazier D. P., Li H.,. Xing W.C., Bishopric N. H. and Webster K. A. (2004) Mitochondrial signals initiate the activation of c-Jun N-terminal kinase (JNK) by hypoxia-reoxygenation. *FASEB J.* **18**, 1060-1070.

Du J., Mitch W. E., Wang X. and Price S. R. (2000) Glucocorticoids induce proteasome C3 subunit expression in L6 muscle cells by opposing the suppression of its transcription by NF-kappa B. *J. Biol. Chem.* **275**, 19661–19666.

Du Y. S., Zhu Y., Stern E. D., Hwang Y. C., Hori O., Ogawa S., Frosch M. P., Connolly E. S., McTaggert R., Pinsky D. J., Clarke S., Stern D. M. and Ramasamy R. (2000) Amyloid beta -peptide-binding alcohol dehydrogenase is a component of the cellular response to nutritional stress. *J. Biol. Chem.* **275**, 27100-27109.

Esler W. P., Marshall J. R., Stimson E. R., Ghilardi J. R., Vinters H. V., Mantyh P. W. and Maggio J. E. (2002) Apolipoprotein E affects amyloid formation but not amyloid growth in vitro: mechanistic implications for apoE4 enhanced amyloid burden and risk for Alzheimer's disease. *Amyloid.* **9**, 1-12.

Ferrer I., Marti E., Lopez E. and Tortosa A. (1998) NF-κB immunoreactivity is observed in association with beta A4 diffuse plaques in patients with Alzheimer's disease. *Neuroopathol. Appl. Neurobiol.* **24**, 271-277.

Fratta P., Engel W. K., McFerrin J., Davies K. J., Lin S. W. and Askanas V. (2005) Proteasome inhibition and aggresome formation in sporadic inclusion-body myositis and in amyloid-ß precursor protein-overexpressing cultured human muscle fibers. *Am. J. Pathol.* **167**, 517–526.

Friedman J., Hyland K., Blau N. and MacCollin M. (2006) Dopa-responsive hypersomnia and mixed movement disorder due to sepiapterin reductase deficiency. *Neurology* **67**, 2032–2035.

Games D., Adams D., Alessandrini R., Barbour R., Berthelette P., Blackwell C., Carr T., Clemens J., Donaldson T. and Gillespie F. (1995) Alzheimer-type neuropathology in transgenic mice overexpressing V717F beta-amyloid precursor protein. *Nature* **373**, 523-527.

Gillardon F., Kloβ A., Berg M., Neumann M., Mechtler K., Hengerer B. and Dahlmann B. (2007) The 20S proteasome isolated from Alzheimer’s disease brain shows post-translational modifications but unchanged proteolytic activity. *J. Neurochem.* **101**, 1483–1490.

Goate A. M., Haynes A. R., Owen M. J., Farrall M., James L. A., Lai L. Y., Mullan M. J., Roques P., Rossor M. N. and Williamson R. (1989) Predisposing locus for Alzheimer's disease on chromosome 21. *Lancet* **1**, 352-355.

Golabek A. A., Soto C., Vogel T. and Wisniewski T. (1996) The interaction between apolipoprotein E and Alzheimer's amyloid beta-peptide is dependent on beta-peptide conformation. *J. Biol. Chem.* **271**, 10602-10606.

Golde T. E. (2003) Alzheimer disease therapy: can the amyloid cascade be halted? *J. Clin. Invest* **111**, 11-18.

Greenfield J. P., Tsai J., Gouras G. K., Hai B., Thinakaran G., Checler F., Sisodia S. S., Greengard P. and Xu H. (1999) Endoplasmic reticulum and trans-Golgi network generate distinct populations of Alzheimer beta-amyloid peptides. *Proc. Natl. Acad. Sci. U. S. A.* **96**, 742-747.

Haass C. and De S. B. (1999) The presenilins in Alzheimer's disease--proteolysis holds the key. *Science* **286**, 916-919.

Halestrap A. P. (1999) The mitochondrial permeability transition: its molecular mechanism and role in reperfusion injury. *Biochem. Soc. Symp.* **66**, 181-203.

Halestrap A. P. and Brenner C. (2003) The adenine nucleotide translocase: a central component of the mitochondrial permeability transition pore and key player in cell death. *Curr. Med. Chem.* **10**, 1507–25.

Ham, J., Eilers A., Whitfield J., Neame S. J. and Shah B. (2000) c-Jun and the transcriptional control of neuronal apoptosis. *Biochem. Pharmacol.* **60**, 1015–1021.

Hansson C. A., Frykman S., Farmery M. R., Tjernberg L. O., Nilsberth C., Pursglove S. E., Ito A., Winblad B., Cowburn R. F., Thyberg J. and Ankarcrona M. (2004) Nicastrin, presenilin, APH-1, and PEN-2 form active gamma-secretase complexes in mitochondria. *J. Biol. Chem.* **279**, 51654-51660.

Hartmann T., Bieger S. C., Bruhl B., Tienari P. J., Ida N., Allsop D., Roberts G. W., Masters C. L., Dotti C. G., Unsicker K. and Beyreuther K. (1997) Distinct sites of intracellular production for Alzheimer's disease A beta40/42 amyloid peptides. *Nat. Med.* **3,** 1016-1020.

He X. Y., Schulz H. and Yang S. Y. (1998) A human brain L-3-hydroxyacyl-coenzyme A dehydrogenase is identical to an amyloid beta-peptide-binding protein involved in Alzheimer's disease. *J. Biol. Chem.* **273**, 10741-10746.

Hensley K, Butterfield D. A., Hall N., Cole P., Subramaniam R., Mark R., Mattson M. P., Markesbery W. R., Harris M. E., Aksenov M., **As**kenova M., Wu J. F and Carney J. M. (1996) Reactive oxygen species as causal agents in the neurotoxicity of the Alzheimer's disease-associated amyloid beta peptide**.** *Ann. N.Y. Acad .Sci.* **786**, 120–134.

Hotta N., Aoyama M., Inagaki M., Ishihara M., Miura Y., Tada T. and Asai K. (2005) Expression of glia maturation factor beta after cryogenic brain injury. *Brain. Res. Mol. Brain Res.* **133**, 71-77.

Hsiao K., Chapman P., Nilsen S., Eckman C., Harigaya Y., Younkin S., Yang F. and Cole G. (1996) Correlative memory deficits, Abeta elevation, and amyloid plaques in transgenic mice. *Science* **274**, 99-102.

Huang Y., Higginson D. S., Hester L., Park M. H. and Snyder S. H. (2007) Neuronal growth and survival mediated by eIF5A, a polyamine-modified translation initiation factor. *Proc. Natl. Acad. Sci. U. S. A.* **104**, 4194 - 4199.

Jarrett J. T., Berger E. P. and Lansbury P. T. (1993) The carboxy terminus of the beta amyloid protein is critical for the seeding of amyloid formation: implications for the pathogenesis of Alzheimer's disease. *Biochemistry* **32**, 4693-4697.

Jemmerson R., Dubinsky J. M. and Brustovetsky N. (2005) Cytochrome C release from CNS mitochondria and potential for clinical intervention in apoptosis-mediated CNS diseases. *Antioxid. Redox Signal.* **7**, 1158–1172.

Jobst K. A., Hindley N. J., King E. and Smith A. D. (1994) The diagnosis of Alzheimer's disease: a question of image? *J. Clin. Psy.* **55 Suppl**, 22-31.

Jones J. A., Lavallee N., Alman J., Sinclair C., Garcia R. I. (1993) Caries incidence in patients with dementia. *Gerodonto.* 10, 76–82.

Karbowski M., Lee Y. J. and Gaume B. (2003). Spatial and temporal association of Bax with mitochondrial fission sites, Drp1, and Mfn2 during apoptosis. *J. Cell Biol.* **159**, 931-938.

Karbowski M., Arnoult D., Chen H., Chan D. C., Smith C. L. and Youle R. J. (2004) Quantitation of mitochondrial dynamics by photolabeling of individual organelles shows that mitochondrial fusion is blocked during the Bax activation phase of apoptosis. *J. Cell Bio.* **164**, 493-499.

Kalousava M., Zima T., Tesar V., Dusilova-Sulkova S. and Skrha, J. (2005) Advanced glycoxidation end products in chronic diseases-clinical chemistry and genetic background. *Mutat. Res.* **579**, 37-46.

Kang J., Lemaire H. G., Unterbeck A., Salbaum J. M., Masters C. L., Grzeschik K. H., Multhaup G., Beyreuther K. and Muller-Hill B. (1987) The precursor of Alzheimer's disease amyloid A4 protein resembles a cell-surface receptor. *Nature* **325**, 733-736.

Keck S., Nitsch R., Grune T. and Ullrich O. (2003) Proteasome inhibition by paired helical filament-tau in brains of patients with Alzheimer's disease. *J. Neurochem.* **85**, 115-122.

Keil U., Bonert A., Marques C. A., Scherping I., Weyermann J., Strosznajder J. B., Muller-Spahn F., Haass C., Czech C., Pradier L., Muller W. E. and Eckert A. (2004) Amyloid beta-induced changes in nitric oxide production and mitochondrial activity lead to apoptosis. *J. Biol. Chem.* **279**, 50310-50320.

Keller J. N., Hanni K. B. and Markesbery W. (2000) Impaired proteasome function in Alzheimer's disease. *J. Neurochem.* **75**, 436–439.

Kenworthy A. K. (2001) Imaging protein-protein interactions using fluorescence resonance energy transfer microscopy. *Methods* **24**, 289-96.

Kessler J., Herholz K., Grond M. and Heiss W. D. (1991) Impaired metabolic activation in Alzheimer's disease: a PET study during continuous visual recognition. *Neuropsychologia* **29**, 229-243.

Kihiko M. E., Tucker H. M., Rydel R. E. and Estus S. (1999) c-Jun contributes to amyloid β-induced neuronal apoptosis but is not necessary for amyloid β-induced c-jun induction. *J. Neurochem.* **73**, 2609–2612.

Kikuchi S., Shinpo K., Moriwaka F., Makita Z., Toshio M. and Tashiro K. (1999) Neurotoxicity of methylglyoxal and 3-deoxyglucosone on cultured cortical neurons: synergism between glycation and oxidative stress, possibly involved in neurodegenerative diseases. *J. Neurosci. Res.* **57**, 280-289.

Kim S. H., Vlkolinsky' R., Cairns N., Fountoulakis M. and Lubec G. (2001) The reduction of NADH Ubiquinone oxidoreductase 24-and 75-kDa subunits in brains of patients with Down syndrome and Alzheimer’s disease. *Life Sci.* **68**, 2741–2750.

Kuan C. Y., Yang D. D., Roy D. R. S., Davis R. J., Rakic P. and Flavell R. A. (1999) The Jnk1 and Jnk2 protein kinases are required for regional specific apoptosis during early brain development. *Neuron* **22**, 667-676.

Kuan C. Y., Whitmarsh A. J., Yang D. D., Liao G., Schloemer A. J., Dong C., Bao J., Banasiak K. J., Haddad G. G. and Flavell R .A. (2003) A critical role of neural-specific JNK3 for ischemic apoptosis. *Proc. Natl. Acad. Sci. U. S. A.* **100**, 15184–15189.

Kuan C. Y. and Burke R. E. (2005) Targeting the JNK signaling pathway for stroke and Parkinson’s diseases therapy. *Curr. Drug Targets CNS Neurol. Disord.* **4**, 63–67.

Kuhla B., Boeck K., Schmidt A., Weigle B., Schmitz M., Ogunlade V., Münch G. and Arendt T. (2005) Age-dependent changes of glyoxalase I expression in human brain. *Neurobiol. Aging* **27**, 815-822.

Kuhla B., Boeck K., Schmidt A., Ogunlade V., Arendt T., Munch G. and Luth H. J. (2007a) Age- and stage-dependent glyoxalase I expression and its activity in normal and Alzheimer's disease brains. *Neurobiol. Aging* **28**, 29-41.

Kuhla B., Haase C., Flach K., Luth H. J., Arendt T. and Munch G. (2007b) Effect of Pseudophosphorylation and Cross-linking by Lipid Peroxidation and Advanced Glycation End Product Precursors on Tau Aggregation and Filament Formation. *J. Biol. Chem.* **282**, 6984-6991.

Kumagae Y., Zhang Y., Kim O. J. and Miller C. A. (1999) Human c-Jun N-terminal kinase expression and activation in the nervous system. *Brain Res Mol Brain Res.* **67**, 10–17.

Lambert M. P., Barlow A. K., Chromy B. A., Edwards C., Freed R., Liosatos M., Morgan T. E., Rozovsky I., Trommer B., Viola K. L., Wals P., Zhang C., Finch C. E., Krafft G. A. and Klein W. L. (1998) Diffusible, nonfibrillar ligands derived from Abeta1-42 are potent central nervous system neurotoxins. *Proc. Natl. Acad. Sci. U. S. A.* **95,** 6448-6453.

Langer A. K., Poon H. F., Münch G., Lynn B. C., Arendt T. and Butterfield D. A .(2006) Identification of AGE-modified proteins in SH-SY5Y and OLN-93 cells. *Neurotox Res.* **9**, 255–268.

Leuner K., Hauptmann S., Abdel-Kader R., Scherping I., Keil U., Strosznajder J. B., Eckert A. and Muller W. E. (2007) Mitochondrial dysfunction: the first domino in brain aging and Alzheimer's disease? *Antioxid. Redox. Signal.* **9,** 1659-1675.

Levy E., Carman M. D., Fernandez-Madrid I. J., Power M. D., Lieberburg I., van Duinen S. G., Bots G. T., Luyendijk W. and Frangione B. (1990) Mutation of the Alzheimer's disease amyloid gene in hereditary cerebral hemorrhage, Dutch type. *Science* **248,** 1124-1126.

Levy-Lahad E., Wasco W., Poorkaj P., Romano D. M., Oshima J., Pettingell W. H., Yu C. E., Jondro P. D., Schmidt S. D. and Wang K. (1995) Candidate gene for the chromosome 1 familial Alzheimer's disease locus. *Science* **269,** 973-977.

Lewis J., Dickson D. W., Lin W. L., Chisholm L., Corral A., Jones G., Yen S. H., Sahara N., Skipper L., Yager D., Eckman C., Hardy J., Hutton M. and McGowan E. (2001) Enhanced neurofibrillary degeneration in transgenic mice expressing mutant tau and APP. *Science* **293,** 1487-1491.

Lim R., Miller J. F. and Zaheer A. (1989) Purification and characterization of glia maturation factor beta a growth regulator for neurons and glia. *Proc. Natl. Acad. Sci. U. S. A.* **86**, 3901–3905.

Lin C. H., Chung M., Chen W. B. and Chin H.(2007) Growth inhibitory effect of the human *NIT2* gene and its allelic imbalance in cancers. *FEBS J.* **274**, 2946-2956.

Lin M. T. and Beal M. F. (2006) Alzheimer's APP mangles mitochondria. *Nat. Med.* **12,** 1241-1243.

Lippa C. F., Nee L. E., Mori H. and St George-Hyslop P. (1998) Abeta-42 deposition precedes other changes in PS-1 Alzheimer's disease. *Lancet* **352**, 1117-1118.

Liu Y., Longo L. D. and De Leon M. (2000) In situ and immunocytochemical localization of E-FABP mRNA and protein during neuronal migration and differentiation in the rat brain. *Brain Res.* **852**, 15-27.

Lopez S. M., Pasquini L., Besio M., Pasquini J. M. and Soto E. (2003) Relationship between β-amyloid degradation and the 26S proteasome in neural cells. *Exp. Neurol.* **180**, 131–143.

Löscher M., Fortschegger K., Ritter G., Wostry M., Voglauer R., Schmid J. A., Watters S., Rivett A. J., Ajuh P., Lamond A. I., Katinger H. and Grillari J. (2005) Interaction of U-box E3 ligase SNEV with PSMB4, the β7 subunit of the 20 S proteasome. *Biochem. J.* **388**, 593-603.

Lovestone S. and Reynolds C. H. (1997) The phosphorylation of tau: a critical stage in neurodevelopment and neurodegenerative processes. *Neuroscience* **78**, 309-324.

Lue L. F., Kuo Y. M., Roher A. E., Brachova L., Shen Y., Sue L., Beach T., Kurth J. H., Rydel R. E. and Rogers J. (1999) Soluble amyloid beta peptide concentration as a predictor of synaptic change in Alzheimer's disease. *Am. J. Pathol.* **155**, 853-862.

Lue L. F., Walker D. G., Brachova L., Beach T. G., Rogers J., Schmidt A. M., Stern D. M. and Yan S. D. (2001) Involvement of microglial receptor for advanced glycation endproducts (RAGE) in Alzheimer's disease: identification of a cellular activation mechanism. *Exp. Neurol.* **171**, 29-45.

Lue L. F., Yan S. D., Stern D. M. and Walker D. G. (2005) Preventing activation of receptor for advanced glycation endproducts in Alzheimer's disease. *Curr. Drug Targets. CNS. Neurol. Disord.* **4**, 249-266.

Lustbader J. W., Cirilli M., Lin C., Xu H. W., Takuma K., Wang N., Caspersen C., Chen X., Pollak S., Chaney M., Trinchese F., Liu S., Gunn-Moore F., Lue L. F., Walker D. G., Kuppusamy P., Zewier Z. L., Arancio O., Stern D., Yan S. S. and Wu H. (2004) ABAD directly links Abeta to mitochondrial toxicity in Alzheimer's disease. *Science* **304**, 448-452.

Luth H. J., Ogunlade V., Kuhla B., Kientsch-Engel R., Stahl P., Webster J., Arendt T. and Munch G. (2005) Age- and stage-dependent accumulation of advanced glycation end products in intracellular deposits in normal and Alzheimer's disease brains. *Cereb. Cortex* **15**, 211-220.

Lyras L., Cairns N. J., Jenner A., Jenner P. and Halliwell B. (1997) An assessment of Oxidative Damage to Proteins, Lipids, and DNA in Brain from Patients with Alzheimer's Disease. *J. Neurochem.* **68**, 2061–2069.

Magistretti P. J., Pellerin L. and Martin, J. L. (2000) Brain Energy Metabolism: An Integrated Cellular Perspective in: *Psychopharmocology, the Fourth Generation of Progress.*

Makowski L. and Hotamisligil G. S. (2004) Fatty acid binding proteins—the evolutionary crossroads of inflammatory and metabolic responses. *J. Nutr.* **134**, 2464S-2468.

Manczak M., Anekonda T. S., Henson E., Park B. S., Quinn J. and Reddy P. H. (2006) Mitochondria are a direct site of A beta accumulation in Alzheimer's disease neurons: implications for free radical generation and oxidative damage in disease progression. *Hum. Mol. Genet.* **15**, 1437-1449.

Marambaud P., Ancolio K., Lopez-Perez E. and Checler F. (1998) Proteasome inhibitors prevent the degradation of familial Alzheimer's disease-linked presenilin 1 and potentiate A beta 42 recovery from human cells. *Mol. Med.* **4**, 147–157.

Marcus D. L., Strafaci J. A., Miller D. C., Masia S., Thomas C. G and Rosman J. (1998) Quantitative neuronal c-fos and c-jun expression in Alzheimer's disease. *Neurobiol. Aging* **19**, 393–400.

Marques C. A., Keil U., Bonert A., Steiner B., Haass C., Muller W. E. and Eckert A. (2003) Neurotoxic mechanisms caused by the Alzheimer's disease-linked Swedish amyloid precursor protein mutation: oxidative stress, caspases, and the JNK pathway. *J. Biol. Chem.* **278**, 28294-28302.

Mattson M. P., Cheng B., Davis D., Bryant K., Lieberburg I. and Rydel R. E. (1992) beta-Amyloid peptides destabilize calcium homeostasis and render human cortical neurons vulnerable to excitotoxicity. *J. Neurosci.* **12**, 376–389.

Mattson M. P. and Kroemer G. (2003) Mitochondria in cell death: novel targets for neuroprotection and cardioprotection. *Trends Mol. Med.* **9**, 196-205.

McGrath L. T., McGleenon B. M., Brennan S., McCol l D., McILroy S. and Passmore A. P. (2001) Increased oxidative stress in Alzheimer's disease as assessed with 4-hydroxynonenal but not malondialdehyde. *Q. J. Med.* **94**, 485-490.

Mckee A. C., Kosik K. S. and Kowall N. W. (1991) Neuritic pathology and dementia in Alzheimer’s disease. *Ann. Neuro*. **30**, 156-165.

Micheva K. D., Kay B. K. and McPherson P. S. (1997) Synaptojanin forms two separate complexes in the nerve terminal. *J. Biol. Chem.* **272**, 27239-27245.

Miyata T., van Ypersele de Strihou C., Imasawa T., Yoshino A., Ueda Y., Ogura H., Kominami K., Onogi H., Inagi R., Nangaku M. and Kurokawa K. (2001) Glyoxalase I deficiency is associated with an unusual level of advanced glycation end products in a hemodialysis patient. *Kidney Int.* **60**, 2351-2359.

Moreira P. I., Santos M. S. and Oliveira C. R. (2007) Alzheimer's disease: a lesson from mitochondrial dysfunction. *Antioxid. Redox. Signal.* **9**, 1621-1630.

Morishima Y., Gotoh Y., Zieg J., Barrett T., Takano H., Flavell R., Davis R. J., Shirasaki Y. and Greenberg M. E. (2001) Beta-amyloid induces neuronal apoptosis via a mechanism that involves the c-Jun N-terminal kinase pathway and the induction of Fas ligand. *J. Neurosci.* **21**, 7551-7560.

Mott R. T. and Hulette C. M. (2005) Neuropathology of Alzheimer's disease. *Neuroimaging Clin. N. Am.* **15**, 755-65.

Mucke L., Masliah E., Yu G. Q., Mallory M., Rockenstein E. M., Tatsuno G., Hu K., Kholodenko D., Johnson-Wood K. and McConlogue L. (2000) High-level neuronal expression of abeta 1-42 in wild-type human amyloid protein precursor transgenic mice: synaptotoxicity without plaque formation. *J. Neurosci.* **20**, 4050-4058.

Mullan M., Houlden H., Crawford F., Kennedy A., Rogues P. and Rossor M. (1993) Age of onset in familial early onset Alzheimer's disease correlates with genetic aetiology. *Am. J. Med. Genet.* **48**, 129-130.

Myung J. K., Gulesserian T and Fountoulakis M. (2003) Deranged hypothetical proteins Rik protein, Nit protein 2 and mitochondrial inner membrane protein, mitofilin, in fetal Down syndrome brain. *Cell. Mol. Biol.* **49**, 739-746.

Norenberg M. D. and Rao K. V. (2007) The mitochondrial permeability transition in neurologic disease. *Neurochem. Int.* **50**, 983-997.

Oddo S., Caccamo A., Shepherd J. D., Murphy M. P., Golde T. E., Kayed R., Metherate R., Mattson M. P., Akbari Y. and LaFerla F. M. (2003) Triple-transgenic model of Alzheimer's disease with plaques and tangles: intracellular Abeta and synaptic dysfunction. *Neuron* **39**, 409-421.

Oh S., Hong H. S., Hwang E., Sim H. J., Lee W., Shin S. J. and Mook-Jung I. (2005) Amyloid peptide attenuates the proteasome activity in neuronal cells. *Mech. Ageing Dev.* **126**, 1292–1299.

Okazawa H. and Estus S. (2002) The JNK/c-Jun cascade and Alzheimer's disease. *Am. J. Alzheimer Dis. Other Demen.*. **17**, 79-88.

Parker W. D., Jr., Parks J., Filley C. M. and Kleinschmidt-DeMasters B. K. (1994) Electron transport chain defects in Alzheimer's disease brain. *Neurology* **44**, 1090-1096.

Pedersen J. S. and Otzen D. E. (2008) Amyloid a state in many guises: Survival of the fittest fibril fold. *Protein Sci.* **17**, 2-10.

Polidori M. C., Griffiths H. R., Mariani E. and Mecocci P. (2007) Hallmarks of protein oxidative damage in neurodegenerative diseases: focus on Alzheimer’s disease. *Amino Acids* **32**, 553-558.

Ricci J. E., Waterhouse N. and Green D. R. (2003) Mitochondrial functions during cell death, a complex (I-V) dilemma. *Cell Death Differ.* **10**, 488–492.

Perl D. P. (2000) Neuropathology of Alzheimer's disease and related disorders. *Neurol. Clin.* **18**, 847-864.

Pirttila T., Soininen H., Heinonen O., Lehtimaki T., Bogdanovic N., Paljarvi L., Kosunen O., Winblad B., Riekkinen P., Wisniewski H. M. and Mehta P. D. (1996) Apolipoprotein E (apoE) levels in brains from Alzheimer disease patients and controls. *Brain Res.* **722**, 71-77.

Raiha I., Kaprio J., Koskenvuo M., Rajala T. and Sourander L. (1996) Alzheimer's disease in Finnish twins. *Lancet* **347**, 573-578.

Ramjaun A. R., Angers A., Legendre-Guillemin V., Tong X. K. and McPherson P. S. (2001) Endophilin regulates JNK activation through its interaction with the germinal center kinase-like kinase. *J. Biol. Chem.* **276**, 28913-28919.

Ranganathan S., Ciaccio P. J., Walsh E. S. and Tew K. D. (1999) Genomic sequence of human glyoxalase-I: analysis of promoter activity and its regulation. *Gene.* **240**, 149–155.

Reddy P. H. (2007) Mitochondrial dysfunction in aging and Alzheimer's disease: strategies to protect neurons. *Antioxid. Redox. Signal.* **9**, 1647-1658.

Reddy P. H. and Beal M. F. (2005) Are mitochondria critical in the pathogenesis of Alzheimer's disease? *Brain Res. Brain Res. Rev.* **49**, 618-632.

Reutens A. T. and Begley C. G. (2002) Endophilin-1: a multifunctional protein. *Int. J. Biochem. Cell Biol.* **34**, 1173-1177.

Richard Eckert. L., Ann-Marie B., Monica R., Nancy R., David Ryan and Kathleen L. (2004) S100 Proteins in the Epidermis. *J. Invest. Dermato*. **123**, 23-33.

Roher AE, Lowenson JD, Clarke S. (1993) Beta-amyloid-(1-42) is a major component of cerebrovascular amyloid deposits: implications for the pathology of Alzheimer disease. *Proc. Natl. Acad. Sci. U. S. A.* **90**, 10836–10840.

Rovner B. (1986) Prevalence of Mental Illness in a Community Nursing Home. *Am. J. Psychiatry.* **143**, 1446-1449.
Ruffels J., Griffin M. and Dickenson J. M. (2004) Activation of ERK1/2, JNK and PKB by hydrogen peroxide in human SH-SY5Y neuroblastoma cells: role of ERK1/2 in H2O2-induced cell death. *Eur. J. Pharmacol.* **483**, 163-173.

Sajithlal G., Huttunen H., Rauvala H. and Munch G. (2002) Receptor for Advanced Glycation End Products Plays a More Important Role in Cellular Survival than in Neurite Outgrowth during Retinoic Acid-induced Differentiation of Neuroblastoma Cells. *J. Biol. Chem.* **277**, 6888 – 6897.

Salmon E., Lespagnard S., Marique P., Peeters F., Herholz K., Perani D., Holthoff V., Kalbe E., Anchisi D., Adam S., Collette F. and Garraux G. (2005) Cerebral metabolic correlates of four dementia scales in Alzheimer's disease. *J. Neurol.* **252**, 283-290.

Sasaki N., Fukatsu R., Tsuzuki K., Hayashi Y., Yoshida T., Fujii N., Koike T., Wakayama I., Yanagihara R., Garruto R., Amano N. and Makita Z. (1998) Advanced glycation end products in alzheimer’s disease and other neurodegenerative diseases. *Am. J. Pathol.* **153**, 1149–1155.

Sasaki N., Toki S., Chowei H., Saito T., Nakano N., Hayashi Y., Takeuchi M. and Makita Z. (2001) Immunohistochemical distribution of the receptor for advanced glycation end products in neurons and astrocytes in Alzheimer's disease. *Brain Res.* **888,** 256-262.

Sato S., Tatebayashi Y., Akagi T., Chui D. H., Murayama M., Miyasaka T., Planel E., Tanemura K., Sun X., Hashikawa T., Yoshioka K., Ishiguro K. and Takashima A. (2002) Aberrant tau phosphorylation by glycogen synthase kinase-3beta and JNK3 induces oligomeric tau fibrils in COS-7 cells. *J. Biol. Chem.* **277**, 42060-42065.

Schaufele F., Demarco I. and Day R. N. (2005) Molecular imaging: FRET microscopy and spectroscopy. **Chapter 4**, 72-94. FRET Imaging in the Wide-Field Microscope.

Schinzel A. C., Takeuchi O., Huang Z., Fisher J. K., Zhou Z., Rubens J., Hetz C., Danial N. N., Moskowitz M. A. and Korsmeyer S. J. (2005) Cyclophilin D is a component of mitochondrial permeability transition and mediates neuronal cell death after focal cerebral ischemia. *Proc. Natl. Acad. Sci. U. S. A.* **102**, 12005-12010.

Schmidt A. M., Hori O., Cao R., Yan S. D., Brett J., Wautier J. L., Ogawa S., Kuwabara K., Matsumoto M. and Stern D. (1996) RAGE: a novel cellular receptor for advanced glycation end products. *Diabetes* **45 Suppl 3**, S77-S80.

Schmidt A., Wolde M., Thele C., Fest W., Kratzin H., Podtelyjnekov A. V., Witke W., Hunttner W. B. and Soling H. D. (1999) Endophilin 1 meidaiates synaptic vescicle formation by transfer of arachidonate to lysophosphatidic acid. *Nature* **401**, 133-141.

Schmidt A. M., Yan S. D., Yan S. F. and Stern D. M. (2000) The biology of the receptor for advanced glycation end products and its ligands. *Biochim. Biophys. Acta* **1498,** 99-111.

Schobel S, Neumann S., Seed B. and Lichtenthaler S. F. (2006) Expression cloning screen for modifiers of amyloid precursor protein shedding. *Int. J. Dev Neurosci.* **24**, 141-148.

Selkoe D. J. (2001) Alzheimer's disease: genes, proteins, and therapy. *Physiol. Rev.* **81**, 741-766.

Selkoe D. J. (2002) Alzheimer's disease is a synaptic failure. *Science* **298**, 789-791.

Selkoe D. J. (2000) Toward a comprehensive theory for Alzheimer's disease. Hypothesis: Alzheimer's disease is caused by the cerebral accumulation and cytotoxicity of amyloid beta-protein. *Ann. N. Y. Acad. Sci.* **924**, 17-25.

Serretti A., Artioli P., Quartesan R. and De Ronchi D. (2005) Genes involved in Alzheimer's disease, a survey of possible candidates. *J. Alzheimers Dis.* **7**, 331-353.

Sherratt H. S. (1991) Mitochondria: structure and function. *Rev. Neurol. (Paris)* **147**, 417-430.

Shinohara M., Thornalley P. J., Giardino I., Beisswenger P., Thorpe S. R., Onorato J. and Brownlee M. (1998) Overexpression of glyoxalase-I in bovine endothelial cells inhibits intracellular advanced glycation endproduct formation and prevents hyperglycemia-induced increases in macromolecular endocytosis. *J. Clin. Invest.* **101**, 1142-1147.

Shoji M., Iwakami N., Takeuchi S., Waragai M., Suzuki M., Kanazawa I., Lippa C. F., Ono S. and Okazawa H. (2000) JNK activation is associated with intracellular beta-amyloid accumulation. *Brain Res. Mol. Brain Res.* **85**, 221-233.

Smeitink J. A., Loeffen J. L., Triepels R. H., Smeets R. J., Trijbels J. M. and van den Heuvel L. P. (1998) Nuclear genes of human complex I of the mitochondrial electron transport chain: state of the art. *Hum. Mol. Genet.* **7**, 1573–1579.

Smeitink J. and van den Heuvel L. W. (1999). Human mitochondrial complex I in health and disease. *Am. J. Hum. Genet.* **64**, 1505-1510.

Smeitink J. A., van den Heuvel L. W., Koopman W. J., Nijtmans L. G. Ugalde C. and Willems P. H. (2004) Cell biological consequences of mitochondrial NADH: ubiquinone oxidoreductase deficiency.*Curr. Neurovasc. Res.* **1**, 29-40.

Smith C. M. and Swash M. (1978) Possible biochemical basis of memory disorder in Alzheimer disease. *Ann. Neurol.* **3**, 471-473.

Smith M. A., Taneda S., Richey P. L., Miyata S., Yan S. D., Stern D., Sayre L. M., Monnier V. M. and Perry G. (1994) Advanced Maillard reaction end products are associated with Alzheimer disease pathology. *Proc. Natl. Acad. Sci. U. S. A.* **91**, 5710–5714.

Song L., Li J., Zhang D., Liu Z. G., Ye J., Zhan Q., Shen H. M., Whiteman M. and Huang C. (2006) IKK{beta} programs to turn on the GADD45{alpha}-MKK4-JNK apoptotic cascade specifically via p50 NF-{kappa}B in arsenite response. *J. Cell Biol.* **175**, 607 - 617.

Souder E. (2005) Neuropathology in Alzheimer's disease: target of pharmacotherapy. *J. Am. Acad. Nurse Pract.* **Suppl**, 3-5.

Staniszewska M., Leszek J., Malyszczak K. and Gamian A. (2005) Are advanced glycation end-products specific biomarkers for Alzheimer's disease? *Int. J. Ger. Psy.* **20**, 896-897.

Stockley J. H. and O'Neill C. (2007) The proteins BACE1 and BACE2 and beta-secretase activity in normal and Alzheimer's disease brain. *Biochem. Soc. Trans.* **35**, 574–576.

Suzuki N., Cheung T. T., Cai X. D., Odaka A., Otvos L., Jr Eckman C., Golde T. E. and Younkin S. G. (1994) An increased percentage of long amyloid beta protein secreted by familial amyloid beta protein precursor (beta APP717) mutants. *Science* **264**,1336-1340.

Tamagno E., Robino G., Obbili A., Bardini P., Aragno M., Parola M. and Danni O. (2003) H2O2 and 4-hydroxynonenal mediate amyloid beta-induced neuronal apoptosis by activating JNKs and p38MAPK. *Exp. Neurol.* **180**, 144-155.

Taguchi A., Blood D. C., Canet A., Lee D. C., Qu W., Tanji N., Lu Y., Lalla E., Fu C., Hofmann M. A., Kislinger T., Ingram M., Lu A., Tanaka H., Hori O., Ogawa S., Stern D. M. and Schmidt A. M. (2000) Blockade of RAGE-amphoterin signalling suppresses tumour growth and metastases. *Nature* **405**, 354-360.

Takeuchi M., Kikuchi S., Sasaki N., Suzuki T., Watai T., Iwaki M., Bucala R. and Yamagishi S. (2004) Involvement of advanced glycation end-products (AGEs) in Alzheimer's disease. *Curr. Alzheimer Res.* **1**, 39-46.

Takuma K., Yao J., Huang J., Xu H., Chen X., Luddy J., Trillat A. C., Stern D. M., Arancio O. and Yan S. S. (2005) ABAD enhances Abeta-induced cell stress via mitochondrial dysfunction. *FASEB J.* **19**, 597-598.

Tobina J. E., Cui J., Wilk J. B., Latourelle J. C., Laramie J. M., McKee A. C., Guttmang M. and Karamohamed S., DeStefano A. L. and Myers R. H. (2007) Sepiapterin reductase expression is increased in Parkinson's disease brain tissue. *Brain Res.* **30**, 1139, 42-7.

Tol J., Roks G., Slooter A. J. and van Duijn C. M. (1999) Genetic and environmental factors in Alzheimer's disease. *Rev. Neurol. (Paris)* **155 Suppl 4**, S10-S16.

Torroja L., Ortuno-Sahagun D., Ferrus A., Hammerle B. and Barbas J. A. (1998) Scully, an essential gene of Drosophila, is homologous to mammalian mitochondrial type II L-3-hydroxyacyl-CoA dehydrogenase/amyloid-beta peptide-binding protein. *J. Cell Biol.* **141**, 1009-1017.

Townsend K. P. and Pratico D. (2005) Novel therapeutic opportunities for Alzheimer's disease: focus on nonsteroidal anti-inflammatory drugs. *FASEB J.* **19**, 1592-1601.

Trevaskis J., Walder K., Foletta V., Kerr-Bayles L., McMillan J., Cooper A., Lee S., Bolton K., Prior M., Fahey R., Whitecross K., Morton G. J., Schwartz M. W. and Collier G. R. (2005) Src homology 3-domain growth factor receptor-bound 2-like (endophilin) interacting protein 1, a novel neuronal protein that regulates energy balance. *Endocrinology* **146**, 3757-3764.

Troy C. M., Rabacchi S. A., Xu Z., Maroney A. C., Connors T. J., Shelanski M. L. and Greene L. A. (2001) Beta-Amyloid-induced neuronal apoptosis requires c-Jun N-terminal kinase activation. *J. Neurochem.* **77**, 157-164.

Veerkamp J. H. and Zimmerman A. W. (2001) Fatty acid-binding proteins of nervous tissue. *J. Mol. Neurosci.* **16**, 133-142.

Vera Adam-Vizi. (2005) Production of Reactive Oxygen Species in Brain Mitochondria: Contribution by Electron Transport Chain and Non–Electron Transport Chain Sources. *Antioxid. Redox Signal.* **7**, 1140-1149.

Verdier Y., Zarandi M. and Penke B. (2004) Amyloid beta-peptide interactions with neuronal and glial cell plasma membrane: binding sites and implications for Alzheimer's disease. *J. Pept. Sci.* **10**, 229-248.

Voss T. C., Demarco I. A. and Day R. N. (2005) Quantitative imaging of protein interactions in the cell nucleus. *Biotech.* **38**, 413–424.

Votyakova T. V. and Reynolds I. J. (2005) Ca^{2+}-induced permeabilization promotes free radical release from rat brain mitochondria with partially inhibited complex I. *J. Neurochem.* **93**, 526–537.

Wallrabe H. and Periasamy A. (2005) Imaging protein molecules using FRET and FLIM microscopy. *Curr. Opin. Biothenol.* **16**, 19-27.

Walsh D. M., Klyubin I., Fadeeva J. V., Cullen W. K., Anwyl R., Wolfe M. S., Rowan M. J. and Selkoe D. J. (2002) Naturally secreted oligomers of amyloid beta protein potently inhibit hippocampal long-term potentiation in vivo. *Nature* **416**, 535-539.

Walsh D. M., Tseng B. P., Rydel R. E., Podlisny M. B. and Selkoe D. J. (2000) The oligomerization of amyloid beta-protein begins intracellularly in cells derived from human brain. *Biochemistry* **39**, 10831-10839.

Wang B. R., Zaheer A. and Lim R. (1992) Polyclonal antibody localizes glia maturation factor beta-like immunoreactivity in neurons and glia. *Brain Res.* **591**, 1-7.

Wang Q., Walsh D. M., Rowan M. J., Selkoe D. J. and Anwyl R. (2004) Block of long-term potentiation by naturally secreted and synthetic amyloid beta-peptide in hippocampal slices is mediated via activation of the kinases c-Jun N-terminal kinase, cyclin-dependent kinase 5, and p38 mitogen-activated protein kinase as well as metabotropic glutamate receptor type 5. *J. Neurosci.* **24**, 3370-3378.

Widera D., Mikenberg I., Elvers M., Kaltschmidt C. and Kaltschmidt B. (2006) Tumor necrosis factor alpha triggers proliferation of adult neural stem cells via IKK/NF-kappaB signaling. *BMC. Neurosci.* **7**, 64-68.

Wilquet V. and De S. B. (2004) Amyloid-beta precursor protein processing in neurodegeneration. *Curr. Opin. Neurobiol.* **14**, 582-588.

Wojcik C. and Di Napol M. (2004) Ubiquitin-Proteasome System and Proteasome Inhibition: New Strategies in Stroke Therapy. *Stroke* **35**, 1506-1518.

Xu X., Raber J., Yang D., Su B. and Mucke L. (1997) Dynamic regulation of c-Jun N-terminal kinase activity in mouse brain by environmental stimuli. *Proc. Natl. Acad. Sci. U. S. A.* **94**, 12655-12660.

Yan S. D., Chen X., Fu J., Chen M., Zhu H., Roher A., Slattery T., Zhao L., Nagashima M., Morser J., Migheli A., Nawroth P., Stern D. and Schmidt A. M. (1996) RAGE and amyloid-beta peptide neurotoxicity in Alzheimer's disease. *Nature* **382**, 685-691.

Yan S. D., Roher A., Chaney M., Zlokovic B., Schmidt A. M. and Stern D. (2000) Cellular cofactors potentiating induction of stress and cytotoxicity by amyloid beta-peptide. *Biochim. Biophys. Acta* **1502**, 145-157.

Yan S. D., Shi Y., Zhu A., Fu J., Zhu H., Zhu Y., Gibson L., Stern E., Collison K., Al-Mohanna F., Ogawa S., Roher A., Clarke S. G. and Stern D. M. (1999) Role of ERAB/L-3-hydroxyacyl-coenzyme A dehydrogenase type II activity in Abeta-induced cytotoxicity. *J. Biol. Chem.* **274**, 2145-2156.

Yan S. D., Stern D., Kane M. D., Kuo Y. M., Lampert H. C. and Roher A. E. (1998) RAGE-Abeta interactions in the pathophysiology of Alzheimer's disease. *Restor. Neurol. Neurosci.* **12**, 167-173.

Yan S. D., Zhu Y., Stern E. D., Hwang Y. C., Hori O., Ogawa S., Frosch M. P., Connolly Jr E. S., McTaggert R. and Pinsky D. J. (2000) Amyloid beta -Peptide-binding Alcohol Dehydrogenase Is a Component of the Cellular Response to Nutritional Stress. *J. Biol. Chem.* **275**, 27100 - 27109.

Yan S. D. and Stern D. M. (2004) Mitochondrial dysfunction and Alzheimer's disease: role of amyloid-beta peptide alcohol dehydrogenase (ABAD). *Int. J. Exp. Pathol.* **86**, 161-171.

Yang S., Lee Y. J., Kim J. M., Park S., Peris J., Laipis P., Park Y. S., Chung J. H. and Oh S. P. (2006) A murine model for human sepiapterin-reductase deficiency. *Am. J. Hum. Genet.* **78**, 575-587.

Yao J., Taylor M., Davey F., Ren Y., Aiton J., Coote P., Fang F., Chen J. X., Yan S. D. and Gunn-Moore F. J. (2007) Interaction of amyloid binding alcohol dehydrogenase/Abeta mediates up-regulation of peroxiredoxin II in the brains of Alzheimer's disease patients and a transgenic Alzheimer's disease mouse model. *Mol. Cell. Neurosci.* **35**, 377-382.

Yong W., Lomakin A., Kirkitadze M. D., Teplow D. B., Chen S. H. and Benedek G. B. (2002) Structure determination of micelle-like intermediates in amyloid beta protein fibril assembly by using small angle neutron scattering. *Proc. Natl. Acad. Sci. U. S. A.* **99**, 150-154.

Zaccolo M. (2004) Use of chimeric fluorescent proteins and fluorescence resonance energy transfer to monitor cellular responses. *Circ. Res.* **94**, 866–873.

Zal T., Zal M. A. and Gascoigne N. R. (2002) Inhibition of T cell receptor-coreceptor interactions by antagonist ligands visualized by live FRET imaging of the T-hybridoma immunological synapse. *Immunity* **16**, 521-534.
Zhang J. Y., Liu S. J., Li H. L. and Wang J. Z. (2004) Microtubule-associated protein tau is a substrate of ATP/Mg2+-dependent proteasome protease system. *J. Neural. Transmi.* **112**, 547-555.

Zhang G. Y. and Zhang Q. G. (2005) Agents targeting c-Jun N-terminal kinase pathway as potential neuroprotectants. *Exper.t Opin. Investig. Drugs* **14**, 1373–1383.

Zhu X., Raina A. K., Rottkamp C. A., Aliev G., Perry G., Boux H. and Smith M. A. (2001) Activation and redistribution of c-jun N-terminal kinase/stress activated protein kinase in degenerating neurons in Alzheimer's disease. *J. Neurochem.* **76**, 435-441.

Zhu X., Lee H. G., Raina A. K., Perry G. and Smith M. A. (2002) The role of mitogen-activated protein kinase pathways in Alzheimer's disease. *Neurosignals* **11**, 270-281.

Zhu X., Raina A. K., Lee H., Casadesus G., Smith M. A. and Perry G. (2004) Oxidative stress signalling in Alzheimer's disease. *Brain Res.* **1000**, 32-39.

Zhu X., Smith M. A., Perry G.., Aliev, G. (2004). Mitochondrial failures in Alzheimer's disease. *Am. J. Alzheimer Dis. Other Demen.* **19**, 345-352.

Appendix 1: List of Suppliers

Supplier	Address
Abcam	Cambridge, UK
Amaxa	Cologne, Germany
American Tissue Culture Collection (ATCC)	Rockville, USA
Amersham- Pharmacia-Biotech	Buckinghamshire, UK
Bachem	Bubendorf, Switzerland
BD Biosciences/Clontech	Oxford, UK
Biomol Interantional	Exeter, UK
Fisher Scientific	Loughborough, UK
Invitrogen/Gibco	Paisley, UK
Millipore	Watford, UK
New England Biolabs/Cell signaling	Hertfordshire, UK

Appendix 2: Antibody specific protocols

Primary antibody: anti-β-actin (Sigma) 1:5000
Secondary antibody: Santa Cruz anti-mouse-HRP 1:5000
Protocol: As described in section 2.4.6

Primary antibody: anti-PSMB4 (Biomol International) 1:2000
Secondary antibody: Santa Cruz anti-mouse-HRP 1:5000
Protocol: As described in section 2.4.6

Primary antibody: anti-NDUFV2 1:5000
Secondary antibody: Santa Cruz anti-rabbit-HRP 1:5000
Protocol: As described in section 2.4.6
Anti-NDUFV2 is a kind gift from Dr Ian Fearnley,
MRC Dunn Human Nutrition Unit, Cambridge.

Primary antibody: anti-Glyoxylase 1 1:2000
Secondary antibody: Santa Cruz anti-rabbit-HRP 1:5000
Protocol: As described in section 2.4.6
Anti-Glyoxylase 1 is a kind gift from Dr Carol Brown,
Department of Cell and Molecular Pharmacology, Hollings Cancer Center.

Primary antibody: anti-GFP (Sigma) 1:1000
Secondary antibody: Santa Cruz anti-mouse-HRP 1:10,000
Protocol: As described in section 2.4.6

Primary antibody: anti-FLAG M2 (Sigma) 1:500
Secondary antibody: Santa Cruz anti-mouse-HRP 1:10,000
Protocol: Block at room temperature 30 minutes 3% milk TBS
Wash 1x TBS
Primary antibody 1:500 3% milk-TBS 30 minutes
Wash 1x TBS 10 minutes
Secondary antibody 1:10,000 3% milk-TBS 30 minutes
Wash 8x 3minutes TBS

Primary antibody: anti-phospho-JNK (Cell signaling) 1: 2000
Secondary antibody: Santa Cruz anti-mouse 1:5000
Protocol: Block overnight 4°C 3% Bovine serum albumin (BSA) TBS/T
Wash 1x TBS/T
Primary antibody 1:2000 3% BSA TBS/T overnight
Wash 3x TBS/T 5 minutes
Secondary antibody 1:5000 3% BSA TBS/T 1 hour

Wash 3x TBS/T 5 minutes

Primary antibody: anti -JNK (Cell signaling) 1: 2000
Secondary antibody: Santa Cruz anti-mouse 1:5000
Protocol: Block overnight 4°C 3% BSA TBS/T
Wash 1x TBS/T
Primary antibody 1:2000 3% BSA TBS/T overnight
Wash 3x TBS/T 5 minutes
Secondary antibody 1:5000 3% BSA TBS/T 1 hour
Wash 3x TBS/T 5 minutes